THE ROLE OF *O*-LINKED GLYCOSYLATION IN VWF FUNCTION

A thesis submitted to Imperial College London

for the degree of

Doctor of Philosophy in the Faculty of Medicine

by

Agata Anna Nowak, BSc,MSc

Centre for Haematology

Faculty of Medicine

Imperial College of London

Hammersmith Campus

January 2011

ABSTRACT

During synthesis Von Willebrand Factor (VWF) undergoes *O*-linked glycosylation (OLG) but the functional significance of this has not been fully explored. In this study the 10 OLG sites in VWF were mutated to alanine, individually and as clusters on either or both sides of the A1 domain: Clus-1 (N-terminal side), Clus-2 (C-terminal side) and double cluster (DC). All mutants demonstrated normal expression, multimeric structure and collagen and heparin binding functions. Furthermore, mass spectroscopy analysis showed that the OLG structures presented on recombinant VWF were similar in structure to those on plasma derived VWF including the presence of a rare disialosyl motif. The variants T1486 (C-terminal side of the A1 domain), Clus-2 and DC were less susceptible to ADAMTS13 proteolysis under static and pseudo-shear stress conditions and showed increased binding to ADAMTS13 when in solution. Using an optimised plate-based ELISA assay, it was demonstrated that mutation of the OLG sites on the N-terminal side of the VWF-A1 domain enhanced sensitivity to ristocetin-mediated binding to recombinant GPIbα. Increased GPIbα binding was also observed with desialylated VWF and this effect was attributed to sialic acid residues on the OLGs. Similar results were obtained using the conventional ristocetin cofactor assay. To further investigate these findings, an *in vitro* flow assay was optimised to analyse the interaction of VWF and platelets under shear stress. Mutation of the OLG sites on the N-terminal side of the A1 domain, increased platelet rolling velocity but did not significantly alter the dissociation rate of the VWF-A1:GPIbα bond. However, they did decrease the number of transient tethering events as a function of time when VWF was immobilised directly on to the flow surface. Interestingly, when compared with wtVWF the T1255A and Clus-1 variants mediated increased platelet capture to collagen under high shear stress.

The data presented in this thesis demonstrates that the OLG clustered at the C-terminal side of the A1 domain alter susceptibility of VWF to ADAMTS13 cleavage. Whilst OLGs clustered at the N-terminal side of A1 modulate its interaction with GPIbα both under static and shear conditions. A unifying hypothesis would be that VWF OLG alter conformational stability around the A1 domain and modulate its interactions with adjacent domains and with other molecules. However different effects may predominate under static and flow conditions. Importantly, VWF-platelet interaction in flow assays depends on the way VWF has been immobilised.

DECLARATION OF ORIGINALITY

I, Agata Anna Nowak, hereby declare that the work presented in this thesis is my own. All work and data analysis of the results were performed by myself, unless otherwise specified in the text.

Agata Anna Nowak

ACKNOWLEDGMENTS

Firstly, I would like to take this opportunity to express my deep and sincere gratitude to both my supervisors Professor Mike Laffan and Dr Thomas McKinnon. I would like to thank Professor Laffan for the opportunity to study in his laboratory, for his excellent and enthusiastic supervision, guidance and immense knowledge.

I could have not imagined having a better mentor for my PhD study than Dr McKinnon; it has always been pleasure and fun to work with you. Thank you for constant encouragement, motivation and enthusiasm and also patience during the writing up period. Tom you are not only an excellent and inspiring supervisor and an amazing scientist but also a truly great friend; not sure how you do it, but I am immensely grateful.

I wish to thank Professor David Lane for important feedback and advice. It is also a pleasure to thank all the past and present members of 5S1 lab especially Dr Alain Chan for invaluable help and advice, Dr Sara Zanardelli for important scientific and non-scientific discussions, also many thanks to Yaozu Xiang, Dr Brenda Luken and Dr Rens de Groot.

I would like to express gratitude, to all the people I've had a chance to collaborate with; Professor Karen Vanhoorelbeke, Professor Anne Dell and Dr James O'Donnell for important contributions and helpful advice to the studies; Dr Anne Riddell and Mrs Gillian Angus for performing VWF:RCo activity assays. Many thanks to Dr Kévin Canis for teaching me the basics of MS and all the help during our studies.

On a personal note, I wish to thank my lovely fellow PhD students. You have made this three years enjoyable and fun. Helena, thank you for being a great friend, for your support great sense of humour and all the fun and crazy stuff we have done over the years. Maria and Verity I am grateful for your support and encouragement in an out of work, your positive energy and all the fun times we shared. And Josefin I've really appreciated your support during the last months of my doctorate.

Finally, the support and encouragement of many friends has been indispensable and I would like to thank particularly; Marta, Adwoa, Hannah, Ania, Lukasz, Amu, Poh-Choo, Julia, Domi and last but not least Paula&Jarek.

Na końcu chciałbym podziewkować mojej rodzinie zwłaszcza rodzicom i Oli, dzięki którym mogłam uczyć się i studiować w komfortowych warunkach. Bez waszego wsparcia, miłości, zrozumienia i motywacji nie bylo było by to możliwe

CONTENTS

TITLE……..……1

ABSTRACT……...……..2

DECLARATION OF ORGINALITY ……..3

ACKNOWLEDGMENTS……..…….4

CONTENTS……...……..5

LIST OF FIGURES……...13

LIST OF TABLES…….19

LIST OF ABBREVATIONS…….20

1 INTRODUCTION 25

1.1 Overview of haemostasis..... 25

1.2 Von Willebrand factor..... 25

1.3 VWF gene structure and transcriptional regulation..... 25

1.3.1 VWF synthesis and processing 26

1.3.2 Tissue Distribution and sites of synthesis 29

1.4 VWF storage and secretion 30

1.5 VWF structure and function 32

1.5.1 VWF tertiary structure 33

1.5.2 The D domains 34

1.5.2.1 Factor VIII binding 35

1.5.2.2 P-selectin binding 36

1.5.3 The A domains 36

1.5.4 The D4 and B domains..... 40

1.5.5 The C domains and the cysteine knot 40

1.6 Collagen binding 40

1.7 ADAMTS13 42
1.7.1 ADAMTS13 role in the haemostasis 43
1.7.2 ADAMTS13 associated disorders 44
1.7.3 ADAMTS13 role in proteolysis of VWF 46
1.7.4 Factors modulating ADAMTS13 proteolysis 47
1.7.5 Mechanism of ADAMTS13 multistep binding to VWF 48
1.8 Thrombospondin I cleavage 49
1.9 VWF and platelet binding 50
1.9.1 Platelet aggregation 56
1.10 Mechanism of transient platelet adhesion under flow 58
1.11 Blood flow dynamics and kinetics 61
1.12 VWF self aggregation 64
1.13 Von Willebrand disease 65
1.14 VWF glycosylation 66
1.14.1 *N*-linked glycosylation 68
1.14.2 *O*-linked glycosylation 70
1.14.2.1 Synthesis of O-linked glycans 71
1.14.2.2 Function of O-linked glycans 73
1.14.3 VWF *O*-linked glycans structure and function 74
1.15 Sialic acid 76
1.16 VWF clearance, role of carbohydrates 77
1.17 Mass spectrometry 80
2 AIMS OF THESIS 82
3 MATERIAL AND METHODS 83
3.1 General molecular biology techniques 83
3.1.1 Site-directed mutagenesis 83
3.1.2 Restriction endonuclease digestion of plasmid DNA 83

3.1.3 Ligation of plasmid vector and insert DNA 83
3.1.4 Agarose gel electrophoresis of DNA 84
3.1.5 Transformation of competent bacterial cells 84
3.1.6 Isolation of plasmid DNA 84
3.1.7 Agar Plates and Luria-Bertani (LB) Media ± Ampicillin, Kanamicin 85
3.1.8 Gel extraction 85
3.1.9 Cloning and expression vectors 85
3.1.10 Generation of human and murine VWF glycan mutants 87
3.1.11 Sequencing 90
3.2 Cell culture 90
3.2.1 General Tissue Culture 90
3.2.2 Cell revival 90
3.2.3 Cell passage 90
3.2.4 Transient transfection of HEK293T cells 91
3.3 General protein techniques 91
3.3.1 Protein determination using the Bicinchoninic acid (BCA) assay 91
3.3.2 SDS polyacrylamide gel electrophoresis (SDS-PAGE) 92
3.3.3 Coomassie staining of SDS-PAGE gels 92
3.3.4 Western Blot 92
3.3.5 Purification of VWF from Haemate P® 93
3.3.5.1 Gel filtration 93
3.3.5.2 Heparin Sepharose affinity chromatography 93
3.3.6 Purification of recombinant VWF 94
3.3.6.1 Ion exchange chromatography 94
3.3.6.2 Heparin Sepharose affinity chromatography 94
3.3.7 Nickel affinity chromatography 94
3.3.8 Botrocetin purification 95

3.4 VWF Analysis 95
3.4.1 VWF ELISA 95
3.4.2 VWF Multimer Analysis 96
3.4.3 Collagen binding assay 96
3.4.4 Nanobody binding assay 97
3.4.5 Plate binding assay between the bacterial A2 domain and VWF variants 97
3.4.6 Immunosorbent assay for VWF-linked T antigen–Peanut agglutinin binding (PNA) binding assay 98
3.4.7 Heparin binding 99
3.4.8 Glycoprotein Ibα binding assay 99
3.5 ADAMTS13 analysis 100
3.5.1 ADAMTS13 ELISA 100
3.5.2 ADAMTS13 activity assays under static conditions 100
3.5.3 ADAMTS13 activity assays under pseudo-shear conditions 101
3.5.4 Assay of ADAMTS13 binding to extended VWF 101
3.5.5 Assay of ADAMTS13 binding to globular VWF 101
3.6 Generation of GPIbα-myc/His construct 102
3.7 Interaction of platelets and VWF variants under conditions of flow 105
3.7.1 Platelets and erythrocytes isolation and labelling 105
3.7.2 Flow chamber and digital image processing 106
3.7.3 Preparation of flow slides 107
3.7.4 Measurements of platelet interaction and rolling velocities in flow 107
3.7.5 Measurement of platelet tethering 108
3.7.6 Measurement of platelet binding by VWF bound to collagen 108
3.8 Statistical analysis 109
3.9 Mass spectrometry techniques 109
3.9.1 Reductive elimination 109

3.9.2 Chemical derivatisation-permethylation 109
3.9.3 MALDI-MS and MS analysis 110
3.9.4 Data analysis 110
4 ANALYSIS OF VWF *O*-LINKED GLYCAN STRUCTURE 111
4.1 Introduction 111
4.2 In silico analysis of VWF 112
4.2.1 Sequence alignment of the VWF-A1 domain flanking regions 112
4.3 Experimental analysis of VWF *O*-linked glycans structure 115
4.3.1 Purification of VWF from Haemate P 115
4.3.2 Purification of recombinant VWF 116
4.3.3 *O*-glycome profile of rVWF 119
4.4 Discussion 123
5 EXPRESSION AND CHARACTERISTION OF VWF *O*-LINKED GLYCOSYLATION MUTANTS 127
5.1 Generation of *O*-linked glycosylation variants 127
5.1.1 Mammalian expression of recombinant VWF 128
5.2 Characterisation of VWF mutants 132
5.2.1 Multimer analysis 132
5.2.2 Collagen binding activity 134
5.3 Functional characteristics of VWF variants 136
5.3.1 Heparin binding 136
5.3.2 Nanobody binding 137
5.3.3 Binding of bacterial expressed VWF A2 domain to VWF 141
5.3.4 Peanut agglutinin binding 144
5.4 Discussion 145
6 INTERACTION OF VWF *O*-LINKED GLYCOSYLATION VARIANST WITH ADAMTS13 150
6.1 ADAMTS13 cleavage of VWF *O*-linked glycosylation variants 150

6.1.1 ADAMTS13 proteolysis of full length VWF variants under static and pseudo-shear conditions 150

6.1.2 Cleavage of D'-A3 VWF with ADAMTS13 154

6.2 Characterisation of binding between ADAMTS13 and S1486A, Clus 2 and DC VWF variants 156

6.2.1 Binding between ADAMTS13 and elongated VWF 156

6.2.2 Binding between ADAMTS13 and VWF in globular conformation 158

6.3 Discussion 160

7 EFFECT OF O-LINKED GLYCANS ON THE INTERACTION OF VWF WITH PLATELET RECEPTOR GLYCOPROTEIN Ibα UNDER STATIC CONDITIONS 171

7.1 Introduction 171

7.2 Expression of recombinant GPIbα 172

7.2.1 GPIbα construct 172

7.2.2 GPIbα/myc-his protein expression and purification 172

7.3 GPIbα binding assay 174

7.3.1 GPIbα binding and VWF multimeric size 174

7.4 GPIbα binding and VWF *O*-linked glycosylation 175

7.5 GPIbα binding and VWF sialylation 184

7.5.1 Desialylation of *O*-linked glycosylation variants 187

7.6 Binding between GPIbα and wtVWF in the presence of botrocetin 190

7.7 Ristocetin co-factor activity assay- Influence of *O*-linked glycans on platelet aggregation 191

7.8 Discussion 192

8 VWF *O*-LINKED GLYCANS ROLE IN VWF-PLATELET INTERACTION UNDER CONDITIONS OF FLOW 201

8.1 Introduction 201

8.2 Expression and purification of D'A3 201

8.3 Flow assay optimisation 202

8.3.1 Experimental setup....202
8.3.2 Flow slides....203
8.3.3 Platelet preparation....204
8.3.4 Coating VWF concentration....205
8.3.5 Optimal collagen source....207
8.4 Kinetics and mechanics of platelet interaction with immobilised VWF-D'A3: method optimisation and data analysis....210
8.4.1 Platelet capture....210
8.4.2 Platelet rolling velocities....213
8.4.3 Dissociation rate constant....218
8.4.4 Transient tethering....220
8.5 Desialylated wtVWF interaction with platelets under shear stress....221
8.5.1 Platelet adhesion and rolling....221
8.5.2 Transient tethering....222
8.6 Platelet accumulation and rolling on wtD'A3 and *O*-linked glycosylation variants....224
8.7 The influence of VWF *O*-linked glycosylation on the kinetics of GPIbα-A1 tether bond....229
8.7.1 Dissociation rate....229
8.7.2 Transient tethering rate....231
8.7.3 Effect of coating concentration on platelet adhesion to VWF-D'A3....232
8.8 Comparison of platelet translocation pattern over immobilised wtD'A3 and *O*-glycosylation variants....235
8.9 Influence of *O*-linked glycosylation variants on VWF mediated platelet adhesion to collagen....237
8.10 Discussion....238
8.10.1 The influence of *O*-linked glycans on platelet interaction with immobilised D'A3-VWF under various shear rates....242
8.10.2 Sialic acid effect on VWF-platelet interaction under conditions of shear flow 247

8.10.3 Platelets interaction with collagen in the presence of VWF under high shear stress the role of *O*-linked glycans 248

9 CONCLUSION AND FUTURE DIRECTIONS 252

9.1 Susceptibility to ADAMTS13 proteolysis 254

9.2 VWF interaction with platelet GPIbα – the role of *O*-linked glycans 255

9.3 VWF *O*-linked glycans as stabilisers of linker regions 259

9.4 Structure of VWF *O*-linked glycans 261

9.5 Sialic acid and VWF function 263

9.6 Role of VWF *O*-linked glycans *in vivo* 263

10 REFERENCES 267

APPENDICES ……...……..297

PUBLICATIONS ARISING FROM THIS WORK…….300

LIST OF FIGURES

Figure 1.1. Posttranslational modifications of VWF 28

Figure 1.2.Dimerisation and multimerisation of VWF 29

Figure 1.3. Domain structure of VWF 33

Figure 1.4 The A domains structure 37

Figure 1.5 ADAMTS13 domain structure 43

Figure 1.6 Putative two step binding interaction between ADAMTS13 and VWF 49

Figure 1.7 GPIbα structure and model of interaction with the VWF-A1 domain 54

Figure 1.8 Schematic representation of bond mechanics 60

Figure 1.9 Schematic representation of blood flow in a vessel 61

Figure 1.10 Types of glycans 67

Figure 1.11 VWF glycosylation 68

Figure 1.12 Pathways specific for the assembly of the *O*-linked glycans 72

Figure 1.13 Major tetrasaccharide structure of the *O*-glycans of VWF 74

Figure 3.1 pcDNAA3.1/myc-His A(+) mammalian expression vector 86

Figure 3.2pBlueScript cloning vector 87

Figure 3.3 Outline of cloning steps used to generate VWF glycosylation mutants 89

Figure 3.4 Cloning steps used to generate GPIbα-*myc*-His construct in expression vector 105

Figure 4.1 Protein sequence alignment of the VWF A1domain linker regions from various species 113

Figure 4.2 Gel filtration of Haemate P 116

Figure 4.3 FPLC purification of rVWF by ion exchange chromatography 117

Figure 4.4 Purification of rVWF by heparin affinity chromatography 118

Figure 4.5 Schematic representation of glycomic strategy used to describe VWF *O*-linked glycome 119

Figure 4.6 MALDI-TOF mass spectrum of permethylated VWF *O*-linked glycans 120

Figure 4.7 MALDI-TOF/TOF mass spectrum of the tri-sialylated *O*-linked glycan (*m/z* 1617) 121

Figure 4.8 MALDI-TOF/TOF MS/MS spectrum of the $[M+ Na]^+$ parent ion at *m/z* 1256 122

Figure 4.9 MALDI-TOF/TOF MS/MS spectrum of the $[M+ Na]^+$ parent ion at *m/z* 1705 123

Figure 5.1 VWF *O*-linked glycosylation sites 128

Figure 5.2 Expression of wtVWF and its glycosylation variants - VWF ELISA 129

Figure 5.3 Expression of *O*-linked glycosylation cluster variants 131

Figure 5.4 Multimer distribution of VWF glycosylation variants 133

Figure 5.5 Binding isotherms of VWF variants to collagen type III 135

Figure 5.6 Analysis of VWF binding to collagen types III (A) and I (B) 136

Figure 5.7 Binding of wtVWF and VWF glycosylation variants to heparin 137

Figure 5.8 Binding isotherm of wtVWF and DC variant to nanobody AU/VWFa-11 in the absence of ristocetin 139

Figure 5.9 Binding of wt and mutated VWF to AU/VWFa-11 nanobody in the presence of 250 μg/ml ristocetin 140

Figure 5.10 Binding isotherm of ristocetin activated VWF to AU/VWFa-11 nanobody 141

Figure 5.11 VWF binding to immobilised bacterial A2 domain 142

Figure 5.12 Binding of the bacterial A2 domain to immobilised multimeric VWF variants 143

Figure 5.13 Binding of the mammalian glycosylated and de-glycosylated VWF-A2 domain to multimeric immobilised VWF 144

Figure 5.14 Binding of peanut agglutinin to VWF cluster variants 145

Figure 6.1 Multimer gel analysis of ADAMST13 cleavage 151

Figure 6.2 Collagen binding analysis of wtVWF, S1486A and Clus 2 and DC variants proteolysis by ADAMTS13 in the presence of urea 152

Figure 6.3 Multimer gel analysis of wt and S1486A VWF proteolysis by ADAMTS13 in pseudo shear assay 153

Figure 6.4 Collagen binding analysis of VWF proteolysis by ADAMTS13 in pseudo shear-vortex assay 154

Figure 6.5 Cleavage of wt-, S1486A-, Clus 2- and DC- D'A3 by ADAMTS13, analysed by western blotting 155

Figure 6.6 Binding of ADAMTS13 to elongated VWF 157

Figure 6.7 Binding between ADAMTS13 and globular VWF 159

Figure 6.8 Binding isotherms of soluble wtVWF and S1486A variant to ADAMTS13 160

Figure 6.9 Model of the A1 and A2 domain in solution with *O*-glycosylation sites indicated 164

Figure 6.10 Proposed crystal structures model of the A1 the A2 unfolded domains with the *O*-linked glycosylation sites indicted 166

Figure 6.11 Predicted model of the A1A2A3 domains complex 168

Figure 7.1 FPLC purification of GPIbα-*myc*/his using a Ni^{2+}-chelating HiTrap column 173

Figure 7.2 SDS-PAGE gel showing the expression and purification of rGPIbα 174

Figure 7.3 VWF multimeric size and ristocetin dependent GPIbα binding 175

Figure 7.4 GPIbα binding by VWF variants in the absence of ristocetin 176

Figure 7.5 Interaction between GPIbα and VWF glycosylation variants in the presence 1mg/ml ristocetin 177

Figure 7.6 Binding between VWF *O*-glycosylation variants (N-terminal side) and recombinant GPIbα in the presence of various ristocetin concentrations 178

Figure 7.7 Binding between VWF *O*-glycosylation variants (C-terminal side) and recombinant GPIbα in the presence of various ristocetin concentrations 179

Figure 7.8 Binding between *O*-linked glycosylation cluster variants and recombinant GPIbα in the presence of various ristocetin concentrations 181

Figure 7.9 Binding between T1679A and T2289A variants and recombinant GPIbα in the presence of various ristocetin concentrations.....182

Figure 7.10 Binding between VWF *O*-glycosylation variants and recombinant GPIbα in the presence of various ristocetin concentrations.....183

Figure 7.11 Comparison of ristocetin mediated GPIbα binding for wtVWF, VWF *O*-glycosylation variants and type 2B VWD variant.....183

Figure 7.12 GPIbα binding for wtVWF and desialylated wtVWF in the absence and presence of ristocetin.....184

Figure 7.13 Interaction between GPIbα and sialyated and desialyated plasma derived and recombinant VWF.....186

Figure 7.14 GPIbα binding by desialyted wtVWF, Clus 1 and Clus 2 variants in the presence of various ristocetin concentrations.....188

Figure 7.15 Binding between GPIbα and desialylated DC variant in the presence of a range of ristocetin concentrations.....189

Figure 7.16 Binding of wtVWF and double cluster variant to GPIbα in the presence of botrocetin.....190

Figure 7.17 Ristocetin co-factor activity assay of recombinant VWF variants.....192

Figure 7.18 The A1 domain diagram.....195

Figure 7.19 Predicted model of the A1-A2 domain complex based on the A1 domain crystal structure and predicted A2 domain structure with sites implicated in GPIbα and ristocetin binding.....196

Figure 7.20 The A1 domain crystal structure.....200

Figure 8.1 SDS-PAGE gel showing the expression and purification of wtD'A3-VWF.....202

Figure 8.2 Experimental setup for flow assays.....203

Figure 8.3 Flow slide-design and setup.....204

Figure 8.4 Preparation of plasma free blood – washing erythrocytes.....205

Figure 8.5 Optimal FL-VWF coating concentrations for the flow assay.....206

Figure 8.6 Optimal D'A3 coating concentration saturating the flow sides.....207

Figure 8.7 Determination of optimal collagen source for the flow assay.....209

Figure 8.8 A step by step diagram showing and explaining the individual stages used to count the number of platelets bound to D'A3-VWF.....212

Figure 8.9 Shear rate dependence of platelet adhesion to wtD'A3-VWF.....213

Figure 8.10 Platelet rolling velocities measurement using Image J.....214

Figure 8.11 Shear rate depended platelets rolling velocity on wtD'A3-VWF.....216

Figure 8.12 Comparison of platelets rolling velocities on various concentrations of immobilised FL-VWF and D'A3 at a shear stress of $1000s^{-1}$.....217

Figure 8.13 Kinetics of dissociation of transiently tethered platelets from wtD'A3 219

Figure 8.14 Shear rate dependence of transient platelet tethering on flow slides coated with wtD'A3 220

Figure 8.15 Platelets attachment to wtD'A3 and desialylated wtD'A3 under shear stress 221

Figure 8.16 Platelet rolling on wtD'A3 and desialylated wtD'A3.....222

Figure 8.17 Shear dependence of transient tethering between platelets and wtD'A3 and desialylated wtD'A3.....223

Figure 8.18 Comparison of platelets attachment to immobilised Clus1-, 1255- , DC-D'A3 variants and wtD'A3 under flow.....225

Figure 8.19 Platelets translocation velocities on the immobilised T1255A-D'A3 and Clus1-D'A3 *O*-linked glycosylation variant under flow.....226

Figure 8.20 The impact of the T1468A mutation on platelet attachment and translocation in flow.....227

Figure 8.21 Comparison of platelet attachment to immobilised full length Clus1-, 1255-DC-VWF variants and wtVWF.....228

Figure 8.22 Kinetics of dissociation of transiently tethered platelets on DC-D'A3 230

Figure 8.23 Platelet tethering to immobilised wtD'A3 and D'A3 glycosylation variants as a function of shear rate.....231

Figure 8.24Interaction of platelets with various concentrations of wtD'A3 and T1255A-D'A3.....233

Figure 8.25 Western Blot analysis of the wtD'A3 and mutated D'A3 fragments coated on a flow slide surface.....234

Figure 8.26 Platelet translocation pattern on immobilised wtD'A3 and T1255-, Cluster1- and DC-D'A3 glycosylation variants.....236

Figure 8.27 Platelet adhesion to collagen type III in the presence of wtVWF and VWF glycosylation variants.....238

Figure 8.28 Illustration of proposed pattern of platelet translocation and transient tethering on immobilised wtD'A3 and the T1255A, Clus1 and DC glycosylation variants under shear stress.....245

Figure 9.1 Platelet numbers and bleeding time after VWF gene transfer in VWF deficient mice.....265

LIST OF TABLES

Table 1.1 Average wall shear rates and wall shear stresses, in various vessels types 63

Table 3.1 Primary and secondary antibodies and their concentrations used for western blotting 93

Table 3.2 Native and permethylated masses of common monosaccharide constituents of glycans.....110

Table 8.1 Collagen sources tested.....208

Table 8.2 Disassociation rate constants for the tether bond between GPIbα- and wtD'A3 and desialyated wtD'A3.....224

Table 8.3 Disassociation rates values for the tether bond between GPIbα- and wild type and mutated D'A3.....230

ABBREVIATIONS

Å	Angstrom
Abs	Absorbance
ADAMTS13	A Disintegrin and Metalloprotease with Thrombospondin like motif
ADP	Adenosine diphosphate
AFM	Atomic force microscopy
As	Asialo
ASGPR	Asialoglycoprotein receptor
BCA	Bicinchoninic acid
B_{max}	Maximal binding
bp	Base pair
BSA	bovine serum albumin
CBA	Collagen binding assay
cDNA	Complementary deoxyribonucleic acid
CHO	Chinese hamster Ovary
CIAP	Calf intestinal alkaline phosphatase
CK	Cysteine knot
CMV	Cytomegalovirus
CU	Complement components C1r/C1s, Uegf and Bone morphogenic protein 1
CV	coefficient of variation
DDAVP	1-deamino-8-D-arginine vasopressin
ddH_2O	double distilled water
DMSO	Dymethyl sulfoxide
DNA	Deoxyribonucleic acid
dNTP	deoxynucleoside triphosphate
ds	desialylated
EBL	Elderberry bark lectin
EC	Endothelial cells

E.coli	Escherichia coli
EDTA	Ethylenediaminetetraacetic acid
ELISA	Enzyme-linked immunosorbent assay
Endo F	endo-β-N-acetylglucosaminidase F
ER	Endoplasmic reticulum
FBS	Fetal bovine serum
FL-VWF	Full length VWF
FPLC	Fast protein liquid chromatography
FVIII	Factor VIII
GP	Glycoprotein
HEK	Human embryonic kidney fibroblast
HMW	High molecular weight
HRP	Horseradish peroxidase
HUVEC	Human Umbilical Vein Endothelial Cells
kb	Kilobase
kd	Dissociation constant
kd(app)	Apparent dissociation constant
K_D	Equilibrium dissociation constant
kDa	Kilodaltons
LB	Luria-Bertani medium
LMW	Low molecular weight
mAU	Milli absorbance unit
MCS	Multiple cloning site
Mins	Minutes
MMW	Medium molecular weight
mRNA	Messanger ribonucleic acid
MW	Molecular weight
N-linked	Asparagine linked
OPD	O-phenylenediamine dihydrochloride

Pa	Pascal
pBS	pBlueScript
PBS	Phosphate buffered saline
PBST	Phosphate buffered saline and Tween 20
PCR	Polymerase chain reaction
PDI	Protein disulphide isomerise
Pd	Plasma derived
PEI	Polyethylenimine
PNA	Peanut agglutinin
PNGase F	Peptide: *N*-Glycosidase F
r	Recombinant
rpm	Revolutions per minute
RT-PCR	Reverse transcription-polymerase chain reaction
Sec	Seconds
SDS-PAGE	Sodium dodecyl sulphate polyacryilamide gel electrophoresis
SPR	Surface plasmon resonance
TBS	Tris buffered saline
TGN	Trans Golgi network
TSR	Thrombospondin repeat
UL-VWF	Ultra large Von Willebrand Factor
UV	Ultraviolet
V	Volts
v/v	volume per unit volume
VWD	Von Willebrand Disease
VWF	Von Willebrand Factor
VWF:Ag	Von Willebrand Factor antigen
VWF:CB	Von Willebrand Factor collagen binding
wtVWF	Wild type VWF
WPB	Weibel-Palade body

Common abbreviations not spelled in the text

˚C	Celsius degrees
g	gram
l	liter
m	meter
M	molar
Mol	mole
SD	standard deviation
U	units
V	volt
%	percentage

Power prefix abbreviations

m	milli
µ	micro
n	nano
p	pico

Sugar abbreviations and symbols

Fucose (Fuc) 

Glucose (Glc) 

Galactose (Gal) 

Mannose (Man) 

N-acetylglucosamine (GlcNac) 

N-actylgalactosamine (GalNAc) 

N-acetlyneuraminic acid (NeuAc) 

N-glycolylneuraminic acid (NeuGc) 

Ammino acid abbrveations

Alanine	Ala	A
Arginine	Arg	R
Asparagine	Asn	N
Aspartic acid	Asp	D
Cyteine	Cys	C
Glutamic acid	Glu	E
Glutamine	Gln	Q
Glycine	Gly	G
Histidine	His	H
Isoleucine	Ile	I
Leucine	Leu	L
Lysine	Lys	K
Methionine	Met	M
Phenylalanine	Phe	F
Proline	Pro	P
Serine	Ser	S
Threonine	Thr	T
Thryptophan	Trp	W

1 INTRODUCTION

1.1 Overview of haemostasis

Haemostasis is a regulated response to maintaining blood flow within the vascular system; preventing blood loss at sites of vessel injury but at the same time maintaining blood fluidity. Haemostasis is maintained by several complex interactions between vessel walls, platelets and plasma proteins. The first stage of the haemostatic system, called primary haemostasis, is initiated by exposure of blood to the subendothelium and results in the formation of a platelet-rich plug. Platelets adhere to the subendothelial matrix and temporarily limit blood loss. The platelet plug is stabilised through the coagulation cascade which results in the generation of thrombin, which converts fibrinogen into fibrin which stabilises the platelet plug into a stable haemostatic clot. At the same time the fibrinolytic system and healing mechanisms ares activated which ultimately remove they clot and repair the tissue.

1.2 Von Willebrand factor

Von Willebrand factor (VWF) is a multimeric plasma glycoprotein that plays a critical role in facilitating primary haemostasis. Firstly, VWF supports platelet adhesion and aggregation at sites of vascular injury.[1] Secondly VWF acts as the carrier protein for blood coagulation Factor VIII (FVIII) being crucial for its survival in the circulation by protecting it from proteolytic degradation.[2] VWF is synthesised and stored in endothelial cells and megakaryocytes and is released into the plasma as a series of multimers with a molecular weight ranging from 500 to 20000kDa, with the largest multimers being the most haemostatically active.

1.3 VWF gene structure and transcriptional regulation

The 178-kilo base pair (kb) gene encoding VWF is localised on the short arm of chromosome 12 (12p13.2). The 8.7 kb messenger RNA (mRNA) is spliced from 52 exons.[3] Exon 1 represents a 5' untranslated sequence exons 2-18 encode signal and propeptide sequences and exons 19-52 encode for the mature VWF subunit.[3,4] A non-processed VWF pseudogene is located on chromosome 22 (22q11) which is ~29kb in length, spanning exons 23-34 of the functional VWF gene and has 97% sequence homology.[5,6] The VWF pseudogene contains multiple stop codons, indicating that it is not a functional human gene.[5]

Regulation of VWF gene expression has been investigated using the promoter sequence linked to a reporter gene.[7] The promoter sequence encompassed base pairs (bp) -487 to +247 (numbered relative to the transcription start site) and was able to mediate endothelial specific expression of the reporter gene. Deletion analysis demonstrated that a 112bp fragment (-90 to +22), contained core promoter activity.[7,8] A core promoter sequence TATA box is present at a position +30 and a CCAAT box (transcription factor binding site) is located +8bp downstream of the TATA box. Deletion analysis also established a strong silencer sequence upstream of the core promoter at base pairs -487 to -312 that is activated by an *NF-1* protein that was shown by DNA footprint analysis to interact with nucleotides -440 to -470.[9]

The effect of the silencer sequence is counteracted by transcription factors of the GATA family, which bind to a positive regulatory sequence in exon 1, at bp +150 to +247. This positive regulatory element is able to overcome the effect of the silencer region and also endothelial cell (EC) specificity on the core promoter.[7] DNA sequence analysis of the positive regulatory sequence predicted a GATA binding site at +222 and an *SP1* binding site at +180. Mutation of the *SP1* site did not influence transcriptional activity, but mutation of the GATA site caused significant reduction of reporter gene expression, demonstrating the positive regulatory sequence with an intact GATA binding site is required to active VWF gene expression in EC.[7] Finally another negatively regulatory element has been located in the region -89 to +244, that is able to bind the *Oct-1* transcriptional repressor.[8]

1.3.1 VWF synthesis and processing

VWF is synthesised exclusively in endothelial cells and megakaryocytes,[10] with the majority of plasma VWF being derived from endothelial cells.[11] Following transcription pre-pro VWF is synthesised and is composed of a 21 amino-acid N-terminal signal peptide, a 741 amino acid pro-peptide and a 2050 amino acid mature protein. Numbering of VWF is taken from the first ATG start codon of the signal peptide. Pre-pro VWF undergoes complex co- and posttranslational modifications (Figure 1.1). The signal peptide directs pre-pro-VWF to the rough endoplasmic reticulum (RER) where the signal peptide is cleaved and 16 *N*-linked high mannose oligosaccharides are added to each pro-VWF monomer.[12] VWF dimers are formed by formation of disulphide bonds between C-terminal subunits of VWF monomers (Figure 1.2)[13,14] *N*-linked glycosylation is necessary for dimerisation to occur, since treatment of endothelial cells

with Tunicamycin, an antibiotic that prevents *N*-linked glycosylation results in the accumulation of pro-VWF monomers in the ER.[15-17] Monomeric VWF is retained in the ER by binding to ER regulatory proteins, such as BiP, and is subsequently degraded.[16,18] VWF dimers are transported to the Golgi apparatus where *N*-linked glycans are modified to produce complex type carbohydrates. Mannose residues are trimmed while *N*-acetylgalactosamine and galactose residues are added.[19] Further carbohydrate processing including the addition of terminal sialic acids and blood group antigens can take place in the trans-Golgi network (TGN) where the A, B and H blood group glycosyltransferases are present.[20] In addition, 10 *O*-linked glycan chains are added to pro-VWF in the Golgi.[12] In the trans-Golgi network (TNG) VWF undergoes sulphation, however inhibition of this process does not affect VWF multimerisation, storage or stability.[21] Finally, multimerisation of pro-VWF dimers occurs in the TGN (Figure 1.2). Multimer assembly involves intermolecular disulphide bond formation between cysteines in the N-terminal part of the pro-VWF.[14,22] The presence of calcium and the acidic pH (6.2) of the TGN [18] as well as the presence of the propeptide[16] are crucial for multimerisation. Treatment of human umbilical vein endothelial cells (HUVEC's) with chelating agents or ammonium chloride which increases pH within acidic organelles was demonstrated to inhibit VWF multimerisation.[16,23] Co-transfection of cells with sequences encoding the VWF propeptide and VWF with the propeptide sequence deleted, resulted in the secretion of fully multimerised VWF, demonstrating that the propeptide does not need to be a continuous part of the VWF structure. It is hypothesised that the propeptide has intermolecular protein disulphide isomerase (PDI)-like enzyme activity, acting as chaperone in a low-pH-dependent oxidoreductase reaction to promote disulphide bond formation.[24] The VWF propeptide is cleaved in the TGN by the enzyme furin which recognises a positively charged sequence downstream of the Arg763-Ser764 cleavage site.[25-27] Mutations in this region result in incomplete removal of the propeptide, and impaired factor FVIII binding.[28] The propeptide (previously also known as VWF AgII) remains non-covalently associated with mature VWF until they are both secreted into plasma.[29] In addition, the propeptide is also necessary for targeting VWF to storage granules and for their formation.[30-32]

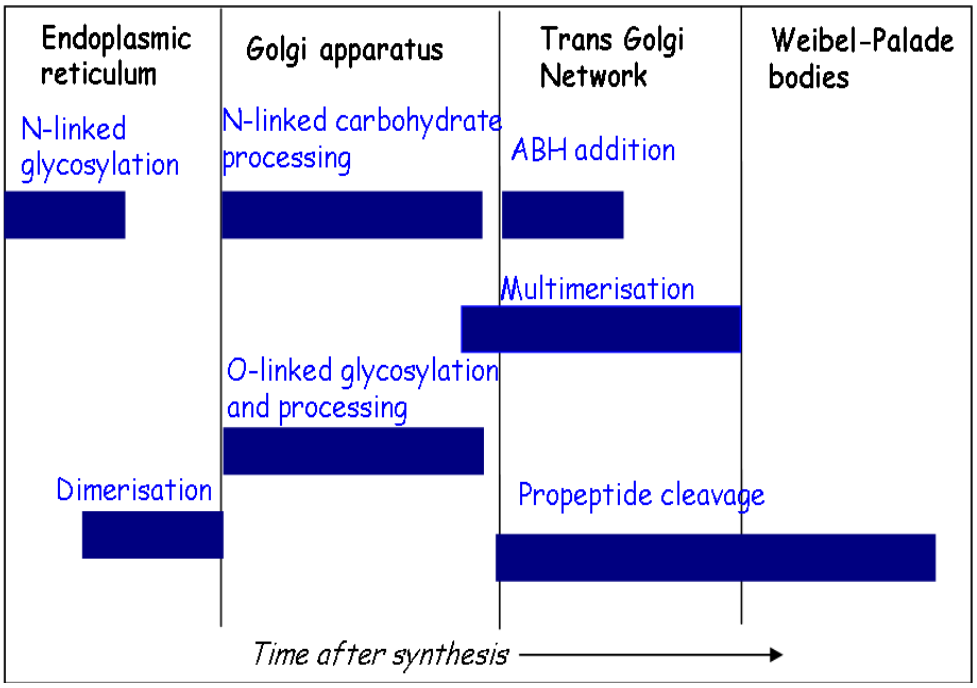


Figure 1.1. Posttranslational modifications of VWF

Following translation VWF undergoes extensive modifications in the endoplasmic reticulum and Golgi network prior to being stored or released. These include glycosylation, including the addition of ABO blood sugars, dimerisation and multimerisation, and finally proteolytic cleavage of the propeptide.

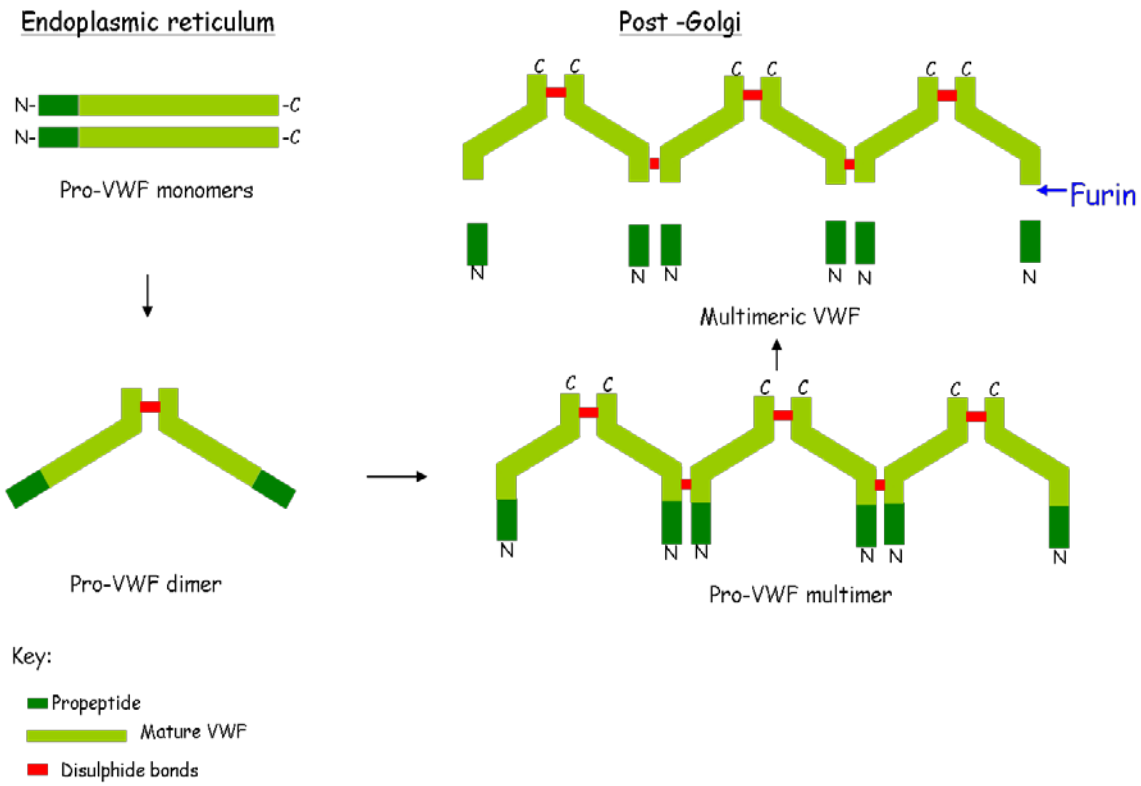


Figure 1.2.Dimerisation and multimerisation of VWF

Within the ER, VWF dimers are formed by formation of disulphide bonds between C-terminal subunits of VWF monomers. Multimerisation of VWF pro-VWF dimers occurs in the trans-Golgi network, and involves intermolecular disulphide bond formation between cysteines in the N-terminal part of the pro-VWF. Subsequently the VWF propeptide is cleaved by furin and remains non-covalently associated with mature VWF.

1.3.2 Tissue Distribution and sites of synthesis

As discussed, VWF biosynthesis is limited to endothelial cells and megakaryocytes. Analysis of VWF expression in mice using quantitative RT-PCR and *in-situ* hybridisation analysis, demonstrated endothelial cells derived from the spleen, aorta and lung had the highest levels of VWF mRNA, while liver, gut and kidney endothelial cells expressed relatively less VWF mRNA. In addition, higher levels of VWF mRNA were detected in endothelium of larger vessels compared to microvessels, and in venous compared to arterial endothelial cells.[33] Similarly VWF protein was predominantly located in the endothelium of larger vessels.[34] Immunohistochemistry performed on porcine blood vessels detected VWF in all venous endothelium, except the pulmonary vein. However, VWF was absent from the majority of arterial endothelial cells, except the distal abdominal aorta, the *vasa vasorum* of the thoracic aorta and the pulmonary artery.[35] The reason for a variable tissue distribution of VWF has not been explained

although it has been postulated that VWF can a play a role in controlling haemostasis in a vascular bed-specific manner.[36,37] A porcine model with hereditary VWF deficiency was utilized to show that, following total body irradiation, transplantation of normal bone marrow restores a normal platelet count, but does not reinstate the plasma VWF pool.[11] VWF circulates in plasma at a concentration of ~10μg/ml with a half-life of ~12 hours.[38]

1.4 VWF storage and secretion

The endothelial mature VWF can be either secreted constitutively or stored in Weibel-Palade bodies (WPBs),[39] whereas megakaryocyte VWF is stored in the α-granules of platelets and is released only upon platelet activation.[40,41] WPBs are large cigar-shaped, regulated secretory organelles that originate from the TGN.[42-45] They are unique to the vascular endothelium but their distribution varies between endothelial beds, with highest numbers present in the pulmonary artery.[33,46] WPBs are 100-200nm in diameter and 1-5μm in length, with a uniform pattern of longitudinal striations[37,45] which represent high molecular weight VWF filaments organised into helical tubules.[47,48] The tubular shape of the WPBs is required for the orderly secretion and haemostatic function of VWF.[49] In addition to VWF a number of other proteins have been shown to be stored in WPBs: Factor VIII, P-Selectin, Endothelin, CD36/lamp3, Interlukin-8, α1,3-Fucosyltransferase VI, tissue-type plasminogen activator, angiopoietin-2 and osteoprotegerin,[29,50-56] suggesting that secretion from these organelles can contribute to the regulation of haemostasis, inflammation and angiogenesis.

VWF is essential for WPB formation, since in its absence endothelial cells do not form WPBs.[57,58] What is more, the expression of VWF in cell lines that normally do not express VWF such as human embryonic kidney 293 cells (HEK293) can result in the generation of organelles that are identical to WPBs.[31,49] Likewise, endothelial cells isolated from a type 3 VWD dog that lack WPBs, were able to re-establish WPB formation when transfected with VWF.[58] The propeptide is essential for WPB formation [32] and WPB-like tubules can be assembled *in vitro* from VWF propeptide and dimeric N-terminal domains of VWF only.[47] Interestingly, the VWF propeptide is also able to target unrelated proteins to storage granules.[59] In addition to VWF, clathrin associated adaptor protein complex AP-1 is another factor crucial for the formation of WPBs.[60]

Endothelial exocytosis is one of the earliest reactions to vascular injury and plays an important role in thrombosis and inflammation. Regulated secretion from WPBs involves their translocation from the cytoplasm and fusion with the plasma membrane. The exocytosis of VWF generally requires an intra-endothelial rise in Ca^{2+} or cAMP and can be induced by number of secretagogues including thrombin, histamine, vascular endothelial growth factor (VEGF), vasopresin, epinephrine or serotonin.[61-66] For example, following vascular injury, thrombin induces a rapid, local response involving elevation of intracellular Ca^{2+} levels that results in WPB exocytosis,[67] whilst epinephrine induces cAMP-dependent release of VWF following physical activity and other acute stresses.[68,69] Additionally, factors such as shear stress or hypoxia have also been shown to trigger VWF secretion.[70,71] What is more, secretion from WBP can be induced artificially, for instance, the vasopressin analogue DDAVP (1-deamino-8-D-arginine vasopressin) is used in the clinical treatment of VWD and several other bleeding disorders to increase the pool of circulating VWF.[72] A variety of diverse agonists can trigger exocytosis, whilst the only factors described to inhibit WPBs exocytosis are nitric oxide (NO)[73,74] and hydrogen peroxide.[75] By limiting exocytosis those two factor can inhibit vascular inflammation and their roles might be important in haemostasis since excessive endothelial exocytosis has been linked to inflammatory and thrombotic disorders such as atherosclerosis and acute coronary syndromes.[74,76,77] Vascular inflammation and atherosclerosis were more severe in mice strains lacking endothelial NO synthase(eNOS),[78,79] and the inability to synthesise NO is a risk factor for the development of atherosclerosis.[80,81] Moreover, it has been shown that deficiency of eNOS and therefore lack of NO in mice results in endothelial VWF release and leads to development of thrombotic microangiopathy.[82]

Several pathways have been proposed to facilitate release of WPB contents under different pathophysiological conditions such as injury or inflammation. Initially it has been demonstrated that WPBs can employ two types of exocytosis; full-collapse and a slow form of 'kiss-and-run' ('lingering kiss'), with the second type allowing for the selective release of small molecules other than VWF.[83] However, in a recent study another type of exocytosis, multigranular exocytosis, has been identified and proposed as a key pathway of VWF secretion. In this study, a novel membrane surrounded structure ('secretory pod') was identified as the site of WPB's coalescence and VWF exocytosis. In addition, small cytoplasmic vesicles were shown to mediate the fusion of WPBs with these secretory pods prior to VWF secretion. The authors suggest this

homotypic fusion of secretory granules prior to regulated exocytosis may facilitate VWF string formation by pooling the content of multiple WPBs.[84]

To date it has been generally accepted that majority of newly synthesised VWF is spontaneously released from non-stimulated endothelial cells through a constitutive pathway and only 5-10% of VWF is stored in WPBs.[38,85-87] However a recent study has shown that blocking the constitutive secretion has only a minor effect on the spontaneous release of VWF, suggesting that majority of VWF was sorted into WPBs and subsequently secreted without the requirement for cell stimulation. This spontaneous release of VWF that has been firstly sorted into the regulated secretory pathway is called basal secretion.[88] It has been demonstrated that 80% of VWF spontaneously released from cultured human umbilical vein endothelial cells (HUVEC) was via the basal secretion pathway. This data suggests that VWF is sorted to the regulated secretory pathway in endothelial cells more efficiently than previously reported.[88]

1.5 VWF structure and function

Mature VWF is assembled from 250kDa subunits into haemostatically active multimers of variable size ranging from 500 to 20000kDa, with the larger multimers having the greatest haemostatic potential. Each pro-VWF monomer is comprised of four types of homologous repeating domains arranged in the sequence:

NH2-D1-D2-D'-D3-A1-A2-A3-D4-B1-B2-B3-C1-C2-CK-COOH

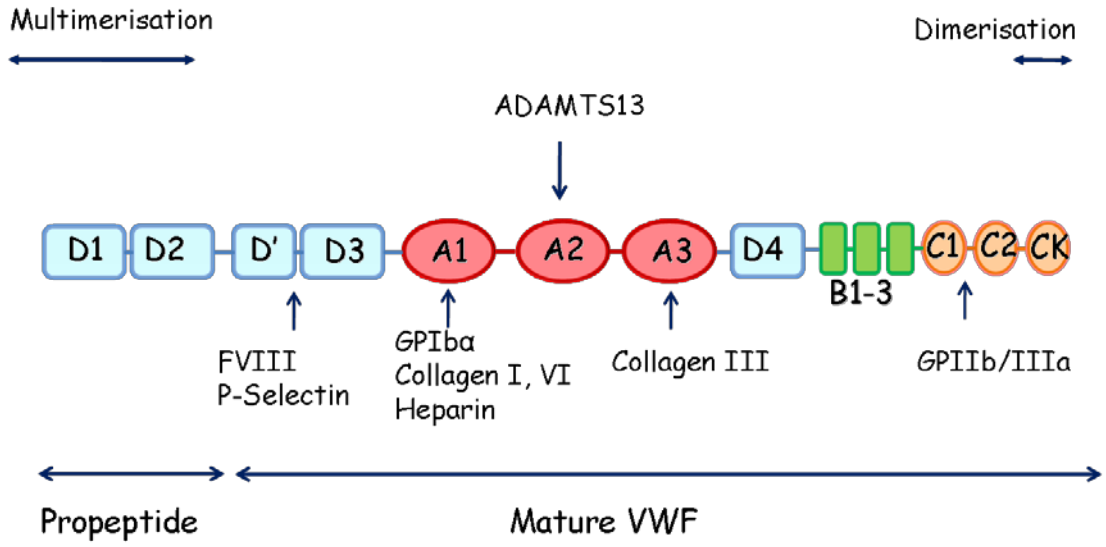


Figure 1.3. Domain structure of VWF

VWF is comprised of four homologous repeating domains: four D domains, a truncated D' domain, three A domains, three B domains, two C domains and a cysteine knot (CK) domain arranged as shown. Binding sites for platelet receptors, collagen, and other ligands as well as the ADAMTS13 cleavage site are indicated. VWF dimers are formed by intramolecular disulphide bonds at the C-terminus and multimers are form by intramolecular disulphide bonds at the N terminus.

1.5.1 VWF tertiary structure

Electron microscopy and atomic force microscopy techniques have been used to visualise the overall structure of VWF and two conformations of multimeric VWF were identified. Firstly in the absence of shear VWF appears as a loosely coiled mass of VWF multimers ('ball of yarn' or globular VWF conformation). However, when subjected to the critical shear stress of 35dyn/cm^2 VWF multimers undergo conformational change from a globular state to an extended conformation and appear as uncoiled filamentous structures- (elongated VWF).[89,90] As will be discussed later this structural transition is essential for exposure of various binding sites and VWF interactions with receptors, therefore for VWF physiological functions.[89] The unravelling effect of shear stress on VWF structure can be imitated *in vitro* by denaturants such as urea and guanidine-HCl or modulators such as the antibiotic ristocetin or the snake venom botrocetin; however it is unlikely that these fully reproduce the conditions *in vivo.*

Numerous studies using electron[90-92] and atomic force[89,93,94] microscopy demonstrate that VWF multimers are flexible strands of various sizes containing globular domains

joined by rod-like connecting structures. A multimeric strand encompasses several dimeric core units or protomers, which are linked by N-terminal disulphide bonds. The protomeric dimers represent two VWF monomers connected end-to-end via the C-terminal disulphide bond. Tapping mode atomic force microscopy was recently used to visualise and compare the structure of recombinant and plasma derived (r & pd) VWF.[94] The minimum multimer size of pd and rVWF was determined to be 53 and 25nm respectively, while the maximum size was 693nm for pdVWF and 910mm for rVWF. Approximately 70% of multimers analysed were in the range from 100 to 300nm. [94] The diameters of the globular core repeating subunits of pdVWF and rVWF multimers were shown to be around 18.6nm and 20.3nm respectively. The diameter of the globular core of VWF dimer, was shown to be in the same range (~22.3nm) as that of multimeric VWF. In addition, the elongated rVWF structure was analysed following exposure to shear stress. Completely extended molecules lengths were in the range of 2300 to 28000nm, and the diameter of the core was around 19.3nm. The length of elongated rVWF was similar to the length of extended pdVWF determined in another EM study.[90] Elongated pdVWF reaching 15µm was previously described, however this probably corresponded to the VWF aggregates rather than individual multimers, since the study used a low-resolution fluorescence microscopy.[95] Interestingly, hydrophobicity of the surface was shown to influence the structure of VWF. On hydrophobic surfaces, VWF displayed a compact tertiary structure, while on hydrophilic surface it appeared in an extended structure.[93]

1.5.2 The D domains

VWF has four D domains, each comprised of 360 amino acids, as well as the D' domain which is 97 amino acids long.[96] D domains have a significant sequence homology and all are rich in cysteine residues.[1,97] The position of the majority of the cysteine residues is conserved, suggesting that D domains have a similar tertiary structure.[96]

The propeptide D1 and D2 domains (residues R34-S746) are essential for the formation of multimers as well as for VWF direction to storage [18,30-32] and they are removed from the mature VWF as previously described. Furthermore, the highly cysteine-rich VWF propeptide has internal protein disulphide isomerase activity and functions as an intramolecular chaperone by positioning VWF into the correct orientation, thereby enabling proper intermolecular disulphide bond formation. [98] The integrity of the

propeptide is essential for its functional activity and deletion of either the D1 or D2 domain prevents VWF multimerisation[30]. In addition, several naturally occurring mutations in the VWF propeptide, impair its function and result in defective VWF multimerisation (T87S,[98] R273W,[99] N528S,[100] G550R,[101] C623W[102] and 625insG[102]).

The D' and D3 (residues P769-L1242) form the N-terminal portion of mature VWF subunit and contain binding sites for FVIII [103] and P-Selectin[55] and are crucial for multimer formation, as deletion of either the D' or D3 domain results in the production of un-multimerised VWF.[22] Moreover, VWF comprised of propeptide, D' and D3 domains only was able to form intermolecular disulphide bonds, showing that it is the only part of VWF involved in multimerisation and that this process is independent of dimerisation.[22]

What is more, as supported by a number of studies, the VWF D3 domain contains the cysteine residues essential for multimer formation.[22] For example, when plasma VWF was digested with V8-protease and trypsin a dimeric fragment spanning residues 1036-1491 was generated, while with the flanking regions were monomeric. This illustrated that all the intersubunit disulphide bonds must occur within these residues.[104] Moreover, cysteine residues C1142, C1130, C1149, C1157 and C1234 have been shown to be requisite for VWF multimerisation to occur.[105-107] In addition, Purvis *et al.*, demonstrated that two cysteines at position 1099 and 1143, are essential for the oxidoreductase mechanism of VWF multimerisation and may form intersubunit disulphide bonds.[108] Conversely, the D' domain does not contain cysteine residues involved in an intersubunit disulphide bonding, but its correct folding and integrity are essential for multimerisation, suggesting it may act as a molecular chaperone in VWF multimerisation.[109,110]

1.5.2.1 Factor VIII binding

As mentioned previously, VWF acts as the carrier protein for FVIII, which circulates in blood at a concentration of 0.3-0.7nM, non-covalently associated with VWF.[2,111] FVIII binds VWF with a K_D of 0.2 -0.3 nM,[112] independently of VWF multimeric size,[113] although the affinity decreases following VWF binding to collagen (K_D=5nM).[114] FVIII is the critical factor in the coagulation cascade, as its deficiency leads to impaired generation of activated factor X and results in the severe bleeding disorder haemophilia A.[111] The survival and the consequent plasma concentration of FVIII are significantly

reduced in the absence of VWF,[115] since VWF stabilizes the FVIII heterodimeric structure,[116] protects it from proteolytic degradation by phospholipid-binding proteins such as activated protein C,[117] inhibits FVIII binding to activated factor IXa[118] and stops FVIII cellular uptake.[119] As will be discussed later it has been demonstrated that FVIII can accelerate cleavage of VWF by ADAMTS13 under conditions of shear stress.[120]

1.5.2.2 P-selectin binding

P-selectin is a membrane protein expressed on the surface of activated endothelial cells and platelets, stored together with VWF in WPBs.[50,121] It has been demonstrated that P-selectin interaction with D'D3 domains of VWF facilitates its recruitment to WPBs.[55] A study by Paddila *et al.*, revealed that P-selectin expressed on the apical membrane of endothelial cells mediates adhesion of ULWF multimers to the vascular endothelium.[122] which then bind circulating platelets and could support leukocyte tethering and rolling.[123]

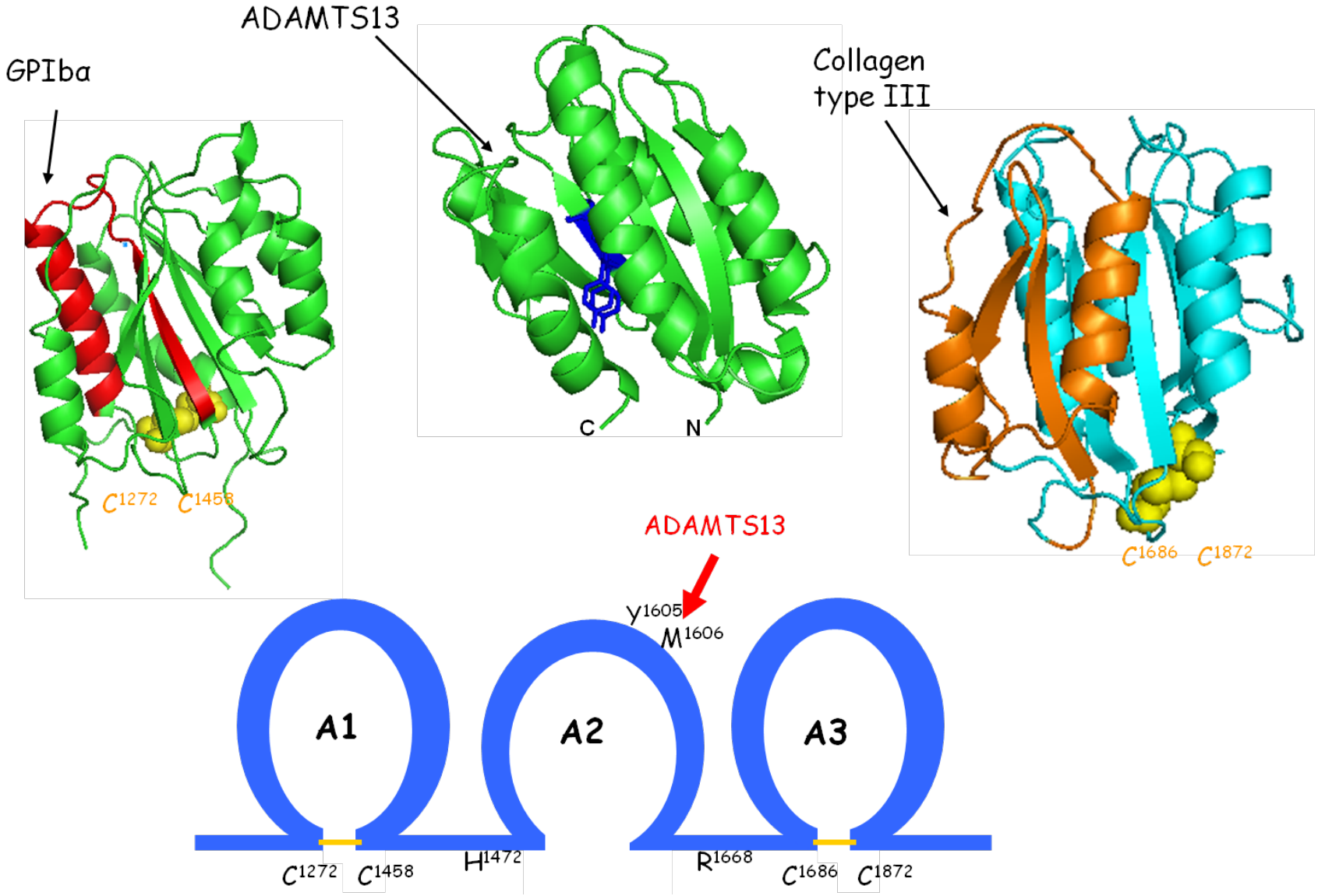
1.5.3 The A domains

VWF contains three A domains that share ~ 30% homology and span residues 1260-1874, (A1 domain 1260-1453, A2 domain 1498-1668, A3 domain 1691-1874).[124]. The crystal structures of all three VWF A domains have been determined.[125-127] Both the A1 and A3 domains contain an intramolecular disulphide bond that forms loops of approximately 187 residues, the A2 domain lacks this disulphide bond, thus its structure is more flexible, which has hindered its crystallisation (Figure 1.4). Nevertheless interesting evolutionary adaptations of the A2 domain have been deduced from its crystal structure, suggesting it acts as a force-sensing domain.[127] In addition the intrinsic thermodynamic stability of the VWF A domains against unfolding was studied in the presence of urea and the A2 domain was shown to be the least stable and most the most susceptible to unfolding.[128]

Next page:

Figure 1.4 The A domains structure

In contrast to the A2 domain, both the A1 and A3 domain contain an intramolecular disulphide bond between cysteine residues (indicated in yellow), resulting in the formation of a loop composed of 187 amino acids. The crystal structures of the three A domains have been resolved as shown. Binding sites for GPIbα located in the A1 domain (in red), collagen type III localised in the A3 domain (in brown), and the ADAMTS13 cleavage site (Y1605- M1606) present in the A2 are shown.


GPIba
ADAMTS13
Collagen
type III
C1272
C1458
C
N
C1686
C1872
ADAMTS13
Y1605
M1606
A1
A2
A3
C1272
C1458
H1472
R1668
C1686
C1872

The A1 domain contains the binding sites for Glycoprotein (GP) Ibα, heparin, cell surface sulfatides, and collagens type VI,[129-131] type I[132] and putatively type III.[133] Its homologous A3 domain has been shown to bind only to collagens type I and III.[134] The A2 domain contains the single ADAMTS13 (A Disintegrin And Metalloproteinase with ThromboSpondin type-1 repeats 13), cleavage site and the linker region between A1 and A2 is involved in leukocyte binding.[135]

The A1 domain contains, as will be discussed further, the only known VWF binding site for platelet glycoprotein receptor GPIbα.[136,137] Interaction of VWF with platelets is controlled by various mechanisms which are necessary to avoid premature formation of platelet aggregates which could occlude the vasculature. In normal conditions in the circulation there is no interaction between platelets and VWF, partially due to the fact that the platelet binding site within A1 domain is shielded by the adjacent D'-D3 domains.[138] Shear stress and immobilization of VWF both induce conformational changes in VWF and lead to exposure of functional sites which enables VWF to bind circulating platelets via the GPIb/IV/X complex.[14,89,129] To mimic this interaction *in vitro* VWF needs to be treated with modulators such as ristocetin or botrocetin.

The A1 domain mediates heparin binding,[129,139-141] with residues K1362 and R1395 and clusters K1332-R1336 and K1405-K1408 being essential for this interaction.[142] A second minor heparin binding site has been found within the N-terminal residues (M1-E272) of VWF.[92] It has been established that heparin binding is largely independent of the multimeric composition of VWF.[143] Presence of a heparin binding site may indicate that VWF can interact with matrix proteoglycans that contain sulphated carbohydrates. Indeed, VWF was reported to bind decorin, a proteoglycan that plays role in the vessel wall matrix assembly.[144]

VWF can bind to sulfated glycosphingolipids (sulfatides) that are present on cellular membranes and may support VWF localisation on injured tissues.[145,146] The sulfatide binding site has been localised to the A1 domain, and was shown to be different from the GPIbα binding site.[147,148] Conversely sulfatides have been shown to block ristocetin dependent platelet aggregation and platelet adhesion under flow conditions.[149]

1.5.4 The D4 and B domains

Limited research has been performed to elucidate the role of the D4 and B domains. Expression of recombinant VWF with the D4 domain deleted did not alter VWF multimeric structure or binding to type III collagen.[150] Interestingly, the VWF region spanning residues G1874 to K2813 which includes the D4 domain was shown to contain a low affinity (K_D=86nM) ADAMTS13 binding site.[151,152] However, this binding site was exposed only when VWF was in globular conformation with the A2 domain buried.[151]

1.5.5 The C domains and the cysteine knot

The C1, C2, and cysteine knot domains comprise the C-terminal part of the VWF monomer. The C1 and C2 domains span residues C2255-L2645 and have sequence homology to cysteine rich domains found in thrombospondin and alpha-procollagen types I and III.[153] The C1 domain contains the RGDS (Arginine-Glycine-Asparagine-Serine) sequence which is essential for binding to the platelet GPIIb/IIIa receptor (integrin $\alpha_{2b}\beta_3$) and also to the HUVEC vitronectin receptor ($\alpha_v\beta_3$).[154] In addition, a peptide antagonist that binds to the VWF C-terminal domains, specifically inhibiting VWF binding to collagen, and consequently suppressing platelet adhesion and aggregation, has been identified using a phage display method.[155]

The cysteine knot (CK) domain spans the final C-terminal residues of VWF (2724-2813) and contains the cysteine residues involved in the formation of VWF dimers.[13,14,156] Given that recombinant VWF with the mutations C2771A and C2773R cannot dimerise, these residues are thought to be significant for the dimerisation process. What is more, mutations of these residues have been found in some patients with type 2A VWD who cannot assemble large multimers.[157]

1.6 Collagen binding

The first step in haemostasis is the interaction of platelets with the exposed extracellular matrix at the sites of vascular injury. Collagen is the main component of the subendothelial matrix[158] as it accounts for up to 40% of the vessel wall protein contents, and provides a scaffold for attachment of other matrix proteins and endothelial cells. Several types of collagen have been identified in the human vasculature: types I, III-VI, VIII and XII-XIV; with fibrillar collagens type I and III being the major components of

blood vessels, and type IV localised in the basement membrane.[159,160] Furthermore, collagen type III is present in the subendothelium and is exposed following limited injury to the vessel wall, while collagen type I is localised deeper in the vessel wall and becomes exposed only as a result of an extensive injury. It is well documented that platelet recruitment to the site of vascular injury under high shear (>600s^{-1}) requires VWF, that binds to exposed collagen and mediates platelet adhesion and activation.[159] VWF binds preferentially to collagen type III and displayed lower affinity for collagens type I, II, IV and V under static conditions.[161] The VWF A1 and A3 domains have been shown to mediate collagen binding, and their respective roles may differ depending on the type of collagen engaged, and the shear stress of blood flow.[131,133] The VWF-A1 domain was shown to interact with collagen types I and III[162] and contain a major binding site for collagen type VI ,[130,131] whilst the A3 domain encompasses the principal collagen type III binding site[134] and can also mediate interaction with collagen type I.[162] Furthermore, the VWF A3 domain was shown to be vital and sufficient for VWF binding to fibrillar collagens *in vitro* since VWF protein lacking the A3 domain showed minimal residual collagen binding, with a normal multimeric pattern.[134,163,164] Additionally, mutagenic studies of the VWF A3 domain demonstrated that residues N1742, S1783 and H1786 are essential for collagen binding; also residues I1738, T1740, V1760, E1764, R1726 and R1779 are important for collagen binding, as their alteration decreases collagen binding at least 10 fold.[165,166] Together these residues define a flat hydrophobic collagen binding site at the front face of the A3 domain.[166-168] Moreover, the analysis of the VWF A3 domain crystal structure suggests that its negatively charged residues interact with positively charged residues on collagen.[126]

Of note, VWF multimeric size directly correlates with its affinity to collagen, with the higher molecular weight VWF multimer exhibiting greater collagen binding affinity, with K_D values of 1-7nM on a subunit basis[*],[150,169] while the recombinant A3 domain alone exhibits a weak binding with much higher K_D of 2μM.[168] Based on the crystal studies of the A3 domain its interaction with collagen is achieved due to interaction of negatively charged residues on the A3 domain and positively charge residues on collagen. The size of the isolated A3 domain limits the number of residues of collagen that can interact with the putative collagen interaction surface and the absence of

[*] To determine the K_D for the interaction of VWF with collagen, the monomeric weight of VWF was taken as 270kDa

pronounced binding grove, which precludes a large van der Waals surface and interaction between the A3 domain and collagen and is consistent with low affinity for a single A3 domain.[126]

It has been demonstrated that the VWF A1 domain can play an important role in VWF binding to the injured vascular wall, by interacting with collagen type VI.[170] In addition, a study has shown that under shear stress the A1 domain can substitute for the A3 domain in platelet recruitment to collagen fibres.[133] Moreover, Morales *et al*., in their studies suggest that binding to collagen via the A3 domain causes a conformational change that exposes a cryptic collagen binding site in the A1 domain that increases the affinity of VWF for collagen.[132] In summary, the synergistic action of A1 and A3 domains can be crucial to support VWF binding to exposed subendothelial matrix containing various collagen types and their roles might vary depending on the shear conditions.

1.7 ADAMTS13

The VWF A2 domain contains the cleavage site for the VWF cleaving metalloprotease, ADAMTS13 (A Disintegrin And Metalloproteinase with ThromboSpondin type-1 repeats),[171] a Zn^{2+} and Ca^{2+}dependent enzyme and a member of the "the disintegrin and metalloprotease with thrombospondin repeats" family.[172,173] It is a large multidomain glycoprotein, and starting at the N-terminus it is composed of a metalloprotease domain, a disintegrin-like domain, a thrombospondin-1-repeat (TSR), a cystein-rich and a spacer domains, seven tandem TSRs and two CUB domains [complement components C1r/C1s, Uegf (epidermal growth factor-related sea urchin protein) and bone morphogenetic protein-1] that are unique for ADAMTS13 (Figure 1.5). ADAMTS13 is primarily synthesized in hepatic stellate cells, but also by endothelial cells, and megakaryocytes or platelets [174-177] and its plasma concentration in healthy individuals is ~1μg/ml (5nM)[178-180] and the estimated half life is 2-3 days.[181]

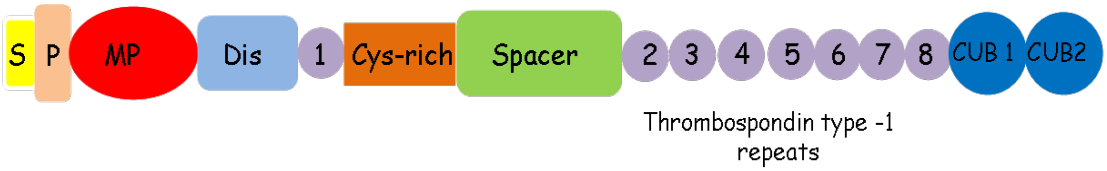


Figure 1.5 ADAMTS13 domain structure

Schematic diagram showing the ADAMTS13 domain structure. ADAMTS13 has a signal peptide (S), which is removed upon entry into ER and a propeptide (P). Mature ADAMTS13 consists of an N-terminal metalloprotease domain (MP), followed by a disintegrin-like domain (Dis), a thrombospondin-1-repeat (TSR), a cystein-rich (Cys-rich) and a spacer domains (spacer), seven tandem TSRs and two CUB domains.

1.7.1 ADAMTS13 role in the haemostasis

ADAMTS13 regulates VWF multimeric size and hence its activity by proteolytic cleavage of the Y1605- M1606 bond located in the VWF A2 domain.[171,182] Although ADAMTS13 is constitutively active,[183] VWF can be proteolysed only once it undergoes substantial changes in its secondary structure that expose the cryptic cleavage site.[182] A fundamental function of ADAMTS13 is cleavage of hyperactive ultra large (UL)VWF multimers anchored at the cell surface following endothelial secretion. This proteolysis results in the formation of smaller multimers that have lost the ability to spontaneously bind platelets and therefore are no longer prothrombotic but still haemostatically active.[184,185] The proteolysis of UL-VWF takes place very rapidly and requires low,[184-186] or almost no shear stress[187,188] and once released cleaved VWF fragments become inaccessible for ADAMTS13.

In addition to controlling the size of newly secreted UL-VWF, ADAMTS13 can also regulate the size of VWF at the sites of haemostatic plug formation. During platelet plug formation VWF binds to the exposed collagen and subsequently unravels due to the shear stress exerted by flowing blood. This conformational change of VWF is not only essential for platelet capture but also exposes ADAMTS13 cleavage site. However, other process involved in primary and secondary haemostasis such as fibrin and platelet GPIIbIIIa interaction with fibrinogen, platelet-platelet binding, and fibrin deposition also stabilise plug formation and therefore the effect of VWF proteolysis is limited. ADAMTS13 can act only at the edges of the developing plug, limiting its growth. This mechanism has been confirmed i*n vivo* as increased platelet binding to the subendothelium and accelerated thrombus formation were observed following arterial

injury in ADAMTS13 deficient mice strain or when ADAMTS13 activity was blocked by antibody in wild type animals. This effect was observed to decrease when recombinant ADAMTS13 was infused into knockout animals.[189]

ADAMTS13 cleaves UL-VWF preferentially due to their greater susceptibility to deformation which results in exposure of multiple binding sites within the A domain when endothelial bound. Furthermore, UL-VWF multimers are able to bind platelets more tightly than smaller multimers and since VWF-platelet complexes are the preferred substrates of ADAMTS13 under fluid shear-stress, ULVWF multimers are more prone to proteolysis.[190]

Another rationale for increased ADAMTS13 proteolysis of endothelial cell-anchored UL-VWF emerged when ADAMTS13 was shown to bind to the endothelial cell plasma membrane.[191] Studies established that ADAMTS13 pre-bound to HUVECS exhibited increased proteolysis of VWF when compared to ADAMTS13 present in solution. ADAMTS13 binding to endothelial cells was specific, reversible, concentration and time dependent, with K_D of 58nM. In addition, the interaction required presence of the C-terminal TSP1 repeats of the protein, and was inhibited by heparin and trypsin.[191]

1.7.2 ADAMTS13 associated disorders

UL-VWF multimers are biologically hyper-active because compared to small multimers they have higher affinity towards the extracellular matrix [192] and platelet GPIbα. [193] As pointed out their size needs to be controlled in order to prevent formation of platelet rich thrombi in the microcirculation (pathogenic thrombosis). Absence or severe reduction in ADAMTS13 is associated with systemic thrombosis, mainly thrombotic thrombocytopenic purpura (TTP). TTP is clinically characterised by microvascular thrombosis, haemolytic anemia, thrombocytopenia, neurological abnormalities, fever, and renal dysfunction.[194,195] Mutations in ADAMTS13 gene cause a congenital form of TTP,[196] while an acquired form results from the development of autoantibodies against ADAMTS13.[197]

On the other hand, mutations in VWF that prematurely destabilise it can increase its susceptibility to ADAMTS13 cleavage. The significant decrease in VWF multimeric size and thereby haemostatic potential at the sites of injury is associated with a congenital bleeding disorder VWD type 2A.[198,199] Moreover, patients with aortic

stenosis which generates high shear in circulation have increased VWF proteolysis and reduced multimer size as compared with healthy individuals.[200,201]

ADAMTS13 activity has been shown to be crucial *in vivo* to protect the brain from ischemia-reperfusion injury by ameliorating post-ischemic hypoperfusion.[202] The possible neuroprotective effect of ADAMTS13 is possibly due to proteolysis of VWF on the surface of thrombi formed on the ischemic endothelial cells since VWF was shown to play a role in the development of ischemic brain injury, however the specific mechanism of its action remains unclear.[184,202-204] Moreover, it has been demonstrated that VWF deficient mice were protected from ischemic brain injury,[205] while mice deficient in ADAMTS13 displayed larger stroke infarction,[206-208] when compared to wild type animals. It has been subsequently demonstrated that interaction of VWF with collagen and GPIbα are critical steps in stroke development in mice, while interaction of VWF with GPIIb/IIIa is not essential.[209]

Interestingly it has been suggested that ADAMTS13 activity can not only down-regulate thrombosis but also inflammation. Firstly, VWF levels were shown to be increased while ADAMTS13 level were reduced in both acute and chronic inflammation.[210] In addition, it has been demonstrated that by cleaving endothelial UL-VWF, ADAMTS13 prevents excessive leukocyte rolling in unstimulated veins and leukocyte adhesion and extravasation under inflammatory conditions.[211-213]

Platelets play a crucial role in thrombus formation in normal haemostasis by adhering to exposed endothelium at sites of vascular insult and participating in thrombus formation, however, this physiological defence mechanism can also lead to thrombotic diseases such as heart attack and stroke. Rupture of an atherosclerotic plaque exposing underlying fibrous matrix can lead to thrombus formation mediated by GPIb-IX-V/VWF and/or GPVI/collagen interactions. On the other hand pathological shear stress in an atherosclerotic coronary or cerebral artery can induce platelet-VWF interaction leading to thrombus formation, which obstructs the blood flow and consequently leads to heart attack or a stroke.[214,215] Many studies have been performed to elucidate whether high plasma concentration of VWF are associated with an increased risk of thrombosis, and some evidence was provided that high VWF levels are associated with a moderately increased risk of arterial thrombosis. Studies in pigs with VWD and in VWF deficient mice have revealed a reduced tendency to develop artherosclerosis.[216] On the other hand

no difference in the size of atherosclerotic plaque has been shown between VWD type 3 patients and healthy individuals, suggesting that VWF does not play a role in the atherosclerotic process but only in the occlusive arterial thrombosis.[217,218]

1.7.3 ADAMTS13 role in proteolysis of VWF

The specificity of ADAMTS13 for proteolysis of VWF is facilitated by multiple cooperative contacts that bind ADAMTS13 to VWF.[151,219,220] ADAMTS13 binds to unfolded VWF with high affinity and the apparent K_D was calculated to be ~14nM.[174,183] The N-terminal ADAMTS13 domains are required and sufficient for recognition of and proteolysis of denatured multimeric VWF, since ADAMTS13 truncated after the spacer domain still efficiently proteolysed VWF whereas ADAMTS13 truncated before the spacer domain did not.[221,222] It has been demonstrated that the spacer domain of ADAMTS13 (in particular residues R568, R660, Y661 and Y665) binds the exosite E1660-R1668 at the C-terminal side of the A2 domain which helps approximate the two proteins.[223-226] Subsequent interaction between the ADAMTS13 disintegrin-like domain with amino-acids close to the VWF A2 cleavage site was shown to be crucial for the proteolysis to occur.[227] Furthermore the ADAMTS13 disintegrin-like domain was shown to assist in proteolysis via an interaction between ADAMTS13 R349 residue and the D1614 residue in VWF helping to position the scissile bond within the active site of ADAMTS13.[227] Once ADAMTS13 is bound to the elongated VWF, its metalloprotease domain can catalyse hydrolysis of the Y1605-M1606 within A2 domain. The metalloprotease domain contains a conserved active site sequence motif HEXXHXXGXXH and adjacent Met-turn that provide Zn^{2+} binding pocket. The bound zinc ion and the active site residue GE225 coordinate a water molecule that impels the hydrolysis of the scissile bond.[228] In addition, a high affinity Ca^{2+} binding site, near the active site is vital for efficient VWF proteolysis.[229]

In vivo ADAMTS13 proteolysis of VWF is initiated by high shear stress that induces unfolding of the cryptic ADAMTS13 cleavage site.[230] To observe ADAMTS13 proteolysis *in vitro* VWF has to be unfolded by mild denaturation with urea[171] or guanidine hydrochloride[182,231] followed by barium or calcium activation of ADAMTS13.[173,182] Cleavage of VWF *in vitro* using denaturants may require long incubation times,[171] whereas cleavage of VWF under flow conditions occurs in minutes.[184] To investigate the interaction of ADAMTS13 with VWF, short recombinant

substrates can be used to avoid the need for denaturants or shear stress. The shortest substrate that can be cleaved by ADAMTS13 is a 73 amino acid fragment (VWF73) spanning residues 1596-1668 of the A2 domain.[173] Other studies have used a VWF115 substrate, spanning residues 1554-1668 of the A2 domain.[232]

It has been suggested that ADAMTS13 distal domains modulate its activity, however, their role has not yet been fully elucidated. Under conditions of high shear stress, Feys *et al.*, did not observe any difference in VWF cleavage or binding for ADAMTS13 recombinant variants truncated after the TSR-8 (delCUB) or the spacer domain (MDTCS), while Zhang *et al*. reported that delCUB and MDTCS had minimal activity against VWF, and that removal of CUB domains reduces VWF binding 5 to 7 fold. [152,174] In addition, the MDTCS variant was able to cleave UL-VWF released form endothelial cells in a parallel flow chamber based assay[226] and had unaltered activity when assayed in the presence of urea or guanidine.[221,222] Interestingly, transgenic mice that expressed ADAMTS13 truncated after the TSR6 domain were reported to have increased thrombogenicity compared to wild type animals, while the plasma VWF multimeric pattern was normal.[233] This could suggest that distal domains of ADAMTS13 are important for VWF cleavage under high shear. Alternatively, altered thrombus formation could be due to removal of ADAMTS13 domains interacting with globular WVF, therefore limiting the amount of ADAMTS13 immediately available at the site of thrombus formation.

1.7.4 Factors modulating ADAMTS13 proteolysis

At the site of vascular injury, VWF can adhere to exposed collagen and this immobilisation under high shear flow allows VWF to unravel, bind platelets, and undergo ADAMTS13 proteolysis. Consequently as described previously, both hydrodynamic forces and immobilisation change the conformation of VWF and the way it interacts with ADAMTS13. Interestingly cleavage is activated by shear when A2 is present in large VWF multimers, but not when present as a much smaller isolated domain, probably because the tensile forces acting on the protein under shear flow increase with protein size.[171,182,200,234] In addition, domains adjacent to A2 as well as VWF ligands can exert a differential effect on ADAMTS13 cleavage. For example, it has been demonstrated that binding of platelet GPIbα to the A1 domain stimulates the cleavage of the A2 domain by ADAMTS13. Recombinant VWF A2A3 was cleaved ~10

fold faster than recombinant A1A2A3, indicating that the A1 domain inhibits cleavage, however this inhibition can be relieved by binding of the A1 domain to GPIbα or heparin.[235] As mentioned earlier, FVIII binding to VWF can also accelerate ADAMTS13 cleavage of VWF under conditions of shear stress.[120] Further analysis demonstrated that binding of both platelets and FVIII to VWF synergistically enhances its proteolysis by ADAMTS13 under mechanically induced shear stress.[236] Furthermore glycosylation status of both VWF (discussed in section 1.14) and ADAMTS13 was suggested to modulate their interaction. ADAMTS13 undergoes both *O*-and *N*-linked glycosylation. Preventing *O*-fucosylation in the TSP-1 repeats resulted in reduced secretion from HEK293T[237] cells while the *N*-linked glycans were shown to modulate both ADAMTS13 secretion and proteolytic activity.[238]

1.7.5 Mechanism of ADAMTS13 multistep binding to VWF

Recently it has been reported that apart from binding to elongated VWF, ADAMTS13 is able to bind with different affinity to VWF in its native conformation. ADAMTS13 was shown to bind to globular VWF with an apparent K_D of 79nM when the interaction was studied using immunoprecipitation experiments[152] and with a K_D of 90nM when binding to VWF captured via a monoclonal antibody was analysed by an ELISA based plate assay.[239] Additionally, a similar K_D of 86nM was calculated for interaction of immobilised ADAMTS13 and globular VWF in solution.[151] Distal ADAMTS13 domains are required for its binding to globular VWF; however their exact role is not yet clear. Zanardelli *at al.* suggested the involvement of TSP5- CUB domains, and Feys *et al.*[152] reported that deletion of CUB domains did not alter native VWF binding and suggested that TSR2-8 are important for the interaction. Nevertheless, the distal ADAMTS13 domains interact with the C-terminal region of VWF, as suggested both by surface plasmon resonance (SPR) experiments and plate binding assays using a series of VWF deletion mutants.[151] Significantly, ADAMTS13 binding to globular VWF does not lead to VWF proteolysis in the absence of shear stress therefore binding of ADAMTS13 to VWF in globular conformation is suggested to be an early step of a multistep interaction that ultimately leads to VWF proteolysis (Figure 1.6). In addition, it has been suggested that globular VWF and ADAMTS13 in plasma may be able to form complexes, as ADAMTS13 and presumably native VWF were co-purified from a commercial factor VIII/VWF concentrate by size exclusion chromatography, [240] while Feys *et al*. were able to detect ADAMTS13 binding to plasma VWF[152].

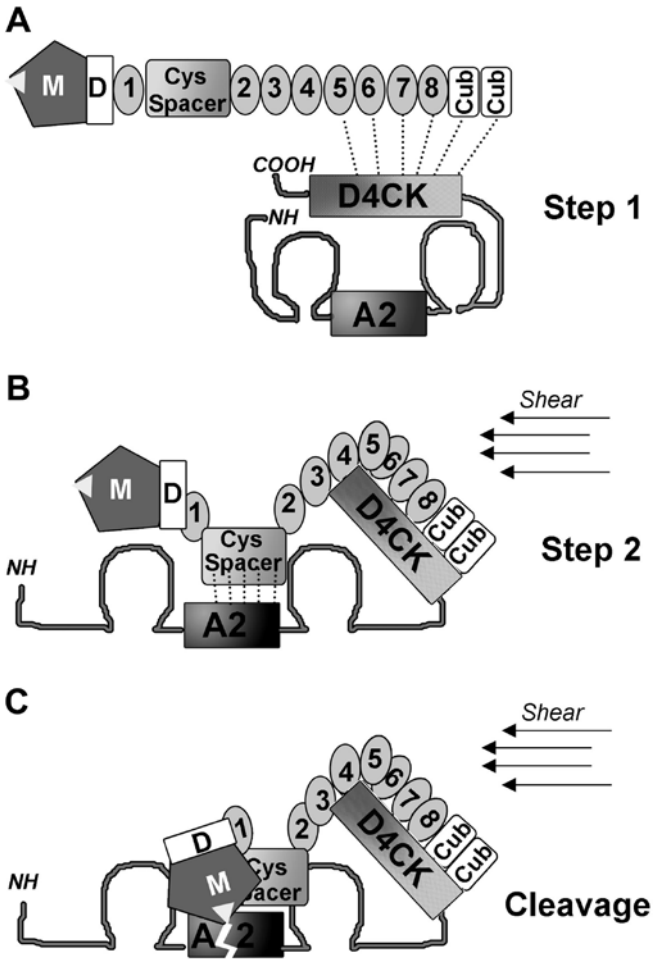


Figure 1.6 Putative two step binding interaction between ADAMTS13 and VWF

Illustration of the proposed initial binding interaction mechanism between ADAMTS13 and VWF that eventually leads to VWF proteolysis. **A)** Diagram of ADAMTS13 domain structure and VWF in globular conformation. The ADAMTS13 cleavage site within the VWF A2 domain is buried. C-terminal domains of VWF can interact with distal ADAMTS13 domains. It is not clear yet exactly which domains participate in the binding. However this step is not necessary for VWF proteolysis to occur **B)** Under conditions of shear stress, VWF unravels and its A2 domain interacts with high affinity with ADAMTS13 spacer domain and **C)** metalloprotease domain can access and cleave the Y1605-M1696 bond in the VWF A2 domain. Figure reproduced from Zanardelli *et al.*, 2009.[151]

1.8 Thrombospondin I cleavage

VWF multimeric size can also be regulated, however to a significantly lesser extent, by a protein disulphide bond reductase, identified as thrombospondin-1 (TSP-1).[241] VWF and TSP-1 incubated together can form thiol dependent complexes, which results in the generation of free thiols in VWF, and a decrease in VWF multimeric size. Furthermore an inverse relationship was observed between the plasma molar ratio of VWF/TSP-1

and VWF multimeric size. Additionally, administration of TSP-1 to mice resulted in a decrease in VWF multimeric size. [241] However, it has also been demonstrated that the average multimer size of plasma VWF in TSP-1 null mice was significantly smaller than in wild type mice.[242] Interaction between VWF and TSP-1 was shown to be mediated by the VWF A3 domain.[241,242] Since ADAMTS13 was also shown to interact with the A3 domain[185] it has been suggested that TSP-1 and ADAMTS13 may compete for binding to the A3 domain, which would limit degree of ADAMTS13 proteolysis. TSP-1 is stored in the α-granules of platelets. Following platelet lysis and activation reduced multimeric size of platelet VWF was observed in wild type but not in TSP-1 null mice. Increased collagen and platelet binding was observed upon platelet lysis and activation only in TSP-1 null mice.[242] This suggests that TSP-1 influences plasma derived and platelet derived VWF differently and may be more relevant to platelet derived VWF.

1.9 VWF and platelet binding

Under physiological conditions platelets and VWF do not interact. Vascular injury leads to exposure of subendothelial matrix i.e. collagen, fibronectin and laminin that initiates VWF and platelet adhesion. The type of interaction depends on the rheological conditions. At low shear conditions platelets can bind directly to collagen via integrin α2β1,[243,244] or to fibrinogen via integrin αIIbβ3.[245] At conditions of high shear rates (exceeding 500-800s^{-1}[246]), shear rates that are normally present in the human arterial circulation, VWF is required to mediate platelet adhesion to the damaged endothelium.[247]

Under conditions of elevated shear stress VWF binds to the subendothelium principally via collagen. This enables VWF to assume an extended conformation and results in exposure of its A1 domain to interact with the platelet membrane glycoprotein (GP) Ib-IX complex and mediates platelet capture. The largest VWF multimers support platelet adhesion most efficiently, since they expose repeating functional sites supporting multiple and more efficient adhesive interactions.[192] This is the first step in a sequence of signalling and adhesion events that generate a haemostatic plug at the site of vessel injury.

The platelet GPIb-IX-V complex is composed of transmembrane leucine rich glycoproteins: GPIbα and GPIbβ that are disulphide linked and non-covalently

associated with GPIX and GPV with minimal stoichiometry of 2:4:2:1 on the platelet surface.[248,249] The VWF binding site lies within the N-terminal 293 residues of GPIbα.[250] The A1 domain contains the only known VWF binding site for GPIbα.[104,137,141] A study using a synthetic VWF peptides showed that the residues D1277-E1305 encompass the major GPIbα binding site.[136] Moreover specific mutations R1287S, G1324S, H1326T, T1357S/E1359A, Q1367R, S1370R[251]and E1260A, N1274A[252] reduced binding between VWF A1 domain and platelets in the presence of ristocetin and botrocetin. The GPIb domain also contains non-identical but overlapping binding sites for other adhesive ligands (e.g. thrombospondin), counter-receptors (e.g. P-selectin and leukocyte integrin $\alpha_M\beta_2$), and coagulation Factors XI and XII, kininogen, and thrombin.[253-256] Therefore GPIb-IX-V also takes part in the adhesion of platelets to activated endothelial cells, in leukocyte recruitment to the sites of vascular damage and in thrombin induced platelet activation. Interaction between the A1 domain and GPIbα is crucial for haemostasis in arterioles and arterial capillaries, and participates in thrombosis in larger arteriessuch as coronary arteries at the sites of stenosis caused by artherosclerotic plaques.[257-260]

Recombinant isolated A1 domain binds to GPIbα but in contrast to the entire molecule does not initiate stable platelet adhesion.[104,261] Binding of GPIbα to VWF facilitates the initial transient tethering of platelets to the vessel wall that can be visualized, both *in vivo* and *in vitro*, as platelet rolling or slow translocation. The interaction between GPIbα and the A1 domain has fast association ("on")[262-264] and dissociation ("off")[262,264,265] rates and by itself cannot provide irreversible adhesion. The torque imposed by flowing blood causes platelets to translocate over immobilized VWF but the interaction between GPIbα and the A1 domain slows the platelet velocity down allowing establishment of additional bonds through other receptors on activated platelets. Those receptors have an intrinsically slower rate of bond formation, but mediate stable interaction and result in definitive arrest of platelets and thrombus formation. The mechanism by which GPIbα-VWF binding produces platelet activation has not been yet fully elucidated. It has been shown that GPIbα interaction with VWF triggers elevation of intracellular Ca^{2+}, phosphoinostide metabolism, protein phosphorylation (PLCγ2, ERK-1/2); activation of myosin light chain kinase and cytoskeletal actin filament rearrangements leading to platelet spreading. Upon activation the platelets undergo a change in morphological shape becoming more spherical and

extrude long pseudopods that enhance interaction with adjacent platelets. The platelet membrane also exposes more negatively charged phospholipids to provide an optimal surface for binding of coagulation factors. Furthermore, platelet granular contents are released (i.e., ADP, platelet derived growth factors, adhesion molecules and coagulation factors).[266,267] This allows the recruitment of additional platelets from the flowing blood. Eventually the activation of platelets leads to activation of platelet receptor GPIIb/IIIa (integrin $\alpha_{IIb}\beta_3$) that interacts with fibrinogen and the RGDS sequence in the VWF C1 domain and to P-Selectin expression on the platelet surface, thus mediating stable platelet adhesion, spreading and aggregation.[164,245]

Binding between VWF and GPIb-IX-V has to be strictly regulated to ensure that platelet plug formation is restricted to the site of vascular injury, since inadvertent binding can lead to both thrombosis and bleeding. For instance gain of function mutations in the VWF-A1 domain affect its conformation and promote spontaneous GPIbα binding. Enhancement of adhesion in the normal circulation can lead to the loss of high molecular weight VWF multimers and a reduction in platelets numbers, resulting in the bleeding disorder, von Willebrand disease (VWD) type 2B.[11,268] The type 2B mutations are clustered in a small region within the lower surface of VWF-A1 domain which is remote from the GPIbα binding site but they were showed to cause a significant change in the crystal structure of the A1 domain, altering the positions of residues implicated in GPIbα binding.[269,270] Platelet-type pseudo-VWD is caused by mutations in the amino terminal region of GPIbα region that increase its affinity for VWF resulting in a phenocopy of type 2B VWD.[271,272] In addition, binding studies of VWD mutants have indicated that both type 2B and platelet type VWD mutation increase platelet adhesion, in part by reducing the GPIbα-A1dissociation rate.[262,265] Lack or dysfunction of the GPIb-IX-V complex causes Bernard-Soulier syndrome (BSS), a rare congenital bleeding disorder characterised by thrombocytopenia, giant platelets, and decreased ristocetin-induced agglutination.[273,274]

The crystal structure of the unaligned VWF A1 domain [125] and extracellular domain of GPIbα[275]and the crystal structure of the VWF A1-GPIbα complex have been solved.[276] The A1 domain with the type 2B gain of function mutation R1306Q and GPIbα with the gain of function mutation M239V were used to facilitate crystallization of their complex.[276] Furthermore, a complex comprised of the extracellular domain of GPIbα

and wild type VWF-A1 domain was crystallised.[277] Conformational rearrangements occurring within the regions directly involved in the GPIbα-A1 binding were suggested by comparing the crystal structures of wild type and mutated protein complexes.

The VWF binding fragment of GPIbα (H1-E282) is elevated from the platelet plasma membrane by a mucin stalk and is composed of an N-terminal disulfide-looped capping sequence (residues 1-35), a leucine rich repeat sequence (residues 36-200), a C-terminal disulphide-looped flanking sequence (residues 201-268), and an anionic/sulphated sequence (residues 269-282).[278](Figure 1.7) The GPIbα central fragment forms an elongated curve that is composed of eight tandem leucine-rich repeats (LRRs); while the N-terminal sequence forms a 14-residue β-hairpin motif defined by a disulfide bond. The tip of the β-hairpin, named a β-finger, protrudes from the protein surface .The C-terminal flanking sequence has a more complex structure with two cysteine bonds and a highly protruding flexible loop between the cysteine bonds named a β-switch.[276] The A1 domain interacts with the concave surface of GPIbα with two main areas of high affinity interaction: the C-terminal β-switch of GPIbα binds near the top of the A1 domain while the β hairpin binds near the base of the A1 domain (Figure 1.7). Upon binding to the VWF A1 domain, the β-switch region undergoes a conformational change forming a β-hairpin that aligns with the central β sheet of the A1 domain forming the major interface of the complex.[276,277] The GPIbα gain of function mutations are located in the β-switch region and are predicted to stabilize the β-hairpin, enhancing the binding affinity. Comparison of the wild type and mutant complex shows that the GPIbα gain of function mutant adopts a more stable β-hairpin conformation, nucleated by a strong γ-turn, while wild type GPIbα has the same β-hairpin structure but a weak γ-turn.[276,277] The gain of function mutations in type 2B VWD are clustered in the bottom face of the A1 domain next to the interaction site with the β-finger of GPIbα. In the free A1 domain the sequence at the N-terminal side of the disulphide bond shields the binding site for the β-finger and this N-terminal extension is displaced when GPIbα binds.[276] The N-terminal extension is inhibitory because recombinant A1 domains lacking this extension bind GPIbα with 5-10 fold higher affinity.[137] The type 2B mutants that are localized within the N-terminal extension are likely to destabilize its interactions with the bottom face of the A1 domain, thereby making the GPIbα β-hairpin binding site accessible. Shear stress induces GPIbα activation by inducing a conformational transition of the β-switch loop to the β-hairpin, thus stabilizing it and facilitating the interaction with the central β-

sheet of the A1 domain, thereby promoting VWF binding.[279,280] VWD type 2B mutations and platelet-type pseudo VWD gain of function mutations affect distinct binding sites and their effect on binding is additive.[276]

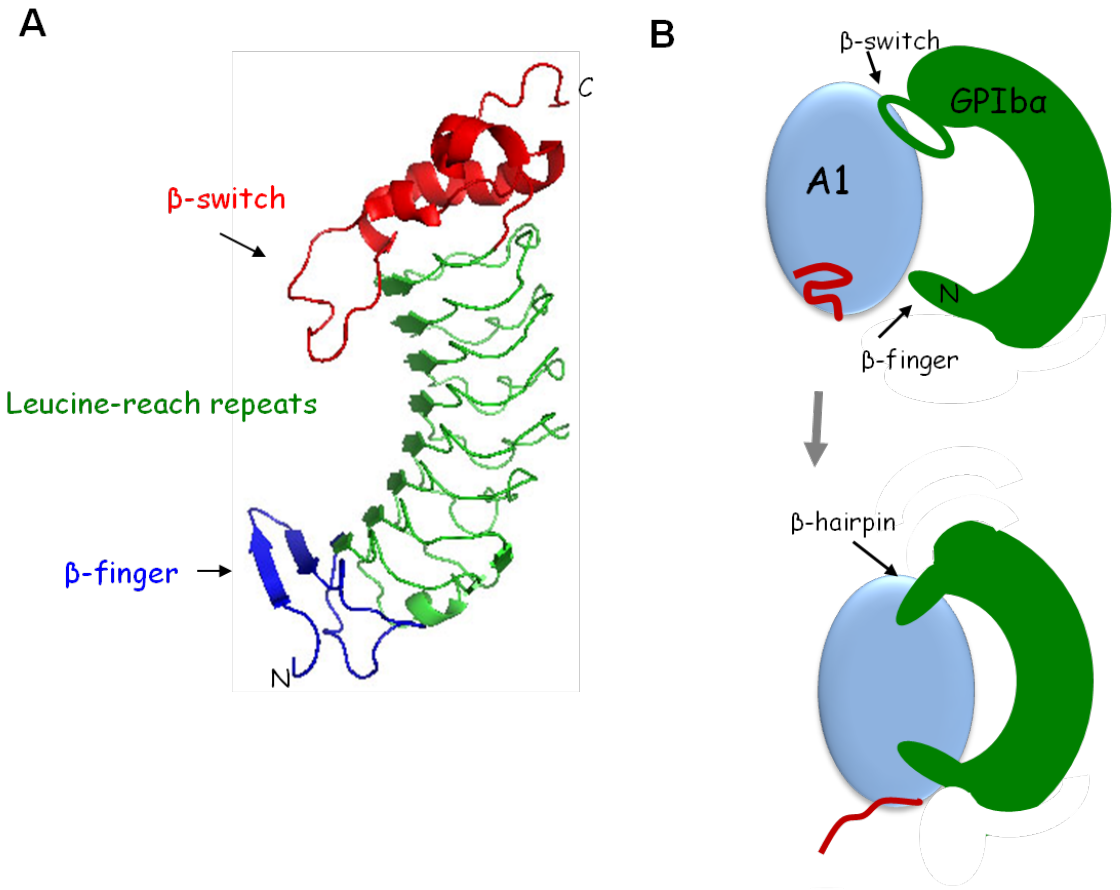


Figure 1.7 GPIbα structure and model of interaction with the VWF-A1 domain
A) GPIbα structure-ribbon representation; N-terminal β-finger region shown in blue, leucine rich repeats region in green, and C-terminal β-switch in red. **B)** Cartoon illustration of VWF interaction with the N-terminal part of GPIbα. Leucine-rich repeats of GPIbα wrap around one side of the A1 domains but do not directly contact it. The N-terminal β-finger region of GPIbα contacts the N-terminal extension of the A1 domain (in pink), and the β-switch region of GPIbα contacts the top of the A1 domain. Binding requires the amino–terminal extension of A1 to move, and induces transformation of the β-switch to a β-strand (figure adapted from Sadler, 2002[281]).

From the crystal structure analysis it appears that interface of the A1-GPIbα complex is characterised by presence of large patches of opposite charges, however charge residues at the interface are not involved in direct contacts between two proteins but are either fully or partially solvated. This suggests that GPIbα and the A1 are attracted by long-range electrostatic interactions, therefore avoiding the energetically adverse de-

solvation of charged residues in the formation of final complex.[276,282] The efficiency of platelet adherence is also dependent on the strength of the tethering force between the VWF-A1 domain and GPIbα, which was shown to be strongly correlated with the stability of the A1 domain.[283]

The isolated A1 domain used for crystallization lacks key structural elements that inhibit GPIbα binding in multimeric VWF. Binding studies using Surface Plasmon Resonance (SPR) in the absence of modulators demonstrated that the isolated A1 domain has notably higher affinity for GPIbα with K_D of 30nM compared to a K_d of more than 1μM determined for multimeric VWF , suggesting that other domains have inhibitory effect on the binding.[276] In addition, it has been demonstrated that the binding strength between GPIbα and the isolated A1 domain is identical to that determined for UL-VWF, in the absence of modulators, e.g ristocetin and botrocetin while plasma VWF bound GPIbα only in the presence of modulators. This suggested that changes in UL-VWF multimer conformation are more significant than their size for capture of platelets and that the intrinsic conformation of the A1 domain remains intact during the structural change of VWF.[193] Furthermore, several studies have shown that GPIbα binding affinity varies between A1 domains depending on the length of regions flanking the cystein bond.[137,284,285]

In multimeric VWF the accessibility of the A1 domain might be limited by the shielding effect of the D'-D3, since the D'-D3 region has been shown to have a negative regulatory role on the VWF-GPIb-IX-V interaction. It has been shown that deletion of the D'-D3 region in VWF results in increased GPIbα binding, while the isolated D'D3 region inhibits binding of platelet receptor GPIb to VWF. Moreover, using a panel of anti-VWF monoclonal antibodies it was shown that the D'D3 region is in close proximity with the A1 domain in soluble but not immobilised VWF.[138] The A2 domain might also participate in regulating the A1 domain activity. It has been demonstrated that the purified bacterial A2 domain binds to the A1 domain when VWF is immobilised or activated by ristocetin and prevents VWF interaction with GPIbα under high-flow conditions.[286]

Binding between GPIbα and VWF can be induced *in vitro* by modulators such as the antibiotic ristocetin and the snake venom protein botrocetin. Ristocetin and botrocetin interact with two distinct regions of VWF and GPIbα, and induce GPIbα binding

through different mechanisms. Ristocetin is an antibiotic from *Nocardia lurida*, that fluctuates many proteins, binds to platelets at high concentration (>1mg/ml) and mediates VWF dependent platelet agglutination (< 1mg/ml ristocetin).[287] Two regions have been implicated in its interaction with VWF: the C1237- P1251 region of VWF at the N-terminal site of the A1 domain[288,289] and the proline-rich sequence, E1463 to N1472, C-terminal to the disulphide bond in the VWF A1 domain.[288-291] Botrocetin is a venom coagglutinin isolated from the rattlesnake *Bothrops jararaca* that specifically binds to VWF and can interact with GPIbα only in the presence of the A1 domain. The botrocetin binding site is localised within the A1 domain (engaging helices α5 and α6 on one side of the VWF-A1) in the close proximity to the GPIbα binding site.[270,292] In contrast to ristocetin, botrocetin does not induce any conformational change in the A1 domain but could provide an additional binding surface for GPIbα.[293,294] It has been demonstrated that botrocetin first binds to the A1 domain but not GPIb and than subsequently slides around the A1 surface to form a new interface. Botrocetin decreases the A1-GPIbα disassociation rate two fold without affecting the association rate.[293,294] Moreover, within the GPIbα receptor, leucine-rich repeats 2 to 4 are critical for ristocetin dependent VWF binding, whereas the sulfated-tyrosine cluster between Asp-269 and 287 is more important for botrocetin dependent VWF binding.[295-298] It is accepted that ristocetin dependent rather than botrocetin dependent VWF-GPIbα binding closely correlates with shear-dependent interaction between VWF and GPIbα.[299] For example, studies showed that the ability of the anti-GPIbα and anti-VWF antibodies to inhibit GPIbα dependent adhesion under flow correlated with their capability to inhibit ristocetin, but not botrocetin dependent VWF binding.[299] In addition, VWF-A1 containing type 2M-VWD mutations were able to support shear induced platelet aggregation in the presence of botrocetin.[300] This thought to reflect the fact that only ristocetin induces conformational change in the A1 domain.

1.9.1 Platelet aggregation

Once platelets have adhered to the site of vascular injury they release VWF stored in α-granules and bind to VWF and fibrinogen, and further platelets are recruited to the site to form the primary platelet plug. This process is mediated, depending on the fluid dynamic, conditions by VWF interacting with GPIbα and integrin αIIbβ3 in the same way as described above and/or fibrinogen interacting with αIIbβ3.[301-303] In addition, immobilised fibrinogen and fibrin can mediate immediate irreversible adhesion of

flowing non-activated platelets via integrin αIIbβ3 at the lower shear stress rates. At low wall shear stress fibrinogen interacting with integrin αIIbβ3 forms the predominant link between aggregated platelets,[304] although VWF competes with fibrinogen for integrin αIIbβ3.[305,306] However at high shear flow, fibrinogen alone is unable to support platelet aggregation and VWF is required to form the platelet aggregate.[302,307,308] The presence of both VWF and fibrinogen is important for the development of stable thrombi as shown by both *ex vivo* studies and knock-out mice[309,310] and supported by observation of altered haemostatic properties of platelets from individuals with isolated congenital deficiency of either fibrinogen or VWF[311,312].

Interestingly, it was demonstrated that GPIbα can mediate activation-independent platelet adhesion and aggregation under very high shear rates above $10000s^{-1}$.[313] Importantly, this process depends on the presence of both soluble and immobilised VWF and can occur without any need for platelet activation or integrin function. Platelet VWF can also be involved in the formation of the platelet plug. However, since it is released from the α-granules of activated platelets it is unlikely to be involved in the initial adhesion of platelets to the site of vascular injury. Platelet VWF has been shown to mediate platelet aggregation at high shear stress and therefore is involved in the extension of the platelet aggregate after the initial adhesion of platelets to the exposed subendothelium.[308]

Collagen can also directly bind activated platelets receptors; integrin $\alpha_2\beta_1$ (GPIa/IIa)[314,315] and glycoprotein VI (GPVI),[316-318] however their relative importance remains debated. The type of binding is dependent on shear stress. Under high shear only previously activated platelets can bind to collagen via their GPVI receptor or via integrin α2β1 to collagen type III. [164,319] It has been suggested that at low shear, platelets bind mainly type I collagen, through integrin $\alpha_2\beta_1$, which is followed by binding via the GPVI receptor and subsequent platelet activation. GPVI is a low-affinity collagen receptor but is very effective in initiating signalling once it is cross-linked by binding to collagen.[320] The integrin $\alpha_2\beta_1$ conformational activation increases its affinity for collagen, and possibly requires inside-out signalling generated by either interaction of GPVI with collagen or activation of integrin $\alpha_2\beta_3$.[321] GPVI has been shown to influence platelet aggregation and thrombus formation on fibrillar collagen type I coated surface under flow conditions.[322-324] Combined deficiency of GPVI and integrin $\alpha_2\beta_1$ in mice results in complete inhibition of thrombus formation, compared to a minor reduction in

thrombus formation resulting from deficiency of only one of the receptors.[316] Interestingly GPVI or integrin $\alpha_2\beta_1$ deficiency in humans does not cause a strong bleeding phenotype.[315,325,326] Nevertheless genetic polymorphism in both GPVI and integrin $\alpha_2\beta_1$ has been suggested as a predisposition to thrombosis and targeting those receptors is considered a potential antithrombotic strategy.[327]

1.10 Mechanism of transient platelet adhesion under flow

Platelets are disc shaped, anulceate blood cells derived from megakaryocytes that are activated to initiate thrombosis only in certain physiological or pathological conditions. As described previously, at the sites of vascular injury, under high shear, VWF is essential to the initiation of platelet adhesion and therefore subsequent plug formation, since it is able to resist hydrodynamic forces and provide a rapid link between extracellular matrix and platelets. As mentioned above, platelet adhesion is initiated by transient interaction between the VWF-A1 domain and platelet receptor GPIbα, though only when both proteins are subjected to high fluid shear stress which exerts a hydrodynamic force on the GPIbα-VWF bonds.[215] Interestingly, flow enhances rather than impedes platelet adhesion, despite the dislodging forces.[245] This unique feature of the interaction between GPIbα and VWF-A1 enables activation-independent platelet tethering to injured vessel wall even when the velocity of blood is elevated whilst at the same time preventing inappropriate platelet agglutination in the normal circulation.

Bonds between adhesion molecules are often mechanically stressed. It used to be assumed that the tensile mechanical force acting on a biological adhesive bond increases the detachment rate and shortens bond lifetimes, since work done by the force could overcome the energy barrier between the bound and free states.[328] However in recent years, several receptor-ligand pairs have been shown to form ‘catch bonds’ whose lifetimes are actually extended by force. Examples of such force-enhanced bonds include the bacterial protein FimH binding to its ligand mannose,[329] leukocyte selectins and *sialyl Lewis*^{X} containing ligands[330] and myosin-actin motor protein interaction.[331] The interaction between GPIbα and VWF under conditions of increasing shear stress was proposed to follow this mechanism with binding observed under high flow conditions and showing a dual response to the force of the flowing blood.

Applied force affects lifetimes of catch bonds in two distinct ways depending on the degree of shear applied. Initially, as force increases, bond lifetime increases until a

maximal value is reached (catch regime). Increased bond life time results in decreasing cell rolling velocity. As the force increases further, bond lifetimes decrease and as a result rolling velocities increase (slip regime).[330] It has been shown that disassociation of the bond is governed by the force that is applied to the bond as a result of the hydrodynamic force acting on the cell. The key property of adhesive catch bonds distinguishing them from slip bonds is their ability to resist applied force. This mechanism allows many adhesive molecules to resist forces in the body that would normally break cell-cell contact. [332,333]

Mechanical properties of individual catch bonds in response to mechanical force (shear) have been analysed using atomic force microscopy,[334,335] optical tweezers,[336] a biosurface force probe,[337,338] and a microneedle cantilever.[339] In these experiments, surfaces coated with receptor and ligand are touched together and then pulled apart while recording forces, and rupture events are analysed. Force can be either; loaded at a constant level and held until the bond breaks-to measure bond life time; or increased steadily until the bond ruptures-to measure the probability of bond rapture and bond strenght.[340-342] A bond can be described as a slip bond when the bond lifetime is shorter at higher forces and the bonds rupture more frequently (Figure 1.8 a,c) A bond can be called a catch bond if the bond lifetime increases with force up to a critical force (this region is called catch regime), and then it enters a slip regime where force shortens the lifetime (Figure 1.8 b). A catch bond has two peaks corresponding to increased probability of bond rapture, that are below and above the critical force (Figure 1.8, d). The proportion of ruptures in each of the peaks is determined by the pace at which the loading force is increased, as bonds only break below the critical force if given enough time. If the force is increased too fast, a bond could be described as slip, which was probably why these bonds were not always detected.

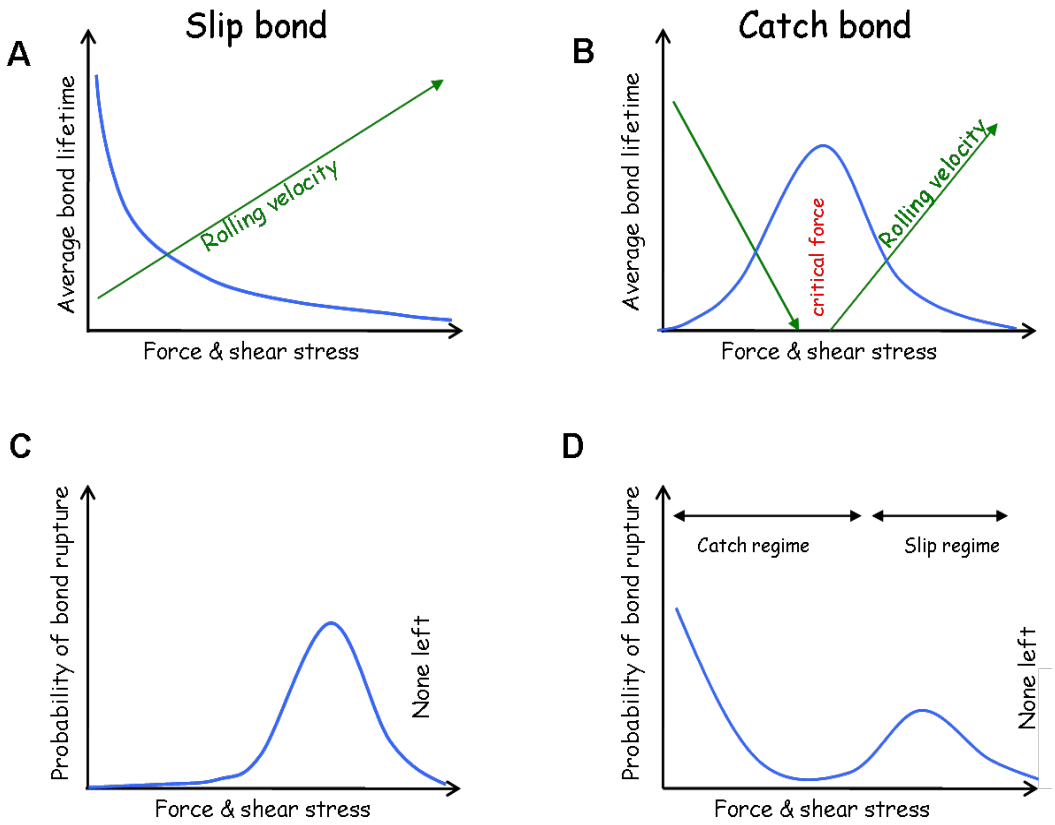


Figure 1.8 Schematic representation of bond mechanics

A) The mean life time of a slip bond decreases, and ligand rolling velocity increases with shear stress. **B)** Mean lifetimes of catch bonds increases with force below a critical force and decreases with force above the critical force. In addition, strength of a slip bond **(C)** and catch bond **(D)** when force is increased until rapture. Slip bonds have one peak at higher forces (shear stress) corresponding to highest chance of rapture and lowest lifetime. Catch bonds have to peaks, above and below critical force, where the bonds break most frequently.

Interestingly, a number of mutations in VWF that result in type 2B VWD can modify the mechanical regulation of the GPIbα-A1 catch bond. Recently single molecule experiments have shown that the mutation R3106 and R1450 linked to type 2B VWD change the properties of the bond by prolonging the bond lifetime at low shear and lowering or eliminating the shear threshold requirement for bond formation and platelet rolling: thus eliminating catch bond behaviour.[335] This may explain the ability of globular VWF with type 2B mutations to induce platelet agglutination in the circulating blood. [343] As mentioned previously, the domains neighbouring A1 and the flanking N-terminal region, have beenshown to inhibit GPIbα binding. It is not clear if this

inhibition is due to allosteric or masking effects, since these parts of VWF were not included in the A1 construct used to examine the catch bonds.[138,286,335]

1.11 Blood flow dynamics and kinetics

Platelets perform their function in the blood under constant fluid motion and the type of flow influences platelet function. Blood is a viscous fluid suspension comprised of a continuous part (plasma) and a suspended part (cells) that may become separated by the action of shear stress, as gravity has a negligible effect in the flowing blood.[344,345] In addition when the cell count is normal, red blood cells constitute majority of the circulating mass and occupay the center of the vessel where the velocity of blood is the highest. As the consequence of lateral migration under shear and erratic motion,[260,346] they occupy most of the lumen, pushing leukocytes and platelets to the sides increasing the platelet concentration adjacent to the vessel wall.[347-349] This distribution facilitates adhesive interactions of platelets with the vessel wall.

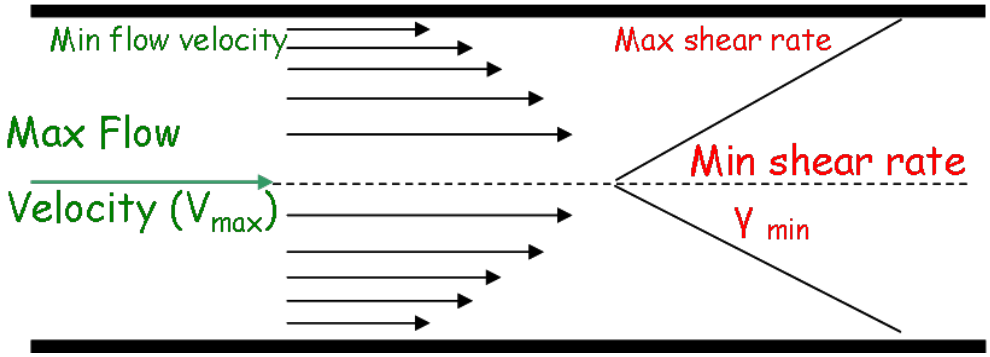


Figure 1.9 Schematic representation of blood flow in a vessel

Blood flow in a vessel follows a laminar model, and can be visualised as a series of fluid layers (laminae) moving at different velocity. It is the difference in the velocity between laminae of the flowing blood that generates shearing forces. The blood has greater velocity at centre of the vessel than near the wall, while the shear rate value is minimal in the centre and increases toward the vessel wall.

A Newtonian fluid is one that has a constant viscosity at all shear rates (i.e. irrespective of velocity fields). Blood has a pulsatile flow in arteries and non-Newtonian behaviour at lower shear rates. However, blood flowing in a vessel wall at shear rates above $200s^{-1}$ can be considered a Newtonian fluid,[260,350] therefore the velocity profile of blood

moving steadily in the vessel with a constant cross-sectional is assumed to follow the laminar flow model. This means that at a given flow rate, blood in the centre of the vessel has maximal velocity which decreases toward the wall.(Figure 1.9) The changing velocity of blood which increases with distance from the vessel wall creates shearing flow, which is a sliding motion between two adjoining laminae moving at different speeds. Shear rate (γ) is the difference in flow velocity as a function of a distance from the wall, and is expressed in cm/s per cm or usually as inverse second (s^{-1}). Shear rates in flowing blood are small at the centre of the vessel, and increase near the vessel wall as a result of drag[215]. Shear stress (τ) is the tangential force per unit area of contact between laminae resulting mainly from pressure differences within the vascular system and can be expressed either in pascals (Pa; $1Pa=N/m^2$) using the International System of Units or as dyn/cm^2 ($1Pa=10dyn/cm^2$) in CGS system. In an ideal Newtonian fluid shear stress and shear rate are linear. Shear stress is a function of shear rate and the viscosity (μ) of the fluid. Fluid viscosity is expressed in Pa·s or dyn/cm^2·s the latter equivalent to Poise (P) where 1P= 0.1Pa·s. Examples of shear rates in vivo are given in Table 1.1. Several specific models have been suggested to describe the effect of the force on association and disassociation of adhesive proteins,[351,352] and VWF-GPIbα interaction, similarly to selectins, is principally described by the Bell model. The Bell model is used to describe the force dependence of the off rate of a receptor-ligand interaction and is expressed as an exponentially increasing function of force. According to this model two mechanisms can regulate rolling velocities in flow. First it may be controlled by the intrinsic kinetics of bond disassociation (k_{off}^0), i.e in the absence of force. Secondly, rolling could be modulated by the relative compliance (σ), which is the susceptibility of the bond disassociation to applied force.[333] Engineering principles have been used to design models to reproduce blood flow *ex vivo* in injured, narrowed, or branched arteries. However it has to be mentioned that the assumption of laminar flow may not be completely relevant *in vivo* where blood flow is more complex and rheological variables related to eddy formation, pulsatility and dynamic constriction may predominate under some physiological and pathological conditions.

Blood vessel	Shear rate (s^{-1})	wall shear stress (dyn/cm^2)
Large arteries	300-800	11.4-30.4
Arterioles	500-1600	19.0-60.8
veins	20-200	0.76-7.6
Stenotic vessels	800-10000	30.4-380

Table 1.1 Average wall shear rates and wall shear stresses, in various vessels types Viscosity of blood assumed to be 3.8,miliPoise. (Reproduced from Kroll et al., 1996)[215]

Viscosity is a very important factor in shear flow as it relates the kinematics of fluid movement (shear rate, units of time $^{-1}$) to shear stress (units of force per area, the product of shear rate and viscosity) and therefore the hydrodynamic forces that are experienced by objects in contact with the fluid. It has been demonstrated that bond formation is a function of shear rate and therefore the kinematics of receptor and ligand movement, but not shear stress. The formation of the bond is limited by the separation distance of the receptor and ligand and the time that the receptor and ligand are in proximity to each other, rather than by the force applied on the bond. Shear rate is a limiting factor in tether formation, because when the velocity of the cell relative to the substrate is too high, it provides insufficient time for a collision to take place between the receptor and the ligand and thus to allow bond formation.[332,353] Dissociation of the bond on the other hand, is a function of shear stress and consequently the force on the bond.

For cells (platelets) in the flow, the formation of an adhesive receptor-ligand interaction is termed 'transient tethering' and can be detected as an abrupt arrest in the movement of cell previously free in the flow, while bond disassociation can be distinguished as the subsequent recommencement of the hydrodynamic movement of the cell.[354] Transient tethers have been shown to take place when the density of the receptor is very sparse, so that it cannot support rolling, therefore they represent a single receptor-ligand bond.[333,354,355] This has been confirmed for the P - and L- selectin by comparing the k_{off} calculated from the Bell model[333,354] at the absence of force and k_{off} measured using SPR.[356,357]

Mody *at al,* investigated the mechanics of platelets tethering to surface immobilised VWF-A1 domain under hydrodynamic flow, and developed a two-dimensional model to calculate the motion of platelets.[358] Through the comparison of theoretical analysis and experimental observation, they have estimated that the tether bond formation between the A1 domain and platelet could take place only in situations where a hydrodynamic compressive force is predicted to act along the platelet length (compressive force), pushing it against the surface, in that way initiating platelet adhesion.[358] They have suggested that the compressive force promotes bond formation by bringing the surfaces into close molecular contact and helping to overcome repulsive long range interactions between surfaces[358,359]

1.12 VWF self aggregation

It has been shown that shear forces can induce VWF lateral self-association in solution. VWF multimers are thought to form fibres, which are organised in a spider web-like structure and therefore have significantly increased platelet capture potential. This property of VWF was first observed by Savage *at al.,* when properties of VWF lacking its A1 domain where investigated in a parallel flow chamber under conditions of high shear flow. VWF lacking the A1 domain and therefore the ability to interact with non-activated platelets, immobilised on a flow slide was able to support platelet adhesion when whole blood containing VWF was perfused over the slide, but did not when plasma free blood used.[360] This implies that VWF present in whole blood, was able to associate with VWF lacking the A1 domain immobilised on the slide, and mediate platelet capture. Subsequently Choi *at al.* showed that some plasma VWF multimers contain surface exposed free thiols, and that shear stress can promote the formation of disulphide bonds utilising these free thiols. Based on that data and additional experiments using a cone-plate viscometer[361] it has been proposed that the VWF self-association is mediated by the formation of new intermolecular disulphide bonds under high shear.[362] Furthermore, VWF with its free thiols blocked had decreased ability to interact with VWF secreted from endothelial cell under shear up to $250s^{-1}$.[363] Interestingly VWF self assembly was also observed under static conditions. A plate binding assay demonstrated that the interaction between immobilised and soluble VWF involves multiple domains but none has been identified as essential.[360,364] In addition VWF self-aggregation has been detected in a solution under static conditions when conformation of the protein was altered by ristocetin.[365]

1.13 Von Willebrand disease

Von Willebrand disease (VWD) is the most common congenital bleeding disorder caused by defects in the concentration, structure, or function of VWF. The disease was first identified by Dr Erik Von Willebrand in 1924 in families from the Aland Islands who suffered bleeding problems distinct from haemophilia. Symptoms vary according to severity of the disease and include epistaxis, gingival bleeding, menorrhagia, prolonged bleeding from minor wounds, skin bruises and haematomas and gastrointestinal bleeding in more severe cases. VWD is a heterogeneous disorder and is classified into three primary categories. Type 1 is a partial quantitative deficiency, type 2 results from qualitative defects, and type 3 results from a total deficiency of VWF.

Type I is the most frequent VWD type (70% of all VWD patients). It is defined as a bleeding disorder resulting from as a simple quantitative deficiency of VWF. However it appears that when analysed in detail VWF from individuals with type 1 VWD frequently shows subtle abnormalities in multimer composition and distribution. This is more consistent with the dominant-negative effect of many type 1 VWD associated mutations.Type I VWD subtype Vicenza is characterised by low plasma VWF levels resulting from the accelerated clearance of VWF.[366-368]

VWD type 2 that results from functional defects of VWF is further divided into four secondary categories: 2A, 2B, 2M, 2N.

Type 2A refers to VWF mutants with decreased platelet adhesion caused by a selective deficiency of the most haemostatically active high and intermediate molecular weight VWF multimers. Two distinct molecular mechanisms can cause the type 2A VWD phenotype and the corresponding causative mutations are subdivided into group I and group II. Group I refers to VWF with mutations localised in the propeptide, the cysteine knot domain or the D3 domain, resulting in defective assembly and secretion of VWF multimers. VWF mutants that are classified to group II undergo normal processing and secretion but loss of large and intermediate molecular weight multimers takes place in plasma, due to increased ADAMTS13 proteolysis caused by mutations in the A2 domain.

Type 2B refers to VWF mutants with increased affinity for platelet GPIbα. The responsible mutations are cluster within or near the A1 domain, which contains the GPIbα binding site. Mutated VWF shows an increased ristocetin-induced platelet

aggregation (RIPA) at abnormally low concentrations of ristocetin. Paradoxically, patients with VWD type 2B do not suffer from thrombosis but bleeding. This can be explained by the increased clearance of both VWF and platelets, leading to absence of haemostatically effective high molecular weight multimers in plasma and a variable thrombocytopenia.

Type 2M refers to VWF mutants with decreased platelet adhesion but normal VWF multimer distribution. The functional defect is caused by mutations in the GPIbα binding site in the A1 domain, which disrupt VWF binding to platelets.

Type 2N refers to mutants with markedly decreased affinity for factor VIII, and consequently low FVIII levels due to enhanced clearance. Mutations that lead to type 2N VWD are localised within the FVIII binding site of VWF domains. Since VWF is physiologically in excess of FVIII the phenotype is autosomal recessive.

1.14 VWF glycosylation

Protein glycosylation is exceptionally abundant and structurally diverse posttranslational modification. A large proportion of proteins and lipids in biological systems are glycosylated. Carbohydrate chains attached to extracellular proteins can act as ligands for receptors and mediate recognition and also modify biochemical properties of proteins, such as charge, folding, solubility and sensitivity towards proteases.[369,370] Moreover, many nuclear and cytoplasmic properties in eukaryotes undergo dynamic glycosylation, which may be an important regulatory modification, reciprocal to phosphorylation, modulating biological processes.[371] Glycosylation can also be used as a way to expand the information of a small genome. For instance, a single gene product such as tissue plasminogen activator (tPA) can be a foundation for over 100 discrete protein glycoforms with different enzymatic activities and plasma clearance.[372] The complexity and heterogeneity of glycans, as well as their template-independent biosynthesis has made it difficult to characterise them or modulate their function.

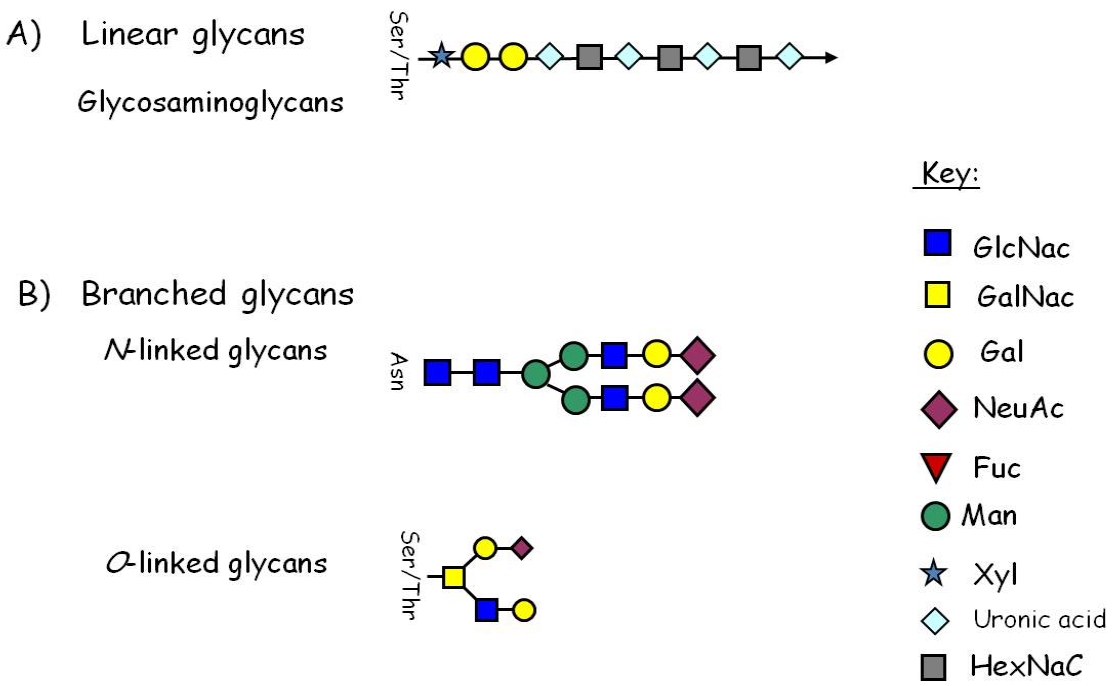


Figure 1.10 Types of glycans

Examples of linear and branched glycans are illustrated. **A)** Glycosaminoglycans (GAGs) are the major category of linear polysaccharides comprised of disaccharide repeat units of alternating uronic acids linked to hexosamines, attached to a core tetrasaccharide. **B)** Branched glycans include *N*- and *O*-linked oligosaccharides. *N*-linked glycans can by divided into high mannose, hybrid, and complex. *O*-linked glycans are further subdivided by core type.

Glycans are categorised into two broad groups: branched and linear (Figure 1.10). Linear glycans are represented by glycosaminoglycans(GAGs) such as heparin sulphate chondroitin or dermatan sulphate[373] while branched glycans are further divided into *N*-linked and *O*-linked oligosaccharides.[374] VWF undergoes posttranslational modifications resulting in addition of *N*- and *O*-linked glycan chains which comprise 18.7% of the total molecular weight[12] (with *N*-linked glycans accounting for 70% of the carbohydrate component and *O*-linked glycans accounting for 30%)(Figure 1.11)[375,376].

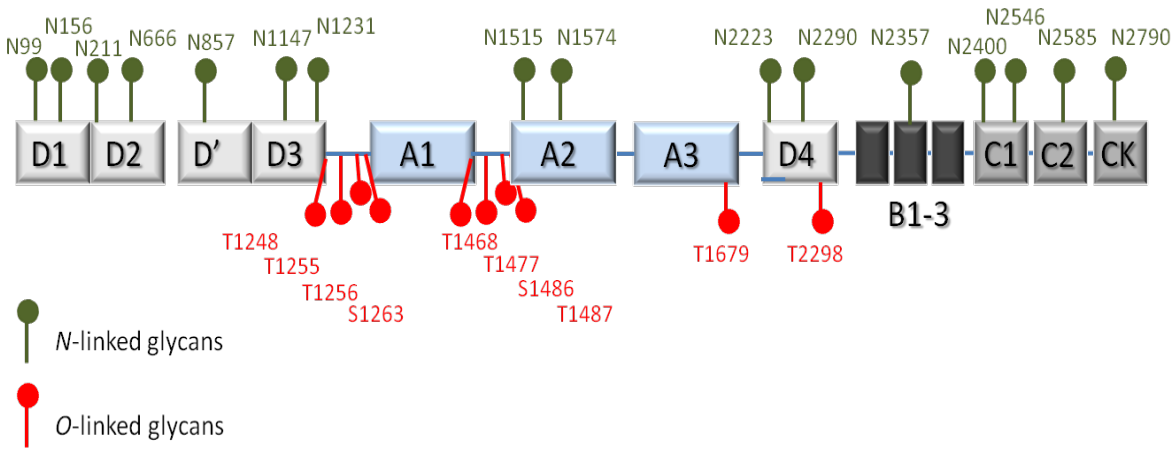


Figure 1.11 VWF glycosylation

VWF contains a predicted 16 *N*- and 10 *O*-linked glycosylation sites. 4 potential N-linked glycan sites are present in the propeptide (D1, D2) and 12 are distributed throughout the mature protein. Conversely 8 *O*-linked glycans are clustered in the A1 domain flanking regions. One *O*-linked oligosaccharide is present in the A3 domain and one in the D4 domain.

1.14.1 *N*-linked glycosylation

N-linked glycosylation is one of the most common co/posttranslational modifications. *N*-linked glycosylation is initiated in the ER by *en bloc* attachment a 14-saccharide moiety ('core' oligosaccharide) onto a nascent polypeptide chain.[19] This core structure (Glc_3 $Man_9GlcNAc_2$) is linked via an *N*-acetylglucosamine residue to an asparagine residue in the sequence NXS/T (or in some cases NXC) where X is any amino acid except proline. Subsequently the terminal glucose residues are removed by Glucosidase I and II. The resulting monoglucosylated structure associates with ER lectin chaperones calnexin and calreticulin, and protein disulphide isomerases including ERp57. When the glycoprotein has folded correctly, the final glucose residue is removed by Glucosidase II, allowing release from calnexin and calreticulin, and transit to the Golgi apparatus. Mannosidases further process the carbohydrate structure. Additional GlcNAc or galactose or N-acetylneuraminic acid residues are added to $Man_3GalNAc_2$ structure to form complex N-linked glycans.[377-380] Endothelial cells can also add terminal fucose residues in an α1-2 linkage to a precursor glycan chain creating the H-antigen , which can be further modified to blood group A or B antigens by addition of GalNAc or galactose residues respectively.[381]

VWF presents sixteen *N*-linked oligosaccharides; four are predicted to be in the propeptide (N99, N156, N211 and N666) and twelve are present in the mature subunit N1515, N1574, N2223, N2290, N2357, N2400, N2546, N2585, N2790.[12] (Figure 1.11) In a number of initial studies VWF glycan structures were isolated and sequenced. A detailed study of VWF *N*-linked glycans was performed by Matsui, Titani and Mizuochi. All studies demonstrated that VWF carries a mixture of complex glycans, with variable number of branches as well as number and identity of terminal sugar residues. A bi-antennary, glycan was shown to be a major *N*-linked glycan type presented by VWF (~70%).[20,382,383]

N-linked glycans fulfil several important functions; for instance they assist in protein folding, disulphide bond formation, prevent aggregation, enhance thermal and kinetic stability of proteins and protect them from proteolysis.[380,384,385] The role of *N*-linked glycans on VWF function and structure has been studied extensively. *N*-linked glycosylation is necessary for dimerisation of VWF since treatment of endothelial cells with Tunicamycin that blocks *N*-linked glycosylation results in the accumulation of VWF monomers within the cell.[16,17] Castanospermine, that prevents initial trimming of glucose residues, was also shown to inhibit VWF secretion, suggesting that interaction with ER chaperones in required to assist in processing of *N*-linked oligosaccharides.[17] Furthermore, presence of certain *N*-linked glycan chains was shown to be important for the proper intracellular processing as well as storage and secretion of VWF, as their removal resulted in protein retention within the ER.[17] Furthermore prevention of glycosylation at individual sites resulted in increase in free thiol reactivity. This suggests that VWF *N*-linked glycans can modulate inter- and intra-molecular disulphide bond formation.[17]

The effect that removal of terminal sialic acid and/or terminal galactose residues from oligosaccharide chains, has on VWF structure and function is not clear. A number of studies have suggested that removal of those residues results in the loss of high molecular weight multimers,[386-388] while others reported that it does not have an effect on VWF multimeric composition. However it is possible that the results from the earlier studies were confounded by the use of impure PNGase enzymes.[389] A recent study clearly demonstrated that removal of the entire *N*-linked glycan chains by PNGaseF does not alter VWF multimeric structure.[239]

VWF *N*-linked glycans have been shown to present ABO group determinants.[20,239] Interestingly, ABO group structures influence the plasma level of VWF, with VWF levels 25% lower in group O than non-O individuals.[376,390,391] In addition, within non-O blood group VWF levels were highest in AB individuals, followed by group B, group A and lowest levels were observed in group O individuals.[392] ABO antigens also influence VWF susceptibility to ADAMTS13 proteolysis, with the O group being the most susceptible.[393]

Finally, removal of *N*-linked glycans increased susceptibility to ADAMTS13 cleavage and allowed cleavage under static conditions in the absence of denaturants.[239] Two *N*-linked oligosaccharides flank the ADAMTS13 cleavage site (N1515 and N1574). Mutation of N1574, to prevent glycosylation at this site, results in increased sensitivity to ADAMTS13 proteolysis. This suggests *N*-linked glycans modulate the interaction between VWF and ADAMTS13.[239]

1.14.2 *O*-linked glycosylation

The most common form of *O*-linked glycosylation in eukaryotes is mucin-type glycosylation, which is initiated by α-O-linking of *N*-acetylgalactosamine (GalNAc) to the β-hydroxyl group of either a serine or a threonine of the polypeptide chain.[394-396] Following addition of the first residue, *O*-linked glycans are synthesised by sequential addition of monosaccharides using specific transferases. Other types of *O*-linked glycosylation are rare or restricted to certain species, tissues or proteins. Examples of alternative types of *O*-linked glycans attached to Ser/Thr include: *β-O*-xylose found on proteoglycans, *α-O*-fucose on epidermal growth factor (EGF)-like domains[397] and α-O-mannose in yeast and mammalian glycoproteins. Moreover, the structure Galβ-*O*-hydroxyLys is found in collagens[398] and Araβ-OhydroxyPro on plant cell wall proteins.[399] Finally, nuclear and cytoplasmic eukaryotic proteins can be glycosylated at multiple sites by single *O*-linked N-acetylglucosamine (O-GlcNAc) residues.[400,371]

Mucins are high molecular weight polymeric glycoproteins present in the mucous gel that protects the mucous epithelium, or cell surface-bound molecules which can take part in cell adhesion. Mucins glycoproteins are very heterogeneous at mRNA, protein, as well as carbohydrate levels. The characteristic property of mucins is the presence of tandem repeat domains that contain identical or similar sequences rich in serine, threonine and proline residues and are highly glycosylated.[401] Mucins are glycoproteins

with dense clusters of *O*-linked sites bearing up to 20 monosaccharides per glycan; however mucin type glycosylation can also take place at singular positions on non mucin proteins.

1.14.2.1 Synthesis of O-linked glycans

The biosynthesis of mucin-type glycosylation takes place in the Golgi apparatus, following N-linked glycosylation, protein folding, and oligomerisation. As mentioned above, *O*-linked glycosylation is initiated by the transfer of GalNAc residue from a nucleotide sugar donor (UDP-αGalNAc) to serine or threonine.[402] This process can be mediated by at least 15 UDP-GalNAc:polypeptide N-acetyl-galactosaminyltransferases that have overlapping but different specificities and are expressed differently among tissues.[403-406] GalNAc transferases are membrane glycoproteins located in variable regions of the Golgi, which may also govern their specificity.[404]

No consensus sequence has yet been determined, but the likelihood of *O*-linked glycosylation occurring can be predicted from comparative studies, basing on the amino acid sequence surrounding the Ser/Thr residue (NetOglyc server www.cbs.dtu.dk/services/netoglyc).[369] *O*-glycosylation will only occur on exposed Ser/Thr residues which are mostly on β-turns of the secondary structure and other regions with extended conformations i.e. rich in proline residues and regions with low hydrophobicity and it will not occur near large amino acid residues. It is suggested that the mucin type glycosylation of multisite substrates occurs in a hierarchical manner, since some of the transferases can only glycosylate peptides which are already glycosylated.[407-409] In addition, studies have showed that the density and glycosylation pattern can affect the activity of transferases; for instance addition of galactose residue to the GalNAc-Ser/Thr moiety can affect the extent of activity on neighbouring sites.[396,410]

The α-*O*-GalNAc-Ser/Thr structure is a foundation for various 'core' structures, which are generated by addition of other monosaccharides to the C-3 and/or C-6 hydroxyl groups of GalNAc. To date, eight core structures have been identified with core 1 and 2 being the most common among both mucin and non-mucin glycoproteins.[411] Unmodified α-O-GalNAc-Ser/Thr structures are seldom found in glycoproteins in normal tissues but are abundant in mucins from cancer cells and are termed Tn antigens.[412] The core structures can be further modified by sialylation, sulphatation,

acetylation, fucosylation, and polylactosamine-extension, and form complex structures such as *sialyl Lewis*^{X} and blood group antigens. The core 1 structure is normally substituted with sulphate, sialic acid or other sugars, but in cancer remains often unsubstituted and constitutes the T antigen.[412] The synthesis, extension and termination of *O*-linked glycans is regulated by transcriptional and translational control, transport of substrates through the Golgi apparatus, concentration of cofactors, as well as interaction of glycosyltransferases (GTs) with other proteins.[412-414]

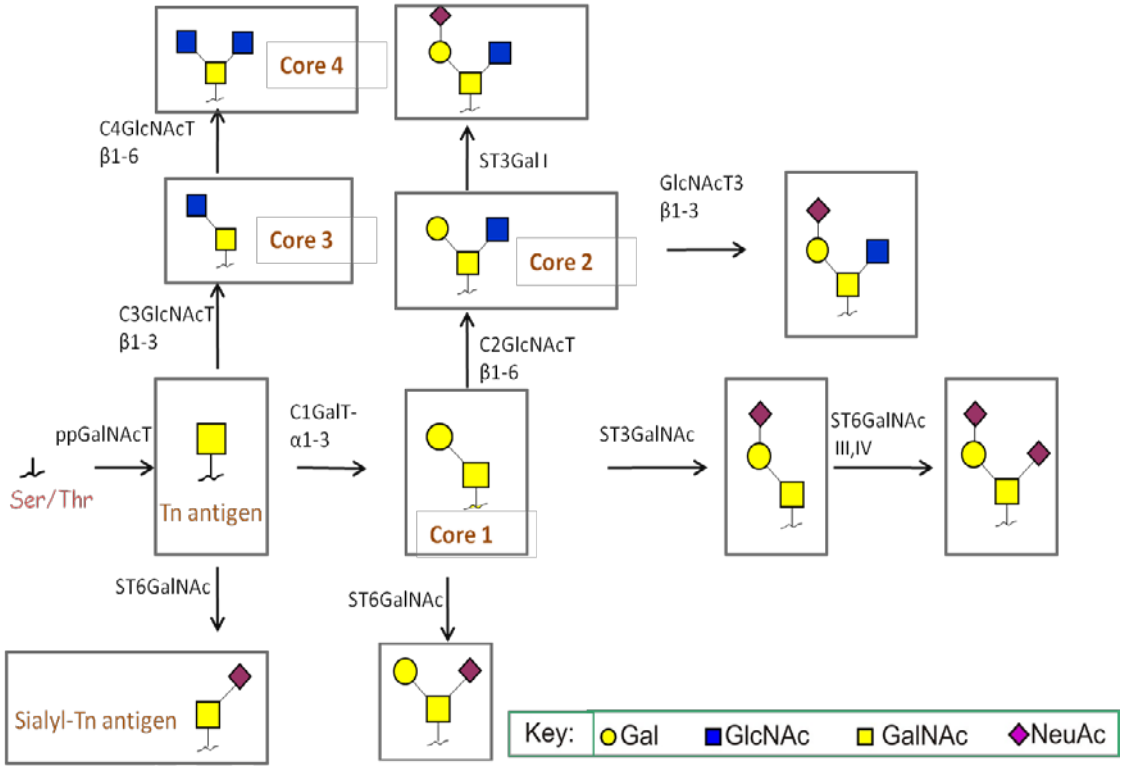


Figure 1.12 Pathways specific for the assembly of the *O*-linked glycans

Schematic illustration of the O-linked glycans biosynthesis. Mucin type glycosylation is initiated by addition of N-acetylgalactosamine (GalNac) residue to serine or threonine of the polypeptide, and then specific transferases (above the arrows) catalyze sequential addition of monosaccharides creating a number of different glycan structures.

More than 80GT families have been identified. Importantly each GT is specific for both the sugar donor and the acceptor substrate. Functions of transferases can be altered by hormones, cytokines and other external factors. Organ specific suppression of specific GTs and up regulation of others results in the formation of cancer-associated changes in

O-linked glycans as demonstrated for breast and colon cancer.[396,415] Changes in the elaboration of *O*-linked glycan chains are associated with a range of diseases, for instance Wiskott-Aldrich syndrome, haematological disorders, cystic fibrosis and cancer.[412,416,417]

1.14.2.2 Function of O-linked glycans

O-linked glycans can constitute 80% of the mucin mass and confer viscous, gel-forming, and adhesive properties, thus providing lubrication and a protective barrier for various body tissues.[401,418,419] Extensively O-glycosylated regions of mucins can block accessibility of the peptide backbone to proteases therefore protecting it from degradation. [420] Mucin type *O*-linked glycans can also regulate the serum half-life of chemokines and hormones, and mediate intracellular trafficking of proteins.[421-424] Moreover, it has been shown that mucin glycans can determine the aggregation state of membrane bound glycoproteins (e.gCD45) thereby modulating signalling and interaction with receptors.[425] Apart from modulating protein function, *O*-linked glycans are often ligands for cell surface receptors and play important roles in the immune system. They have been shown to interact with natural killer cells, lymophocytes, dendritic cells, and other leukocytes. For instance the sialyl-Lewis^x structure is a ligand for selectins (E-, L-, P) and mediates leukocyte adhesion to sites of inflammation as well as the rolling of leukocytes along the endothelial surface.[426-428] In addition, *O*-linked glycans were demonstrated to play roles in cell-adhesion events during sperm-egg interaction,[429] host-microbe contacts[430] and viral infections[431]. *In vitro* experiments showed that *O*-linked glycans on cancer cells can bind to selectins and endothelial cells, which can contribute to the invasive and metastatic properties of tumours. [432,433]Glycosylation with an O-GlcNAc moiety of nuclear and cytoplasmic proteins such as c-myc, p53, RNA polymerase II, and tau, is reciprocal to phosphorylation. It is highly dynamic and responsive to changes in cellular stages and signalling and may have a reverse function to phosphorylation, thus is thought to take part in regulation of transcription, nuclear transport and cytoskeletal assembly.[371,434-437]

O-linked glycosylation may also influence the secondary, tertiary, and quaternary structure of the folded protein. Glycans introduce steric hindrance, and the polypeptide they are attached to can adopt a rigid, extended conformation, with length up to hundreds of nanometers in length as demonstrated by AFM, light scattering and nuclear

magnetic resonance studies[438-445] For example, removal of *O*-linked glycans from the ovine submaxillary mucin causes change of its structure from elongated filamentous to globular.[446-448]

Another interesting aspect of glycosylation is the presence of the *O*-glycosylated Ser/Thr/Pro rich domains, for example in the hinge regions of immunoglobulins IgD and IgA. The *O*-linked glycan chains in this region can extend the peptide chain, due to repulsion between the charge sugars, and protect the region from protease cleavage. *O*-linked glycans in the hinge also mediate the IgA and IgD binding to a lectin site on T-lymphocytes *in vitro*.[449,450] In individuals with IgA nephropathy the *O*-linked glycans in the IgA hinge region express less sialic acid and/or galactose residues, which results in the kidney deposition of immunoglobulins.[451]

1.14.3 VWF *O*-linked glycans structure and function

Ten *O*-linked oligosaccharides are added to each VWF molecule. Eight of the *O*-linked oligosaccharides are clustered in the A1 domain flanking regions (T1248, T1255, T1256, S1263, T1468, T1477, S1486, T1487 aa), one is present between the A2 and A3 domains (T1679 aa) and one is attached within the D4 domain (S2298 aa)[12] (Figure 1.11). A major structure of *O*-linked glycan has been determined as a di-sialylated core 1 structure known as the sialylated T-antigen[12,452,453] (Figure 1.13).

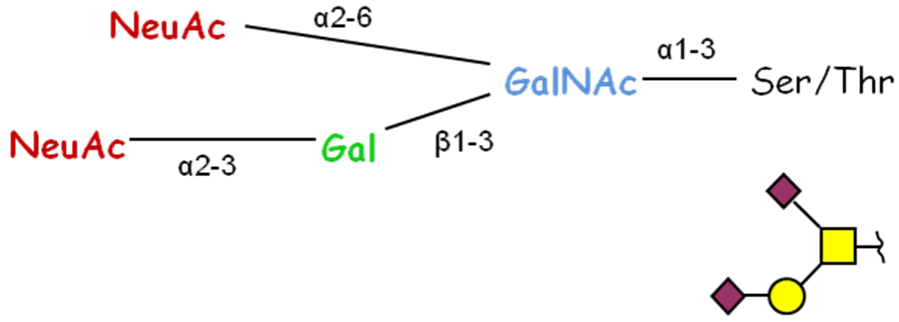


Figure 1.13 Major tetrasaccharide structure of the *O*-glycans of VWF

VWF is predicted to contain 10 *O*-linked glycan sites with the major structure to be disialyated core 1 also known as the T-antigen. Two sialic acid residues are linked to C-3 of galactosyl and C-6 of N-acetylgalactosaminitol residues. (NeuAc- N-acetylneuramic acid, GalNAc- N-acetylgalactosamine)

The VWF region containing the A domains is particularly enriched in glycan side chains. 8 of 10 *O*-linked glycans are positioned near regions designated as important for platelet binding suggesting they might be part of mechanisms regulating the exposure of the GPIbα binding site.[289] Four *O*-linked glycans are clustered in the N-terminal extension of the A1 domain which interacts with the β-finger of GPIbα, therefore the presence and composition of the *O*-linked glycans might alter the binding between VWF and GPIbα. As mentioned beforehand *O*-linked glycans can provide rigidity to a peptide backbone and stabilize otherwise flexible regions.[439] *O*-linked glycan clusters in VWF might stabilise the potentially flexible linker regions flanking the A1 domain and thus modulate A1 domain interactions. In addition interactions between the A1 and the A2 domains could be affected by glycan residues in the vicinity of these domains.

The properties of recombinant VWF lacking *O*-linked glycosylation have been previously investigated, however often with conflicting results. VWF expressed in Chinese hamster ovary cells with a defect in carbohydrate synthesis (CHO ldl-D), therefore lacking *O*-linked oligosaccharides, was shown to be synthesized, multimerised and secreted in the same way as fully glycosylated form.[454] Moreover, when devoid of *O*-linked glycans, VWF bound heparin and collagen type I with normal affinity but exhibited diminished reactivity with GPIbα, and platelet agglutination in the presence of ristocetin. However platelet binding potential was normal in the presence of botrocetin.[454]

Conversely, the isolated VWF-A1 domain expressed in COS-7 cells under *O*-glycosylation blocking conditions exhibited increased platelet aggregation potential compared to the fully glycosylated protein. Simultaneous mutation of S1253, T1255 and T1256 residues to prevent predicted *O*-linked glycosylation of these sites resulted in increase platelet aggregatory responses. However, deletion of only one *O*-linked oligosaccharide (T1468) led to decreased platelet aggregation.[455]

There are limited data regarding the correlation between VWF levels and its *O*-linked glycosylation profile. Firstly, recombinant VWF expressed under glycosylation blocking conditions displayed a reduced half-life when administered in rats. [456] More recent studies examined the association between VWF levels and the presence of the major VWF *O*-linked oligosaccharide sialylated core 1 structure (T antigen; Gal-GalNAc-Ser/Thr). To investigate that, an immunosorbent assay has been developed, in

which peanut agglutinin (PNA) binds to core 1 structure of desialylated VWF. Interestingly, an inverse nonlinear association between PNA binding and VWF plasma levels was observed, suggesting that variations in glycosylation of VWF with *O*-linked sialylated T antigen are associated with its plasma levels. In addition, a linear correlation between PNA binding and propeptide/VWF ratios has been demonstrated, suggesting a putative relationship between the extent of VWF *O*-linked glycosylation and VWF survival. Moreover, VWF released from WPBs following treatment with DDAVP, exhibited a decrease in PNA binding, implying that the *O*-linked glycosylation pattern of VWF stored in WPBs differs from VWF that circulating in plasma.[457]

1.15 Sialic acid

Sialic acids are a family of electronegatively charged monosaccharides including around 50 members, which are derivatives of neuraminic acid (Neu Neu 5-amino-3,5-dideoxy-D-*glycerol*-D-*galacto*-non-2-ulopyranosonic acid). The most common sialic acid is N-acetylneuraminic acid (NeuAc). Sialic acids are essential in higher organisms because inhibition of their biosynthesis (by inactivation of the key enzyme of sialic acid biosynthesis UDP-N-acetlyglucosamine-2-epimerse/N-acetylmannosamine kinase) during early development of mice is lethal.[458] Glycans can be terminated with the sialic acid in α2-3 and 2-6 linkage to Gal residues or α2-6 to GalNAc. Sialylation typically stops chain growth and further branching; however in some cells sialic acid polymers, where sialic acid residues are connected via α2-8 linkages are formed.[402] Three families of sialyltransferases have been identified; α3-sialyltransferse -ST3Gal, α6-sialyltransferse ST6GalNAc-I and II, and ST6GalNAc-III and IV. Sialyltransferases have various specificities towards both the acceptor glycan and the type of sialic acid linkage formed.[459] All ST3Gal enzymes can add sialic acid to Galactose residues, while ST3Gal-I and IV can sialylate the Galβ1-3 residue attached to GalNAc-Thr. ST6GalNAc acts on the GalNAc or Galβ1-3GalNAc residues.[460,461] The sialic acid-containing glycans can exhibit a dual role, as they can either shield underlying antigens, or become ligands and determinants for cell adhesion molecules like lectins or bacteria and viruses.[462] Desialylation can lead to recognition of macromolecules and cells by the complement and immune system, and targeting cells to specific sites often for degradation.[414,463] It has been recognised for a long time that removal of terminal sialic acid and exposure of Gal residues leads to increased clearance of various plasma glycoproteins and cells (ceruloplasmin, fetuin, hormones, erythrocytes, prothrombin and

bacteria.[463-466] Therefore hypersialylation is often used as a protective mechanism, as observed for bacteria.

Both the *N*- and *O*-linked glycan chains of VWF contain terminal sialic acid residues,[20,375,452] and enzymatic removal of these residues can alter glycoprotein conformation.[452] It has been shown that the removal of sialic acid from the carbohydrate chains of VWF by treatment with neuraminidase results in increased sensitivity to proteolysis by trypsin, chymotrypsin and plasmin, within the N-terminal region.[467] Therefore it clear that sialylation is important in protecting VWF against plasma serine and cysteine proteases. A different study has demonstrated that desialylation of VWF/VIII leads to decrease in ristocetin dependent platelet aggregation and facilitates its rapid clearance.[468] Even though sialic acid protects VWF from proteolytic degradation by plasma proteases it was shown it specifically enhances proteolysis by ADAMTS13.[469] Specifically, expression of α2-6 linked sialic acid, predominantly on the *N*-linked glycans appears to mediate this effect. [20,383,469]

1.16 VWF clearance, role of carbohydrates

The mechanism by which VWF is cleared from plasma is not well understood. Several parameters have been shown to influence VWF clearance such as glycosylation and a number of VWF missense mutations. For example, accelerated VWF clearance is a pathophysiological mechanism in some cases of VWD type I (VWD Vicenza). However, no dominant clearance receptors that mediate the cellular uptake of VWF have been characterised.

As pointed out before ABO blood groups greatly influence circulating VWF levels, with the group O individuals having the lowest VWF values and the mechanism underlying variation has been extensively investigated.[470] A number of studies suggest that ABO groups influence VWF survival but not its synthesis or release from endothelial cells. Firstly, the VWF propeptide to VWF antigen ratio, which is used for predicting an increase VWF clearance was shown to be significantly higher in the O than non- O subjects. In addition, the elimination half-life of VWF following DDAVP treatment was significantly shorter in individuals with blood group O when compared to non-O. [471]

Furthermore, it has been suggested that different susceptibility to ADAMTS13 proteolysis,[393] possibly mediated by the ABO antigen structures on the *N*-linked

glycans, particularly H-antigen expression[390] may be one of the reasons for variability in VWF levels between blood groups. To support this, in a study using Duch Kookier dogs with VWF deficiency, HMW VWF was demonstrated to have a longer high life than LMW VWF.[472] The opposite effect was observed in a study using rats, in which HMW VWF were shown to be cleared from circulation faster than VWF dimers.[456] On the other hand, a recent study on VWF knock-out mice model demonstrated that high and low molecular weight multimeric VWF have a similar survival.[368] and another study found no difference in the survival and clearance between the wtVWF and a proteolysis-sensitive VWF variant in the rat model.[456] Therefore, to date, no convincing difference in the clearance of intact VWF and VWF cleaved by ADAMTS13 has been shown. Furthermore, no association between ADAMTS13 levels and the survival of post-desmopressin VWF from patients with VWD type 1 or haemophilia could be detected, further implying that VWF cleavage by ADAMTS13 is not involved in its survival.[473] Finally, mice strains deficient in ADAMTS13 and/or deficient in VWF were used to look at endothelial and hepatocyte derived-VWF clearance.[474] In this study, clearance of endogenous VWF in both the wild type ADAMTS13 and ADAMTS13 deficient mice was equivalent. Moreover, VWF expressed by hepatocytes following hydrodynamic tail injection in VWF deficient mouse strain, was eliminated from the circulation at the same rate in the ADAMTS13 deficient and wild type mice.[474] These results demonstrate that ADAMTS13 proteolysis of VWF is not associated with VWF clearance, at least in an *in vivo* mice model.

In order to establish the role of various domains VWF in its clearance, a VWF knock-out mouse model has been used to examine the survival of truncated VWF variants. To begin with, studies using this animal model demonstrated that clearance rates of the recombinant A1A2A3 were comparable to FL-VWF suggesting that major receptor site for clearance could be located in the A1A2A3 domains.[368] Moreover, deletion of D'-D3 region resulted in increased VWF clearance, suggesting that this region is important in preventing VWF clearance.[368] Interestingly, mutation of R1205S localised in the D3 domain caused accelerated clearance, suggesting that this mutation abrogated the protective role of the D'D3 domains. In addition, deletion of the C-terminal D4-CK domains resulted in markedly reduced clearance, whereas simultaneous deletion of D'D3 and D4-CK regions had no effect.[368] Another study utilised the same mice model to demonstrate increased clearance of VWF with mutations of cysteine residues at

positions C1130, C1149 and C2671, further emphasizing the role of D'D3 domains in VWF clearance.[106]

O-linked glycans could also play a role in VWF clearance, since expression of VWF under *O*- glycosylation blocking conditions results in expression of VWF with a notably reduced half-life: whether the effect was due to removal of terminal residues or entire oligosaccharide remains to be established.[456]

The clearance of various plasma glycoproteins has been shown to be influenced by both, glycan chains and their terminal sialic acid residues.[464,475] Therefore it has been considered that carbohydrate status might modify VWF clearance. For example, VWF with terminal sialic acid residues enzymatically removed has been cleared more rapidly from the circulation in the rabbit model, and the clearance was inhibited by simultaneous infusion of asialo-α-1-acid glycoprotein that binds to the asialoglycoprotein-receptor (ASGPR).[468] Moreover, *in vitro* assays demonstrated that desialylated VWF was able to bind ASGPR with similar affinity to asialo-α-1-acid glycoprotein, while wt VWF showed negligible interaction with the receptor.[468] VWF with both sialic acid and then galactose residues removed was not able to bind the ASGPR, indicating that Galβ1-4GalNAc is the carbohydrate structure recognised.[476] In addition, ASGPR can also recognise glycans terminating with sialic acid α2-6 GalNAc.[477]

Sialic acid is attached to VWF by one of six sialyltransferases (ST3Gal I-VI). ST3Gal-IV and ST6Gal-I can produce α2-3 and α2-6 sialic acid linkages respectively that can block recognition of VWF by asialoglycoprotein receptors (ASGPR) that recognise exposed Gal and GalNAc residues.[476,478] Interestingly no change in PNA binding was observed in mice deficient in ST6Gal-I suggesting that this enzyme is not crucial for VWF sialylation of *O*-linked glycans.[468] Subsequently, in order to study the role of sialic acid in VWF clearance, a murine model was established in which expression of ST3Gal-IV has been inhibited, to produce VWF with decreased α2-6 sialic acid content and as result increased exposure of Gal residues. Interestingly, mice with ST3Gal-IV deficiency had the half-life of VWF reduced 2-fold and reduced VWF and platelets levels were detected.[478] This observation suggested that VWF sialic acid averts VWF clearance via ASGPR receptor. Additionally, to support this theory, in a group of patients with bleeding disorder, reduced sialylation and increased exposure of β-linked

Gal or GalNAc was observed and shown to be associated with reduced plasma VWF levels.[478] Furthermore it has been established that the RIIIS/J mice with naturally reduced plasma VWF levels, expresses N-acetylgalactosaminyltransferase in the vascular endothelial cells instead of intestinal epithelial cell as happens in normal humans and animals. Expression of this transferase resulted in modification of VWF glycan structure, with increased GalNAc presentation. This atypically glycosylated VWF was then showed to be cleared via ASGPR significantly faster than the wild type VWF. [479-482]

Several studies have investigated which routes and which types of receptors participate in the removal of VWF from the circulation. The VWF knockout mouse model has been used to investigate *in vivo* VWF clearance and identify cells that contribute to the uptake of VWF. It has been suggested that VWF binds to macrophages in both the liver and the spleen. Bound VWF is subsequently rapidly internalised and degraded suggesting that macrophages in the liver and the spleen have the capacity to remove VWF from the circulation.[483] In addition, VWF was demonstrated to be a ligand for the Ashwell receptor, which is a major lectin of hepatocytes, responsible for removal of sialo- and asialo-glycoproteins from circulation, implying that hapatocytes are also involved in the clearance of VWF.[484] Furthermore, it has been shown that Man/GlcNAc, Fuc, phosphomannosyl residues can be recognised by other carbohydrate receptors in the liver, therefore recognition via these residues could also contribute to VWF clearance.[475] Despite a great deal of circumstantial evidence, the structural basis for VWF clearance remains obscure and it is not clear which of the possible or which combination of mechanisms is most important or whether the pathological examples use these or other clearance mechanisms.

1.17 Mass spectrometry

Mass spectrometry (MS) is an analytical technique used to determine masses of particles, elemental composition of samples and to elucidate the chemical structure of molecules such as peptides or oligosaccharides. Mass spectrometers generate ions, and separate them according to their mass to charge (m/z) ratio and measure their respective abundance. They consist of three main components; an ionisation source, one or more mass analysers and a detector. In this project a matrix assisted laser desorption ionisation (MALDI) was used as a source of ionisation. Other sources are electrospray

ionisation (ESI) or electron ionisation/impact (EI). In MALDI-MS, the sample is co-crystallised with a low molecular weight matrix on a metal target and introduced into the high vacuum MALDI source. Irradiation by laser pulses induces desorption of the sample and its ionisation by proton transfer between the photo-excited matrix and the analyte. Charged molecules can then be accelerated by an electrical field and send into the analyser.

The two most common analysers are quadrupole and time-of-flight (TOF) analysers. The tandem mass spectrometry techniques (MS/MS) combine two or more analysers. In quadrupole analysers, ions are separated according to their (*m/z)* ratio using the stability of their trajectories in oscillating electrical fields. In TOF analysers, the separation and measurement of ions are based on the kinetic energy relation ($Ek = ½ mv^2$, then $m = 2Ek / v^2 = 2Ek / [dd/dt]$, where Ek is the kinetic energy, m is the mass and v the velocity of the analyte, d being the distance and t the time of flight). According to the equation when the kinetic energy as constant, ions of different mass travel through a field-free region at different velocities. Ions formed in the source are simultaneously accelerated into a linear flight tube and reach the detector after travelling a known distance. The (*m/z*) ratios are determined by based on the time it takes for ions to travel through the field-free region. In the tandem MS, the first mass analyser allows only selected (*m/z*) precursor ion to pass through and become fragmentised and then resulting fragment ions are re-analysed in the second analyser.

2 AIMS OF THESIS

The aim of this thesis is to fully characterise the role of VWF *O*-linked glycans on the function of the VWF molecule. Initially I will produce recombinant VWF *O*-linked glycan variants and determine if these have altered expression and function o using a wide range of assays. Additionally, detailed mass spectroscopy analysis will be performed to determine the nature of the *O*-linked glycans presented on recombinant VWF and how similar they are to plasma derived material. Specifically, this thesis will then focus on two important aspects of VWF biology; firstly the effect of *O*-linked glycans and their terminal sialic residues in mediating susceptibility to proteolysis by ADAMTS13 and secondly, the role that O-linked glycans play in mediating VWF interaction with platelets. To investigate the interaction of VWF with platelets I will develop a static plate binding assay to provide a reproducible measure of the interaction of VWF with GPIbα. Subsequently I will then optimise an *in vitro* flow based assay to investigate the functional role of VWF *O*-linked glycans under conditions of physiological shear stress. This assay will be used to investigate the role of *O*-linked glycans and sialic acid on the ability of VWF to capture platelets and mediate platelet translocation, and to determine kinetic parameters for the interactions such as the k_{off} and k_{on} rate constants.

3 MATERIAL AND METHODS

3.1 General molecular biology techniques

3.1.1 Site-directed mutagenesis

Mutations were introduced into VWF cDNA using the QuickChange® XL site-directed mutagenesis kit (Stratagene) in accordance with manufacturers' instructions. The polymerase chain reaction (PCR) reaction mixture consisted of 2.5U high fidelity *Pfu* ultra DNA polymerase, 125ng of complementary primers containing the desired mutation, 10ng of dsDNA template, 1X reaction buffer, 10mM dNTP's and 3µl of QuickSolution in a final volume of 50µl. The primers used in each amplification reaction are shown in Appendix A. The PCR amplification consisted of an initial denaturation (95ºC, 1 min); 18 cycles of: denaturation (95ºC, 50 sec), annealing (60ºC, 50 sec) and extension (68ºC, 1 min for 1kb); and final extension (68ºC, 7 min).

PCR products were digested with 10 U of DpnI for 1 hour at 37ºC to digest the methylated template DNA. The mutagenesis reactions were transformed into XL-10 gold cells as described in section 3.1.5.

3.1.2 Restriction endonuclease digestion of plasmid DNA

Restriction endonucleases recognise specific sequences in double stranded DNA and induce strand breaks, creating cohesive or blunt ends. Restriction digests were performed using New England Biolabs restriction enzymes and buffers. Reaction mixtures consisted of ~5ng DNA, 20U of the appropriate enzyme and buffer. The reaction mixture was than incubated at the optimum temperature for 1 hour. After cleaving the DNA, digestion products were analysed and separated with agarose gel electrophoresis (see section 3.1.4) and purified using the gel extraction kit (Qiagen, UK).

3.1.3 Ligation of plasmid vector and insert DNA

DNA ligase catalyzes the formation of a phosphodiester bond between the 5' phosphate of one strand of DNA and the 3' hydroxyl of another. Ligation reactions were carried out after both insert and vector DNA had been digested with the appropriate enzymes to generate compatible ends for cloning (see section 1.2). The standard ligation mixture contained vector and insert DNA at the ratio of 1:3, 2µl 5X ligase buffer, 0.5µl T4 DNA

ligase and sterile water to final volume of 10µl. The mixture was incubated overnight at 4°C and then used for transformation (section 3.1.5).

3.1.4 Agarose gel electrophoresis of DNA

Horizontal agarose gel electrophoresis was the technique used to separate DNA molecules depending on their size (according to the methodology of Sambrook *et al.*, 1989). To prepare a gel, agarose powder was mixed with Tris-borate-EDTA buffer (TBE- 40 mM Tris base-40nM boric acid, 1 mM EDTA, pH 8.0) to the desired concentration and then heated in a microwave oven until completely melted. The solution was cooled and SYBR™ was added to facilitate visualization of DNA after electrophoresis (final concentration in gel 5 µg/ml). Gels were then poured and allowed to polymerise for 20mins at 4°C. Samples were prepared by mixing with 6X gel loading buffer (40% (w/v) sucrose in deionised water containing 0.1% bromophenol blue) and loaded into the wells. Electrophoresis was carried out for approximately 1 hour at a constant voltage of 75V. DNA ladder molecular weight markers (NEB) were run alongside the samples in order to determine the molecular size of DNA fragments. The gel was examined on a Bio-Rad FluorS machine equipped with a UV filter to enable visualization of the DNA fragments.

3.1.5 Transformation of competent bacterial cells

20µl of competent cells [XL10-Gold ultra competent *E.coli* cells (Stratagene); NEB Turbo; One Shot®Top10 (Invitrogen)] were thawed on ice and 0.5-2µl of ligation or plasmid samples were added and then incubated on ice for 30 min. Heat shock was performed at 42ºC for 30sec and then the cells were incubated on ice for 2 min at 4ºC. 200µl SOC media (Invitrogen) was added to each transformation reaction and then incubated for 1 h at 37ºC in shaking incubator. Following this they were plated onto LB agar plates containing the appropriate antibiotic, and incubated overnight at 37ºC.

3.1.6 Isolation of plasmid DNA

Isolation of plasmid DNA was performed using; plasmid Miniprep kits (Qiagen,UK) for small scale plasmid isolation (up to 20µg DNA) and plasmid endo-free Maxiprep kits (Qiagen, UK) for large scale plasmid isolation (up to 500µg DNA), both according to manufacturers' instructions. Both kits operate on a principle of bacterial cell lysis,

followed by precipitation of denatured proteins, chromosomal DNA and cellular debris and then elution of plasmid DNA.

3.1.7 Agar Plates and Luria-Bertani (LB) Media ± Ampicillin, Kanamicin

Laura-Bertani media or agar were dissolved in distilled water according to manufacturer's instructions (Invitrogen,UK) and subsequently autoclaved. Once the temperature of the media was below 55°C, either sterilised Ampicillin or Kanamicin were added to a final concentration of 100µg/ml and 50µg/ml respectively. For agar plates, 20ml of molten LB agar was poured into a $10cm^2$ petri dish and allowed to set. LB media and LB agar was stored for a maximum of 2 weeks at 4°C.

3.1.8 Gel extraction

After electrophoresis the bands of interest were excised from agarose gels and purified using the QIAquick gel extraction kit (QIAgen, UK) as per manufactures instructions. Briefly, bands of interest were excised from the gel using a clean razor blade, weighed and solubilised with 3 volumes buffer QG for 10mins at 50°C. Subsequently 1 x volume of isopropanol was added to the dissolved bands and the sample applied to the silica-gel column and centrifuged for 1min at 13000rpm to bind DNA. Flow through was discarded and 0.5ml Buffer QG was applied to the column and centrifuged for 1min to remove traces of agarose, then the 0.75ml Buffer PE was applied to the column and centrifuged to wash the DNA. The column was centrifuged for an additional 1min to remove all traces of wash buffer. Finally, DNA was eluted by the addition of 30µl Buffer EB and centrifugation for 1min at 13000rpm

3.1.9 Cloning and expression vectors

pcDNA3.1/Myc-His (A+)

The pcDNA3.1 (Invitrogen) is a 5.5kb vector that contains the following elements: a human cytomegalovirus (CMV) and immediate-early promoter/enhancer that permits efficient, high level gene expression in mammalian cells; a multiple cloning site; pUC origin that allows high-copy number replication and growth in *E.coli*; an SV40 early promoter and origin that allows episomal replication in cells expressing SV40 large T antigen and ampicillin and neomycin resistance genes, to allow selection in *E.coli* and mammalian cells respectively.(Figure 3.1) The pcDNA vector used also contained a

myc epitope to facilitate immunodetection, and a 6xHis C-terminal tag to allow purification. However these were not needed for expression of full length VWF.

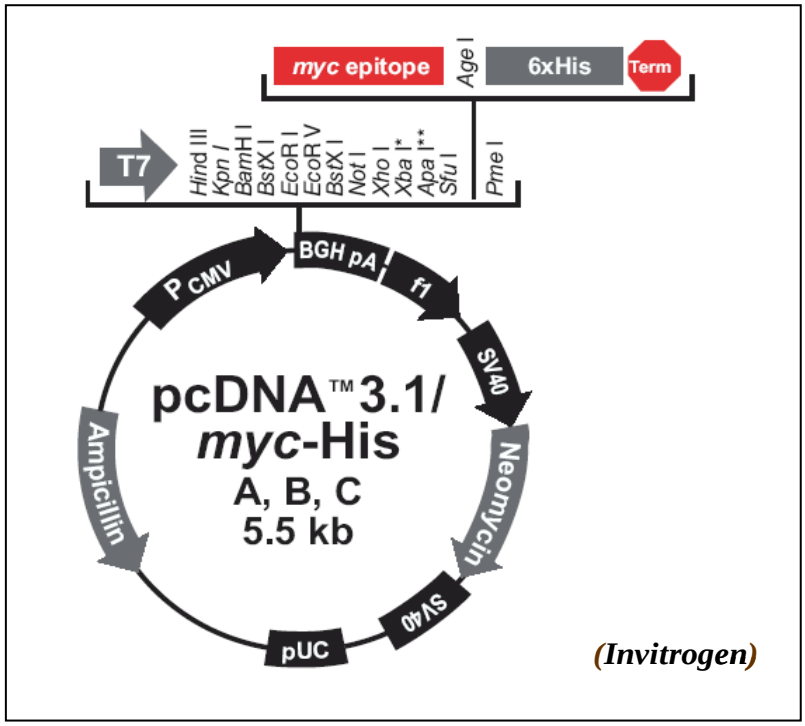


Figure 3.1 pcDNAA3.1/myc-His A(+) mammalian expression vector

pBlueScript

The pBlueScript® II SK Phagemid vector (Stratagene), is a 3 kb, high copy cloning vector. The MCS, T7 and T3 RNA polymerase promoter sequences are present in the N-terminal portion of a lacZ gene fragment (Figure 3.2). A β-galactosidase coding sequence is interrupted by the large polylinker (MCS), which allows screening for bacterial colonies that contain the desired insert because these have the lacZ gene interrupted and will appear white instead of blue. The vector also contains the pUC origin that enables high-copy number replication in *E.coli* and an ampicillin resistance gene to allow for selection.

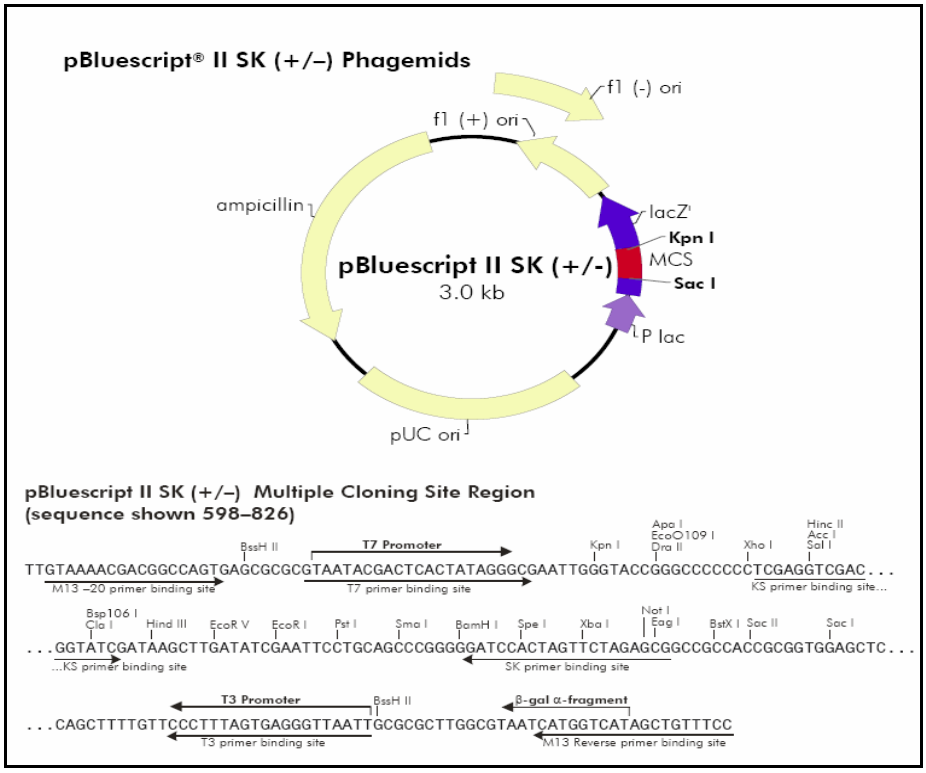


Figure 3.2pBlueScript cloning vector

pGEM-7Zf(+)

pGEM-7zf(+) (Promega) is a 3kb cloning vector that shares the same features as the pBS vector.

3.1.10 Generation of human and murine VWF glycan mutants

The ~2.kb Xho1-KpnI fragment of VWF was cloned into the 3kb cloning pGEM-7Zf(+) vector and used for site-directed mutagenesis of VWF. The XhoI-KpnI fragment contained the VWF sequence between amino acid residues 786-1584, encompassing the putative eight O-linked glycan sites T1248, T1256, T1256, S1263, T1468, T1477, S1486, T1487. This vector was therefore used to mutate the threonine or serine residues to alanine residues, to prevent glycosylation at these sites. The A2-CK fragment of VWF was cloned into the pcDNA3.1 vector and used for site directed mutagenesis of two putative O-linked glycan sites T1679 and T2298 by mutating the threonine residues to alanine residues. Ten single mutations and two cluster mutations (Cluster 1: T1248A, T1256A, T1256A, S1263A; Cluster 2: T1468A, T1477A, S1486A, T1487A) were generated using Quick QuikChange® XL site-directed mutagenesis kit (Stratagene), as described (section 3.1.1).The cluster mutants were produced by successive mutagenesis reactions. The sequence of the mutants was verified and fragments of VWF containing

mutations were subcloned into a vector containing full length VWF. Briefly pGEM (XhoI-KpnI) vector and pcDNA 3.1 with sequence coding full length VWF cloned into multiple cloning site (MCS) and with one KpnI restriction site removed, (FL-VWF^{-KpnI}) were digested with BamHI and KpnI. The digested BamHI–KpnI DNA fragment was ligated into a vector containing FL-VWF that had been digested with the same enzymes. For mutations in pcDNA3.1-A2-CK, the KpnI-AgeI fragment was digested from this vector and subcloned into pcDNA 3.1 FL-VWF^{-KpnI} that had been digested with the same enzymes.(Figure 3.3)

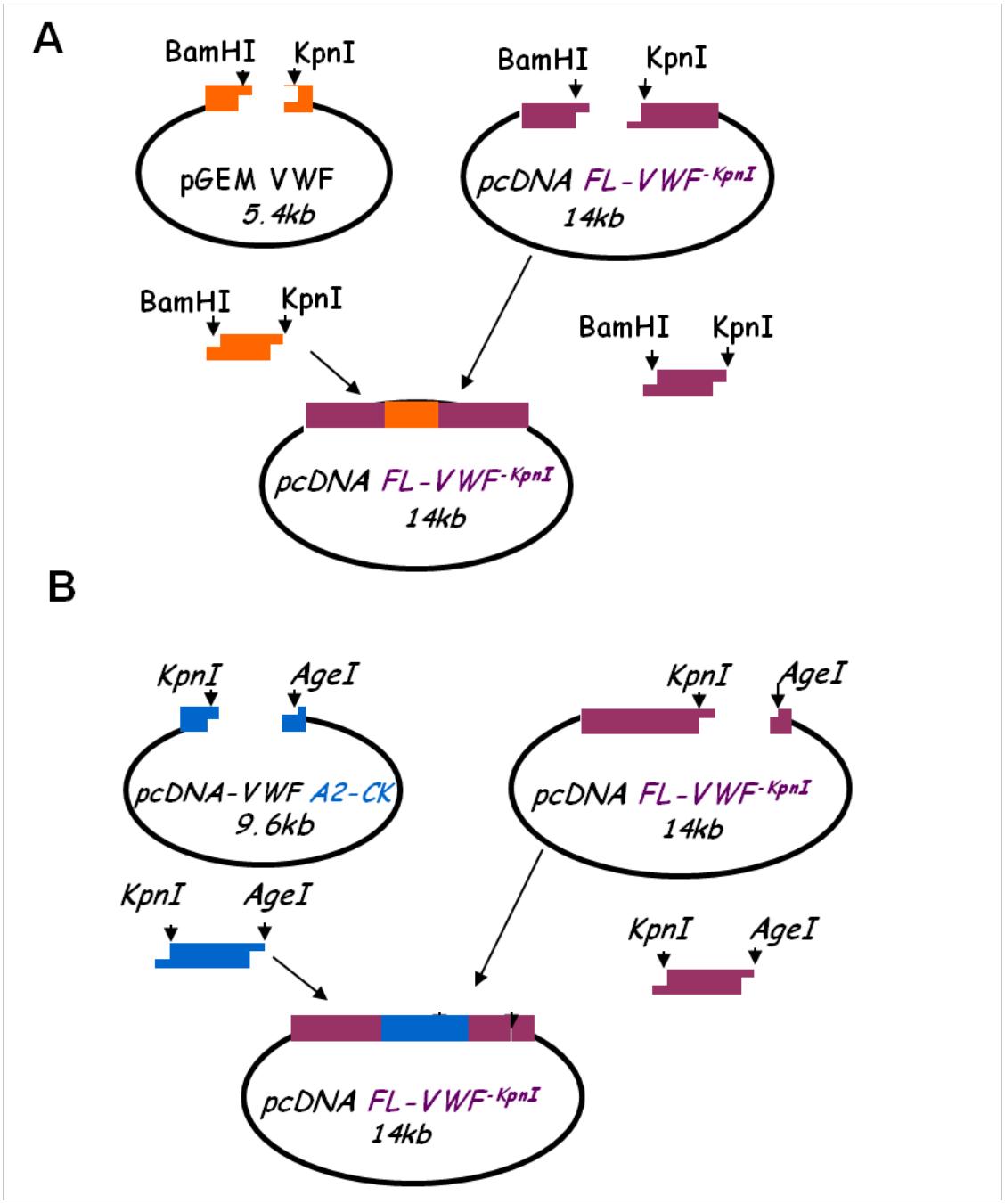


Figure 3.3 Outline of cloning steps used to generate VWF glycosylation mutants

Subcloning of mutated BamHI- KpnI fragment from pGEM VWF **(A)** or mutated KpnI-AgeI fragment from pcDNA A2-CK **(B)** into full length VWF in pcDNA FL-VWF^{-KpnI}.

3.1.11 Sequencing

All the vectors and mutations generated were verified by sequencing to ensure the absence of any unwanted PCR-introduced errors and to check the presence of mutations introduced by site-directed mutagenesis. DNA sequencing was performed at the Imperial College-MRC Genetics Core Facility using an ABI 3700 DNA analyser (Perkin-Elmer).

3.2 Cell culture

3.2.1 General Tissue Culture

All tissue culture was performed in a class II flow cabinet (FASTER BHG 2004, JENCONS-PLS) in a separate laboratory designated specifically for tissue culture. Aseptic technique was used at all times. Cells lines were grown in humidified incubators (BIOHIT, Biological Instrumentation Service, Lancashire, UK) at 37ºC, in 5% CO_2. Frozen cells were kept in a liquid nitrogen container, at a temperature around -180ºC. Cultured cells were visualised under an inverted microscope CK2 (Olympus, Japan).

3.2.2 Cell revival

HEK293T and HEK293 cells stored in 10% DMSO in liquid nitrogen were thawed at 37ºC, then placed in a T75 tissue culture flask (Nunc) with 4ml of growth media [Minimal Essential Medium (MEM) (Sigma), supplemented with 10% Fetal Bovine Serum (FBS) (Biosera), 5mM Penicillin/Streptomycin (Invitrogen), 5mM L-Glutamine (Invitrogen) and 1 x non-essential amino acids (NEAA) (Sigma).] Cells were allowed to attach for 2 hours, then the media was changed to remove residual DMSO and dead cells.

3.2.3 Cell passage

Once cells had reached 80-100% confluency they were passaged into larger culture flasks or split into more flasks. Cells were washed twice with autoclaved phosphate buffer saline (PBS) then detached from the flask surface with 0.5-1ml 0.25% trypsin/EDTA (Sigma). Trypsin was inactivated by the addition of growth media and cells seeded appropriately.

3.2.4 Transient transfection of HEK293T cells

Transient transfection is used to produce recombinant protein without integrating DNA into the cell genome. HEK293T cells express high levels of SV40 large tumour (T) antigen, which allows episomal replication of SV-40 origin-containing plasmids (i.e. pcDNA 3.1). HEK293T cells at ~70% confluency were transfected using 10mM polyethyleneimine (PEI). A control transfection was also performed using an empty pcDNA3.1 vector. 2-3µg/ml of DNA and PEI at the ratio of 2.25:1 (PEI: DNA) were diluted in sterile 150mM NaCl to a required volume. The PEI solution was then added drop-wise to the DNA solution and allowed to incubate for 20mins at room temperature. During the incubation, growth media was removed from the cells and they were washed once with sterile PBS and then Optimem conditioned medium (Invitrogen) was added. The DNA:PEI mixture was then applied to the cells and they were incubated for 3 days at 37ºC, 5% CO_2. The conditioned medium was collected, filtered and if required, concentrated using 100kDa cut off spin filters (Amicon) or a Tangential flow filtration (TFF) apparatus.

3.3 General protein techniques

3.3.1 Protein determination using the Bicinchoninic acid (BCA) assay

The Bicinchoninic acid (BCA) assay is a biochemical assay for determining the total level of protein in a solution. This method is based on the ability of proteins to reduce Cu^{+2} to Cu^{+1} (cuprous ion) in an alkaline medium. The purple-coloured reaction product is formed by the chelation of two molecules of bicinchoninic acid (BCA) with one cuprous ion. The colorimetric intensity correlates with the protein concentration. The assay was performed in flat bottomed uncoated 96 well plates. BCA reagent was prepared immediately before use by adding 1 ml cupric sulphate pentahydrate to 50ml of bicinchoninic acid. Bovine serum albumin (BSA) was used as a standard and a series of dilutions of known concentrations (range 15-2000µg/ml) were prepared. Serial dilutions of the unknown sample were prepared simultaneously. 25µl of each standard or unknown sample were applied in duplicate to the wells of a plate. 200µl of the BCA reagent were added to each well and incubated at 37°C for 30 minutes on a plate shaker. The absorbance was measured at 540 nm using a plate reader (Biotek). The protein concentration of the unknown sample was determined by reading from the BSA standard curve.

3.3.2 SDS polyacrylamide gel electrophoresis (SDS-PAGE)

Different sizes of NuPAGE Bis-Tris precast polyacrylamide gels (Invitrogen) were used to resolve proteins of different molecular weights using SDS polyacrylamide gel electrophoresis (SDS-PAGE). Samples to be analysed under non-reducing conditions were diluted with 4 X SDS loading buffer, (200mM Tris, 8%SDS, 0.4% Bromophenol blue, and 50% glycerol). Samples to be analysed under reducing conditions were diluted with the same buffer containing 4% w/v β-mercaptoethanol. A pre-stained molecular weight protein marker (Invitrogen) was run in parallel with all samples. Samples were heated for 15mins at 90ºC,and loaded onto a gel. Electrophoresis was then performed at a constant voltage of 200V for approximately 40mins.

3.3.3 Coomassie staining of SDS-PAGE gels

Following SDS-PAGE the gel was removed from the apparatus washed with ddH_2O, then placed in SimplyBlue™ SafeStain (Invitrogen, UK) for 1 h at room temperature. The background was destained with ddH_2O overnight at room temperature. Gels were dried using a gel Dryer 583 (Biorad, UK) for two hours.

3.3.4 Western Blot

Proteins were transferred from the polyacrylamide gels to nitrocellulose membranes (Amerham Pharmacia, UK) using Transfer buffer [0.2M glycine, 0.02M Tris, 20 (v/v) methanol] prepared in advance and chilled at 4˚C. Transfer was carried out for 60 min at a constant 35V. After washing in phosphate buffered saline with 0.1 % (v/v) Tween (PBST), membranes were incubated in blocking buffer containing 2.5% (w/v) non-fat milk powder in PBST for either 1 hour on a shaker at room temperature (RT) or overnight at 4ºC. They were washed 3 times for 10 min with PBST and incubated in relevant horseradish peroxidise (HRP) conjugated antibody diluted in PBST on a shaker at RT for 1 hour. Excess antibody was removed by extensive washing with PBST. If the primary antibody was not HRP conjugated the membranes were washed 3 times for 10 min in PBST and incubated with HRP-conjugated secondary antibody, diluted in PBST for 1 hour at RT. Antibodies used in this study are listed in Table 3.1.After washing, protein was detected with an ECL chemiluminescence kit (Immobilion, Milliopore). Briefly, equal amounts of solutions A and B are applied to the membrane for 5 min then the membrane is exposed to Hyper-Film (Amersham Pharmacia, UK) and developed.

Primary Antibody	Concentration	Secondary Antibody	Concentration
Rabbit polyclonal Anti-VWF-HRP (Dako)	1/1000	N/A	N/A
Mouse Anti-myc (Invitrogen)	1/5000	Goat Anti-mouse-HRP (Dako)	1/2000
Goat polyclonal anti-CD42b (SantaCruz)	1/1000	Anti-goat HRP (Dako)	1/5000
Anti-His -HRP	1/5000	N/A	N/A

Table 3.1 Primary and secondary antibodies and their concentrations used for western blotting

HRP horse-radish peroxidise

3.3.5 Purification of VWF from Haemate P®

3.3.5.1 Gel filtration

Gel filtration or size exclusion chromatography which separates proteins on the basis of size was used to remove large quantities of albumin and factor VIII and isolate high molecular weight VWF from Haemate P®. A Sepharose 2B-CL gel filtration column (Amersham Pharmacia, UK) (600mm × 26mm, 318.5ml volume) was pre-equilibrated overnight with 2 column volumes of buffer A (100mM NaCl, 20mM Tris-HCl, pH7.4). Haemate P® was resuspended in water and the sample was loaded onto a column at a flow rate of 0.7ml/min, then eluted at flow rate 1ml/min and 5ml fractions were collected. VWF concentration was determined by VWF antigen ELISA, multimeric composition was analysed by VWF multimer gels and collagen binding assay and used for functional assays or VWF containing fractions were pooled for further purification.

3.3.5.2 Heparin Sepharose affinity chromatography

VWF purification was carried out by affinity chromatography using a heparin column (Heparin-Sepharose 6 fast flow) equilibrated with 2 column volumes of a 20 mM Tris, 100 mM NaCl pH 7,4 buffer. Briefly, mixed gel filtered fractions were loaded at a flow rate of 0.4 mL/min. The column was washed until the UV_{280nm} absorbance had returned to zero. VWF was then eluted using a 20 mM Tris, 300 mM NaCl pH 7,4 buffer then dialysed into a 20 mM Tris pH 7,4 buffer for 24 h at 4ºC and quantified.

3.3.6 Purification of recombinant VWF

3.3.6.1 Ion exchange chromatography

An SK-16 chromatography column (Amersham Pharmacia, UK) was packed with 30ml of Fractogel-EMD-TMAE$^+$ (Merck) according to manufacturer's instructions. Briefly, the empty SK-16 column was washed with ddH_2O and the bottom outlet tube connected to an AKTA FPLC machine. The Fractogel resin was prepared by removing ethanol from the slurry by repeated centrifugation and washing. After decanting the last wash the slurry was resuspended in an equal volume of 300mM NaCl. The column was flushed with 20mM Tris-HCl pH 7.4, and then 35ml of Fractogel-EMD-TMAE$^+$ fast flow was poured into the column chamber with a smooth continuous motion. The remaining column space was filled with 20mM Tris-HCl, 150mM pH 7.4 and the plunger inserted into the top of the column. The Fractogel was allowed to settle for 1min, before a flow rate of 10ml/min was applied to the column for 20 min to ensure the resin was fully packed. The plunger was then pushed ~5mm into the top of the resin. The final column had a volume of 30ml and a maximum flow rate of 4ml/min. VWF expression medium was filtered through a 0.4µm filter and applied to the previously equilibrated column at a flow rate of 1.5 ml per minute. Next, the column was washed until the UV_{280nm} absorbance had returned to zero. The VWF was then eluted using 20mM Tris, 500mM NaCl, pH 7.4 and dialysed into 20mM Tris, 150mM NaCl, ph.7.4 buffer for 24 hours at 4°C quantified and further purified an a Heparin-Sepharose column.

3.3.6.2 Heparin Sepharose affinity chromatography

This was performed as described before in section 3.3.5.2

3.3.7 Nickel affinity chromatography

The recombinant protein (VWF-D'A3, ADAMTS13, and GPIbα) containing culture media was subjected to nickel affinity chromatography using Nickel charged columns that bind His-tagged proteins allowing contaminants to be removed. The media was dialysed into 20mM Tris-HCl, 500mM NaCl, 20mM imidazole, pH 7.8 and was passed over a 5ml Ni^{2+} His trap chelating column (Amersham Pharmacia, UK). The column was then washed, and bound protein eluted with 20mM Tris-HCl, 500mM NaCl, 500mM imidazole, pH 7.8 using an isocratic elution. Eluted fractions were dialysed into 20mM Tris-HCl (pH 7.8) using a 10kDa molecular weight cut-off dialysis membranes

(Pierce, UK). Protein concentration was assessed using ELISA, or BCA (section 3.3.1), purity was assessed using SDS-PAGE in 4-15% gels followed by Coomassie staining (section 3.3.2).

3.3.8 Botrocetin purification

Snake venom from *Bothrops jararaca* (Sigma) was resuspended in 20mM NaH_2PO_4, 150mM NaCl, pH 7.35 and at centrifuged to pallet debris. Supernatant was loaded on a anion exchange column-Source 15Q (GE Healthcare) previously equilibrated with 20mM NaH_2PO_4, 150mM NaCl, pH 7.35 at a flow rate of 0.5ml/min. The column was then washed and by applying a gradient of 1M NaCl in 20mM NaH_2PO_4, pH 7.35: first 150 to 400nM of NaCl for 20 min and than 40nM to 1M NaCl for 10 minutes. All fractions were collected and analysed by SDS-PAGE followed by Coomassie Blue Stain. Fractions containing botrocetin was dialysed into 20mM Tris-HCl, and amount of protein estimated using a BCA assay.

3.4 VWF Analysis

3.4.1 VWF ELISA

VWF antigen (VWF:Ag) was measured by sandwich enzyme-linked immunosorbent assay (ELISA). 96 well microtitre plates (MaxiSorp, Nunc) were coated by overnight incubation at 4˚C with 100 µl per well of rabbit polyclonal anti-human VWF antibody (Dako) diluted in 50mM sodium bicarbonate buffer, pH 9.6 to a final concentration of 7.5µg/ml. Following the incubation, the plates were washed with PBST. Next the plates were blocked for 1 hour at RT with 2.5% BSA-PBST. Following washing, wells were incubated with serial dilutions of recombinant protein and reference plasma; each dilution was assayed in duplicate. After 2 hours incubation at RT, the plate was washed to remove any unbound protein. Bound protein was detected with anti- rabbit polyclonal anti-VWF HRP diluted to a final concentration of 5µg/ml at RT for 1 hour. After a final wash step, to detect bound antibody, 180µl substrate solution (Sigma colour fast OPD tablets) was added to the wells, the reaction stopped with 50µl of 1M H_2SO_4, and the absorbance measured at 492nm using a plate reader. Concentration of VWF in each sample was determined using standard curve generated using reference plasma (VWF concentration 10µg/ml). A standard curve was generated plotting VWF concentration on the x-axis against absorbance on the y-axis. The concentration of reference plasma was taken as being 10µg/ml and diluted serially 1:10 to 1:1280.

Graphs were plotted in Microsoft Excel and the equation-of-the-line and R^2 values were calculated using the "add trendline" function. The equation-of-the-line was given in the format:

$$y = mx + c$$

Where: y is the absorbance value, m is the gradient of the slope, x is concentration of VWF y intercept. To calculate the VWF of unknown samples the equation was rearranged to:

$$x = (y - c) / m$$

Absorbance values (y) of the unknown samples were substituted into the equation and returned a VWF value. Unless stated, all VWF concentration were expressed in μg/ml.

3.4.2 VWF Multimer Analysis

The multimeric pattern of VWF may be visualised by analysis in agarose gels under non-reducing conditions. VWF multimer analysis was performed using a method optimised by Dr. McKinnon. Low resolution (0.8%) and high resolution (1.4%) agarose gels (1.5mm diameter) were prepared by dissolving respectively 0.8g and 1.4g high gelling temperature agarose (Seakem) in 100ml of gel buffer [200mM Tris, 100mM glycine, 0.1% sodium dodecyl sulphate (SDS), pH 9.0] and cast using a Bio-Rad mini-gel casting system. Samples were diluted with sample buffer (10mM Tris, 1mM EDTA, 2% SDS, 8M urea, 0.01% bromophenol blue, pH 8.0) and incubated for 30 min at 60°C. Gels were assembled in a Bio-Rad mini-gel electrophoresis tank and chilled running buffer (100mM Tris, 150mM glycine, 0.1% SDS, pH 8.4) applied to the tank placed in an ice box. 10μl of each sample was applied and electrophoretic separation performed first at 60V for 20 min and than at 35V until the tracking dye had reached the end of the gel. After electrophoresis, Western Blot and immuno-staining with HRP-conjugated polyclonal anti-human VWF antibody was performed (section 3.3.4).

3.4.3 Collagen binding assay

Collagen binding activity (VWF:CB) is recognised as a sensitive measure of high-molecular weight VWF (HMV-VWF). The highest molecular weight multimers bind collagen with the greatest affinity. VWF:CB of recombinant VWF was analysed using

an ELISA based collagen binding assay (CBA). Type III collagen prepared from human placenta by trypsin digestion (Sigma) was dissolved for 16 hours at 4°C in 0.2M acetic acid to final concentration of 0.1mg/ml. A 96 well microtitre plate was coated with 100µl per well of 0.5µg/ml collagen in 50mM sodium bicarbonate buffer, pH 9.6. Following an overnight incubation at room temperature plates were washed with PBST and blocked with 2.5% BSA-PBST for 1 hour at RT. Following washing, wells were incubated with serial dilutions of reference plasma and recombinant VWF. Each dilution was assayed in duplicate. After incubation for 2 hours at RT, wells were washed and rabbit anti-human VWF –HRP polyclonal-antibody added as described above (section 3.4.1).

3.4.4 Nanobody binding assay

The interaction between a nanobody AU/VWF a-11 and VWF was investigated using a modified ELISA based plate assay. The AU/VWFa-11 is a Llama-derived antibody fragment that recognises VWF in its active conformation. To investigate VWF binding, microtiter plates were coated overnight at 4°C with 5µg/mL AU/VWFa-11 in 50mM sodium bicarbonate buffer, pH9.6. Following washing with PBST, wells were blocked with 2.5% BSA PBST for 1 hour at room temperature. Recombinant VWF was prepared in the absence or presence of ristocetin (500µg/mL). All VWF samples were diluted in PBST to reach a concentration between 4 and 0.5nM, and 100µl of sample was loaded into each well and incubated for 1 hour at 37°C. To determine the effect of ristocetin concentration on nanobody binding, VWF at a concentration of 0.5nM was incubated with ristocetin at concentrations between 0 and 500µg/ml. After incubation, bound protein was detected with HRP-conjugated polyclonal rabbit anti-human VWF antibody as described above (section 3.4.1).

3.4.5 Plate binding assay between the bacterial A2 domain and VWF variants

The interaction between the purified bacterial VWF A2 domain (expressed in *E. coil*, kindly donated by Dr Alain Chion) and immobilised or globular VWF was investigated using a modified ELISA based plate assay. To investigate the binding of the A2 domain to immobilised VWF, microtitre plates were coated by overnight incubation at 4˚C with 100 µl per well of VWF variants diluted in 50mM sodium bicarbonate buffer, pH 9.6 to a final concentration of 1µg/ml. Following the incubation, the plates were washed with PBST. Next the plates were blocked for 1 h at RT with 2.5% BSA-PBST. Following

washing, wells were incubated with increasing concentrations of the A2 protein (0-5µm); each dilution was assayed in duplicate. After 1 hour incubation at RT, the plate was washed to remove any unbound protein. Bound protein was detected with anti-Xpress antibody (Invitrogen) diluted in 1 in 1000 at room temperature for 1 hour followed by washing and 1 hour incubation with HRP conjugated polyclonal goat anti-mouse IgG antibody (Dako). After a final wash step OPD substrate solution was added and reaction stopped with H_2SO_4 and the absorbance measured at 492nm using a plate reader.

A modified version of the assay was used to assess the binding of globular VWF to immoblised VWF-A2 domain. Briefly, the microtitre wells were coated with bacterial A2 domain at 5µg/ml. After blocking with 2.5%BSA PBST, soluble VWF (0-35nM) was added for 2 hours and bound VWF was detected using an HRP-conjugated polyclonal anti-VWF antibody as described previously.

3.4.6 Immunosorbent assay for VWF-linked T antigen–Peanut agglutinin binding (PNA) binding assay

Peanut agglutinin (PNA) is a lectin that recognises a desialylated core 1 structure of *O*-linked glycans (T-antigen) and thus can be used to determine the presence of this structure on VWF. The interaction between VWF and PNA (Dako) was investigated using a modified ELISA plate binding assay. Briefly, microtitre plates were coated with polyclonal anti-VWF antibodies at final concentration of 7.5 µg/ml diluted in 50mM sodium bicarbonate buffer, pH 9.6 overnight at incubation 4°C. Wells were then washed with PBST and blocked with 2.5 % BSA-PBST for 1 hour at RT. Following washing wells were incubated with serial dilutions of reference plasma and recombinant VWF. Each dilution was assayed in duplicate. To remove terminal sialic acid residues from oligosaccharide chains VWF samples applied to the wells were incubated in advance with the α 2-3, 6, 8 neuraminidase (from *Clostridium perfringe*ns, New England BioLabs, UK) at a final concentration of 5mU/ml, for 2 hours at 37ºC. Following incubation with VWF wells were washed and biotinylated. PNA (5µg/mL) was added in Tris buffered saline (50mM Tris, 150mM NaCl) with 0.1mM $CaCl_2$, 1mM Mg Cl_2, 1mM $MnCl_2$ and incubated for 1 hour at 37ºC. Following washing wells were incubated with HRP-conjugated streptavidin. Bound PNA was detected by measuring HRP activity using OPD as the substrate, as described previously (section 3.4.1)

3.4.7 Heparin binding

VWF binds to heparin via its A1 domain, allowing the binding between two proteins to be investigated using heparin-Sepharose^{TM}(GE Healthcare, Sweden). Firstly, Heparin-Sepharose agarose was washed with PBS. Briefly, resin was centrifuged at 800g for 5 min and supernatant discarded, PBS was then added, mixed thoroughly, centrifuged, and supernatant was discarded. Once the resin was washed 200 µl of each VWF variant diluted with PBS to a final concentration of 2µg/ml was added to 100µl of Sepharose and incubated on up an over mixer for 30 min at RT. Samples were then centrifuged at 800g for 5 min and supernatant containing unbound VWF was collected. The concentration of VWF before and after incubation with heparin-Sepharose was measured using VWF-ELISA (as described in section 3.4.1) and percentage of binding calculated for each of the variants.

3.4.8 Glycoprotein Ibα binding assay

To investigate binding between recombinant GPIbα fragment and VWF an ELISA based binding assay was optimised. 96 well microtitre plates were coated by overnight incubation at 4°C with 100µl per well of goat polyclonal antibody raised against a peptide mapping to the N-terminus of human CD42b (GPIbα). Antibody was diluted to a final concentration of 5µg/ml in 50mM sodium bicarbonate. Following washing with PBST wells were blocked with 2.5% BSA PBST for 1 hour at room temperature. Following washing, 100µl of recombinant purified GPIbα diluted in PBST at a concentration of 1µg/ml was added to each well and incubated for 1 hour at RT. VWF samples were diluted in PBST to a concentration of 1µg/mL in the absence or presence of ristocetin (0.3-1mg/ml; Helena Labs) to investigate the GPIbα binding at various ristocetin concentrations. To investigate GPIbα binding kinetics, VWF was diluted in PBST to a concentration between 5-0.125µg/ml and 1mg/ml of ristocetin was added to each sample. Samples were applied to the wells and incubated for 1 hour at 37°C. Following washing, bound protein was detected with rabbit polyclonal anti human VWF antibody (final concentration 5µg/ml in PBST) as described above (section 3.4.1). Binding curves were fitted to the one-site binding model using GraphPad Prism 4.0 software, to determine $K_{D(app)}$.

Given that two modulators; ristocetin and botrocetin, induce binding VWF-GPIbα via different mechanisms, GPIbα binding assays were also performed in the presence of botrocetin. Briefly, VWF was diluted serially in PBS starting at 5µg/ml and 4 µg/ml of

purified botrocetin was added to each sample. Samples were applied to GPIbα coated and blocked wells and plates were incubated at 37°C for 2 hours. Following washing, bound protein was detected with rabbit polyclonal anti-human VWF as described above (section 3.4.1).

3.5 ADAMTS13 analysis

3.5.1 ADAMTS13 ELISA

To determine the concentration of ADAMTS13, 96 well microtitre plates were coated by overnight incubation at 4˚C with 100 µl per well of 100ng rabbit polyclonal anti-ADAMTS13 antibody depleted of antibodies against the TSP2-4 domains, diluted in 50 mM sodium bicarbonate buffer, pH 9.6. Following the incubation, the plates were washed with PBST. Next the plates were blocked for 2 hours at RT with 2.5% BSA-PBST. Following washing wells were incubated with serial dilutions of rADAMTS13 protein and reference plasma; each dilution was assayed in duplicate. After 2 hours incubation at room temperature, the plate was washed to remove any unbound protein. Biotinylated anti-ADAMTS13 polyclonal antibody directed against TSP2-4 domains was added to each well at a final concentration of 0.1µg/ml and incubated at 37˚C for 1hour. Bound antibodies were detected by 1 hour incubation with HRP-conjugated streptavidin (at a final concentration 5µg/ml). Hence ADAMTS13 was quantitated by measuring HRP activity using OPD as the substrate. Astandard curve was plotted as described for the VWF:Ag ELISA(section 3.4.1). Reference plasma diluted 1:10 was taken to be 1µg/ml ADAMTS13.

3.5.2 ADAMTS13 activity assays under static conditions

To investigate the cleavage of FL-VWF by ADAMTS13 *in vitro,* purified (section 3.3.7) recombinant ADAMTS13 was used. VWF was unfolded into a conformation suitable for cleavage, by exposing the ADAMTS13 cleavage site in the A2 domain with urea. ADAMTS13 was activated by pre-incubation with calcium. Recombinant FL-ADAMTS13 or was preincubated without substrate at 37° C for 45 minutes in reaction mixture containing 5mM CaCl2, 150 mM NaCl and 20mM Tris-HCl (pH 7.8). Activated ADAMTS13 was then used to digest 15µg/ml of recombinant full length VWF or D'A3 VWF fragment, in the presence of 1.5M urea. Subsamples were removed at designated time points and the reaction stopped with 5mM EDTA. Full length VWF proteolysis was analysed using collagen binding (section 3.4.3) and multimer pattern

(section 3.4.2). Cleavage of D'A3 was analysed using SDS-PAGE followed by western blot (section 3.3.2&4) and detection of the. C-terminal cleavage product by immunostaining with a murine anti- *c-myc* antibody and a secondary HRP conjugated anti-mouse IgG antibody.

3.5.3 ADAMTS13 activity assays under pseudo-shear conditions

Cleavage of FL-VWF by ADAMTS13 was also investigated without the presence of denaturants but under *pseudo shear stress*. VWF at final concentration of 15µg/ml was added to preincubated ADAMTS13 at a concentration of 15nM in 20nM Tris-HCl buffer containing 0.25% BSA, 5mM $CaCl_2$, and $NaCl_2$ (total volume, 20 µL) in a 0.2mL thin walled PCR tube with domed caps (Fisherbrand). The reaction mixture was placed on a vortex at a fixed rotation rate of approximately 2500rpm. Subsamples were removed from the vortex at designated time points. The VWF proteolysis was analysed using collagen binding assay (section 3.4.3) and multimer gel electrophoresis (section3.4.2).

3.5.4 Assay of ADAMTS13 binding to extended VWF

VWF variants, 30nM each, in 50mM sodium bicarbonate buffer (pH9.6) were immobilised onto a 96-well microtitre plate by overnight incubation at 4°C. Wells were washed with PBST, and blocked with 2.5% BSA-PBST for 2 hours at RT. Following washing, increasing concentrations of purified wild-type ADAMTS13 (0-300nM) in PBST in the presence of 10mM EDTA, were applied for 2 hours at 37°C. Bound ADAMTS13 was detected as described for ADAMTS13 ELISA in section 3.5.1. Binding curves were fitted to the one-site binding model using GraphPad Prism 4.0 software, to determine $K_{D(app)}$.

3.5.5 Assay of ADAMTS13 binding to globular VWF

ADAMTS13 binding to soluble VWF was investigated using an immunoprecipitation method. Binding reactions were prepared in 0.2ml PCR tubes (Fisherbrand, UK) and contained 10µg/ml of recombinant VWF, 30nM inactive ADAMTS13 (E225Q) variant in PBS, and incubated for 30 min at 37°C. Subsequently binding reactions were incubated for 30 min on the up and over mixer with 30µl magnetic beads (Dynabeads Protein G, Invitrogen) coupled according to manufacturer's instructions to anti-VWF CK antibody diluted to 5µg/ml in PBS. The magnetic beads were separated from the

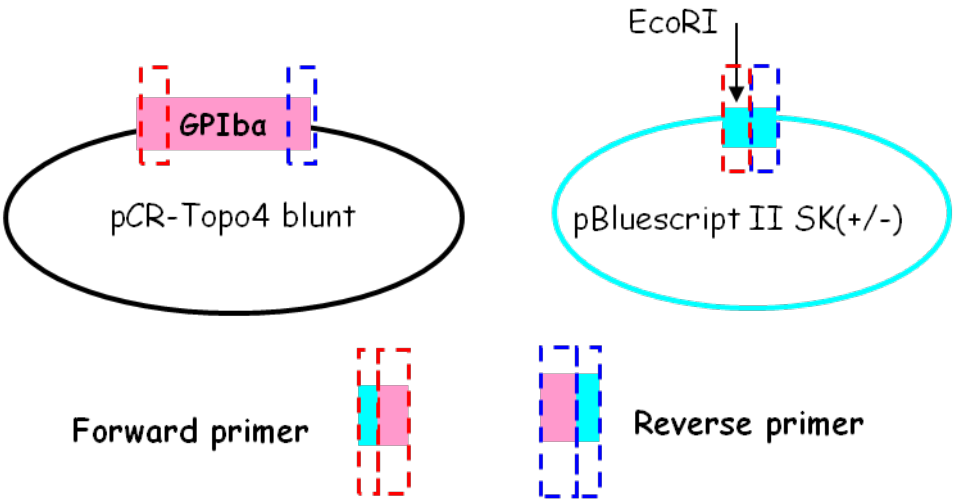
supernatant using a magnetic rack and washed with PBS. The protein coupled to beads was then eluted by heating the beads with 2x reducing buffer (200mM Tris, 8%SDS, 0.4% Bromophenol blue, and 50% glycerol, l4% w/v β-mercaptoethanol) at 60°C, for 20 minutes. Immunoprecipitated proteins were resolved SDS-PAGE, followed by western blotting, and immunostaining with polyclonal anti-VWF antibodies and anti-*c-myc* antibodies to detect ADAMTS13.

3.6 Generation of GPIbα-myc/His construct

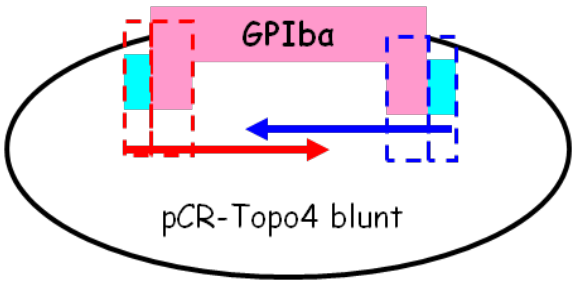
Dr Tom Mckinnon has previously established a clone of GPIbα spanning the first 290 amino acids by PCR from cDNA isolated from HUVEC lysate and reverse transcription of mRNA. This has been verified by DNA sequencing and is present in the cloning vector pCR TOPO4 flanked by EcoRI and XbaI restriction sites. GPIbα was cloned into pBluescript II SK (+/-) vector, and was than subcloned into a pcDNA3.1/ *myc*-His vector in frame with the *myc*-his tag. Briefly, the GPIbα fragment was inserted into a pBluescript II SK (+/-) vector using a site directed insertion method. The first step was amplification of GPIbα sequence (918bp) from pCR-Topo by PCR using ultra high-fidelity KOD polymerase. The PCR reaction mixture consisted 0.5µl KOD DNA polymerase, forward and reverse primers with 0.75µl of dsDNA template, 10X reaction buffer, 2.5µl dNTP's and 1.5µl of 25mM $MgSO_4$ in a final volume of 25µl. The PCR amplification consisted of an initial denaturation (95ºC, 2 min); 27 cycles of: denaturation (95°C, 20 sec), annealing (55°C, 10sec), extension (70° C, 14 sec); and final extension (70°C, 4 min). Following PCR, the reaction mixture was subjected to agarose gel electrophoresis. Amplified GPIbα sequence was purified from the agarose gel using Gel Extraction Kit and quantified on a gel. Next, PCR with Pfu Turbo DNA polymerase was used to insert the DNA fragment encoding GPIbα into the pBluescript vector. The PCR reaction mixture consisted of 1µl Pfu Turbo polymerase, 5µl dNTP's, 3µl QuickSolution, 10X reaction buffer, ~100ng pBluescript (template DNA), and 200~300ng GPIbα sequence (used as primer for this reaction) and ddH20 in the final volume of 50µl. The PCR reaction consisted of an initial denaturation (95°C, 1 min); 18 cycles of: denaturation (95°C, 30 sec), annealing (55°C, 35 sec) extension (68°C, 4 min); and final extension (68°C, 7 min). PCR products were digested with 10 U of DpnI for 1 hour at 37ºC to digest methylated template DNA that did not contain the GPIbα insert.

Following sequencing, GPIbα was subcloned into a pcDNA3.1/*myc*-His vector in frame with a *myc*-His tag. Briefly, the GPIbα sequence was excisedusing EcoRI and XbaI enzymes. This fragment was then ligated into a pcDNA3.1 containing a *myc*-His tag digested with the same enzymes. Ligation reactions were used to transform competent cells, colonies were selected plasmids DNA was isolated and sequenced. The vector containing GPIbα with the *myc*-His tag was amplified, purified and GPIbα-*myc*-His protein expressed in HEK293T as described (section 3.2.4), purified (section 3.3.7) and used for functional assays.

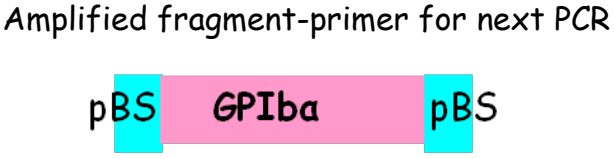
Step1. Primer design- primers for GPIbα amplification, including flanking sides for insertion into the pBluescript vector



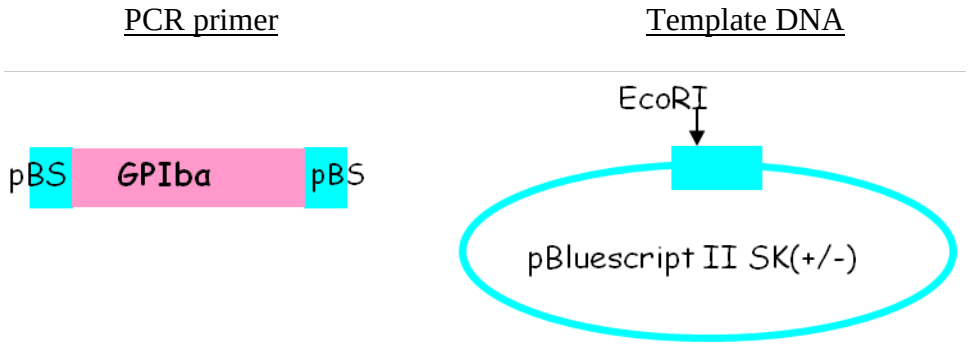
Step2. GPIbα amplification by PCR



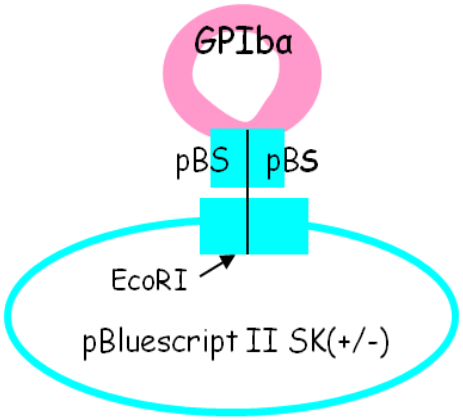
Step3. Fragment purification and quantification



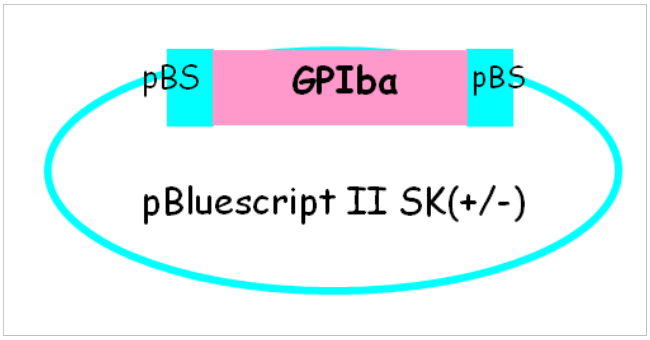
Step4. Mutagenesis to insert GPIbα fragment into pBluescript



PCR



PCR product



Step5. Subcloning EcoRI-XbaI fragment form pBluescript/GPIbα into pcDNA3.1/*myc*-His

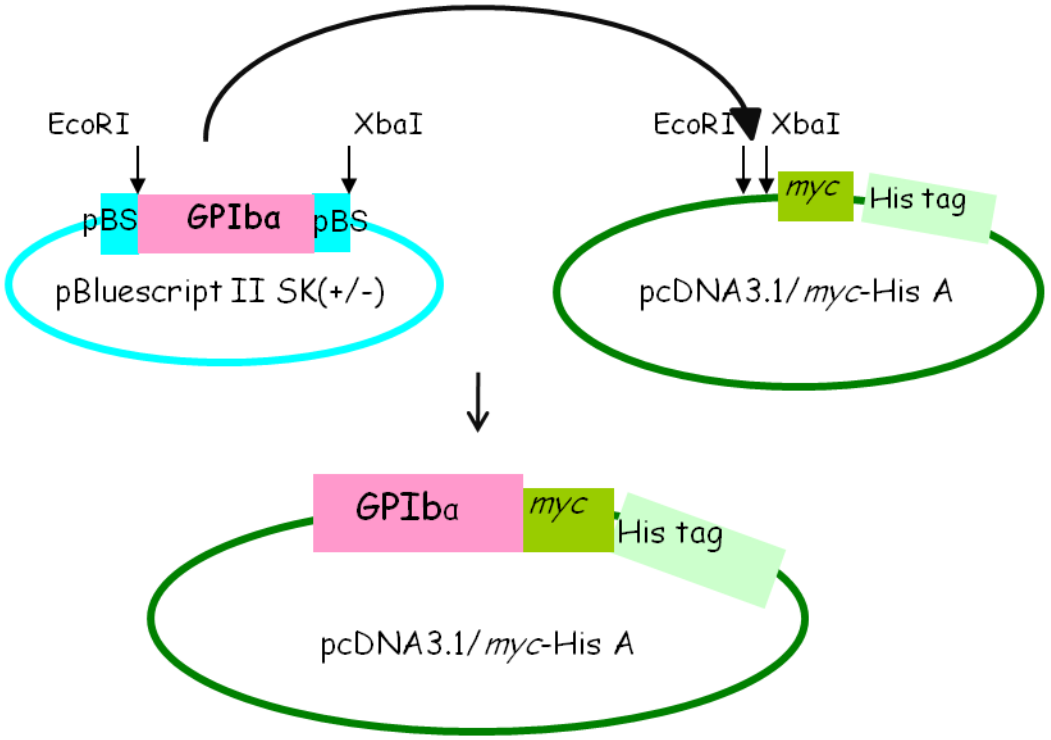


Figure 3.4 Cloning steps used to generate GPIb*α*-*myc*-His construct in expression vector

3.7 Interaction of platelets and VWF variants under conditions of flow

3.7.1 Platelets and erythrocytes isolation and labelling

Whole blood was collected from healthy donors into an anticoagulant solution; 1:6 sodium citrate (ACD; 85mM sodium citrate, 111 mM glucose, 71nM citric acid, pH 4.5). All the centrifugation steps were performed without a brake at 20-25°C, and a 10 min rest-period was taken before each spin. Moreover all used solutions were pre-warmed to room temperature. In order to eliminate potential effects of VWF and other plasma proteins in performed experiments blood cells were prepared as followed. Firstly, erythrocytes and platelet rich plasma (PRP) were separated by centrifugation at 120g for 15min. The top phase containing PRP was placed into a separate tube and 10% v/v ACD, 100mU Apyrase garde VI (Sigma) and 100nM prostaglandin E1 (PGE1; Sigma) were added to prevent platelet activation and centrifuged for 15 min at 1200g to isolate platelets. Next the platelet poor plasma in the supernatant was discarded or

stored for further analysis and the pellet containing platelets was re-suspended in 500µl of platelet wash buffer (36mM Citric acid, 5mM glucose, 5mM KCl, 1mM $MgCl_2$, 100mM NaCl, 2mM $CaCl_2$, pH 6.5) containing 100mU Apyrase, 100nM PGE1 and 3.5 mg/ml BSA. The re-suspended platelets were incubated in the dark for 15min with 4nM calcein-AM, an acetoxymethyl ester, which is fluorescent once cleaved with nonspecific esterases inside the cell. Subsequently 14 ml of wash buffer was added to the fluorescently labelled platelets; the sample was mixed by inverting the tube and centrifuged for 12 min at 1200g. Supernatant was than discarded and pelleted platelets re-suspended in HEPES/Tryodes buffer (10mM HEPES, 137mM NaCl, 2.68mM KCl, 0.42mM NaH_2PO_4 1.7mM $MgCl_2$, 11.9mM $NaHCO_3$, 5mM glucose, pH7.4) supplemented with 3.5mg/ml BSA. Red blood cells were prepared as follows. Following PRP removal 50% v/v of 0.9% saline was added to erythrocytes containing fraction, gently inverted to mix and centrifuged at 1200g for 15 minutes. The supernatant was removed and erythrocytes were re-suspended 50% v/v of 0.9% saline and centrifuged as previously described, this washing procedure was repeated two further times. After the final centrifugation, the supernatant was discarded and erythrocytes re-suspended with HEPES/Tryodes buffer supplemented with 3.5mg/ml BSA to the original starting volume of blood, to maintain a normal hematocrit and the required amount of labeled platelets were added.

3.7.2 Flow chamber and digital image processing

Plasma free blood substituted with fluorescently labelled platelets was perfused through a flow slide (Ibidi) placed on an inverted epifluorescent microscope (Olympus-CKX41). All experiments were recorded in real time using a QImaging camera (Rollera XR) and Q Capture pro software. The digitalised images were collected, processed and analysed using ImageJ software (MacMaster Biophotonics) and Virtual Dub utility. Uncoated µ-Slides as well as fitting tubing and adapters manufactured by Ibidi were used for parallel perfusion assays. Desired flow rates were achieved by adjusting the diameter of syringe and flow rate depending on a slide size according to conversion tables provided by the manufacturer. Slides were connected to a syringe pump Aladdin-1000 (World Precision Instruments) to generate a continuous laminar flow at specific wall shear rates.

3.7.3 Preparation of flow slides

The slide channels were coated with purified D'A3-VWF constructs diluted in sodium bicarbonate buffer, pH 9.6 to 30µg/ml for rolling and 2µg/ml for tethering experiments and incubated for 1 hour at RT. Subsequently the coating solution was aspirated completely and channels were rinsed carefully 3 times with PBS (10 times channel volume), and blocked for 15 min with 1.5% BSA in PBS, and washed with PBS. To compare coating efficiency with immobilised D'A3 variants, the solution containing unbound protein was recovered after coating as were three successive aliquots of PBS used to rinse the slide. The amount of each VWF variant coated was compared by calculating the difference between the total amount added for coating and that recovered in the coating and wash solutions.

To investigate VWF mediated platelet adhesion to collagen, flow slides were coated with collagen type III (Sigma). Collagen was diluted with acetic acid (25mM) to a final concentration of 5µg/ml. And applied to a flow well, and slides incubated overnight at 4°C. As described above slides were washed, blocked with 1.5% BSA in PBS and washed again before use.

3.7.4 Measurements of platelet interaction and rolling velocities in flow

To investigate the ability of VWF variants to support GPIbα dependent platelet rolling, plasma free blood substituted with platelets was passed over D'A3 VWF immobilised onto flow slides at a coating concentration sufficient to saturate the surface. The platelet count in reconstituted blood was lowered to aproximately14000 platelet per µl. Platelet attachment and translocation were analysed at a range of shear rates (125-5000s^{-1}) and movies were recorded after 4 min of flow. Subsequently movies were processed and the number of platelets that remained attached per unit area throughout 3 frames (0.15 s) was measured using Image J software. The number of adherent platelets at a given shear rate was counted for three separate experiments, at 3 fields of view for each experiment.

Rolling velocities were measured by tracking an individual platelet frame by frame at an interval of 0.05s, in the direction of flow and mean velocity was calculated by Image J. The time that one platelet spent continuously moving while mainlining contact with VWF coated surface is defined as the rolling duration, and rolling velocity was calculated by Image J from the distance that the platelet translocated during this period. For each D'A3 variant, approximately 25-40 platelets were tracked in 3 random fields

of views, and 3 separate experimental runs were completed for each flow rate. The data from all experiments was pooled, plotted and used to calculate the mean velocity and variance of velocity for each VWF variant at a range of shear rates.

3.7.5 Measurement of platelet tethering

The duration of tether bonds, the smallest unit of adhesion observable in flow was investigated for platelets and the D'A3 domains. The lowest coating concentration of D'A3 capable of supporting these brief adhesive events was determined by determining the percentage of platelets that paused but did not roll. Only one tethering event per platelet (in the field of view) was counted during the observation period. A transient tether was defined as a flowing platelet that suddenly arrested, without evidence of translocation and then resumed a velocity equivalent to that of a non-interacting platelet. The dissociation rate constants of transient tethers were calculated for coating concentrations of protein that only supported these transient tethers i.e. interaction of an individual platelet with a single VWF-A1 domain. The duration of tethers was determined by recording images at a rate of 22 frames per second and measuring a time each platelet remained bound to the surface at a given shear rate. The dissociation rate constants were then determined by plotting the natural log of the number of platelets that interacted as a function of time after the initiation of tethering. For first-order dissociation kinetics, the resultant plot is a straight line, and the slope of the line = $-k_{off}$

The video data was analysed using Virtual Dub utility. On average, 150 tethering events were measured to determine k_{off} in each independent experimental run. In addition, the number of transient tethering events per 5s was calculated for each variant, at a range of shear rates. Measurements were taken at 3 random fields of view on three separate occasions.

3.7.6 Measurement of platelet binding by VWF bound to collagen

The interaction between platelets and full length VWF mutants bound to collagen was investigated as follows. Plasma free blood substituted with full count of washed labelled platelets and recombinant VWF variants, at final concentration of 10µg/ml was perfused over collagen coated slides for 5 minutes at a shear rate of $1500s^{-1}$. Short movies (1s) were recorded every 30 seconds of flow, and experiment was repeated 3 times on separate occasions. The number of accumulated platelets at each time point assessed as surface coverage (%) was measured using Image J programme.

3.8 Statistical analysis

Analysis of data was performed using the Prism software package (GraphPad {Prism version 4.0 Software for Science, San Diego,USA. All data are expressed as mean with SD. Data were analysed using a t-test and analysis of variance (ANOVA). P values ≤ 0.05 were considered significant.

3.9 Mass spectrometry techniques

3.9.1 Reductive elimination

O-linked glycans were released from PNGase F digested VWF glycopeptides by reductive elimination. Firstly samples were incubated with 55 mg/ml potassium borohydrate (KBH_4) and 0.1M potassium hydroxide solution for 24 hours at 45°C. The reaction was stopped by drop-wise addition of glacial acetic acid. Released *O*-linked glycans were purified via an ion-exchange 50W-X8 Dowex® column previously equilibrated in 5% (v/v) acetic acid. Samples were eluted with 5% (v/v) acetic acid and dried using a Savant Speed-Vac. Surplus borates from the reductive elimination were eliminated by successive co-evaporations using 10% (v/v) acetic acid in methanol solution and dried under a stream of nitrogen and lyophilised.

3.9.2 Chemical derivatisation-permethylation

O-linked glycans were permethylated using a sodium hydroxide procedure on purified and lyophilised glycans. Briefly, sodium hydroxide pellets were crushed with dimethyl sulfoxide to form a slurry which was then added to glycans with 1mL of methyl iodide. The mixture was vigorously mixed on an automatic shaker for 10 min at RT. and the reaction was stopped by addition of water. Permethylated glycans were recovered by chloroform extraction and washed several times with water, and chloroform was evaporated under a stream of nitrogen.

Permethylated glycans were subsequently purified using a reverse-phase C_{18} Sep-Pak column. The Sep-Pak cartridge was attached to a glass syringe and conditioned successively with methanol (5ml), water (5ml), acetonitrile (5ml), and water (3x5ml). The sample was dissolved in 1:1 (v/v) methanol/ water, loaded onto the cartridge, washed with water and eluted with 3ml of 15%, 35%, 50% and 75% (v:v) aqueous acetonitrile solution. The organic solvent was removed by on a Savant Speed-Vac and samples were lyophilised.

3.9.3 MALDI-MS and MS analysis

Matrix assisted laser desorption ionisation MS (MALDI-MS) and MS/MS data on permethylated samples was acquired in a reflector positive ion mode using a 4800 MALDI-time-of-flight (TOF) TOF/TOF (Applied biosystems) mass spectrometer. The instrument was calibrated using the 4700 calibration standard, calmix, as the external calibrant for the MS mode and human [Glu1]-fibrinopeptide G was used as the external calibrant for the MS/MS mode. The collision energy was set to 1 kV, and argon was used as collision gas. Samples were dissolved in 20µl of methanol, and 1 µl was mixed at a 1:1 ratio (v/v) with 2,5-dihydrobenzoic acid (20 mg/ml)1 in 50% (v/v) methanol in water) as the matrix. Data was acquired using 4000 Series Explorer Instrument Control Software and were processed using Data Explorer MS processing software. MS/MS spectra were assigned and annotated with the help of the GlycoWorkbench tool.[485]

3.9.4 Data analysis

The mass of the glycans was determined based on the monoisotopic from of each monosaccharidic constituent (Table 3.2). The reducing and non-reducing extremities of the glycan (e.g a molecule of water and the replacement of two hydrogens by methyl group) and the addition of a sodium atom have to be considered when calculating the mass of permethylated glycan.

Family	Monosaccharide examples	Monoisotopic mass (Da)	
		Native	Permethylated
Hexose	Glucose, galactose, mannose	162	204
Hexosamine	N-acetylglucosamine, N-actylgalactosamine	203	245
Sialic acid	N-acetylneuraminic acid	291	361
Deoxy-hexose	fucose	146	174

Table 3.2 Native and permethylated masses of common monosaccharide constituents of glycans

4 ANALYSIS OF VWF *O*-LINKED GLYCAN STRUCTURE

4.1 Introduction

A significant proportion, ~20%, of the molecular weight of VWF is comprised of *N*- and *O*-linked glycan chains. Based on the primary amino acid sequence and the original sequencing of the VWF protein, VWF contains 16 *N*-linked and 10 *O*-linked glycosylation sites.

An analysis of the *N*-linked glycan structures of VWF was first performed by Matsui *et al* on de-sialyated fragments using chemical techniques.[20] A more detailed mass spectrometric study was recently performed on *N*-linked glycans released from plasma derived VWF by digestion with PNGase F (unpublished data by Dr. K. Canis). Firstly, an additional thirteenth *N*-linked glycosylation site suggested to be unoccupied by Titani, was found to be consistently glycosylated. From these studies, it has been demonstrated that the VWF *N*-linked glycome comprises a large variety of structures (at least 300 distinct structures), the majority of which are multi-antennary complex glycans, with bi-antennary structures being the most common (~80%). Moreover, most structures terminated in sialic acid or fucose residues. In agreement with previous studies the ABH blood group antigens were detected. Interestingly a proportion of the VWF *N*-linked glycan population was shown to have sulphate groups, which are important for recognition in other proteins. VWF *N*-linked glycans have been studied extensively, whilst *O*-linked glycan function is still poorly characterised and a detailed study regarding the VWF *O*-glycome composition was only recently published.[486] It has been demonstrated that the pdVWF *O*-glycome encompasses a heterogeneous population of 18 structures. Both the core 1 and core 2 structures were identified, with the core 1 family being the most abundant. The majority of the structures were sialylated and the di-sialyl core 1 accounted for about 75% of the overall population in accordance with previous studies.[452,486] Interestingly a proportion of core 1 structures (~40%) contained one or two disialosyl motifs; that is two sialic acid residues linked via an α2-8 linkage (NeuAcα$_{2\text{-}8}$NeuAc). In addition, some core 1 structures were show to carry atypical N-glycolylneuraminic acid residues. Strikingly, the majority of core 2 structures were shown to carry ABH blood group antigens (~1% of the *O*-linked glycom). Therefore it can be suggested that similarly to *N*-glycans, *O*-linked glycans, by carrying ABO blood group antigens, could have an influence on VWF plasma levels.[390,392,470]

The pdVWF glycome has been characterised, however no information regarding the structure and composition of *O*-linked glycans of recombinant VWF is available. Since in this project rVWF expressed in non-endothelial cell line was used to study the function of *O*-linked sugars, it was necessary to characterise its *O*-linked glycom and compare it to that of pdVWF.

To begin with the glycan structure of VWF, the primary VWF protein sequence was analysed using neural network algorithms to predict the probability of potential glycosylation sites being occupied. Furthermore, parts of the human VWF protein sequence were aligned with the VWF sequence of other species and with other proteins sharing homologous domains.

Importantly a purification method of rVWF was optimised. Finally purified VWF expressed in HEK293T cells was sequenced and analysed by state-of-the art Mass Spectrometry methods previously optimised for pdVWF.

4.2 In silico analysis of VWF

4.2.1 Sequence alignment of the VWF-A1 domain flanking regions

In order to elucidate whether O-linked glycans are functionally important to VWF, I decided to examine if the sequences that enclose them are conserved across species. To investigate if the *O*-glycosylation sites are conserved, a protein sequence alignment was performed to align the sequences of linker region between the D3-A1 domains and A1-A2 domains of human VWF against other species with known VWF A1 domain flanking sequences. Sequences were obtained from the Swiss-Prot protein database,

(http://www.expasy.org/cgi-bin/sprot-search- de?von%20willebrand%20factor)

and were aligned using AliBee Multiple Alignment (available at: http://www.genebee.msu.su/services/malign_reduced.html)

Both linker regions flanking the A1 domain appear to be conserved. In the D3-A1 linker region the three *O*-glycosylation sites: T1248, T1255, T1256 are highly conserved throughout the species analysed. Interestingly, the S1263 site is not conserved with all the species analysed, with the exception of the Indian elephant, having a proline residue instead of a serine at position 1263. However, in these species, there is a threonine residue at position 1262 which could potentially be glycosylated. The A1-A2 linker

region contains another cluster of 4 *O*-linked glycan chains in human VWF. The *O*-glycosylation sites T1468 and T1477 are highly conserved, whilst the sites S1486 and T1487 appear to be less conserved amongst organisms. (Figure 4.1b) The high conservation of *O*-linked glycosylation sites could suggest their functional importance.

Next page-

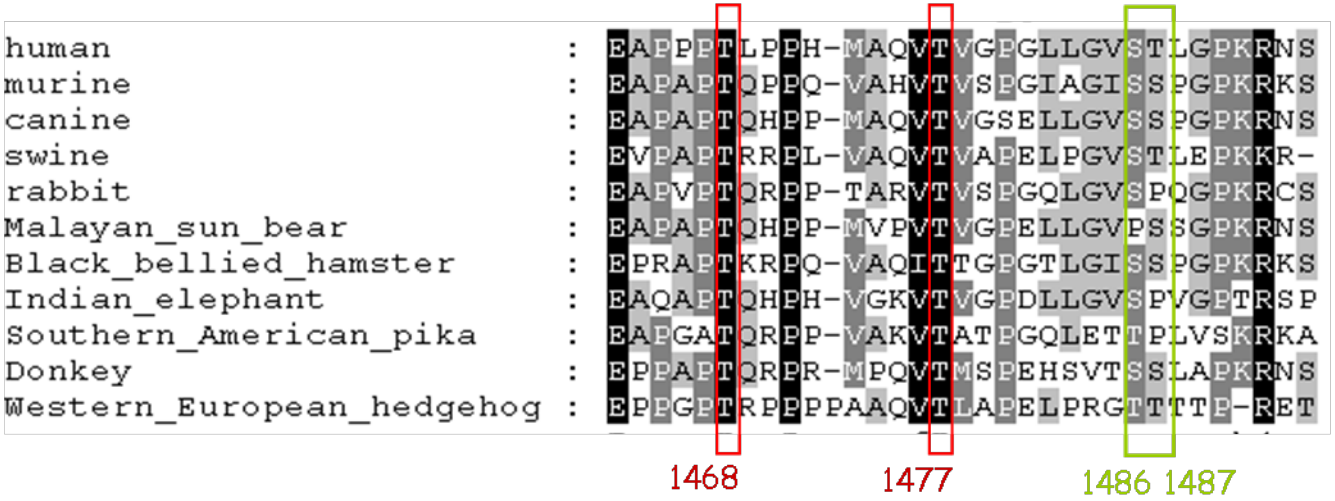
Figure 4.1 Protein sequence alignment of the VWF A1domain linker regions from various species

The amino acid sequence of the VWF A1domain flanking regions from 10 different species was aligned using a protein sequence alignment programme. **(A)** Illustration of sequences of the D3-A1 linker region. The human VWF *O*-linked glycosylation sites T1248, T1255, T1256 are conserved among other species (red boxes). The S1263 residue is present only in the Indian elephant, other organisms have a proline in this position (green box). However in those organisms the position 1262 is occupied by threonine (arrow). **(B)** Illustration of sequences of the A1-A2 linker region. The human VWF *O*-linked glycosylation sites T1468 and T1477 are highly conserved (red boxes). The S1486 and T1487 are conserved in majority of species (green box).

A


human : EPGGLVVPPTDAPVSPTTLYVEDISPPPLHDFYCSRLLDL
murine : EPGGLVAPPTDAPVSSTTPYVEDTPPPPLHNFYCSKLLDL
canine : EPGSLVVPPTEGPIGSTTSYVEDTPPPPLHDFHCSRLLDL
swine : EP----VPPTEGPVSPTTPYEEDTPPPPLHDFFCSKLLDL
rabbit : EPGGMVVPPTDAPVRSTTPYMEDTPPPPLHDFYWSNLMDL
Malayan_sun_bear : ----------
Black_bellied_hamster : ----------
Indian_elephant : RPGELVPPSTVAPVSVTTPFVEDISPPPLXDLYCSKLLDL
Southern_American_pika : EPGGLVVPPTDVPARPTTPYVEDTPPPPLHNFYCSKLLDL
Donkey : ----LEVPPTEGPVGPTTXYVEDTPPPPLHDFYCSKLLDL
Western_European_hedgehog : ----------
1248
1255 1256
1263

B


human : EAPPPTLPPH-MAQVTVGPGLLGVSTLGPKRNS
murine : EAPAPTQPPQ-VAHVTVSPGIAGISSPGPKRKS
canine : EAPAPTQHPP-MAQVTVGSELLGVSSPGPKRNS
swine : EVPAPTRRPL-VAQVTVAPELPGVSTLEPKKR-
rabbit : EAPVPTQRPP-TARVTVSPGQLGVSPQGPKRCS
Malayan_sun_bear : EAPAPTQHPP-MVPVTVGPELLGVPSSGPKRNS
Black_bellied_hamster : EPRAPTKRPQ-VAQITTGPGTLGISSPGPKRKS
Indian_elephant : EAQAPTQHPH-VGKVTVGPDLLGVSPVGPTRSP
Southern_American_pika : EAPGATQRPP-VAKVTATPGQLETTPLVSKRKA
Donkey : EPPAPTQRPR-MPQVTMSPEHSVTSSLAPKRNS
Western_European_hedgehog : EPPGPTRPPPPAAQVTLAPELPRGTTTTP-RET
1468
1477
1486 1487

4.3 Experimental analysis of VWF *O*-linked glycans structure

4.3.1 Purification of VWF from Haemate P

To determine the *O*-linked glycome of both plasma derived and recombinant VWF (rVWF), high purity VWF was required. Plasma derived VWF was purified from a commercial VWF-FVIII concentrate: Haemate P. Haemate P has been shown to contain a high proportion of high molecular weight multimers and has a multimer pattern resembling normal human plasma.[487,488] Lyophilised Haemate P was re-suspended in ddH_2O, then gel filtered through a Sephacryl 400 gel filtration column and 5ml fractions were collected. Protein began to elute from the column typically at fraction A10 (Figure 4.2a). Early eluted fractions and selected later fractions were analysed by SDS-PAGE under reducing conditions followed by Coomassie staining. Fractions A10-B3 demonstrated a major 250kDa band, consistent with monomeric VWF (Figure 4.2b). To remove contaminating proteins and to concentrate the VWF samples, fractions A10-B3 were pooled and further purified using Heparin-Sepharose affinity chromatography. Purified, fully multimeric pdVWF was used as a control in the MS studies and was also used in several other assays described throughout this thesis.

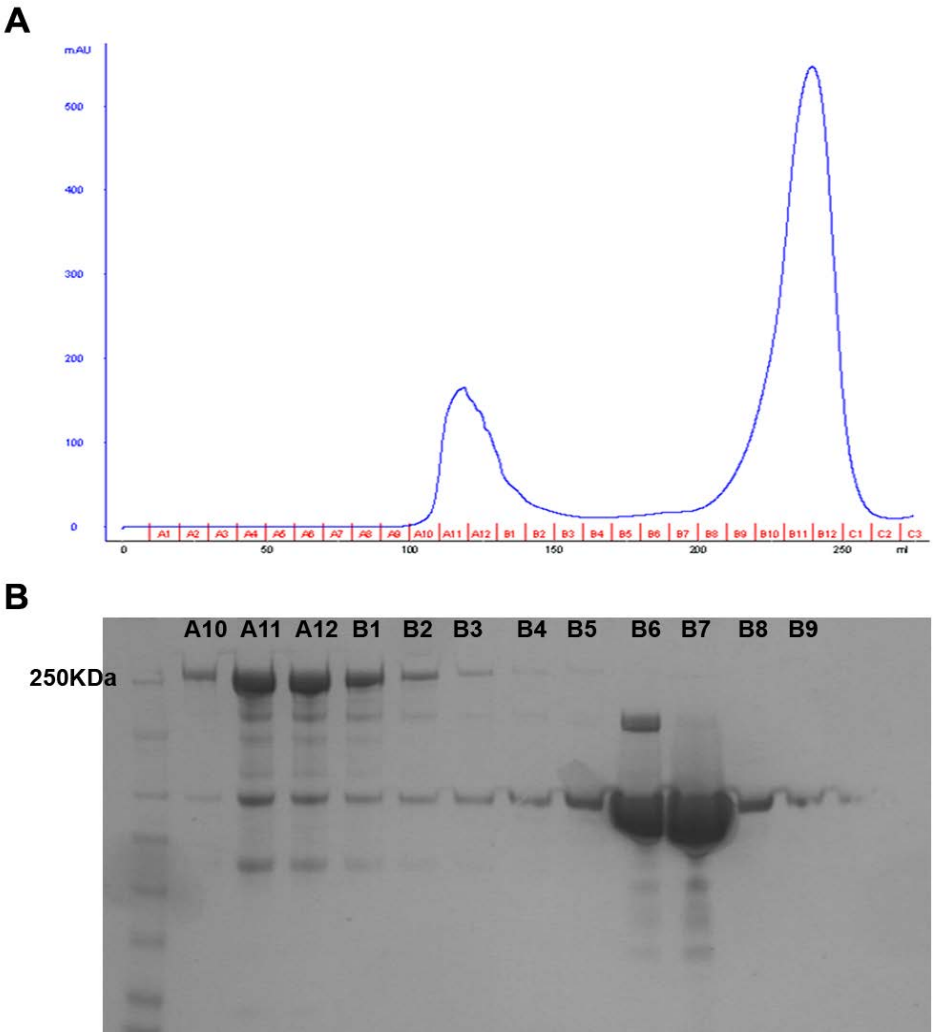


Figure 4.2 Gel filtration of Haemate P

Haemate P was gel filtered through a Sephacryl 400 gel filtration column and 5ml fractions were collected. (A) As demonstrated on chromatogram protein began to elute from the column typically at fraction A10 (**B**) Early eluted fractions and selected later fractions were analysed using reducing SDS-PAGE followed by Coomassie staining. Fractions B6-D12, contained a major 250kDa band corresponding to a monomeric VWF, were pooled and VWF was further purified by Heparin-Sepharose chromatography.

4.3.2 Purification of recombinant VWF

In order to analyse the glycan content of rVWF, large scale transient transfections of HEK293T cells were performed. Approximately 250ml of expression media was collected and filtered and VWF purified by ion exchange chromatography using a previously equilibrated Fractogel-EMD-TMAE+ column. VWF was eluted with 500mM NaCl (Figure 4.3) and all fractions were collected and analysed by SDS-PAGE

under reducing conditions followed by Coomassie staining. The elution fraction contained a band of ~250kDa corresponding to monomeric VWF, however other proteins were still present (Figure 4.4b, lane 1). Some of the bands were detected with ant-VWF antibody, suggesting they correspond to VWF degradation product. To remove contaminating proteins the elution fraction was therefore dialysed against 20mM Tris and further purified using Heparin-Sepharose affinity chromatography (Figure 4.4a). Bound protein was eluted using 500mM NaCl. Gel filtered pdVWF was purified via Heparin affinity chromatography in the same way. Purity of the eluted material was analysed using SDS-PAGE under reducing conditions, followed by Coomassie staining while the multimeric pattern was determined by agarose multimer gel electrophoresis, and the concentration determined by VWF-ELISA. As illustrated on Figure 4.4b (lane 2) a single ~250kDa, band consistent with monomeric VWF, was present in the eluted fraction, indicating a high level of purity. Moreover purified VWF exhibited a normal multimeric pattern, when compared to the non-purified material (Figure 4.4c). The typical VWF recovery after the first purification was 85-90% and 44% after the second.

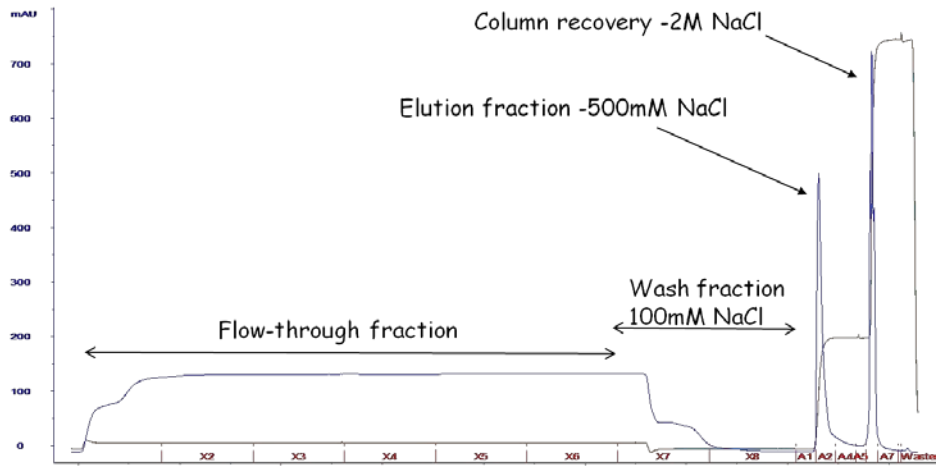


Figure 4.3 FPLC purification of rVWF by ion exchange chromatography

A representative chromatogram of a typical rVWF purification using an ion exchange chromatography. Filtered condition media was loaded onto a Fractogel column. Some proteins pass through the column and did not bind (flow through fraction). Column was washed extensively with 100mM NaCl/20mM Tris to ensure that majority of contaminant proteins were removed from the column with (wash fraction) prior to elution with 500mM NaCl/20mM Tris. Column was recovered with 2M NaCl.

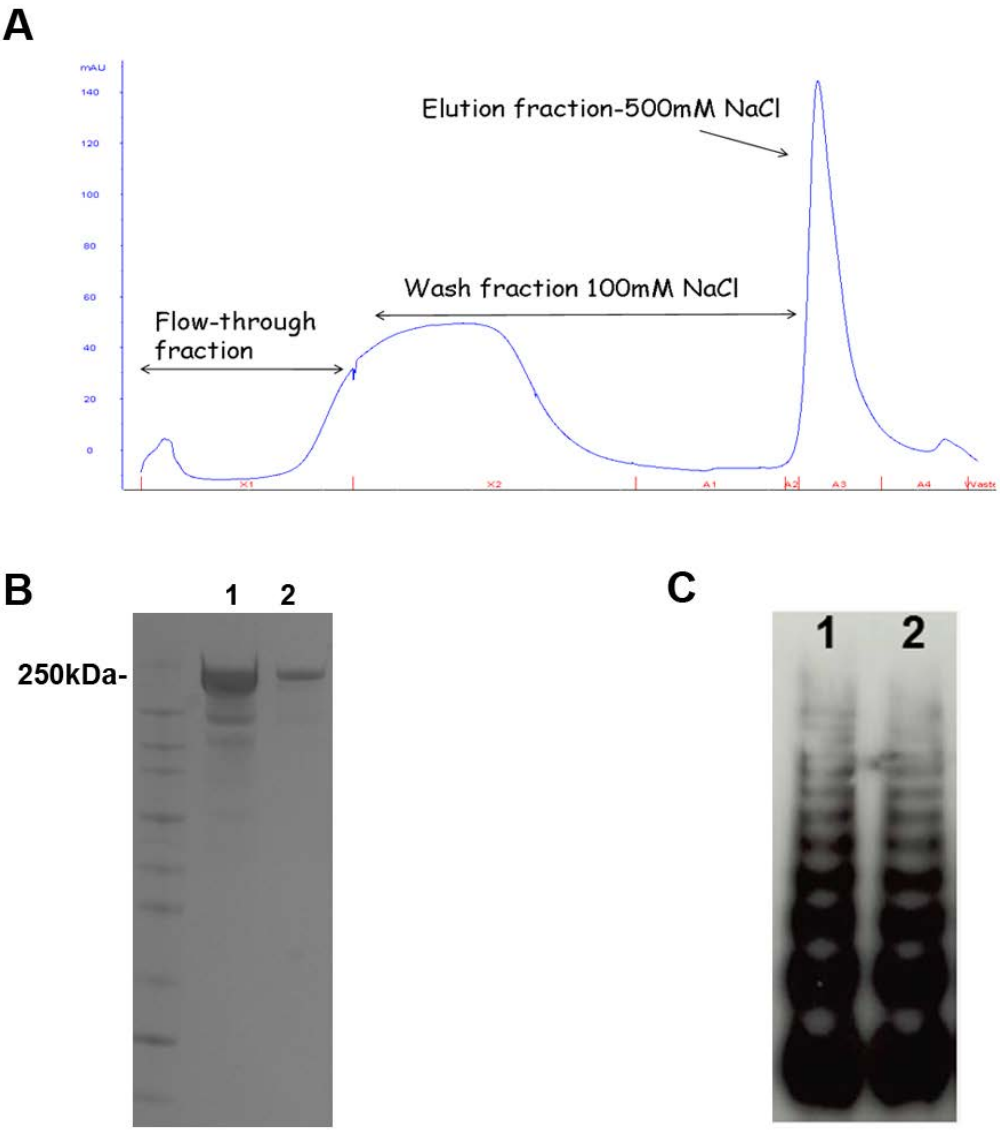


Figure 4.4 Purification of rVWF by heparin affinity chromatography

(**A**) A representative chromatogram of a typical rVWF purification using a Heparin-Sepharose column. Dialysed elution fraction from the ion-exchange chromatography was passed through a column, which was then washed with 100mM NaCl/ 20mM Tris and bound protein was eluted with 500mM NaCl. (**B**) The elution fraction was analysed for purity by reducing SDS-PAGE followed by Coomassie staining. As illustrated only one band of 250 kDa corresponding to monomeric VWF was detected (lane 2) which is in contrast to elution fraction from ion-exchange purification only (lane 1) which had additional bands present. (**C**) Multimeric pattern was determined using a VWF multimer analysis. Purified VWF (lane 2) has comparable multimeric composition as VWF from expression media (lane 1).

4.3.3 *O*-glycome profile of rVWF

State-of-the-art mass spectrometry was used to determine the *O*-linked glycan structures present on purified rVWF. Initially, rVWF purity was further assessed using a mass spectrometry (MS) based proteomic technique by Dr. K. Canis using an off-line nano-LC MALDI-TOF/TOF and data interrogated using the MASCOT program. This analysis confirmed a high level of purity with only trace levels of contaminating peptides present.

The approach used to characterise the rVWF *O*-glycom is illustrated on Figure 4.5 and had been previously optimised for pdVWF.[486] Briefly, VWF was subject to a reduction and carboxymethylated and was then digested with trypsin. Next the *N*-linked glycans were release by incubation with PNGase F and separated from the peptides and *O*-glycopeptides by reverse phase chromatography. (These experiments were performed by Dr. Canis) The *O*-linked glycans were then released from the post-PNGase F glycopeptides by reductive elimination. They were subsequently purified by ion-exchange chromatography, permethylated and purified using a reverse-phase chromatography. The *O*-glycans were finally subject to the matrix-assisted laser desorption and ionization-time of flight (MALDI-TOF) profiling.

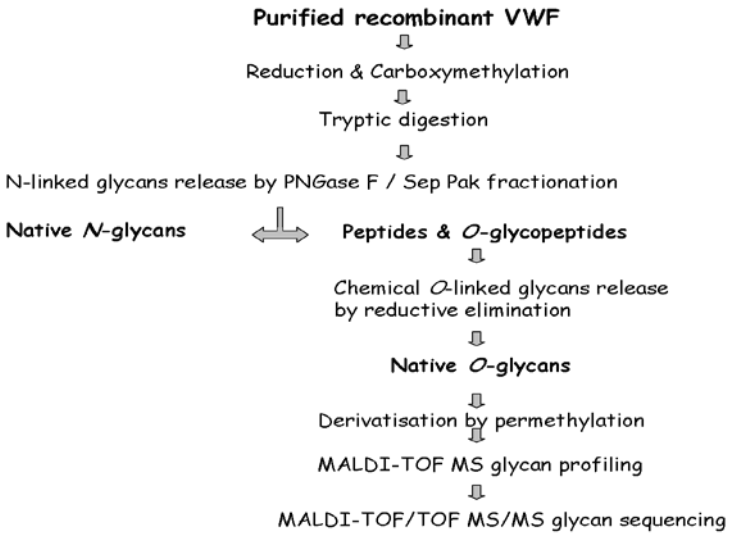


Figure 4.5 Schematic representation of glycomic strategy used to describe VWF *O*-linked glycome

Protocols I have performed are described in Material and Methods section.

As demonstrated on Figure 4.6 six relevant molecular ions were identified, including both core 1 and core 2 moieties, with the core 1 structure being the most abundant. The majority of structures appeared sialylated. Moreover, the major signal corresponded to a di-sialylated core 1 moiety ($HexNAc_1$ $HexNeuAc_2$; *m/z* 1256) but mono (*m/z* 895, 1286) species were also present. Strikingly an uncommon tri-sialylated core 1 structure was also detected (*m/z* 1617). This structure carries a disialosyl group in which two sialic acids are linked together. In addition, a monosialylated core 1 structure and core 2 structures with an unusual sugar N-glycolylneuraminic acid were detected (*m/z* 1286 and *m/z* 1736 respectively). All VWF *O*-linked glycans appear to be processed, as core 1 and core 2 precursors ($Hex_1HexNAc_1$ and $Hex_1HexNeuAc_2$) were not detected.

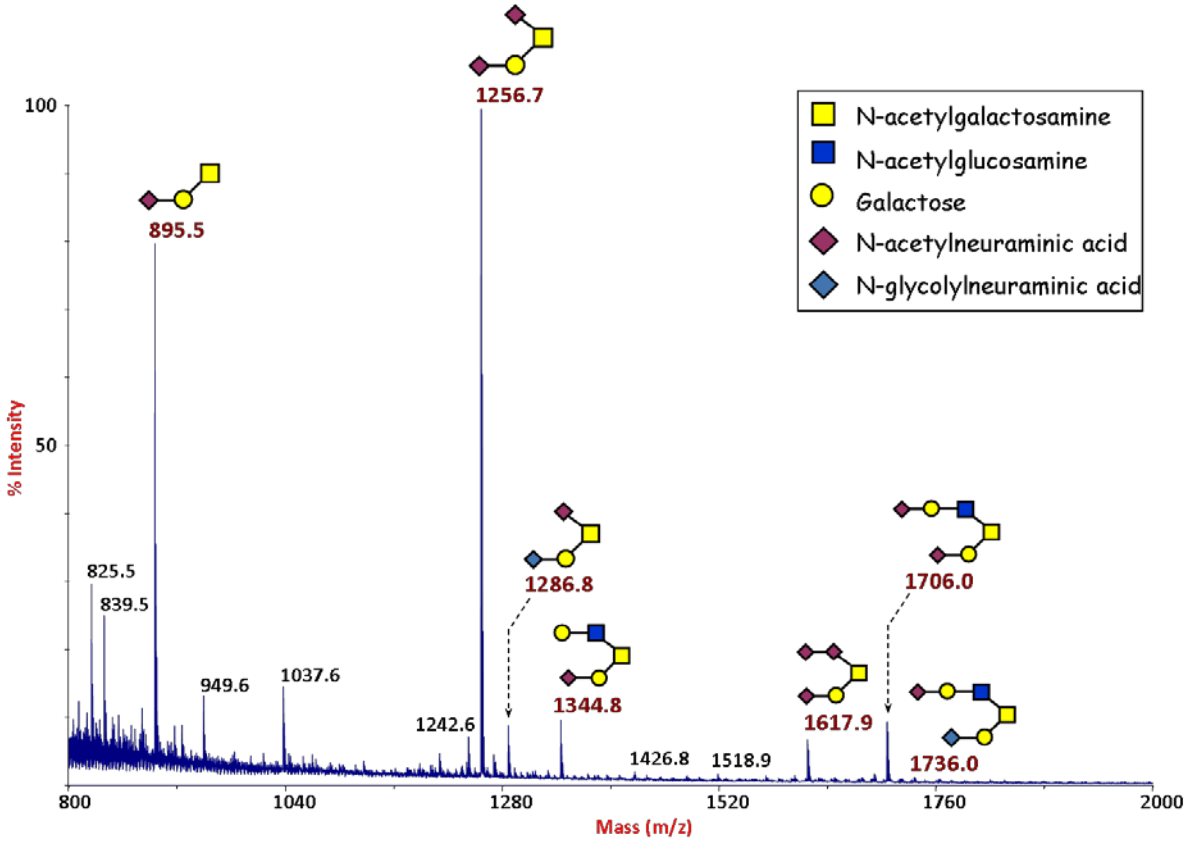


Figure 4.6 MALDI-TOF mass spectrum of permethylated VWF *O*-linked glycans

MALDI-TOF analysis showed VWF *O*-linked glycans contain both core 1 and core 2 structures. The profile is dominated by sialylated core 1 structures (*m/z* 895, 1256, 1617) but also shows presence of core 2 structures (*m/z* 1344, 1706). In addition a core 1 and core 2 structures with a terminal N-glycolylneuraminic acid were detected (*m/z* 1286 and 1736 respectively) No relevant molecular ion has been observed below *m/z* 895.

The ion at *m/z* 1617 suggest the presence of a core 1 structure with a disialosyl group, to further confirm this, MALDI-TOF/TOF analysis of that ion was performed (Figure 4.7). The MS/MS fragmentation of the 1617 parent ion revealed the presence of characteristic fragment ions *m/z* 384, 759, 1020, confirming the presence of disialosyl groups. In addition, it is clear that this motif is carried by the 6-arm as indicated by the presence of *m/z* 1020 and absence of *m/z* 981 ion.

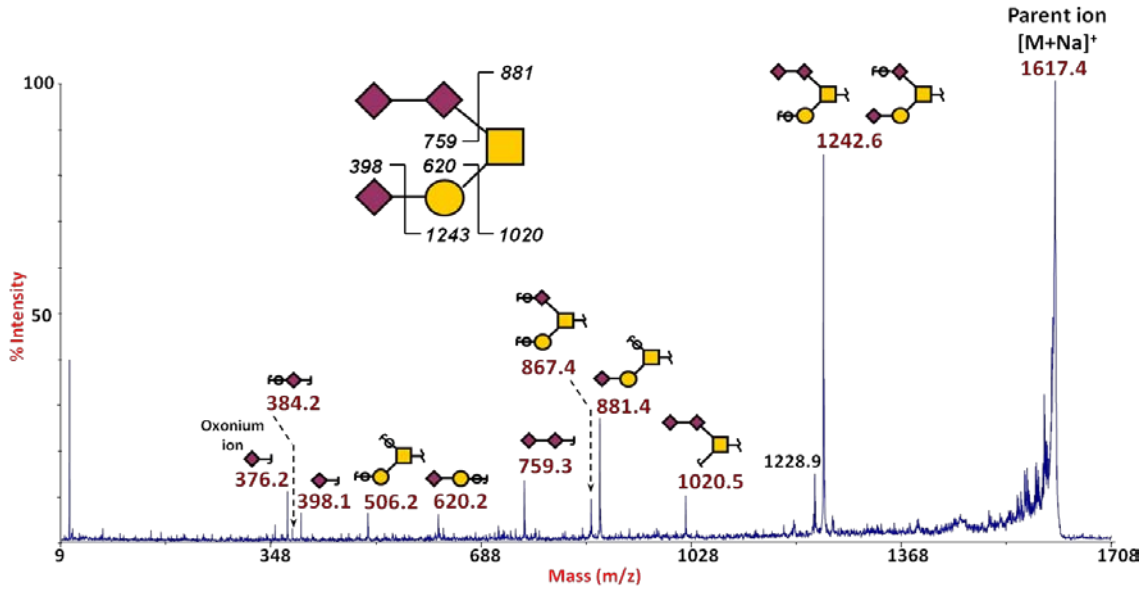


Figure 4.7 MALDI-TOF/TOF mass spectrum of the tri-sialylated *O*-linked glycan (*m/z* 1617)

MALDI-TOF/TOF analysis was performed to further investigate the molecular ion at *m/z* 1618 suggestive of tri-sialylated core 1. Fragmentation of the parent ion provided fragment ions at *m/z* 759, 1020 which allowed characterisation as a core 1 with the tri-sialylated *O*-linked glycan structure that contains an unusual disialosyl motif. Diagnostic m/z.1020 fragment ion revealed that disialosyl group is carried by the 6 arm. In the spectrum all fragment ions carry sodium except the sialic acid residue at mz/ 376 which is an oxonium ion.

Also the parent ion *m/z* 1256 was subject to fragmentation by MALDI-TOF/TOF MS/MS analysis. This was done in order to elucidate whether the di-sialylated core 1 structure (*m/z* 1256) carries a single sialic residue on each arm, or a disialosyl group on one arm, or if the signal corresponds to both isoforms. As illustrated on Figure 4.8 the rVWF *O*-glycome contains only a di-sialylated core 1 structure, which carries a terminal sialic acid on each arm. This was revealed by presence of fragment ions at *m/z* 506, 620

and 659. The absence of core 1 structures with a disialosyl motif was inferred from the absence of characteristic fragments ions at *m/z* 759 (corresponding to two sialic acids linked together) and ions *m/z* 520 and 1020.

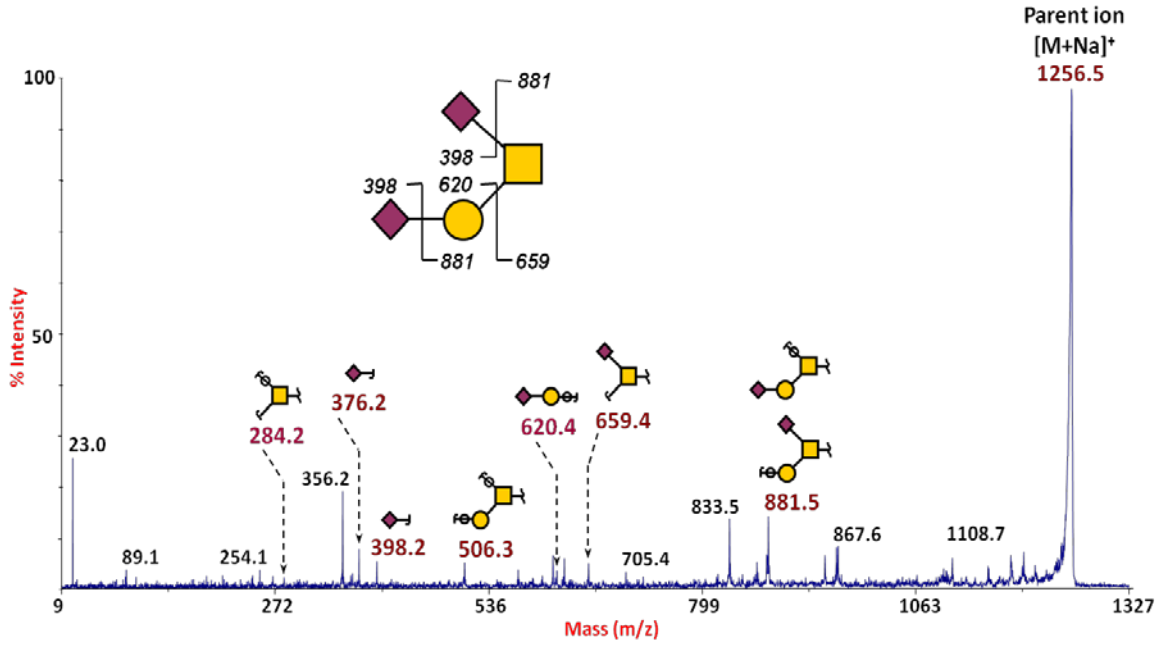


Figure 4.8 MALDI-TOF/TOF MS/MS spectrum of the [M+ Na]$^+$ parent ion at *m/z* 1256

The fragmentation of *m/z* 1256 parent ion confirms the presence of di-sialylated core 1 structure. The characteristic fragment ions at *m/z* 506, 620 and 659 allow the characterisation of the structure as core 1 with a sialic acid residue on each arm. In the spectrum all fragment ions carry sodium except the sialic acid residue at *m/z* 376 which is an oxonium ion.

Finally, as an example for core 2 structure the fragmentation pattern of the parent ion at *m/z* is graphically illustrated on Figure 4.9 .

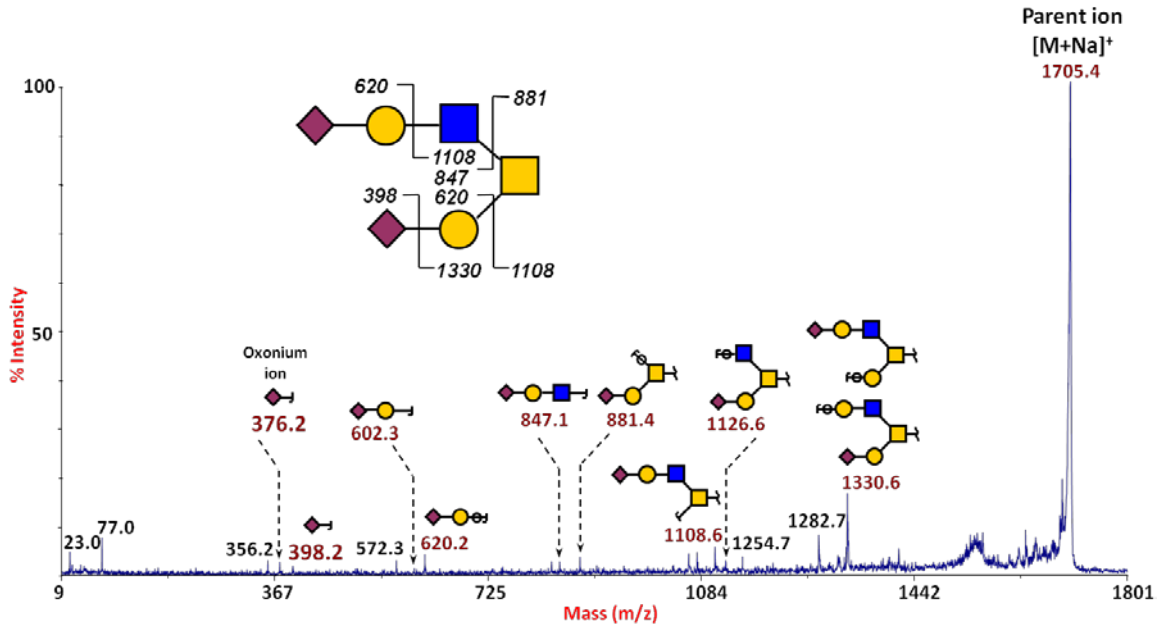


Figure 4.9 MALDI-TOF/TOF MS/MS spectrum of the [M+ Na]$^+$ parent ion at *m/z* 1705

The fragment ions at *m/z* 620, 660, 881, 921 and 1143 allow a full characterisation of the structure as being a core 2 *O*-linked glycan. .In the spectrum all fragment ions carry sodium except the sialic acid residue at *m/z* 376 which is an oxonium ion.

4.4 Discussion

The VWF oligosachcarides account for approximately 15-20% of its total molecular weight. *N*-linked glycans comprise 70% of the carbohydrate and *O*-linked chains the remaining 30%.[375] In contrast to *N*-linked glycans there is no consensus sequence for *O*-linked glycosylation. Nevertheless, the likelihood of *O*-linked glycosylation occurring can be predicted from comparative studies, basing on the amino acid sequence surrounding the Ser/Thr residue. Titani.[12] The prediction of *O*-linked glycosylation sites has to be taken with a degree of caution, but might be more useful to identify the glycosylated regions in a protein rather than specific sites.

Since the two *O*-linked glycan clusters are localised in the linker regions flanking the A1 domain I have aligned the human sequence of the linker regions against known sequences from 10 other species. The protein alignment shows that three *O*-glycosylation sites in the D3-A1 linker are highly conserved. Interestingly, most organisms lack the glycosylation site at position S1263 however they have a vicinal

threonine residue which could potentially undergo glycosylation. Furthermore, the protein alignment of the A1-A2 linker region shows that two *O*-glycosylation sites most proximal to the A1 domain (T1268 and T1477) are highly conserved while the other two residues (S1486 and T1487) appear conserved in the majority of analysed organisms. The highly conserved nature of the *O*-glycosylation sites could suggest that both sites are important and are required for proper VWF structure/function. Interestingly it has been previously suggested that glycosylated threonine or serine residues are less likely to be precisely conserved than a non-glycosylated ones.[369] It has been suggested that *O*-linked glycosylation would be conserved more as a bulk property, as *O*-glycans functions are not highly dependent on the exact number or position of glycosylated residues.[369] However these studies have been mostly performed on heavily glycosylated mucin type proteins where the exact position of S and T residues is not likely to be important as long as they abundant. The individual mucin-type glycosylation sites can be highly specific and highly conserved between species. The fact the VWF *O*-linked glycosylation sites are highly conserved further confirms their importance.

We have recently determined and published the *O*-linked glycan profile of pdVWF.[486] However since the majority of the experiments described in this thesis were performed on recombinant VWF, in collaboration with Prof Anne Dell and Dr Kevin Canis I characterised the rVWF *O*-glycome profile. In order to achieve this, rVWF was first purified from HEK293T expression media by a combination of ion exchange and Heparin-Sepharose chromatography. Heparin-Sepharose affinity chromatography exploits the ability of VWF to bind to heparin.[139] By combination of two purification steps I have successfully obtained highly pure rVWF in quantities large enough for the MS profiling.

The *O*-glycome of rVWF was subsequently analysed using MS techniques previously optimised for pdVWF. Firstly it has been demonstrated that similarly to pdVWF,[452,486] the major *O*-linked glycan moiety of rWVF is a desialylated core 1 structure. Moreover, akin to pdVWF, the rVWF *O*-glycome mostly consisted of sialylated core 1 structures. In addition, core 2 structures were also detected. In contrast to pdVWF, rVWF did not contain any fucosylated *O*-linked oligosaccharides, therefore no ABO- blood group antigens are presented on rVWF *O*-glycans. In addition, both core 1 and core 2 structures with an unusual sugar *N*-glycolylneuraminic acid were detected, which was

also observed for pdVWF. Humans are not able to synthesise N-glycolylneuraminic acid, however traces level of this monosaccharide were observed on several human proteins and it has been shown that the incorporation can occur from dietary sources. In the case of recombinant VWF the fetal calf serum present in the HEK293T tissue culture media could be the source of *N*-glycolylneuraminic acid.

Interestingly it has been demonstrated that similarly to pdVWF, the rVWF *O*-linked glycans carry a rare disialosyl motif. However in contrast to pdVWF, rVWF glycans presented only tri-sialylated core 1 structures, with no tetra-sialylated core 1 structure detected. Therefore a single core 1 glycan carries only one disialosyl group, which we detected primarily on the 6 arm of the structure. The α2-8 linkage of the two sialic acid residues is mediated by a specific $\alpha_{2,8}$-sialyltransferase (ST8Sia), which can synthesise polysialic structures of more than 100 residues as observed in the Neural cell adhesion molecule (NCAM).[489,490] The expression of polysialic acid is significantly upregulated during brain development, and modulates the adhesion properties of NCAM and affects neuronal and glial cell migration, outgrowth and sprouting of axons.[491] Interestingly in the case of proteins such as vitronectin and plasminogen or MUC1[492,493] as well as VWF, the number of connected sialic acid residues does not exceed two. Since the disialosyl motif appears to be very specific it could be inferred that it is important for VWF function. Interestingly a recently published review[494] suggests that VWF can interact with Siglec 7 protein, which is expressed on monocytes and NK cells. Since Siglec 7 has been shown exhibit a high affinity for the disialosyl epitope,[495] it is suggested that VWF *O*-linked glycans could play a role in the interaction of VWF with Siglec expressing cells.

In addition, sialic acid residues confer a negative charge to glycoproteins and since they are abundant on the *O*-linked glycans clustered in the A1 domain flanking regions they could mediate the interaction of the A1 domain with vicinal domains. It has been previously demonstrated that D'D3 domains modulate the accessibility of GPIbα binding site within the A1 domain[138] therefore it is hypothesised that sialic acid residues or the entire *O*-linked glycans in the D3-A1 linker region could modulate this interaction. In addition, interaction between the A1 domain and isolated A2 domain has been documented, suggesting those domains interact with each other.[286] Consequently the terminal sialic acid residues on *O*-linked glycans clustered in the A1-A2 linker

region could influence the accessibility of the ADAMTS13 cleavage site by determining rigidity of the linker region and proximity of the A1, A2 domains.

In conclusion, the *O*-glycome profile of rVWF appears very similar to the profile of pdVWF. The only major, but expected difference is absence of ABO blood group antigens. Moreover, compared to pdVWF, *O*-linked glycans of rVWF lack the tetra-sialylated structures, nevertheless those were quite infrequent in pdVWF *O*-glycome and the rVWF *O*-linked glycans still present the rare disialyl motif.

The functional implications of mutating the *O*-linked glycocyslation site in rVWF are investigated in the subsequent chapters.

5 EXPRESSION AND CHARACTERISTION OF VWF *O*-LINKED GLYCOSYLATION MUTANTS

Current data regarding the role of VWF *O*-linked glycans are limited and often contradictory; therefore the aim of this study was to establish the importance of *O*-linked glycans in modulating VWF expression, structure and function. Since there is no universal enzyme for the release of *O*-linked glycans from the protein backbone, recombinant VWF lacking *O*-linked glycans was produced. As demonstrated in the previous chapter, the types and relative abundance of *O*-linked sugars was similar on plasma derived VWF and recombinant VWF expressed in HEK293T cells, therefore this cell line was chosen to express wtVWF and VWF lacking *O*-linked oligosaccharides. As described, the VWF monomer contains 10 *O*-linked glycosylation sites; therefore VWF variants were generated to prevent glycosylation at one or more of these sites (T1248A, T1255A, T1256A, S1263A, T1468A, T1477A, S1486A, T1487A, T1679A and T2298A) (Figure 5.1). Firstly, the expression and secretion of proteins lacking only one *O*-linked glycan chain or lacking all four of the glycans flanking each (N- or C-terminal) or both sides of the A1 domain was investigated. In order to assess the multimeric composition of expressed VWF variants, multimer gel analysis and collagen binding assays were used. Subsequently VWF functions; collagen type I and III and heparin binding were assessed. Also the impact of the removal of *O*-linked sugars on the conformation of the VWF was probed using a Llama derived nanobody, and isolated VWF A2 domain. In addition, the lectin peanut agglutinin was employed to examine presence of core 1 *O*-linked glycan structure on VWF variants.The interaction of *O*-linked glycosylation variants with ADAMTS13 and platelets was also investigated and is going to be discussed in following chapters.

5.1 Generation of *O*-linked glycosylation variants

To determine the individual roles of VWF *O*-linked glycan chains, specific Thr/Ser residues were mutated to prevent glycosylation. The VWF cDNA encoding for full length (FL) VWF has been previously cloned into the mammalian expression vector pcDNA3.1 by Dr Tom McKinnon. A silent mutation at G100 was introduced to remove the KpnI site within the D1 domain leaving a unique KpnI site within the A2 domain to facilitate efficient subcloning of the VWF cDNA. To aid mutagenesis the XhoI – KpnI fragment of VWF (sequence for residues 768-1590) has also been previously sub-cloned into the cloning vector pGEM Z(+). This vector was used to mutate the 8 *O*-

linked glycan sites located either side of the A1 domain; T1248, T1255, T1256, S1263, T1468, T1477, S1486, T1487, changing the Serine or Threonine residue to Alanine. Following confirmation of the desired mutations by DNA sequencing, the XhoI–KpnI fragment was sub-cloned back into pcDNA FL-VWF. In addition, three cluster variants were constructed mutating all of the four sites either side of the A1 domain or all eight sites around the A1 domain. These were designated cluster 1(Clus 1, N-terminal), cluster 2 (Clus 2, C-terminal) or double cluster (DC) respectively.

To generate *O*-linked glycan mutants at sites T1679 and T2298 the KpnI–Age I fragment of VWF (residues 1590–end) was digested from pcDNA FL-VWF and sub-cloned into pcDNA3.1 and used for mutagenesis. All the mutants were successfully generated and the sequences verified by DNA sequencing.

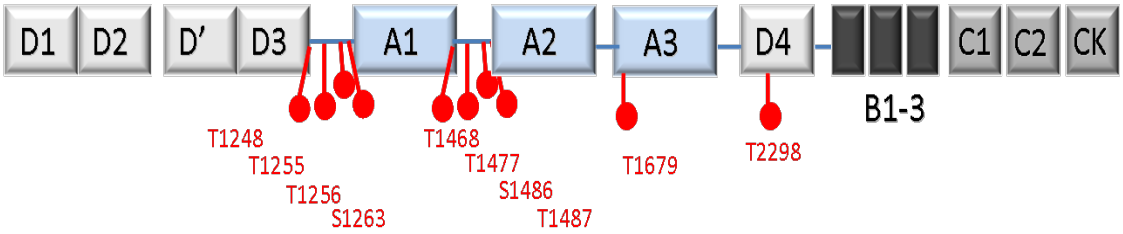


Figure 5.1 VWF *O*-linked glycosylation sites

VWF contains 10 *O*-linked glycosylation sites.[12] Eight glycans are clustered around the A1 domain, four on each side. One oligosaccharide is present in the A3 domain and one in the D4 domain.

5.1.1 Mammalian expression of recombinant VWF

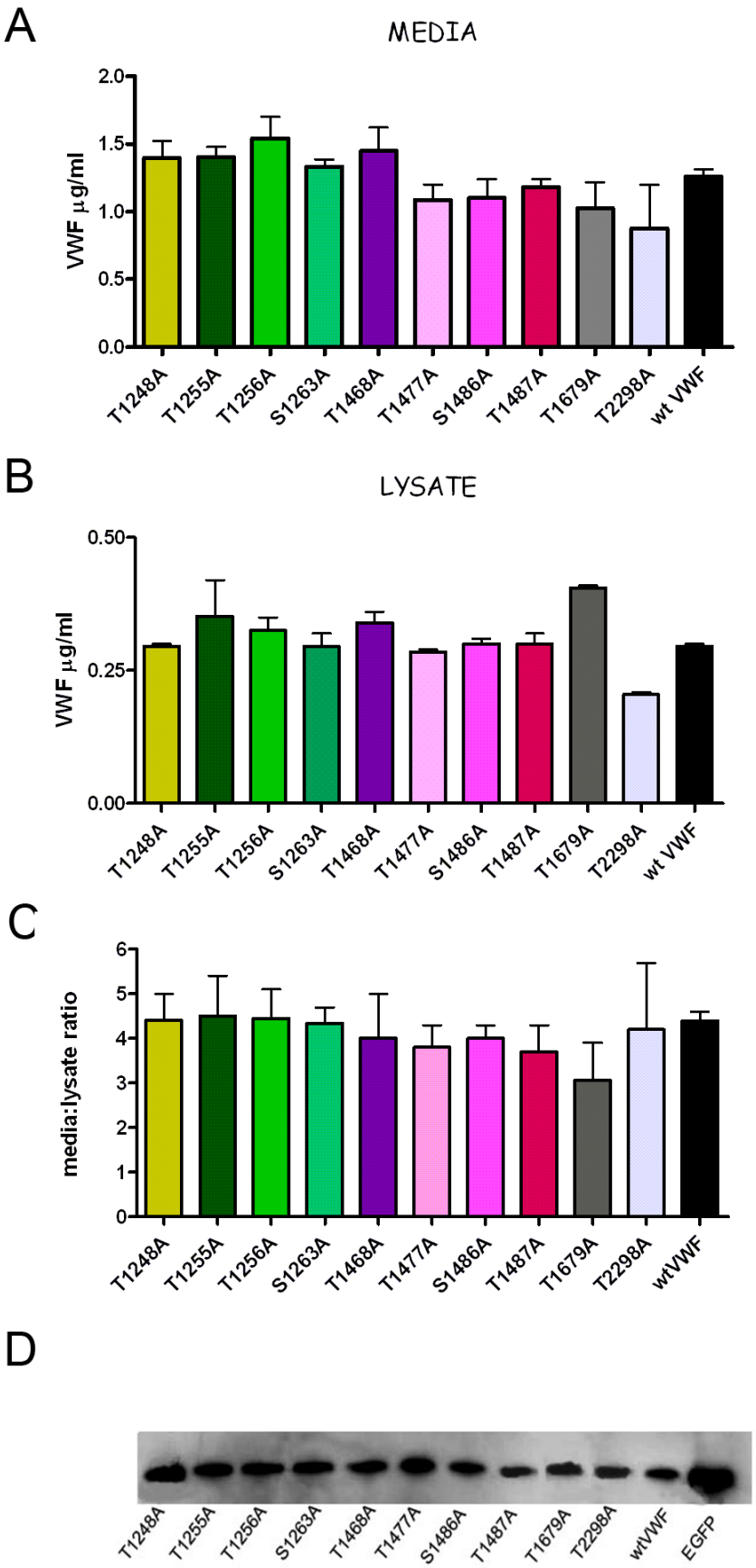
Wild type and mutated recombinant VWF variants were transiently expressed in mammalian HEK293T cells using PEI as the transfection agent. Initial transfections to investigate whether any of the *O*-linked glycan chains play a role in the effective secretion of VWF were performed in 6 well plates. The concentration of each VWF variant in the conditioned media and cell lysate was than compared by VWF ELISA. All VWF variants including the cluster mutants were expressed and secreted into the conditioned medium at similar levels to wild type VWF (wtVWF), also the media to lysate ratio was comparable for all the variants (Figure 5.2a and Figure 5.3b). Co-transfection with enhanced green fluorescent protein (eGFP) was used as a control of transfection efficiency. Conditioned media was subject to SDS-PAGE under reducing

conditions and western blotting with anti-eGFP antibody. Similar eGFP expression was observed for each VWF variant, indicating similar transfection efficiency (Figure 5.2c). In addition, in all transfection experiments control cells were transfected with empty pcDNA3.1 vector, and no VWF expression was observed. The expression of the VWF *O*-linked glycan variants was then scaled up and expressed proteins were concentrated or purified for functional analysis.

Next page :

Figure 5.2 Expression of wtVWF and its glycosylation variants - VWF ELISA

To study the effect of *O*-linked glycosylation on the secretion of VWF, VWF antigen levels in condition media (**A**) and cell lysate (**B**) were analysed using VWF ELISA. Similar amounts of each VWF variant and wtVWF protein was expressed and retained within the cell. (Values shown here are SEM of 3 separate transfections performed in duplicate). (**C**) Media to lysate ratio was determined to be similar for wtVWF and each VWF variant. (**D**) In addition, conditioned medium from each transfection was subjected to SDS-PAGE under reducing conditions followed by western blot with anti-eGFP antibody, showing equal effectiveness of transfection. ($p>0.05$)


A
MEDIA
VWF µg/ml
2.0
1.5
1.0
0.5
0.0
T1248A
T1255A
T1256A
S1263A
T1468A
T1477A
S1486A
T1487A
T1679A
T2298A
wt VWF
B
LYSATE
VWF µg/ml
0.50
0.25
0.00
T1248A
T1255A
T1256A
S1263A
T1468A
T1477A
S1486A
T1487A
T1679A
T2298A
wt VWF
C
media:lysate ratio
6
5
4
3
2
1
0
T1248A
T1255A
T1256A
S1263A
T1468A
T1477A
S1486A
T1487A
T1679A
T2298A
wtVWF
D
T1248A
T1255A
T1256A
S1263A
T1468A
T1477A
S1486A
T1487A
T1679A
T2298A
wtVWF
EGFP

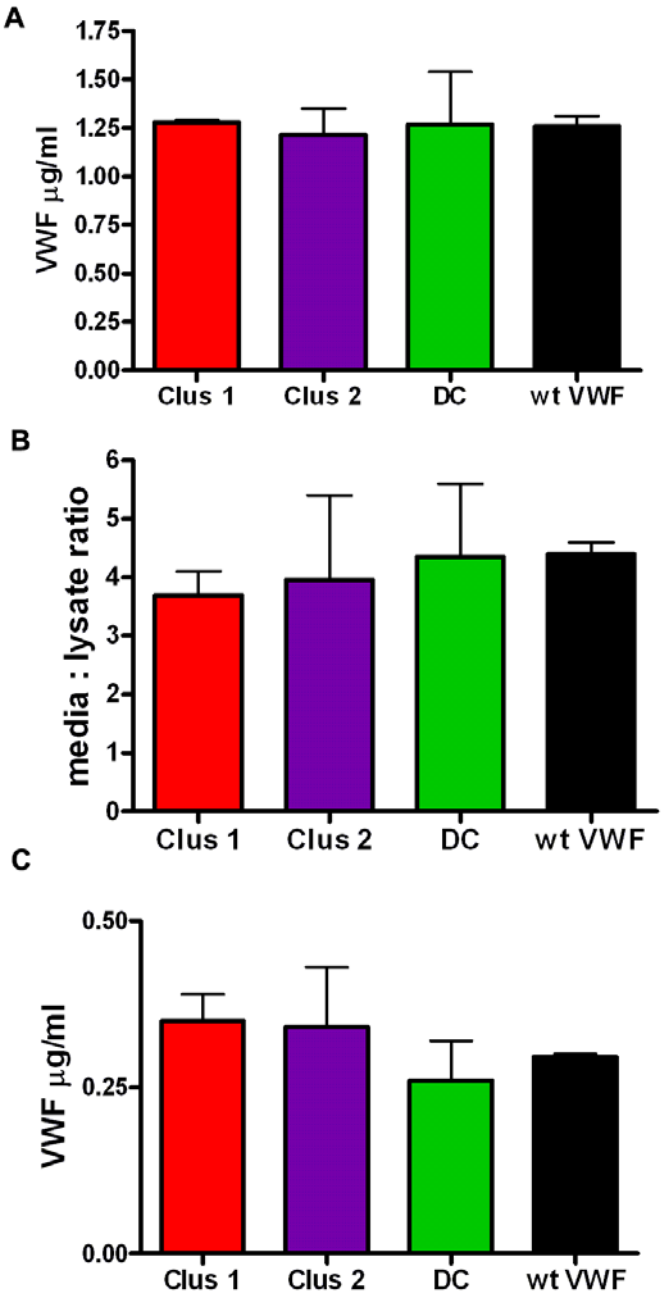


Figure 5.3 Expression of *O*-linked glycosylation cluster variants

To investigate the effect of *O*-linked glycan cluster on the secretion of VWF, VWF antigen levels in the conditioned media (**A**) and cell lysate (**B**) were measured by VWF ELISA. Similar amounts of each VWF variant and wtVWF protein were expressed and retained within the cell. (Values shown here are SEM of 3 separate transfections performed in duplicate). (**C**) Media to lysate ratio was determined to be similar for wtVWF and each VWF cluster variant.($p>0.05$).

5.2 Characterisation of VWF mutants

5.2.1 Multimer analysis

The multimeric composition of expressed VWF was analysed by agarose gel electrophoresis followed by Western Blotting. Equal amounts of VWF were loaded on to the gel and the multimeric composition of the VWF glycosylation variants was compared to that of recombinant wtVWF and plasma derived VWF (pdVWF). All cluster variants and single glycosylation mutants demonstrated multimeric patterns similar to that of wtVWF (Figure 5.4). Compared to pdVWF, rVWF has a different multimeric composition, with the multimer pattern skewed towards medium and lower molecular weight multimers.

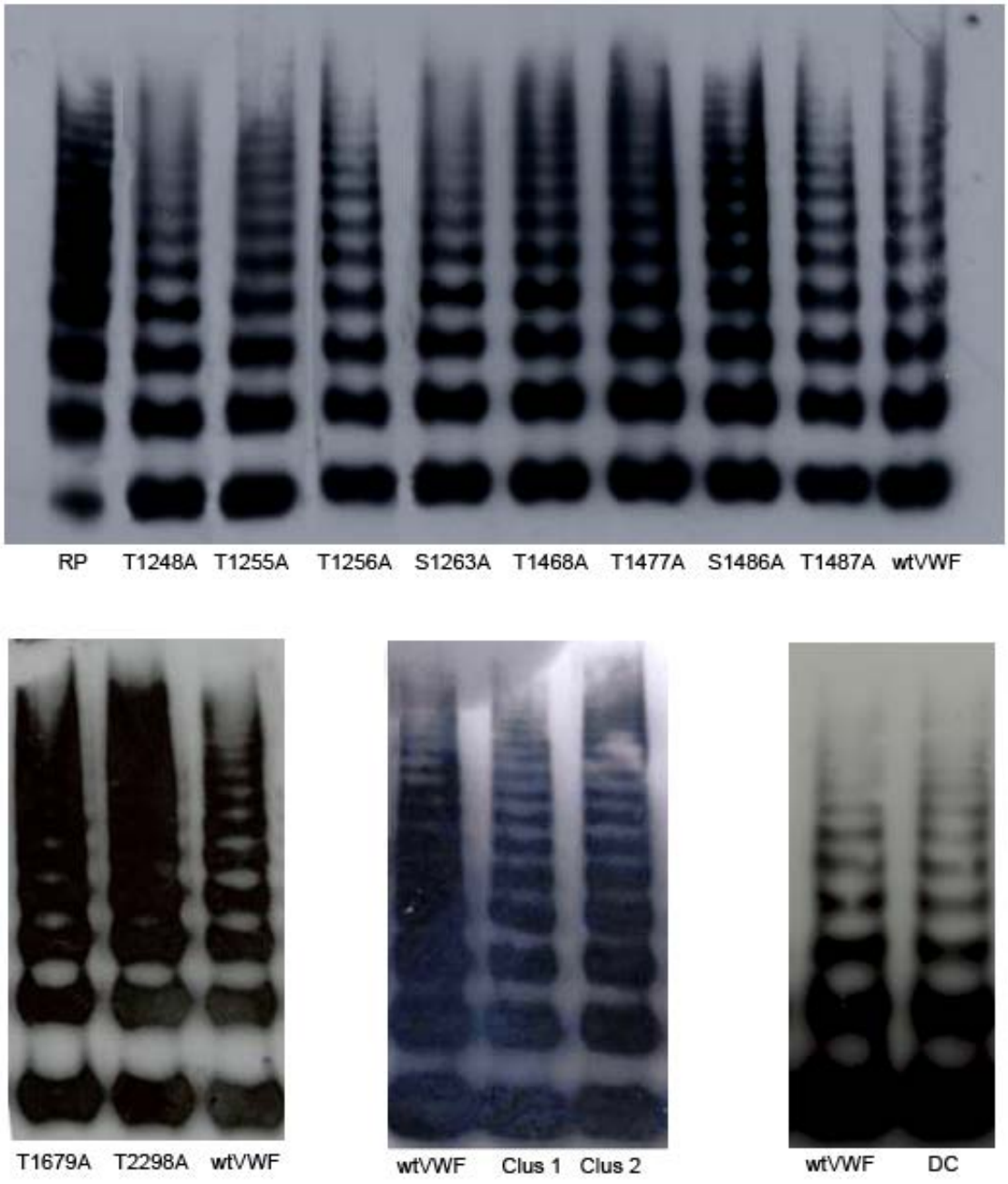


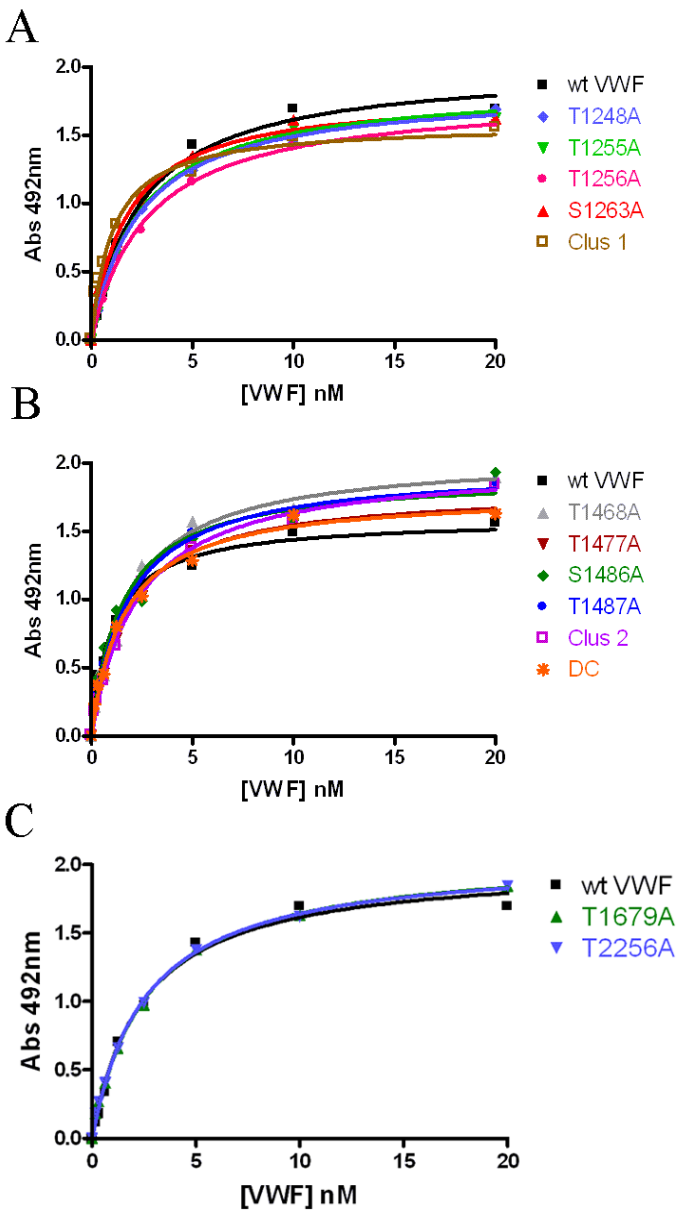
Figure 5.4 Multimer distribution of VWF glycosylation variants

The multimeric pattern of VWF single and cluster glycosylation variants was visualised on in 1.4 % agarose gels. The multimeric patterns of VWF *O*-linked glycosylation variants are indistinguishable from that of recombinant wtVWF. (RP-reference plasma).

5.2.2 Collagen binding activity

The collagen binding function of VWF is highly sensitive to VWF multimeric size with high molecular weight multimers binding collagen with greater affinity. Since all the VWF variants were shown to have a similar multimeric pattern, any alterations in collagen binding are likely to reflect changes in binding affinity rather than an effect of multimerisation. The effect of mutations on binding to collagen types III and I was assessed by an ELISA based collagen binding assay. Immobilised collagen type III was incubated with increasing concentrations of rVWF to generate binding. Binding curves were calculated using a one site binding model which has been previously shown to give appropriate fitting curves. The $K_{D,app}$ was ~2nM for wtVWF* and all the VWF *O*-linked glycan variants demonstrated similar binding affinity demonstrating that they do not affect collagen binding.(Figure 5.5) The VWF collagen type I and III binding function was also investigated as a ratio of collagen binding to VWF antigen (VWF:CB/VWF:Ag). The normal observed ratio for pdVWF is >0.7. WtVWF had a VWF:CB/VWF:Ag ratio of 0.4. This difference in collagen binding is due to differences in multimeric pattern, with plasma derived VWF having more high molecular weight multimers. All single and cluster glycosylation variants showed collagen type III and I binding similar to that of wtVWF confirming that the *O*-linked glycans do not alter binding to collagen (Figure 5.6).

*To determine the K_D for the interaction of VWF with collagen, the monomeric weight of rVWF was taken as 270kDa



D

	$K_{D,app}$ (nM)
wt VWF	1.9 ±0.1
T1248A	2.3 ±0.1
T1255A	2.3 ±0.1
T1256A	2.1 ±0.3
S1263A	1.7 ±0.2
Clus 1	1.0 ±0.2
T1468A	1.8 ±0.2
T1477A	1.7 ±0.2
T1486A	1.5 ±0.3
T1487A	1.7 ±0.2
Clus 2	2.2 ±0.2
DC	1.6 ±0.2
T1679A	2.6 ± 0.2
T2298A	2.5 ±0.2

Figure 5.5 Binding isotherms of VWF variants to collagen type III

Collagen type III binding affinity of VWF *O*-linked glycosylation variants was analysed using an ELISA based plate assay. $K_{D,\ app}$ values were calculated by fitting the data to the one site binding equation and compared to that of wt VWF. Collagen binding curves for glycosylation variants located on the N-terminal side of the A1 domain (**A**) on the C-terminal side of the A1 domain and double cluster (**B**) and the T1679A and T2289A (**C**) variants were shown to be similar to wtVWF. (**D**) The calculated K_D values for all glycosylation variants are listed in the table and are similar collagen binding affinity obtained for wtVWF. Values shown here are SEM of 3 separate experiments performed in duplicate.

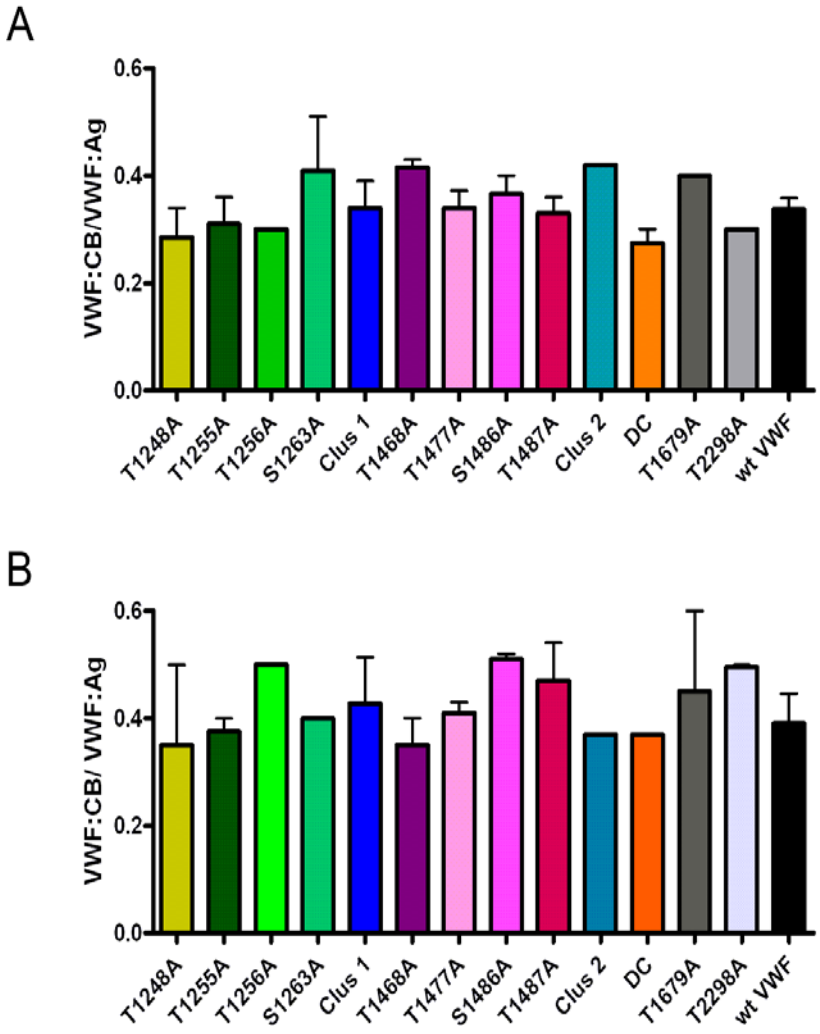


Figure 5.6 Analysis of VWF binding to collagen types III (A) and I (B)

VWF *O*-linked glycosylation variants were tested for their ability to bind collagen. Results from three separate ELISA experiments on VWF samples demonstrate that all variants bound to immobilized collagen types III (**A**) and I (**B**) with the same affinity as wt VWF. (Values shown here are SEM of 3 separate experiments performed in duplicate; $p>0.05$).

5.3 Functional characteristics of VWF variants

5.3.1 Heparin binding

The major heparin binding site of VWF is localised to the A1 domain, and therefore, removal of the *O*-linked glycans chains that flank both sides of the A1 domain disulphide loop could potentially influence the ability of VWF to interact with heparin. Moreover, since I planned to purify recombinant VWF using heparin affinity chromatography I investigated the ability of the VWF *O*-linked glycan variants to bind to Heparin. The heparin-binding properties of the VWF variants were investigated by

incubating a fixed quantity of VWF or its variants with Heparin-Sepharose beads and measuring the amount of VWF remaining unbound by VWF ELISA. It has been established that heparin binding is largely independent of the multimeric composition of VWF.[143] The concentration of VWF was low enough to prevent saturation of the beads. As demonstrated in Figure 5.7 no significant difference in heparin binding between wtVWF and the VWF variants was observed, indicating that removal of *O*-linked glycans does not influence heparin binding.

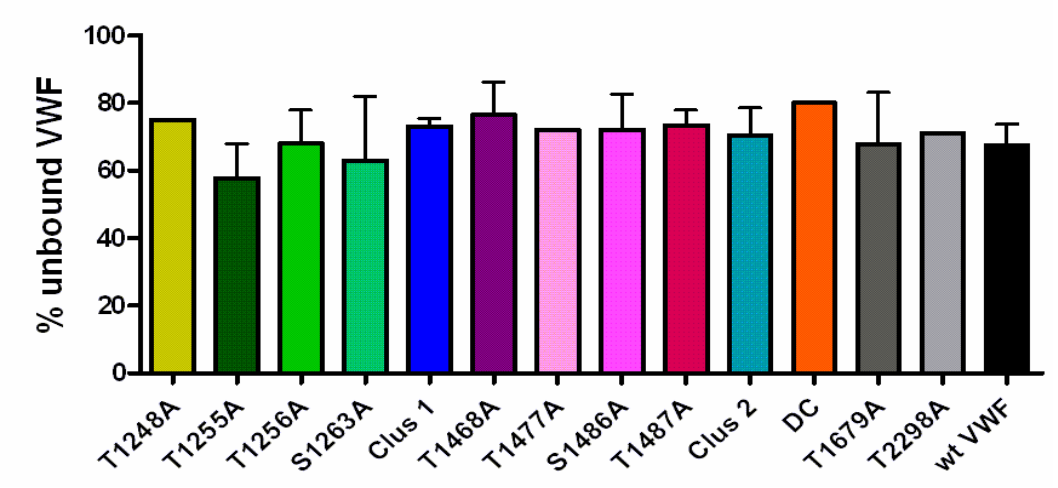


Figure 5.7 Binding of wtVWF and VWF glycosylation variants to heparin

Effect of VWF *O*-linked glycans on the interaction with heparin was investigated using heparin-Sepharose resin and unbound VWF was detected using VWF ELISA. Results are expressed as the percent of heparin unbound, when for each variant the concentration of VWF prior incubation with heparin-Sepharose beads was taken as 100%. The heparin binding capacity for each *O*-linked glycosylation variant was similar to that for wtVWF. (Values shown here are SEM of 3 separate experiments performed in duplicate; $p>0.05$).

5.3.2 Nanobody binding

VWF circulates in plasma in a globular inactive conformation, which is unable to spontaneously interact with platelets. Transition from the non-binding to the GPIbα-binding form of the A1 domain is necessary to induce formation of the VWF-GPIbα complex. This physiological activation occurs when VWF elongation is induced following its binding to collagen or under conditions of high shear stress. The presence of 'activated' VWF (i.e. VWF in its GPIbα-binding conformation) in solution can be

detected using a nanobody (AU/VWFa-11), which is a homodimer of a Llama derived immunoglobin heavy chain.[496] Although the nanobody binds a site within VWF distinct from the GPIbα binding site itself, it can detect VWF in its activated form, which is, for instance, induced by immobilization, ristocetin, or VWD type 2B mutations.

I postulated that removal of the *O*-linked glycans that flank the A1 domain could alter VWF or the A1 domain conformation and therefore enable nanobody binding. To investigate the influence of *O*-linked glycans on VWF conformation and nanobody binding an immunosorbent binding assay in the presence and absence of ristocetin was used. Firstly, in the absence of ristocetin only minimal nanobody binding was observed for wtVWF when compared to wtVWF incubated with 250 µg/ml of ristocetin (Figure 5.8). Similarly, with the exception of the double cluster mutant, no substantial nanobody binding was observed for any of the VWF glycosylation variants in the absence of ristocetin. However, when compared with wtVWF, a slight increase in nanobody binding in the absence of ristocetin was detected for the double cluster variant. (Figure 5.8) This would suggest that removal of all the *O*-linked glycans flanking the A1 domain partially increases the ability of VWF to interact with the nanobody without the need for ristocetin, however it does not appear to fully 'activate' the A1 domain, since the extent of interaction is still minimal compared to ristocetin activated VWF.

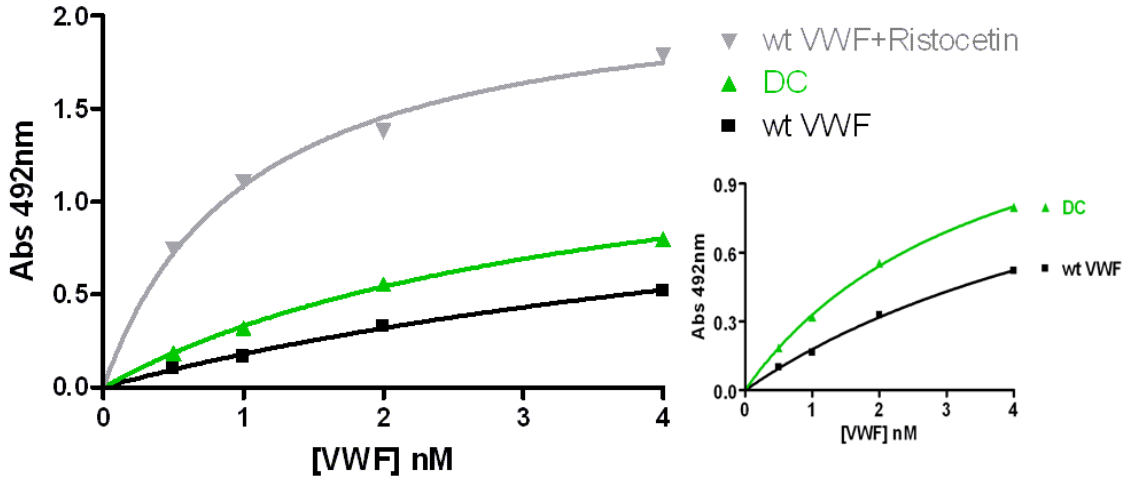


Figure 5.8 Binding isotherm of wtVWF and DC variant to nanobody AU/VWFa-11 in the absence of ristocetin

Binding of wtVWF and all glycosylation variants to nanobody in the absence of ristocetin was determined. Apart from the double cluster all VWF variants showed binding similar to that of wtVWF; for simplicity graph illustrates binding curves for wtVWF and the DC variant only. Inset is with larger scale ordinate. In the absence of ristocetin, wtVWF in solution weakly interacted with the nanobody, and slightly increased binding was observed for the double cluster however accurate binding curves or K_D values could not be derived. For comparison, the much greater binding observed for wtVWF activated with ristocetin is shown.

Subsequently the interaction between ristocetin-activated VWF and the nanobody was investigated. Since maximal binding to the nanobody for wtVWF was reached at a ristocetin concentration of 250µg/ml this concentration was used to compare binding of the nanobody to the VWF variants. The double cluster variant displayed a slight increase in binding, consistent with the slightly increased binding in the absence of ristocetin, while the cluster 2 variants demonstrated a slight decrease in nanobody binding in the presence ristocetin when compared with wtVWF (Figure 5.9). None of the other glycosylation variants showed a significant change in ristocetin dependent nanobody binding in this static assay. To further examine this, the binding parameters of ristocetin activated VWF to nanobody were quantified. Briefly nanobody coated plates were incubated with various concentrations of rVWF (0.5-4nM) in the presence of 250µg/ml ristocetin. Binding isotherm and binding parameters were estimated by fitting the data to the one site binding equation using GraphPad Prism. Figure 5.10 shows binding data from a representative experiment. It was determined that wtVWF bound

the nanobody with a $K_{D,app}$~1.2±0.1nM The T1477A, S1486A, T1487A, Clus2 and the DC showed somewhat decreased nanobody binding in the presence of ristocetin when compared to wtD'A3 and all other glycosylation variants showed similar binding variants were shown to bind with a similar $K_{D,app}$ suggesting that the removal of *O*-linked glycans does not significantly affect VWF-nanobody binding.

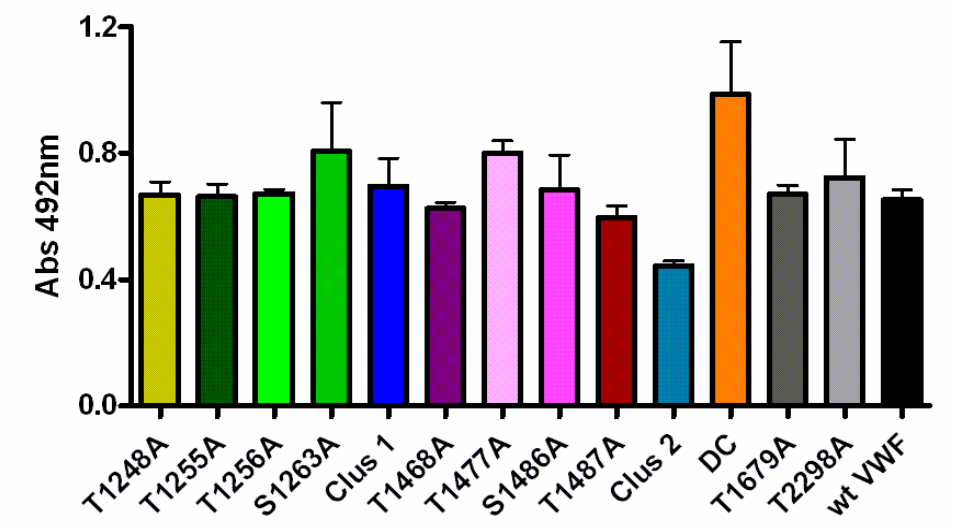
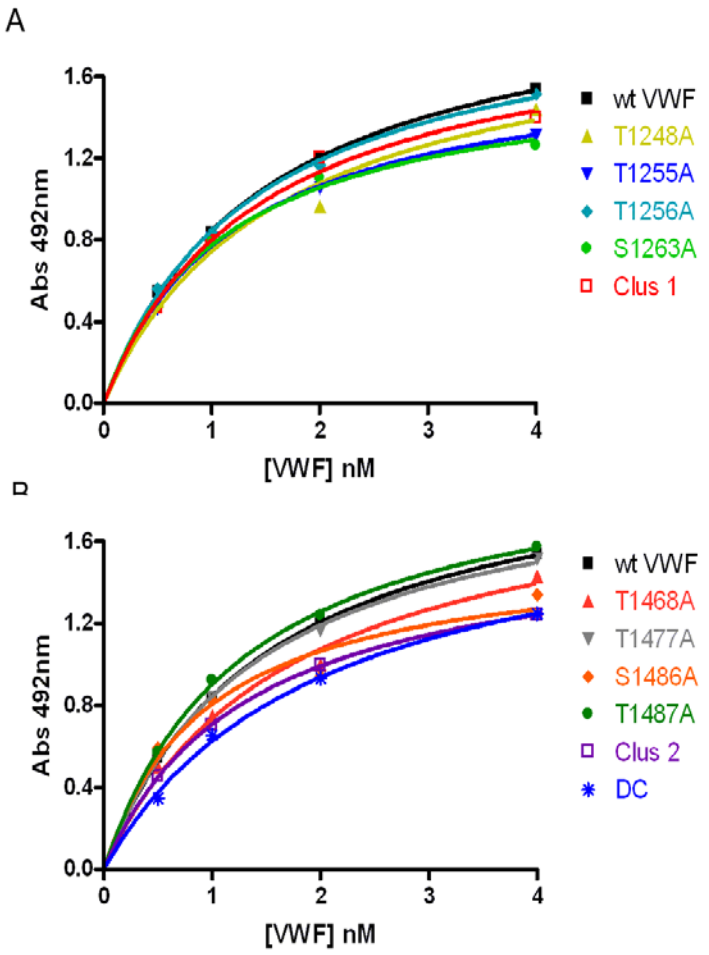


Figure 5.9 Binding of wt and mutated VWF to AU/VWFa-11 nanobody in the presence of 250 µg/ml ristocetin

The concentration of ristocetin that induced maximum binding of VWF to nanobody was determined to be 250µg/ml and this concentration was chosen for the binding assays. The double cluster exhibited increased and cluster 2 decreased nanobody binding while all other mutants have binding similar to that of wtVWF. Each value represents SEM of three independent sets of duplicate determinations.



C

	$K_{D,app}$ (nM)
wt VWF	1.2 ± 0.1
T1248A	1.0 ± 0.1
T1255A	1.1 ± 0.2
T1256A	1.1 ± 0.1
S1263A	0.9 ± 0.1
Clus 1	1.2 ± 0.1
T1468A	1.4 ± 0.4
T1477A	1.8 ± 0.4
S1486A	1.6 ± 0.3
T1487A	1.1 ± 0.1
Clus 2	1.7 ± 0.3
DC	1.9 ± 0.1
T1679A	1.3 ± 0.1
T2298A	1.1 ± 0.1

Figure 5.10 Binding isotherm of ristocetin activated VWF to AU/VWFa-11 nanobody

Nanobody coated plates were incubated with various concentrations of rVWF (0.5-4nM) in the presence of 250µg/ml ristocetin. Binding isotherm and binding parameters were estimated by fitting the data to the one site binding equation. (**A,B**) Representative binding curves illustrated. (**C**) The calculated $K_{D,app}$ values for all variants are listed in the table. (Standard error values are given) Estimated nanobody binding $K_{D,app}$ for wtVWF was approximately 1.2nM. The T1477A, S1486A, T1487A, Clus2 and the DC showed somewhat decreased nanobody binding in the presence of ristocetin and all other glycosylation variants showed similar binding.

5.3.3 Binding of bacterial expressed VWF A2 domain to VWF

It has been previously reported that isolated VWF A2 domain expressed in bacterial cells can bind to the VWF A1 domain when the A1 domain in its 'active' conformation and that this blocks the interaction with GPIbα under high shear.[286] The data obtained from the nanobody binding assays suggested that the double cluster and cluster 2 variants may have an altered conformation. Therefore, I investigated whether the

removal of *O*-linked glycans clustered around the A1 domain could affect the interaction between bacterial expressed A2 domain and the A1 domain of the VWF *O*-linked glycosylation variants.

To begin with, binding of the VWF variants to immobilised bacterial A2 domain was studied as a function of VWF concentration in the absence of ristocetin using an ELISA based plate assay. As previously reported, no binding to the A2 domain was detected for wtVWF in solution. However, ristocetin activated wtVWF was able to bind to the isolated A2 domain with high affinity (Figure 5.11). Similarly to wtVWF, none of the glycosylation variants, when in solution, were able to bind to the isolated A2 domain. (Binding for selected mutants illustrated on Figure 5.11) Subsequently the interaction between the isolated A2 domain and immobilised VWF variants was studied. In agreement with the previous study, the isolated A2 domain binds to wtVWF in a concentration dependent and saturable manner, with half-maximal binding observed at 0.5µM. Consequently VWF variants were also assayed and showed a similar interaction with the immobilised isolated A2 domain, comparable to the wild type protein. Binding curves for selected VWF variants are shown on Figure 5.12. This further confirmed that absence of *O*-linked oligosaccharides flanking the A1 domain does not alter the interaction between multimeric VWF and the bacterial isolated A2 domain.

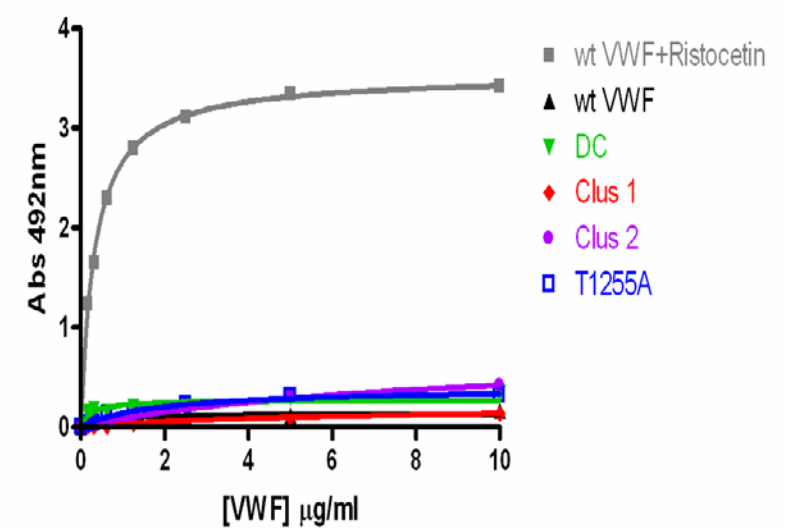


Figure 5.11 VWF binding to immobilised bacterial A2 domain

The wtVWF in solution did not bind to the purified A2 domain even at the highest concentration (10µg/ml). Conversely wtVWF in the presence of ristocetin therefore in an 'active' (GPIbα binding conformation) was able to interact with the bacterial A2 domain with half-maximal binding at a concentration of ~ 1µg/ml. Moreover none of

the *O*-linked glycosylation variants in solution bound to the A2 domain. (For clarity only selected variants shown)

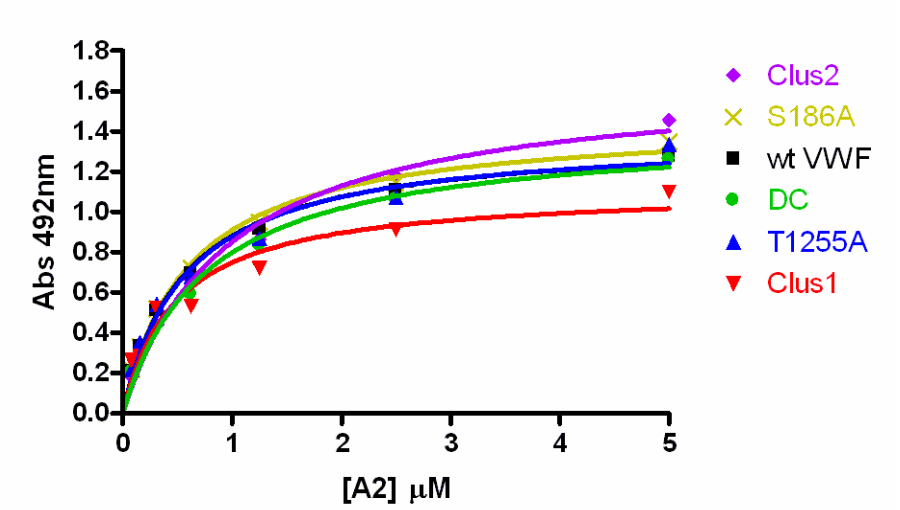


Figure 5.12 Binding of the bacterial A2 domain to immobilised multimeric VWF variants

Effect of the *O*-linked glycans on the binding of the isolated A2 domain was examined using an ELISA based plate assay. Binding isotherm and binding parameters were estimated by fitting the data to the one site binding equation. Half maximal binding was observed at 0.5μm for wtVWF and comparable $K_{D,app}$ values were detected the for *O*-linked variants. For simplicity selected variants are shown on the graph.

Since bacterial expressed proteins do not undergo glycosylation I tested the ability of the purified A2 domain expressed in HEK293T cells, to interact with VWF. In contrast to the bacterial form, the glycosylated mammalian A2 domain was unable to interact with the immobilised FL-VWF. However a notable increase in binding was observed for the A2 domain when the *N*-linked glycans were removed by incubating with PNGase F (Figure 5.13). In addition, VWF appeared to bind to the de-glycosylated mammalian A2 to a lesser extent than to the bacterial A2. This suggests that the *N*-linked glycosylation of the A2 can prevent the interaction that was previously shown to occur between the A1 domain and the bacterial A2 domain devoid of glycans.

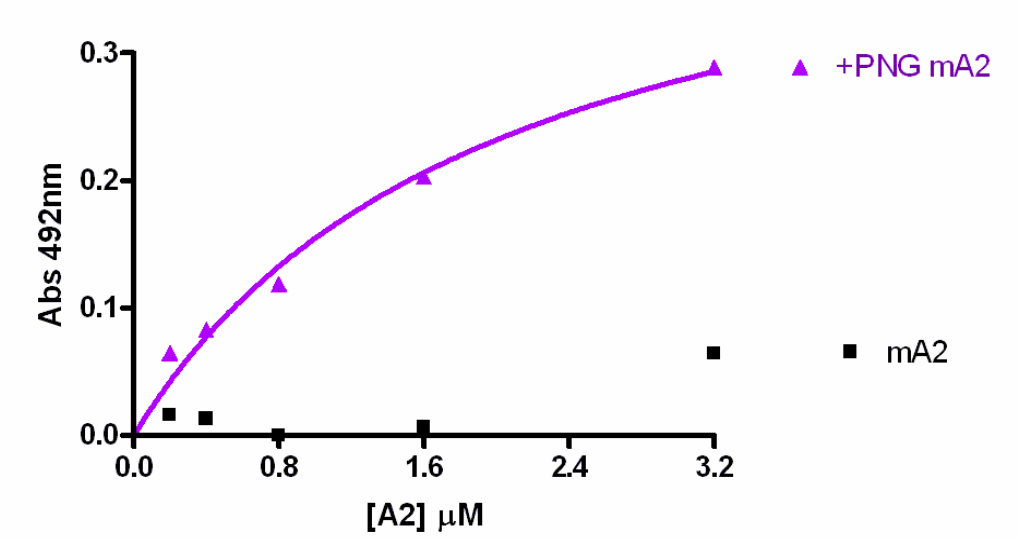


Figure 5.13 Binding of the mammalian glycosylated and de-glycosylated VWF-A2 domain to multimeric immobilised VWF

Interaction between immobilised VWF and the A2 domain expressed in HEK293T cells was assessed using an ELISA base plate assays. No binding of the fully glycosylated VWF-A2 domain was detected (mA2, in black). De-glycosylation of the A2 domain, by treatment with PNGase F resulted in a considerable increase in the binding to the immobilised multimeric VWF (+PNG mA2, in purple).

5.3.4 Peanut agglutinin binding

The majority of *O*-linked glycans terminate with the sialylated core 1 structure (also termed the T-antigen), and variations in the extent of glycosylation of VWF with this structure have been suggested to correlate with VWF plasma levels.[457] The core 1 structure can interact with the lectin peanut agglutinin (PNA), therefore this lectin was used in an immunosorbent assay to assess the relative amount of core 1 structure on the VWF cluster variants compared to wtVWF. In this assay VWF-linked carbohydrates are desialylated using neuraminidase, which allows subsequent detection of the core 1 structure by PNA. No PNA binding was detected when neuraminidase treatment was omitted, confirming specificity of PNA for desialyted core 1 structures. As shown on Figure 5.14, PNA binding was detected for desialylated wtVWF, confirming it contains T-antigen structures. Furthermore a marked decrease in PNA binding was observed for the DC variant that lacks eight of the ten *O*-linked glycan. PNA binding was reduced to a similar level for the Clus 1 variant that has 4 glycans flanking the N-terminal side of the A1 domain missing. The Clus 2 VWF variant, devoid of 4 *O*-linked glycan chains on the C-terminus of the A1 domain exhibited decrease in PNA binding compared to wtVWF, however the reduction in binding was less than for Clus 1 and DC.

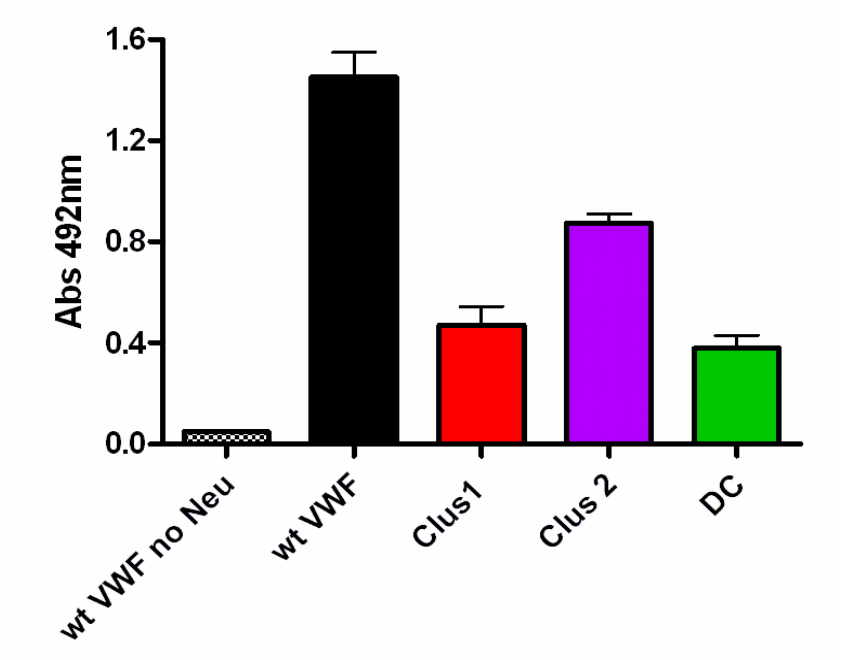


Figure 5.14 Binding of peanut agglutinin to VWF cluster variants

Serial dilutions of neuraminidase (Neu) treated VWF were added to microtiter plates coated with anti-VWF antibodies, and peanut agglutinin (PNA) binding was detected. WtVWF that was not incubated with neuraminidase, therefore with terminal sialic acid residues present was used as a negative control and this did not bind PNA (wtVWF no Neu). In contrast, PNA was able to bind to wtVWF and cluster VWF following removal of terminal sialic acids with neuraminidase. When compared to wtVWF all the cluster variants exhibited diminished PNA binding. A marked reduction in PNA binding was observed for Clus 1 and DC variants while the Clus 2 demonstrated smaller reduction in PNA binding. Data represents the mean of 3 independent experiments.

5.4 Discussion

The properties of recombinant VWF lacking all *O*-linked glycans have been previously investigated, however, often with conflicting results. VWF produced in Chinese Hamster Ovary (CHO) cells that lacked the ability to synthesize *O*-linked glycans was shown to be secreted and multimerised in the same way as the fully glycosylated form.[454] Therefore in this project VWF mutants were made to prevent *O*-linked glycosylation at the ten identified sites and their properties studied in more detail. In addition to this, three cluster variants were constructed by mutating all of the 4 sites either side of the A1 domain (cluster 1 and cluster 2) or all 8 sites around the A1 domain (double cluster). Mutations deleting the remaining two sites were also prepared

separately. Threonine or serine residues were mutated to alanine since it the typically used change to prevent *O*-linked glycosylation at specific side and it is the most conservative change one could apply. Alanine amino acid has a similar size as threonine and serine, and has a hydrophobic side chain instead a polar uncharged side chain, which should not significantly interfere with the conformation of the peptide. As described these were expressed in HEK293T cells and expression and function analysed. The expression and secretion analysis of VWF *O*-glycosylation variants created in this project confirm that absence of *O*-linked glycans does not affect VWF expression and secretion with all the individual point mutations and the cluster mutations being synthesized and secreted to a similar extent. Variations in the extent of glycosylation of VWF with *O*-linked sialylated T-antigen have previously been shown to affect VWF plasma levels.[457] However, the similar expression of VWF *O*-linked glycosylation variants in this study suggests this effect is not due to changes in VWF secretion.

Furthermore, I have confirmed that the removal of *O*-linked glycans has no effect on VWF multimeric structure, with all recombinant variants exhibiting a full range of multimers, similar to wtVWF. The distribution of multimers for recombinant VWF expressed in HEK293T cells was slightly different from that of pdVWF, with the multimeric composition of rVWF being skewed towards the medium and small multimers that are less haemostatically active and as a result having reduced collagen binding per unit antigen. However, wtVWF and all glycosylation variants had a similar affinity for collagen with $K_{D,app}$ ~2nM and VWF:CB/VWF: Ag ratio of 0.4. The value for the $K_{D,app}$ refers to the monomeric concentration of VWF and was calculated based on a VWF monomeric weight of 250kDa, and was in keeping with previously published values. [150] These results suggest that *O*-linked glycans does not affect either multimeric structure or collagen binding affinity.

Heparin binding function, mediated by the VWF-A1 domain, was also examined with all the mutants showing normal heparin binding. Therefore the *O*-linked glycans of VWF do not affect the interactions with heparin, allowing the use of heparin-Sepharose chromatography as a second step of VWF purification.

In order to bind GPIbα, VWF requires a conversion from its resting state into an active GPIbα binding conformation. A previously described llama-derived nanobody can

distinguish between resting and activated VWF.[496] In this study the binding between the immobilised nanobody and rVWF variants in solution was investigated first in the absence of ristocetin. Neither wtVWF, nor any of the glycosylation variants (with the exception of the DC variant) were able to bind appreciably to the nanobody in the absence of ristocetin, showing that those mutations do not induce a conformational change that renders the VWF-A1 domain constitutively active. For the double cluster variant, slightly increased nanobody binding in the absence of ristocetin was detected. This observation could suggest that removal of all *O*-linked glycans flanking the A1 domain alters VWF configuration at least partially, allowing nanobody binding. In the presence of ristocetin the nanobody binding was increased for the double cluster variant and slightly decreased for the Clus 2 variant when compared to wtVWF. The reason for this effect is not fully explained. Removal of glycan chains from the A1 domain N-terminal flanking region could introduce flexibility into the peptide backbone and this could induce a conformational change or alter stability of the A1 domain or the way the A2 or D'D3 domains interact with the A1 domain. This change in conformation could enhance the exposure of either the nanobody binding site or ristocetin binding site allowing more VWF to bind. To further examine the effect of *O*-linked glycans flanking the A1 domain on its interaction with vicinal domains, a previously described A2 binding assay was employed.

A previous study has shown that bacterial expressed VWF A2 domain is able to bind to the A1 domain of VWF when the A1 domain is in its active conformation. In addition it has been shown that the R1405A gain-of function mutation that results in increased platelet binding in the isolated A1 domain diminishes its interaction with the isolated bacterial A2 domain.[132,335,497] Moreover, denaturation and differential scanning calorimetry experiments performed on mammalian wild type and mutated (R1405A) A1A2A3 tri-domain protein have shown that the destabilisation of the A1 domain results in a reduced interaction between the three domains and enhances the binding to GPIbα.[497] However a direct association between the A1 and A2 domain has not been demonstrated in the context of full-length VWF. In the view of these data I used bacterial expressed VWF A2 domain as a tool to investigate if the removal of VWF *O*-linked glycans could alter the conformation of the A1A2A3 complex, resulting in "activation" of the A1 domain. In keeping with previous work, wtVWF did not bind to immobilised bacterial A2 domain in the absence of ristocetin and binding was only

induced when ristocetin was included in the assay. Similar to wtVWF, none of the tested VWF *O*-linked glycosylation mutants bound to bacterial A2 domain in the absence of ristocetin suggesting that either they are not in an "active" conformation or the removal of the *O*-linked glycosylation is unable to produce a significant conformational change to allow binding to bacterial derived VWF A2 domain in the absence of ristocetin. Similarly, when wtVWF or the *O*-linked glycan variants were immobilised and incubated with soluble VWF A2 domain, the A2 domain bound with equal affinity to wtVWF and the mutant proteins. This confirms that immobilisation of VWF to microtitre plates "activates" the molecule and furthermore suggests that the extent of activation (or at least activation detected by isolated A2 domain) by immobilisation is not altered by removal of the *O*-linked glycan chains. Bacterial derived VWF A2 domain is not routinely used in our laboratory due to aggregation of the protein (McKinnon and Chan unpublished observations) and we prefer to express VWF A2 domain in HEK293T cells. Importantly, the VWF A2 domain contains 2 *N*-linked glycan sites, one of which, N1574, has been shown to be crucial for VWF function.[239] In light of this, I determined the ability of mammalian VWF A2 domain to interact with active VWF. Interestingly, unlike its bacterial counterpart, mammalian VWF A2 domain failed to bind to immobilised full length VWF. Following PNGase F digestion to remove the two *N*-linked glycan chains, the mammalian A2 domain was again able to interact with immobilised VWF. These data suggest that the *N*-linked glycan chains present on the A2 domain may influence the way it interacts with the VWF–A1 domain and warrants further investigation. Furthermore this data also highlights differences between proteins expressed in bacterial and mammalian systems

A basic view of *O*-linked glycan structure of the VWF cluster variants was determined by lectin analysis. Lectins are proteins (usually derived from plants) that specifically recognise and reversibly bind carbohydrate moieties. The lectin Peanut agglutinin (PNA) that binds to the core 1 (galactosyl β-1,3 N-acetylgalactosamine) glycan sequence was used, since the majority of VWF *O*-linked glycans are composed of sialylated core 1 structures.[452] As demonstrated by PNA analysis, compared to wtVWF, the DC variant demonstrated greatly reduced PNA binding consistent with the loss of 8 *O*-linked glycan chains. Some PNA binding capacity was retained with the DC variant, implying that the *O*-linked glycan/s at position T1679 and S2298 could be core 1 structures. Consistent with the loss of 4 *O*-linked glycans, the Clus2 variant had less

PNA binding then wtVWF, but more binding than the DC variant. Curiously, the Clus1 variant demonstrated PNA binding similar to the DC variant. The reason for this is not fully understood, however it may be suggested that the *O*-linked glycans on the N-terminal side of the A1 domain are composed of mainly Core 1 structures and the *O*-linked glycans on the C-terminal side are mainly core 2 structures. As such, when the four N-terminal glycans are not present (as with the Clus1 variant) PNA binding is reduced to the same extent as the DC variant. Further detailed mass spectroscopy analysis will be required to confirm the exact structure of the *O*-linked glycan clusters. Alternatively, the C-terminal glycans may be more inaccessible that the N-terminal ones to PNA binding, further structural analysis will be required to confirm this.

In summary, *O*-linked glycans have no influence on VWF expression, secretion or multimeric structure. Moreover, they do not alter the ability of VWF to bind to collagen or heparin. In addition, VWF *O*-linked glycans have a marginal effect on binding to a nanobody designed to recognise the GPIb binding conformation of the A1 domain, but no influence on the interaction of VWF with isolated bacterial A2 domain. In the next chapter the role of *O*-linked glycans in the interaction of VWF with ADAMTS13 is going to be discussed.

6 INTERACTION OF VWF *O*-LINKED GLYCOSYLATION VARIANST WITH ADAMTS13

6.1 ADAMTS13 cleavage of VWF *O*-linked glycosylation variants

6.1.1 ADAMTS13 proteolysis of full length VWF variants under static and pseudo-shear conditions

To investigate the influence of VWF *O*-linked glycans on the interaction with ADAMTS13, cleavage assays were performed initially under static conditions. This assay required the presence of 1.5M urea to denature VWF and cause a conformational change that allows ADAMTS13 access to the otherwise buried cleavage site. The extent of proteolysis was determined by multimer gel analysis and CBA.

The multimeric pattern for the single glycosylation mutants before and after ADAMTS13 proteolysis in the presence of urea is shown in Figure 6.1. At time point zero, all the single glycosylation VWF variants have similar multimeric composition. After 4 hours incubation with ADAMTS13, the HMW multimers are lost, with only the medium to low molecular weight multimers remaining, however the extent of the loss of HMW multimers was noticeably less for the S1486A variant than for the others variants. This suggests that VWF-S1486A is less susceptible to ADAMTS13 cleavage compared to wtVWF. To provide a more quantitative measure of VWF proteolysis, cleavage assay samples were analysed using the collagen binding assay to detect the reduction in multimer size. Supporting the multimer gel analysis, the CBA showed that the S1486A variant was cleaved appreciably slower than wtVWF with less reduction in collagen binding at all time points. Furthermore, cleavage of the Clus 2 (which contains S1486) and DC variants was also assessed in this way. Interestingly the Clus 2 variant was also cleaved to a similar extent to VWF-S1486A and the DC variant was proteolysed by ADAMTS13 to an even lesser extent (Figure 6.2). All other variants exhibited unaltered susceptibility to ADAMTS13 proteolysis (data not shown).

.

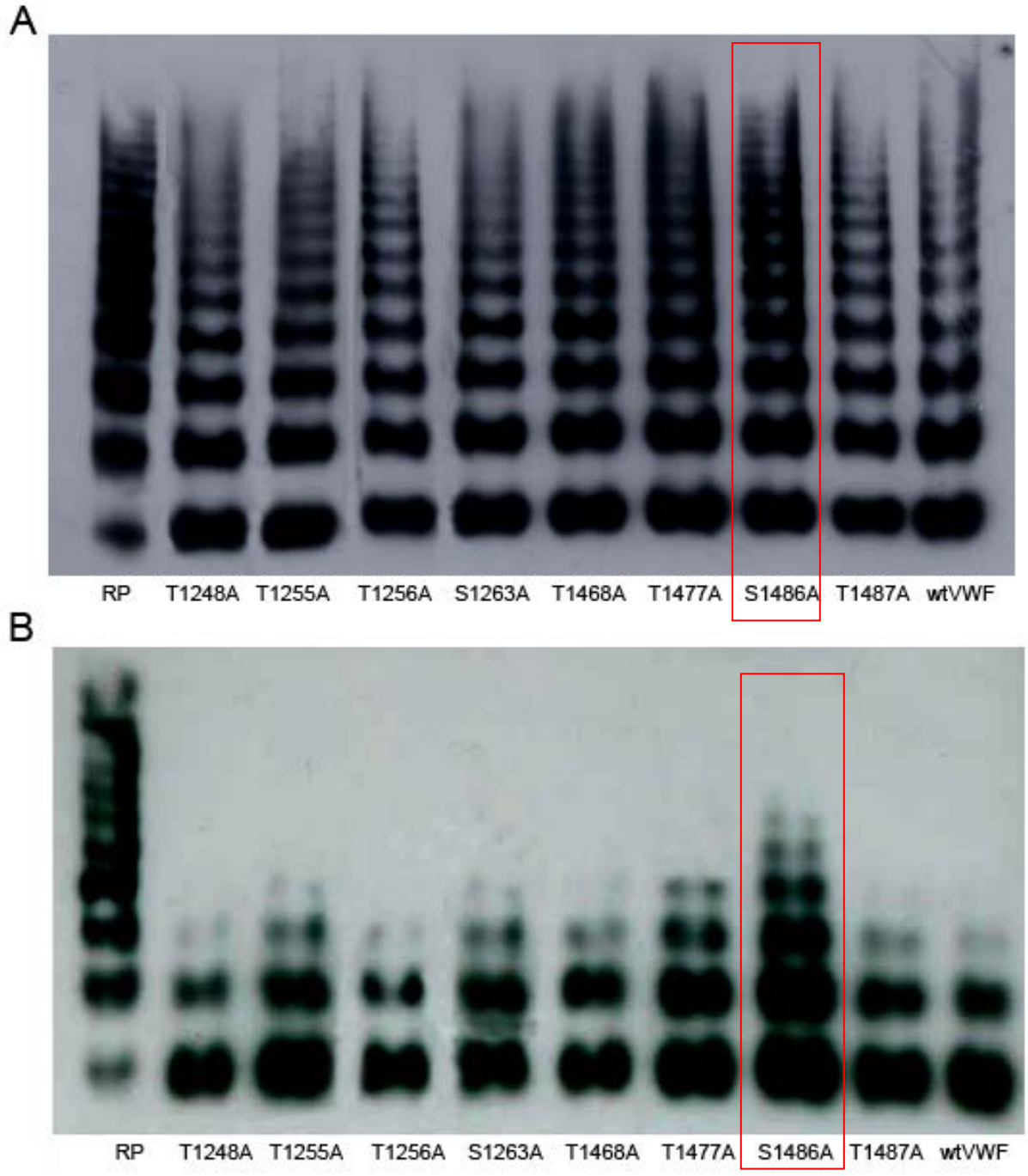


Figure 6.1 Multimer gel analysis of ADAMTS13 cleavage

Multimer gel electrophoresis was used to assess the extent of VWF proteolysis of single glycosylation variants by ADAMTS13. **(A)** VWF multimeric content prior to ADAMTS13 proteolysis. (**B)** VWF multimeric pattern after four hour incubation with ADAMTS13 in the presence of 1.5M urea. Single glycosylation variants were proteolysed very similarly to the wtVWF, with the exception of S1486A (red box) that was proteolysed at a markedly slower rate. The T1477A variant might also seem to be cleaved more slowly, however CBA analysis and cleavage assays showed that it to be the same as wtVWF. RP-reference plasma (no ADAMTS13).

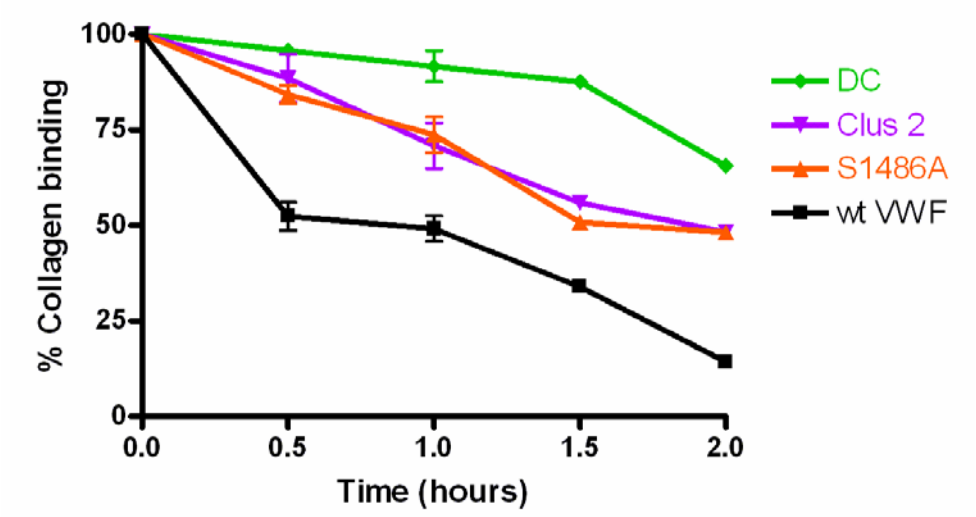


Figure 6.2 Collagen binding analysis of wtVWF, S1486A and Clus 2 and DC variants proteolysis by ADAMTS13 in the presence of urea

VWF variants were subject to ADAMTS13 proteolysis in the presence of urea and the extent of cleavage was analysed by collagen binding assay. Results are expressed as percentage reduction of collagen binding from baseline. The results show that the S1486A, cluster 2 and double cluster variants are cleaved significantly slower than the wtVWF. (Values shown are SEM of 3 separate experiments performed in duplicate).

The requirement for denaturants is a major limitation of static cleavage assays since it does not accurately reflect conditions *in vivo.* To examine the cleavage of VWF under more physiological conditions, experiments were repeated using a simple shear-stress based assay.[120] In this assay a bench top vortex mixer is used to generate mechanical shear stress that results in exposure of the ADAMTS13 cleavage site without the need for urea. As with the static assays, cleavage was assessed by multimer gels and CBA. In keeping with the data obtained under static conditions all of the single *O*-linked glycan variants with the exception of S1486A were proteolysed to a similar extent by ADAMTS13 in the vortex assay. As illustrated by multimer gel analysis, after 2 minutes incubation on the vortex mixer, the loss of HMW multimers is greater for the wtVWF than the S1486A variant indicating slower proteolysis and supporting the data obtained under static conditions (Figure 6.3).

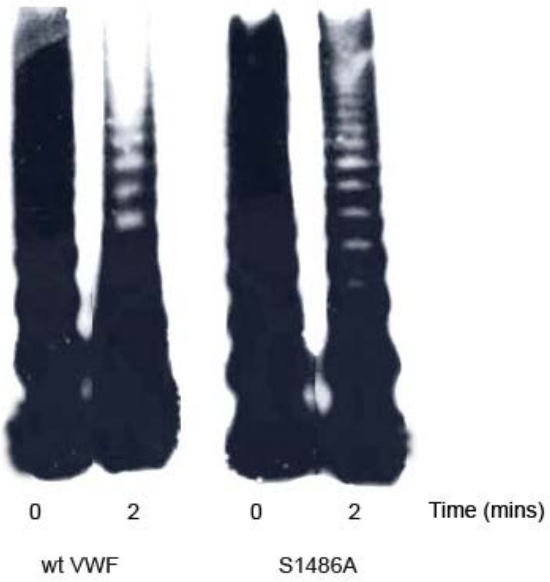


Figure 6.3 Multimer gel analysis of wt and S1486A VWF proteolysis by ADAMTS13 in pseudo shear assay

Multimer gel electrophoresis of VWF variants subjected to ADAMTS13 proteolysis under pseudo shear to show the extent of VWF proteolysis. Single glycosylation variants were proteolysed at very similar extent to the wtVWF, with the exception of S1468A that was cleaved more slowly. Before the start of the assay both wtVWF and S1486A variant have similar multimeric pattern, while after 2 minutes incubation with ADAMTS13 under pseudo-shear conditions the S1486A sample still contains high molecular weight multimers while the wtVWF samples has been reduced to medium weight multimers.

Subsequently, the extent of cleavage under pseudo shear stress was assessed by collagen binding analysis (Figure 6.4). VWF-S1486A, the cluster 2 and the double cluster mutants were shown to exhibit more collagen binding potential than wtVWF after 2 minutes incubation on the vortex mixer, indicating that have decreased susceptibility to ADAMTS13 proteolysis, again corroborating the observations seen under static conditions. However it should be noted that the double cluster variant showed substantially decreased susceptibility to ADAMTS13 cleavage when compared to wtVWF in the presence of urea while the decreased in proteolysis under pseudo-shear conditions was not as significant.

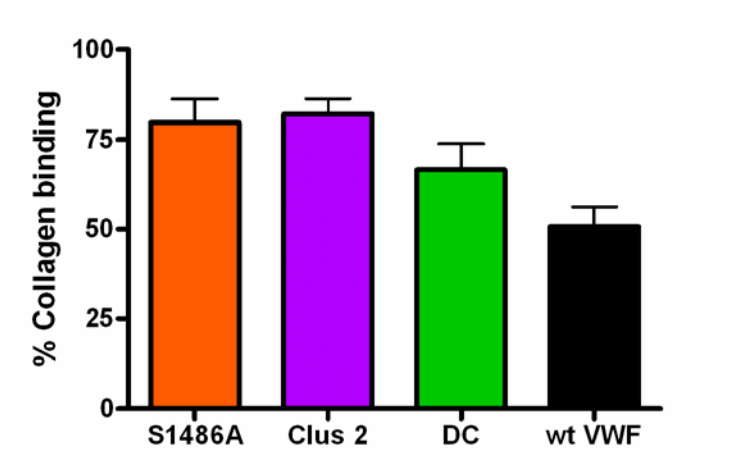


Figure 6.4 Collagen binding analysis of VWF proteolysis by ADAMTS13 in pseudo shear-vortex assay

Bar graph illustrates the reduction in collagen binding following 2 minute incubation with ADAMTS13 on a vortex used to generate shear stress. The extent of cleavage was analysed by CBA. The S1486A, Clus 2 variants are cleaved significantly slower when compared to wtVWF as demonstrated by the lesser reduction in collagen binding activity. Also DC variant exhibited moderate decrease in ADAMTS13 proteolysis. Other single glycosylation variants and cluster 1 have the same susceptibility to ADAMTS13 proteolysis as wtVWF (data not shown). (Error bars are SEM of 3 separate assays performed in duplicate)

6.1.2 Cleavage of D'-A3 VWF with ADAMTS13

In order to establish if the effects of the *O*-linked glycans on ADAMTS13 cleavage are due to alterations in the local conformation of the VWF monomer, ADAMTS13 cleavage assays were also performed on VWF from the D' to A3 (i.e. D'D3A1A2A3) . Experiments were performed in the presence of urea on purified wtD'A3-VWF and D'A3 containing either S1486A, Clus 2 or DC mutations, since these variants in full length VWF had altered susceptibility to ADAMTS13 cleavage.

The D'A3 protein contained a C-terminal c-*myc*/his tag and therefore the C-terminal cleavage product at specific time points was visualised with mouse anti c-*myc* antibodies. The intensities of the bands produced by the cleavage products of wtVWF, S1486A, Clus 2 and DC at specified time points were compared. There was found to be no significant reduction in cleavage between wtVWF and the S1486A variant, but a marked reduction in cleavage between wtVWF and the cluster 2 and double cluster variants (Figure 6.5). This suggests that removal of all *O*-linked glycan chains form the

linker region between the A1 and A2 domain alters the susceptibility of D'A3 to ADAMTS13 proteolysis.

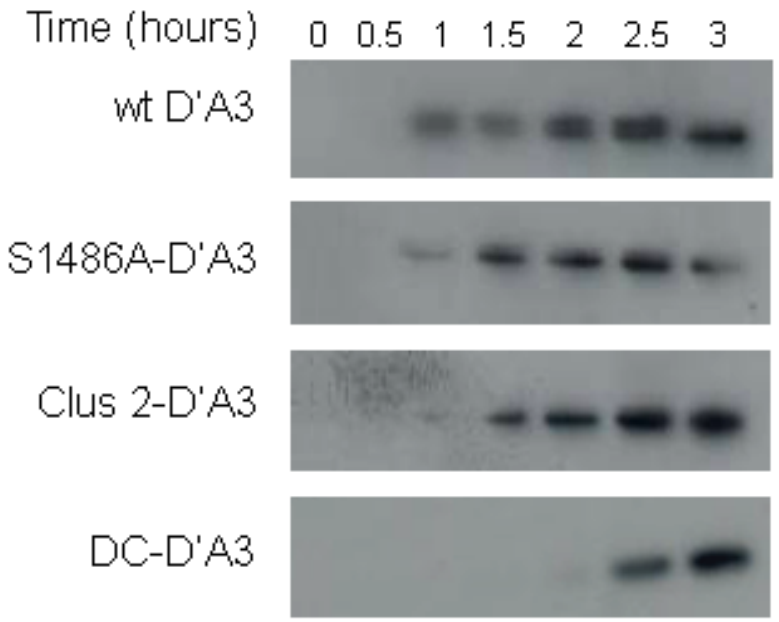


Figure 6.5 Cleavage of wt-, S1486A-, Clus 2- and DC- D'A3 by ADAMTS13, analysed by western blotting

Purified VWF-D'A3 fragments containing either S1486A, Clus 2 or DC mutations were incubated with activated ADAMTS13 in the presence of urea and the extent of proteolysis over time was examined by SDS-PAGE and Western blotting. C-terminal end cleavage products were detected with anti-c-*myc* antibodies as illustrated above. Prior to incubation (time point 0) and after 0.5 hour incubation with ADAMTS13, there are no cleavage products for any of the VWF samples. After 1 hour, weak bands for cleavage products for both wtD'A3 and the S1486A-D'A3 could be detected but no appreciable band for Clus 2-D'A3 or DC-D'A3. The cleavage of Clus 2 was detected after 2 hours. The first visible band for the DC-D'A3 variants was only visible after 2.5 hours and is still weaker in comparison to that of wtVWF and other variants. This suggests that the cleavage of Clus 2- and DC-D'A3 in the presence of urea is significantly slower than that of wt D'A3 and S1486A-D'A3.

6.2 Characterisation of binding between ADAMTS13 and S1486A, Clus 2 and DC VWF variants

6.2.1 Binding between ADAMTS13 and elongated VWF

In order to further elucidate the changes in proteolysis identified, I proceeded to investigate they were associated with altered ADAMTS13 binding to VWF in either its elongated or globular conformation.

First, I assessed the efficiency of VWF at coating microtitre plates. To do this the purified recombinant wtVWF, S1486A, Cluster 2 and double cluster glycan variants were directly coated onto a plate and bound VWF was detected with polyclonal rabbit anti-human VWF. The results showed that the wild type protein and all glycosylation variants analysed were immobilised at similar level (Figure 6.6a) therefore binding assays could be performed. Subsequently, binding of ADAMTS13 to elongated full length VWF was carried out by immobilising wtVWF, S1486A, Clus 2 and DC variants on a microtitre plate and incubation with serial dilutions of full length E225Q-ADAMTS13 mutant is proteotyically inactive. The E225 residue participates in water molecule coordination that impel the hydrolysis of the scissile bond and the inactive ADAMTS13 has been previously created and expressed in our lab (provided by Dr S.Zanardelli). Immobilisation of VWF leads to exposure of exosites in VWF that interact with ADAMTS13 allowing subsequent proteolysis. As shown on (Figure 6.6b) no appreciable difference in binding between wtVWF and the glycosylation variants was observed and the $K_{D,app}$ values were all within the same range.

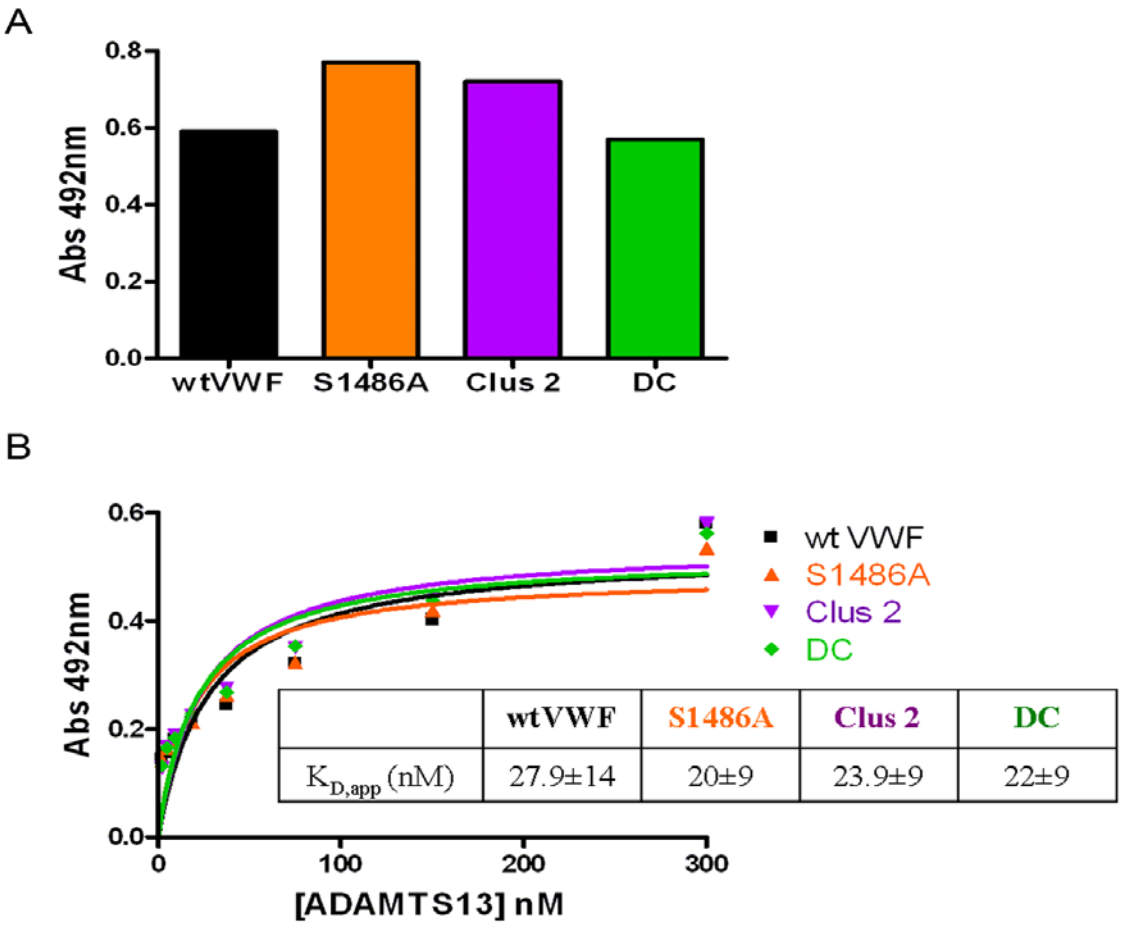


Figure 6.6 Binding of ADAMTS13 to elongated VWF

Binding between elongated VWF and ADAMTS13, was investigated by a plate binding assay**.** (**A**) Firstly coating efficiency of wtVWF and mutated proteins was compared and as shown on the graph all recombinant protein coated with the same effectiveness. (**B**) Binding of ADAMTS13 to the immobilised VWF variants was studied as a function of ADAMTS13 concentration. Binding isotherm and binding parameters were estimated by fitting the data to the one site binding equation. ADAMTS13 shows no difference in binding to full length wtVWF when compared to S1486A, Cluster 2 and DC glycan mutants. The insert table shows K_D estimations and standard error, which are within the same range.

6.2.2 Binding between ADAMTS13 and VWF in globular conformation

ADAMTS13 has been shown to bind weakly to VWF in its globular conformation (K_D ~80nM) with the A2 domain buried, and the binding is mediated by C-terminal parts of both proteins. In the view of the decreased susceptibility to ADAMTS13 proteolysis but normal binding of elongated S1486A, Cluster 2 and double cluster to ADAMTS13 observed I proceeded to investigate if the removal of *O*-linked glycans can influence binding of VWF in solution (i.e. globular VWF) to ADAMTS13. This was assessed by co-immunoprecipitation essentially as previously described.[152] E225Q-ADAMTS13 was incubated with wtVWF and S1486A-, Clus1- and DC-VWF variants and immunoprecipitated with anti-VWF-CK antibodies. Magnetic beads with bound VWF-ADAMTS13 complexes were washed to remove unbound proteins. The VWF and ADAMTS13 were then eluted, and subject to SDS-PAGE under reducing conditions followed by Western Blotting. As shown on Figure 6.7b bands of ~260kDa corresponding to VWF were detected with generally the same intensity for all the samples apart from the sample with VWF omitted, indicating equal immunoprecipitation of VWF by the anti-VWF antibody. Interestingly as shown on Figure 6.7a the glycan variants S1486A- Cluster 2 and DC-VWF (lanes 2, 3, 4 respectively) showed increased ADAMTS13 co-precipitation when compared to wtVWF (lane1), apparent in reduced band strength. No ADAMTS13 was detected when ADAMTS13 (lane 5) or VWF (lane 6) were omitted in the immunoprecipiated mix. These results indicate that S1486A- Cluster 2 and DC-VWF variants in globular conformation have increased ability to bind ADAMTS13.

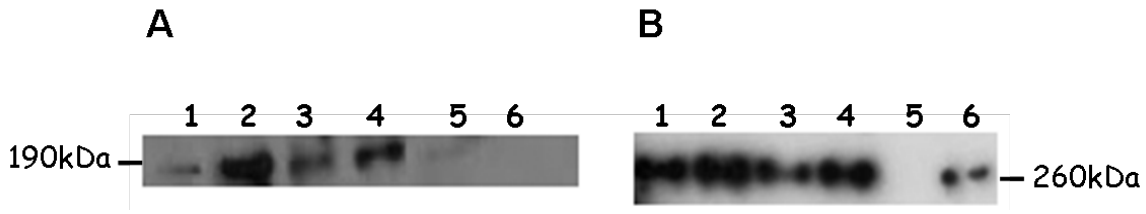


Figure 6.7 Binding between ADAMTS13 and globular VWF

ADAMTS13 binding was studied for wtVWF, S1486A, Clus 2 and DC variants in solution using an immunoprecipitation method. Solutions containing wtVWF and VWF variants and E225Q-ADAMTS13 were immunoprecipitated with anti-VWF-CK domain antibody. Immunoprecipitated proteins were eluted and analysed by SDS-PAGE under reducing conditions and western blotting with **(A)** anti-c-myc (tagged to ADAMTS13) **(B)**or anti-VWF antibodies. Molecular weight markers are indicated. As shown in panel **(A)** less ADAMTS13 was bound to wtVWF (lane 1) than to S1486A-VWF (lane 2), Clus2-VWF (lane 3) or DC-VWF (lane 4). As a control no ADAMTS13 protein was detected when VWF (lane 5) or ADAMTS13 (lane 6) were excluded from the mix. As shown on panel (**B)** similar amounts of wtVWF (lane1) and S1486A, Clus 2 and DC VWF glycosylation variants (lanes 2-4 respectively) were immunoprecipitated with anti-VWF antibody. No ADAMT13 was immunoprecipitated when VWF was omitted (lane 5).

To further confirm this results, binding between wtVWF and the S1486A variant in solution to ADAMTS13 was assessed by an ELISA based plate assay as previously described.[151] As illustrated on Figure 6.8 wtVWF weakly bound to immobilised ADAMTS13 with a $K_{D,app}$ value of 91 ±30nM, which was in accordance with previously published values (85.6± 8nM).[151] Interestingly, the S1486A variant exhibited markedly increased ADAMTS13 binding with $K_{D,app}$ values of 14±5nM. This result further confirms the observation that the absence of an *O*-linked glycan chain at a position S1486 increases binding between VWF in its globular conformation and ADAMTS13.

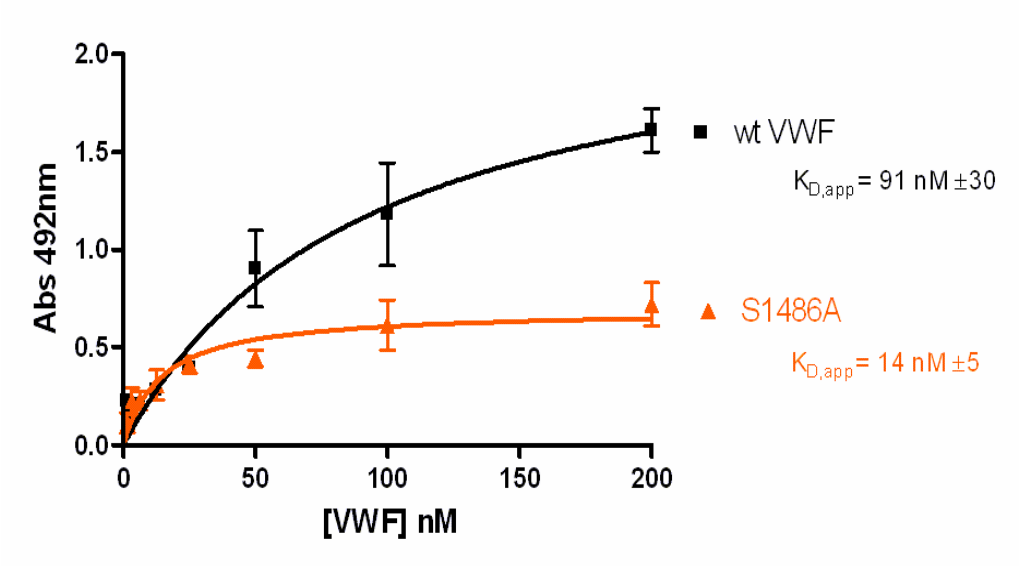


Figure 6.8 Binding isotherms of soluble wtVWF and S1486A variant to ADAMTS13

Binding between ADAMTS13 and globular wtVWF or S1486A-VWF, was investigated as a function of VWF concentration. Binding isotherm and binding parameters were estimated by fitting the data to the one site binding equation. The S1486A-VWF variant in globular conformation had an increased affinity to ADAMTS13 as indicated by a $K_{D,app}$ value of 14nM when compared to $K_{D,app}$ of 91nM estimated for the wtVWF.(Error bars are the SEM of 2 separate assays performed in duplicate).

6.3 Discussion

Cleavage of wild type and mutant rVWF by ADAMTS13 in the presence of urea was assessed by collagen binding and multimer analysis and demonstrated that the S1486A, cluster 2 and double cluster variants were proteolysed slower than wtVWF. In the absence of urea no cleavage was observed, and all samples retained 100% collagen binding when incubated without ADAMTS13, indicating that preparations were stable over the duration of the reaction and that no other contaminating proteases were present. Since the inclusion of urea in this assay to induce a conformation change in VWF is not physiological, the ability of ADAMTS13 to proteolyse VWF was investigated using a bench top vortex mixer to generate shear stress and obviate the need for urea. It is questionable whether this assay generates a shear stress that accurately reflects the shear forces encountered by VWF in the circulation because VWF is not anchored at any point in this assay. The effect is most likely mechanical shear that induces a conformation change in the VWF molecule. Nonetheless, this assay has been

successfully used in several studies and provides a useful alternative to standard *in vitro* assays. Interestingly, the results obtained using the vortex assay demonstrated similar results to those obtained under static conditions, in that the S1486A, Cluster 2 and DC variants were less susceptible to ADAMTS13 proteolysis.

Intriguingly even though the S1486 and T1487 glycosylated residues are next to one another, only the mutation of the S1486 residue has an effect on the ADAMTS13 cleavage. This may be explicable when one considers the specificity of N-acetlygalactosaminyltransferases (GalNAcTs) that initiate glycosylation by attachment of GalNAc to Seronine or Threonie residues. It has been previously demonstrated that the initial *O*-linked glycosylation of the peptide can influence the subsequent glycosylation events by inducing conformational changes in the peptide backbone and adjusting the accessibility of particular glycosylation sites for GalNAcTs.[409,410,423,498,499] For example it has been shown that complete glycosylation of MUC1 tandem repeat peptide is dependent on several transferases that act in a highly ordered and hierarchical manner and can have highly restricted acceptor substrates.[500] A similar observation; that prior glycosylation of a peptide backbone with GalNAc has a positive effect on subsequent glycosylation of nearby residues, was shown for the MUC5AC motif peptide[501] and may explain the formation of clustered *O*-linked glycans on mucins. An analogous mechanism can be postulated for VWF *O*-linked glycosylation: mutation of S1486A preventing addition of GalNAc sugar to this residue may then prevent glycosylation of the adjacent T1487 residue. Conversely, the lack of a GalNAc residue at T1487A may not be necessary for the glycosylation of S1486. We have attempted to clarify this by mass spectrometry analysis however to date it has not proved possible.

Decreased susceptibility to ADAMTS13 cleavage observed for the cluster 2 and the double cluster proteins could therefore either be a result of the loss of a single *O*-linked oligosaccharide at S1486 or from a cumulative response resulting in loss of the whole C-terminal glycan cluster. The removal of *O*-linked glycans from the N-terminal flanking region of the A1 domain does not alter susceptibility to ADAMTS13 cleavage. Therefore diminished proteolysis of the double cluster variant is only a consequence of loss of *O*-linked glycans from the C-terminal cluster.

The exact mechanism by which *O*-linked glycosylation can influence susceptibility of VWF to cleavage by ADAMTS13 is unknown. It could be hypothesised that the altered

susceptibility to ADAMTS13 cleavage is due to a change in accessibility to the A2 domain, which in turn reflects a change in VWF conformation.

O-linked glycans are known to provide rigidity to a peptide backbone and stabilize otherwise flexible regions thus stabilising protein conformation.[439] Glycans introduce steric hindrance, and the polypeptide they are attached to can adopt a rigid, extended conformation, with length up to hundreds of nanometers in length as demonstrated by AFM, light scattering and nuclear magnetic resonance studies[438-445] Clustering of GalNAc-based glycans linked by α-linkages to Ser/Thr induces a stable and extended structure to glycopeptides. Importantly, it has been shown that the attachment of a first GalNAc residue by α-linkage to Ser/Thr has a profound effect on the overall conformation of peptide backbone, in which specific interactions between the peptide and the sugar moiety play a crucial role. It has been suggested that stereochemical constraints imparted by the α linkage place the first sugar moiety in close proximity to the peptide backbone.[400,502] The GalNAc residues stabilises the peptide via hydrogen bonding between the amide proton of the GalNAc residue and the oxygen atom of the carbonyl group of the amino acid it is attached to.[438,503] However, a study on the MUC7 protein demonstrated that hydrogen bonding does not occur in serine glycosylated peptides, and therefore they have more rotational freedom around the glycosidic bond and assume a more apical position.[502] In addition, the peptide structure is stabilised by close association of several methyl groups. It has been proposed that the N-acetyl methyl groups of GalNAc interact with methyl groups of nearby amino acids, shielding the hydrophobic surfaces. Rigid and extended *O*-glycosylated peptide have been identified for glycophorin A and it has been suggested the GalNAc residues are located alternatingly on opposite sides of the peptide backbone, further reducing its flexibility.[504] Ovine submaxillary gland mucin (OSM) is another protein whose structure is controlled by *O*-linked glycans. OSM has a highly extended conformation when in its native from, asialo OSM has a somewhat less extended structure, but protein with the *O*-linked glycans removed looses its linear structure and becomes globular. [441]*O*-linked glycans clusters are also present in the hinge regions of the IgA or IgD proteins, where they extend the peptide chain, due to repulsion between charged sugars such as sialic acids, and protect the region from protease cleavage.[450,451]

It could be suggested that removal of glycans from the linker region between the A1 domain and the A2 domain may change flexibility of this region, altering any potential

interactions between the A1 and the A2 domains, and as a result, altering the accessibility of ADAMTS13 cleavage site. In addition, it is known that terminal sialic acid confers a negative charge to glycoproteins due to its carboxyl group dissociating a proton at physiological pH.[505] The removal of *O*-linked glycan(s) and therefore sialic acid may decrease the charge on the A1-A2 linker region and allow VWF to adopt a more tightly folded conformation making it more difficult for ADAMTS13 to access the cleavage site within the A2 domain. It has been previously suggested that the A2 domain is mechanically stabilised by the A1 and A3 domains,[506] therefore I propose that *O*-linked glycans might participate in this stabilisation.

The reason why mutation of only one glycosylation site (S1486A) in the glycan cluster at the C-terminal side of the A1 domain has an effect on ADAMTS13 cleavage may also become better understood when a model of the proposed structure of the VWF A1&A2 domains is analysed. As illustrated on Figure 6.9 when VWF is in its globular conformation, threonine residues 1468 and 1477 are exposed on the surface of the A1 domain while residues S1486 and T1487 are buried within the A2 domain in the vicinity of ADAMTS13 cleavage site. However, this model needs to be interpreted with a degree of caution, since the crystal structures of the A1 and predicted structure of the A2 domains do not include the linker region between the two domains. Indeed, only the crystal structures of the A1 domain obtained by Huizinga et al.,[276] included the *O*-linked glycan site S1468 and this was derived from bacterial cells and thus would not have been *O*-linked glycosylated in any case.

In addition, it is surprising that the two glycosylation sites T1486 and T1487 could be buried within the A2 domain, since these sites have been shown to occupied by *O*-linked glycans. *O*-linked glycosylation occurs once the protein is folded therefore it would be difficult for galactosyltransferases to access the glycosylation site if they were indeed buried. However, the predicted model of the VWF A1A2A3 domains based on the crystal structures is still a valuable model.

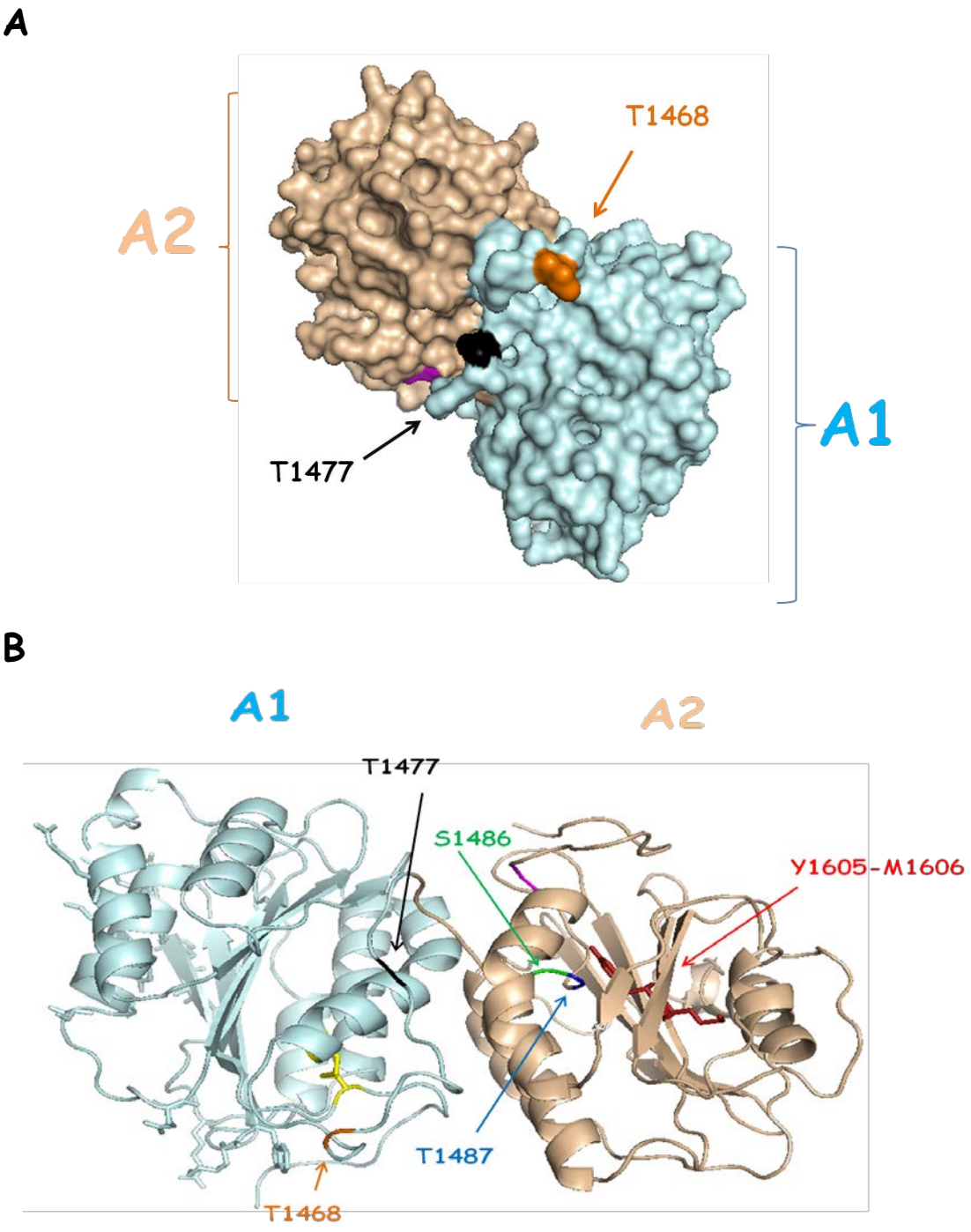


Figure 6.9 Model of the A1 and A2 domain in solution with *O*-glycosylation sites indicated

Model is based on the crystal structure of the A1 domain and predicted crystal structure of the A2 domain and was provided by Wei Chen (**A**) Two *O*-linked glycosylation sites in the A1-A2 linker region mapped to the surface of the A1 domain are indicated, the T1468 residue in orange and the T1477 amino acid in black. (**B**) Ribbon representation of the A1 and A2 domains, the S1486 (in green) and the T1487 (in blue) glycosylation site appear to be buried within the A2 domain, close to the ADAMTS13 cleavage site (Y1605-M1606, in red).

As discussed, the VWF *O*-linked glycans are potentially responsible for maintaining rigidity of the A1-A2 linker region and could prevent excessive shielding of the A2 domain by the A1 domain. Alternatively, *O*-linked glycans can have a more local effect on the stability of the ADAMTS13 cleavage site, since as suggested by the VWF A1A2A3 structural model, the glycans attached to the S1486 and T1487 residues are positioned next to the Y1605-M1606 cleavage site in the partially unfolded A2 domain (Figure 6.10). *O*-linked glycans have been shown to increase stability of various proteins,[385,507-510] and it has been suggested that rather than stabilising the folded state of the protein, they destabilise the unfolded state by increasing its enthalpy. (e.g. by breaking some residual structural elements).[508] Moreover, presence of *O*-linked glycans can prevent aggregation of unfolded or partially unfolded proteins.[508] Furthermore it has been demonstrated that the degree of stabilisation depends on the position of the glycosylation sites and their number, but only very weakly on the type or a size of the glycan.[385,508] Therefore it is postulated that the *O*-linked glycans can force the unfolded VWF-A2 domain to adopt a more extended conformation allowing efficient exposure of the ADAMTS13 cleavage site. Furthermore, they could prohibit the formation of residual interactions within the A2 domain and allow exposure of residues that interact with ADAMTS13 allowing for subsequent proteolysis of the Y1605-M1606 bond. The absence of *O*-linked glycans might induce more flexibility into the structure and allow formation of nonspecific interactions within the A2 domain, therefore impeding ADAMTS13 binding and cleavage as observed for the S1486A, cluster 2 and double cluster variants. Moreover absence of *O*-liked glycans chains could alter the arrangement of the metalloprotease domain in the binding pocket, subsequently impairing the catalytic efficiency of metalloprotease domain.

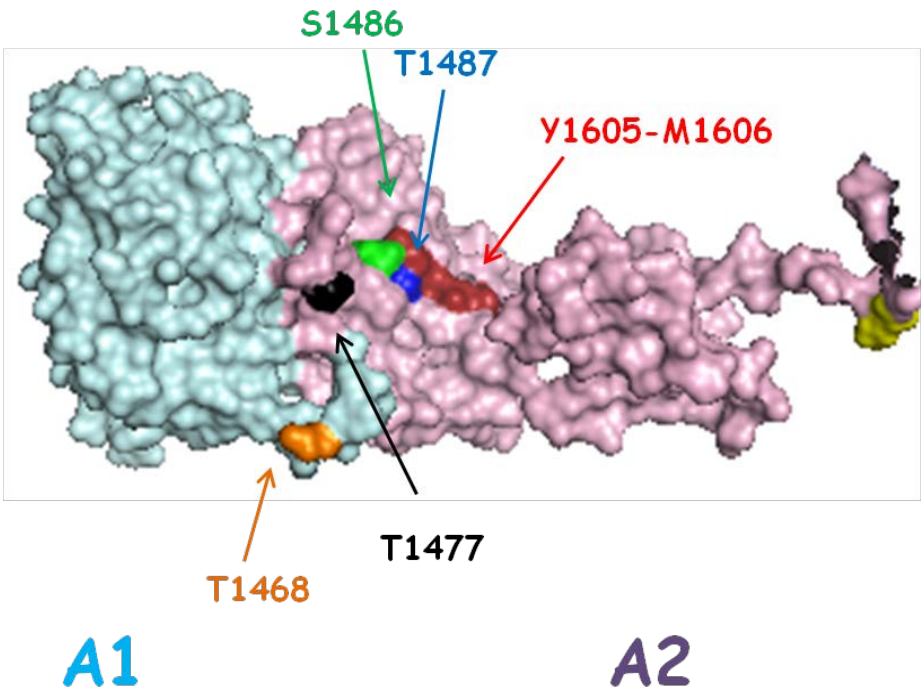


Figure 6.10 Proposed crystal structures model of the A1 the A2 unfolded domains with the *O*-linked glycosylation sites indicted

Model is based on the crystal structure of the A1 domain and predicted crystal structure of the A2 domain and was provided by Wei Chen. Unfolding of the A2 domain results in the exposure of ADAMTS13 cleavage site (in red) and *O*-linked glycosylation sites S1486 and T1487 (green and blue respectively) Suggesting that two oligosaccharides attached to these amino acids, will be present in vicinity of the scissile bond. The other glycosylation sites are T1468 in orange and T1477 in black.

In order to investigate if removal of VWF *O*-linked glycans has a more local effect the susceptibility to ADAMTS13, cleavage reactions were also performed using a shorter substrate D'A3 fragment of VWF. This fragment of the protein was chosen for number of reasons. Firstly it is unable to form dimers or multimers, but contains VWF regions that can influence ADAMTS13 proteolysis. It encompasses both *O*-glycosylated linker regions flanking the A1 domain, as well as all three A domains that are thought to interact with each other. In addition, it contains the D'D3 domains that have been shown to shield the A1 domain. Finally D'A3-VWF was successfully and efficiently expressed and secreted in HEK293T cells.

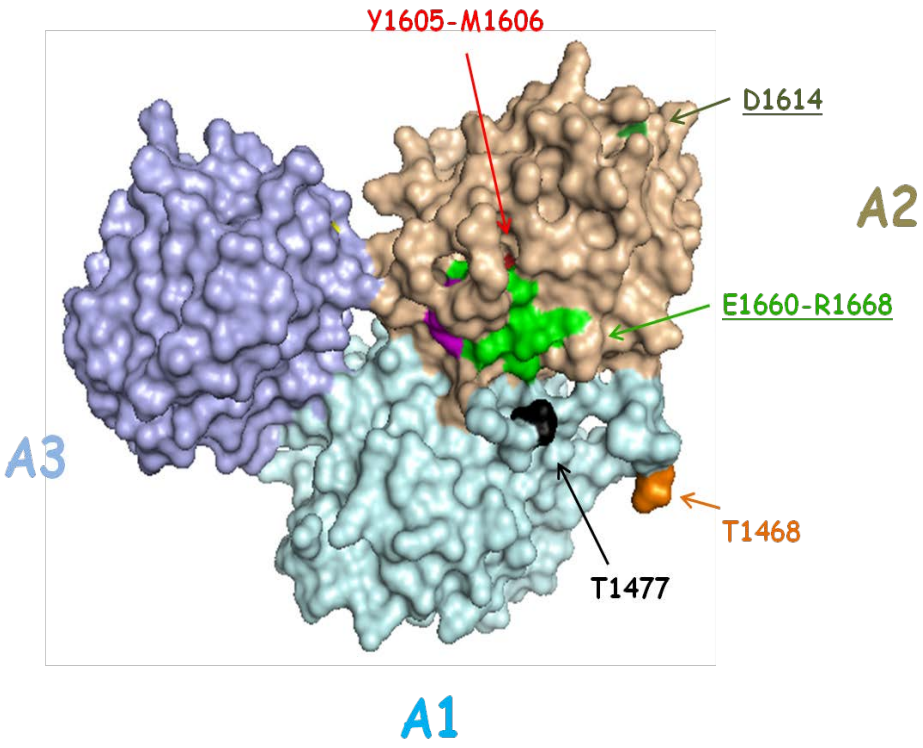
Interestingly, ADAMTS13 cleavage of the D'A3 cluster 2 and double cluster variants showed significantly reduced cleavage in comparison to wtVWF, whereas the D'A3

S1486A VWF mutant did not show any appreciable difference. The reason for the why the absence of a single glycan chain at position S1486 has an effect on cleavage of full length VWF but not the D'A3 fragment is not obvious. It is hypothesised that in the full length protein, the C-terminal end of VWF may be exerting an effect on the conformation or stability of the A2 domain and the removal of only a single glycans chain from this VWF fragment does not modify this.

To further assess how *O*-linked glycans affect the susceptibility of VWF to ADAMTS13 cleavage, the binding interaction between the two proteins was investigated. It has been previously shown that when VWF is coated onto microtitre plates it undergoes a conformational change that exposes the ADAMTS13 binding site within the A2 domain and allows high affinity binding of ADAMTS13 to VWF. Interestingly, the VWF S1486A, Clus2 and DC variants, which were all cleaved to a lesser extent by ADAMTS13, bound ADAMTS13 in this assay with similar affinity.

The binding of ADAMTS13 to elongated VWF is a multistep interaction that engages different exosites in the A2 domain. The ADAMTS13-VWF binding interaction is initiated by the binding of the ADAMTS13 spacer domain with VWF residues E1660-R1668 which helps to approximate two proteins.[223-226] As illustrated on Figure 6.11a the ADAMTS13 spacer domain binding site is positioned near the *O*-linked glycosylation sites when VWF is in its globular conformation. However, in the unfolded VWF-A2 domain, residues E1660-R1668 are distant from the glycosylated A1-A2 linker region (Figure 6.11b). The spacer domain binding allows for subsequent vital interaction between the ADAMTS13 disintegrin-like domain residue R349 and the VWF-A2 domain D1614 residue, which helps to position the scissile bond within the active site of ADAMTS13.[227] Interestingly D1614 is close to the *O*-linked glycans and the ADAMTS13 cleavage site when the VWF A2 domain is partially unfolded (Figure 6.11b), but is distant from the linker region in the folded VWF (Figure 6.11a). Based on the predicted model of the VWF A1A2A3 domain complex the remoteness of the 1660-1668 spacer binding site and *O*-linked glycans in the elongated conformation could explain why the *O*-linked glycans did not influence ADAMTS13 binding in this situation. However since *O*-linked glycans are located close to D1614 residue they could have an effect on downstream binding by the ADAMTS13 disintegrin-like domain, which may not be detected by the binding assay used in this study.

A



B

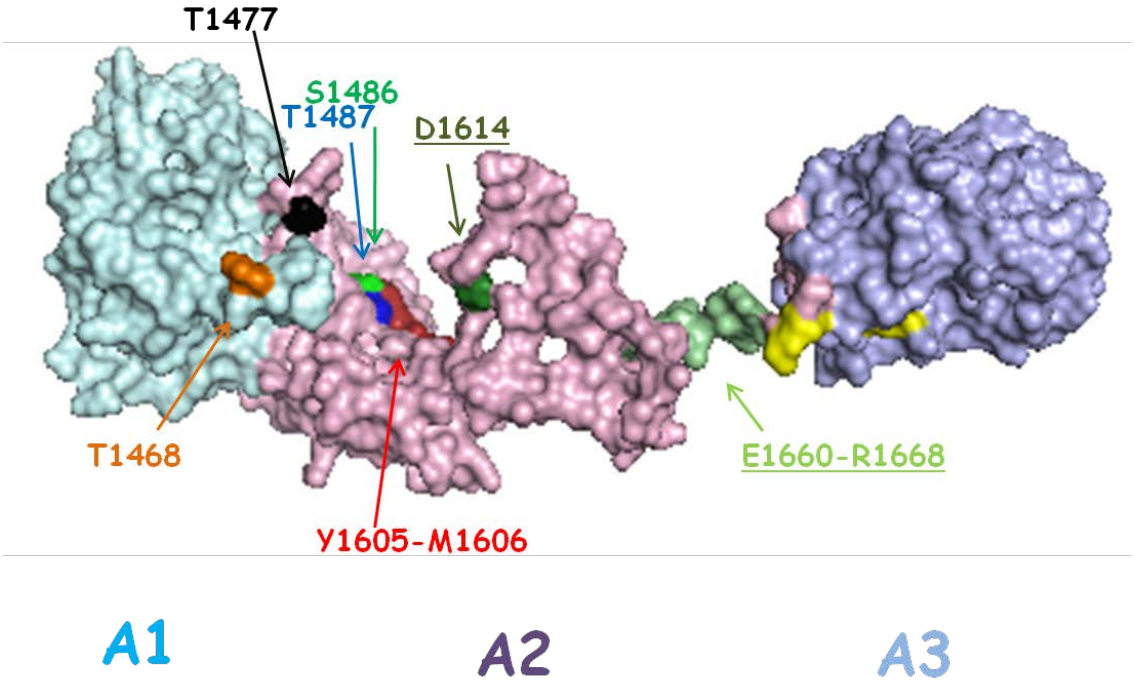


Figure 6.11 Predicted model of the A1A2A3 domains complex

Legend next page:

Model is based on the crystal structure of the A1 and A3 domains and predicted crystal structure of the A2 domain and was provided by Wei Chen (**A**) Illustration of the unfolded A domains complex surface. Exposed *O*-linked glycan sites are indicated T1468 in orange and T1477 in black. The ADAMTS13 cleavage site indicated in red (Y1605-M1606) is buried within the A2 domain. Residues crucial for VWF binding to ADAMTS13 spacer domain, E1660 to R1668 are shown in light green. The D1614 residue that interacts with the disintegrin like domain is labelled in dark green. (**B**) Unfolding of the A2 domain results in the exposure of ADAMTS13 cleavage site and two additional *O*-linked glycosylation sites S1468 and T1487 (green and blue respectively). In addition ADAMTS13 exosites become exposed. With the D1614 residue positioned near the cleavage site and *O*-liked glycosylation sites.

In addition, it may be implied that the observed differences in the interaction of the VWF variants with ADAMTS13 are due to the amino acid change and not the absence of *O*-linked oligosaccharides, however this is unlikely to be the case. Firstly, change of alanine to threonine is typically used to prevent glycosylation at specific sites since it the most conservative change one could apply. Alanine has a similar size as threonine and serine, and has a hydrophobic side chain instead of a polar uncharged side chain, which should not significantly interfere with the conformation of the peptide. Moreover, no change in ADAMTS13 cleavage is observed for the T1487A mutation which is adjacent to the S1486A mutation.

Recently it has been reported that apart from binding to elongated VWF, ADAMTS13 is able to bind with low affinity to VWF, when VWF in its native globular conformation,[152,232] the effect of *O*-linked glycans on this interaction was therefore studied. Intriguingly, the mutations that resulted in decreased susceptibility to ADMATS13 proteolysis enhanced binding of VWF in solution to ADAMTS13. It is not unfeasible, as to our knowledge binding between globular VWF and ADAMTS13 is not necessary or linked to VWF cleavage in the presence of urea. It is hypothesised that the improvement in binding is due to a change in overall conformation of VWF due to removal of *O*-glycan chains. As discussed beforehand absence of *O*-linked glycan chain can induce flexibility of the A1-A2 linker region thus alter the position of both domains in relation to not only each other but also towards other domains. Therefore it is suggested that change in local conformation can alter the exposure of binding sites, on all other domains in globular VWF.

In summary, it has been demonstrated *O*-linked glycans alter VWF interaction with ADAMTS13, possibly by modifying the interface and stability of the A1 and A2 domains. In the next chapter the role of *O*-linked glycans on the interaction of VWF with GPIbα is going to be discussed.

7 EFFECT OF O-LINKED GLYCANS ON THE INTERACTION OF VWF WITH PLATELET RECEPTOR GLYCOPROTEIN Ibα UNDER STATIC CONDITIONS

7.1 Introduction

The *O*-linked glycans clustered around the A1 domain are positioned near regions designated as important for platelet binding, suggesting they may be part of mechanisms regulating the exposure of the GPIbα binding site.[289] Indeed, it has been reported that VWF lacking *O*-linked glycans exhibits reduced binding to GPIbα and limited ability to agglutinate platelets in the presence of ristocetin.[454] Conversely, VWF A1 domain (residues 1236-1476) expressed in *E.coli*, or under *O*-linked glycosylation blocking conditions exhibited increased platelet aggregatory responses when compared with the fully glycosylated forms.[261,455] It is obvious that the existing data is contradictory, therefore the aim of this study was to fully characterise the influence of *O*-linked glycans on the VWF A1 domain interaction with platelets.

Traditionally the interaction of VWF with platelets (via GPIbα) is investigated using the ristocetin cofactor assay and this assay was first used to examine platelet agglutination by *O*-linked glycosylation variants. However, a number of studies have recently utilised a recombinant fragment of GPIbα, spanning the first 290 amino acids to investigate the interaction between GPIbα and the VWF-A1 domain. Consequently I have expressed and purified this recombinant GPIbα fragment (rGPIbα) and a subsequently optimised its use in an ELISA based plate binding assay. This assay was then used to explore the role of *O*-linked glycans in the GPIbα-VWF interaction under static conditions in the absence and presence of various ristocetin concentrations and also in the presence of botrocetin.

VWF sialylation status has also been previously shown to influence platelet aggregation, with several studies suggesting that desialylated-VWF (dsVWF) can induce spontaneous platelet aggregation in the absence of ristocetin and increase ristocetin mediated aggregation.[511,512] However, other studies have detected decreased ristocetin mediated platelet aggregation by dsVWF,[468,476] or have not shown any difference in ristocetin mediated or independent platelet aggregation by dsVWF.[386,387,513] Again, the results of previous studies are conflicting and because the *O*-linked glycans terminate predominantly in negatively charged sialic acid residues, the role of sialic acid on the VWF interaction with GPIbα was also investigated.

7.2 Expression of recombinant GPIbα

7.2.1 GPIbα construct

The N-terminal part of GPIbα has been shown to mediate the interaction between platelets and VWF; therefore Dr TAJ Mckinnon has previously established a clone of GPIbα spanning the first 290 residues and cloned this into the cloning vector pCRTOPO4. In this study the GPIbα fragment from pCRTOP4 was cloned into a pBluescript II SK (+/-) vector using site directed insertion PCR. This fragment was then subcloned into the mammalian expression vector pcDNA3.1/*myc*-his vector in frame with a *myc*-his tag as described in detail in section 3.6.

7.2.2 GPIbα/myc-his protein expression and purification

In initial experiments pcDNA-GPIbα/myc-his was transiently expressed on a small scale in HEK293T cells. Western blot analysis of the expression media demonstrated a band of ~45kDa when probed with anti-*myc* and anti-GPIb antibodies indicating the presence of recombinant GPIbα. To provide sufficient quantities of protein for further assays, rGPIbα was transiently expressed on a large scale in HEK293T cells and purified by Nickel affinity chromatography (Figure 7.1). Eluted fractions were analysed by SDS-PAGE followed by Coomassie staining to determine the purity and presence of rGPIbα (Figure 7.2). The protein was successfully eluted from the column with 250mM imidazole and visible as a single band of 45kDa; however some contaminants were still present in the GPIbα positive fraction (Figure 7.2, lane 3), indicating this purification method provides partial purification of GPIbα. To improve purity and purification was repeated on the eluted material. As shown on the chromatogram (Figure 7.1) some protein was eluted with 10 and 100nM imidazole and those elution fractions were analysed by SDS-PAGE followed by Coomassie staining and immunoblotting using anti-*myc* antibody to determine their purity. Fusion protein was detected by a Western Blot as a single band of 45kDa in the fraction eluted with 100nM imidazole. As shown on SDS-PAGE gel (Figure 7.2, lane 4), all contaminants were successfully removed and only one band of 45kDa corresponding to GPIbα-*myc*/His was visible.

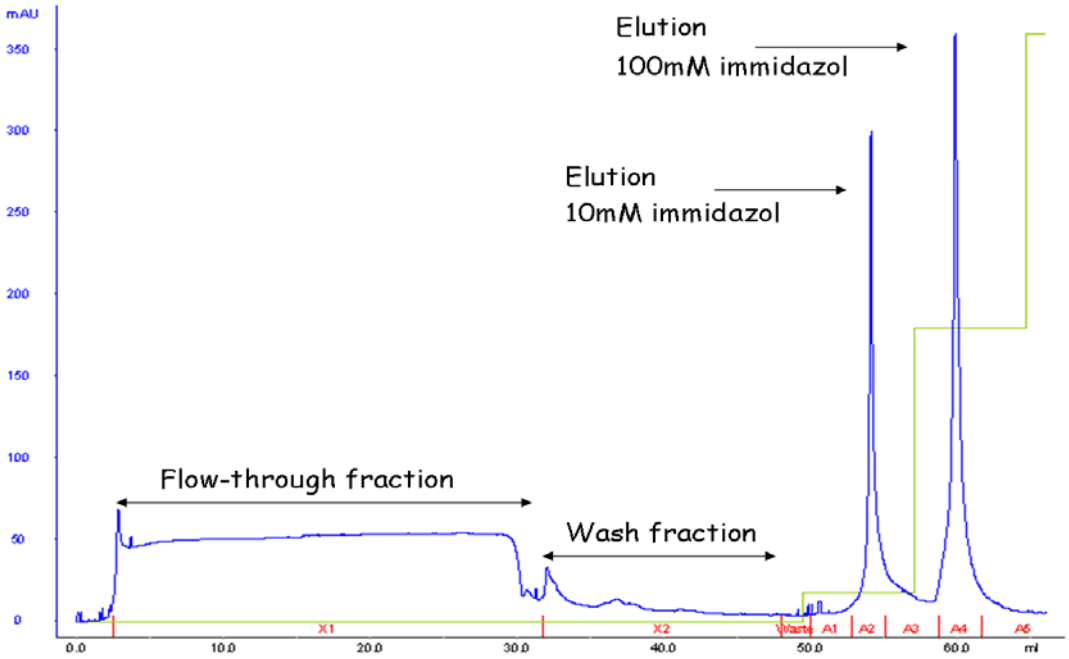


Figure 7.1 FPLC purification of GPIbα-*myc*/his using a Ni^{2+}-chelating HiTrap column

A representative chromatogram of a typical GPIbα purification. The His tag of the protein was exploited in the purification. Filtered and concentrated condition media was loaded onto a column. Some proteins pass through the column and did not bind (flow through fraction). Columns were washed extensively with 20mM Tris, 100mM and 2mM imidazole to ensure that majority of contaminant proteins are washed from the column (wash fraction) prior to isocratic elution (20mM Tris-HCl, 500mM NaCl, 500mM imidazole, pH 7.8). Protein was eluted with 10 and 100nM imidazole. All the fractions were collected and analysed with SDS-PAGE and Western Blotting.

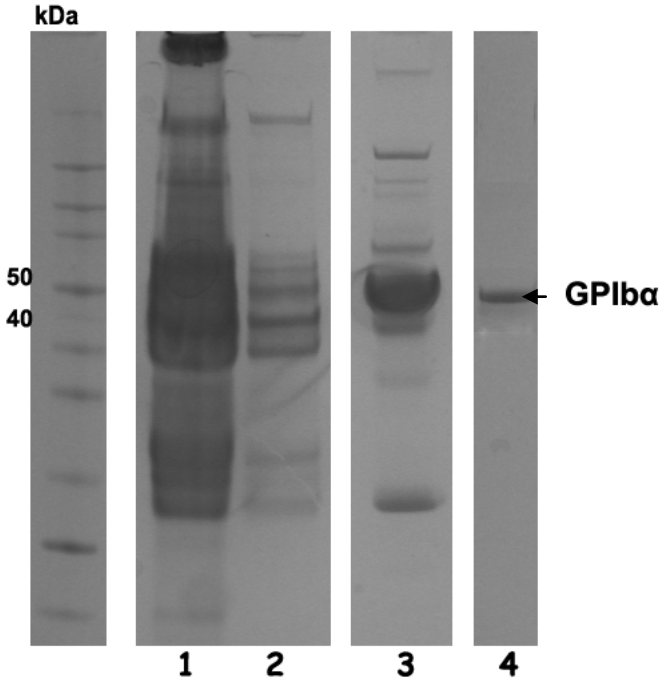


Figure 7.2 SDS-PAGE gel showing the expression and purification of rGPIbα

GPIbα-*myc*/his protein was expressed in HEK293T cells and purified using Nickel affinity chromatography. Fractions from purification were analysed by SDS-PAGE followed by Coomasie blue staining. Lane 1, total mixture of proteins in the culture medium. Lane 2, flow through- material that did not bind to the column X1 fraction on chromatogram), demonstrates presence of contaminant proteins. Lane 3, rGPIbα -*myc*/His containing elution fraction from the first purification, with some contaminants still present. This elution fraction (A2) was re-purified and as shown in Lane 4: pure GPIbα-*myc*/His protein was eluted.

7.3 GPIbα binding assay

The rGPIb fragment was used to establish a plate based assay to investigate the binding of VWF to GPIbα. In brief, microtitre plates were coated with a polyclonal anti-GPIb antibody (anti-CD42b) and this was then used to capture rGPIbα at concentration of 1µg/ml. The microtitre plates were then incubated with VWF in the absence or presence of ristocetin or botrocetin.

7.3.1 GPIbα binding and VWF multimeric size

In order to validate the assay, I initially assessed the effect of VWF multimerisation on the interaction with GPIbα. It has been previously reported that larger VWF multimers bind GPIbα with the greatest affinity. To this end, different VWF fractions with decreasing multimeric size were purified from Haemate P by gel filtration, and were

incubated with immobilised GPIbα in the presence of ristocetin (1mg/ml). Multimer size was determined by VWF multimers analysis and CBA, with the largest multimers (fractions 1 and 2) having a CBA/VWF:Ag ratio of 2.2 and the smallest multimers (fraction 6), a CBA/VWF:Ag ratio of 0.2. In keeping with published data, there was a direct relationship between VWF multimer size and GPIbα binding, with the greatest GPIbα binding observed with the fraction containing the largest VWF multimers. (Figure 7.3) This confirms sensitivity of the assay to VWF molecular weight.

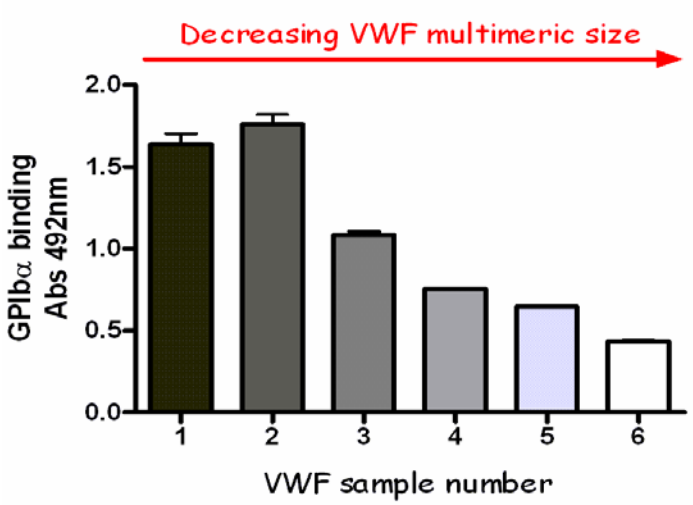


Figure 7.3 VWF multimeric size and ristocetin dependent GPIbα binding

Microtitre plates coated with GPIbα were incubated with different multimeric size pdVWF in the presence of 1mg/ml of ristocetin. PdVWF multimeric size was previously assessed by CBA. Collagen binding corrected for VWF antigen levels (CBA/VWF) of 2.2 corresponded to highest molecular weight multimers and collagen binding of 0.2 to low molecular weight multimers. Calculated CBA/ VWF for sample 1 – was 2.2, sample 2 -1.8, sample 1.6, sample 3- 1, sample 4-0.5, sample 5- 0.5 and sample 6-0.2. GPIbα binding gradually decreases with VWF multimeric size

7.4 GPIbα binding and VWF *O*-linked glycosylation

Since eight of the VWF *O*-linked glycan chains are clustered around the A1 domain they could potentially affect the interaction of VWF with GPIbα. Using the GPIbα plate binding assay I investigated the effect of the *O*-linked glycan variants on the binding of VWF to GPIbα in the absence and presence of ristocetin.

GPIbα coated plates were incubated with 4nM VWF in the absence or presence of 1mg/ml ristocetin. As expected no GPIbα binding was detected for wtVWF when

ristocetin was omitted. (Figure 7.4) In contrast, notable binding was detected following addition of ristocetin (wtVWF +R; Figure 7.4). GPIbα binding assay in the absence of ristocetin was repeated for all glycosylation variants, in order to determine whether removal of any of the glycans results in VWF conformational change that would allow spontaneous GPIbα binding. None of analysed VWF variants could bind VWF without addition of ristocetin (Figure 7.4).

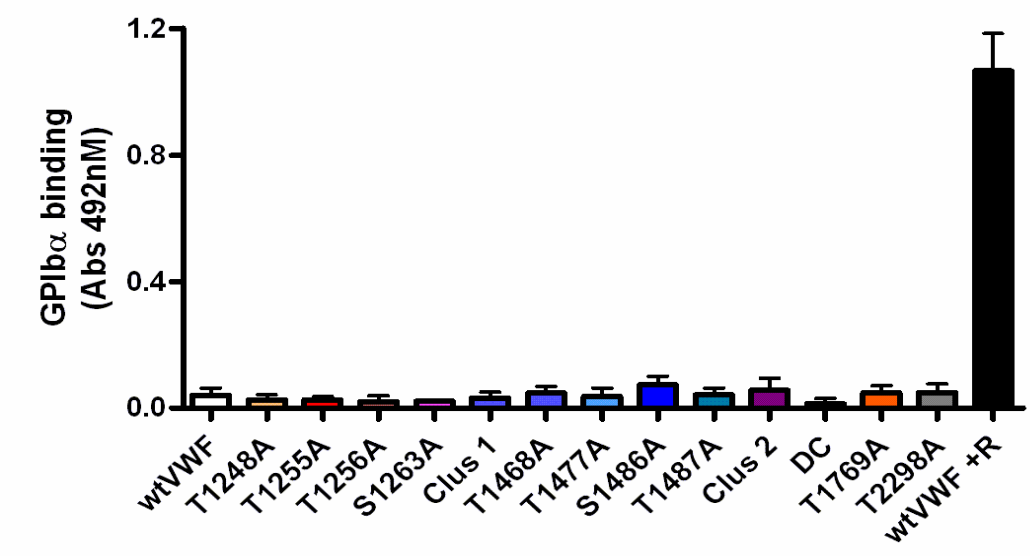


Figure 7.4 GPIbα binding by VWF variants in the absence of ristocetin

wtVWF and VWF variants were applied onto a microtitre plate coated with recombinant GPIbα in the absence of ristocetin. As expected no GPIbα binding was observed for wtVWF. Similarly all *O*-linked glycosylation variants were unable to bind to GIbα without ristocetin. As a control, wtVWF was shown to bind to GPIbα. in the presence of 1mg/ml ristocetin (wtVWF +R).

Since removal of *O*-linked oligosaccharides had no effect on GPIbα binding in the absence of ristocetin, the influence of *O*-linked glycans on ristocetin dependent binding was examined. For this, microtitre plates were coated with GPIbα as beforehand incubated with VWF variants at a concentration of 4nM in the presence of ristocetin. The concentration of 1mg/ml ristocetin was used in this assay as it is used in the traditional Ristocetin Cofactor activity assay and previously described plate assay[514]. Interestingly, compared to wtVWF markedly increased GPIbα binding was detected for the T1255A variant which is localised in the D3-A1 linker region. (Figure 7.5) Furthermore an even greater increase in ristocetin dependent GPIbα binding was detected for the Clus 1 variant, devoid of all *O*-linked glycan chains flanking the N-terminal side of the A1 domain. Moreover, enhanced GPIbα binding was detected for

the DC variant. Conversely, the T1468A and T1477A variants demonstrated reduced binding to GPIbα in the presence of 1mg/ml ristocetin (Figure 7.5), however, despite the Clus2 variant encompassing both of these mutations, its binding to GPIb was unaltered.

Mutation of the other *O*-linked glycosylation sites did not alter the ability of VWF to bind GPIbα in the presence of ristocetin. These data suggest that the *O*-linked glycans clustered at the N-terminus of VWF-A1 domain can have a negative effect on the interaction of VWF with GPIbα, at least in the presence of saturating concentrations of ristocetin. In contrast the lack of *O*-linked sugars at positions T1468 and T1477 in the C-terminus of VWF-A1 domain can decrease the ability of VWF to interact with GPIbα in the presence of ristocetin.

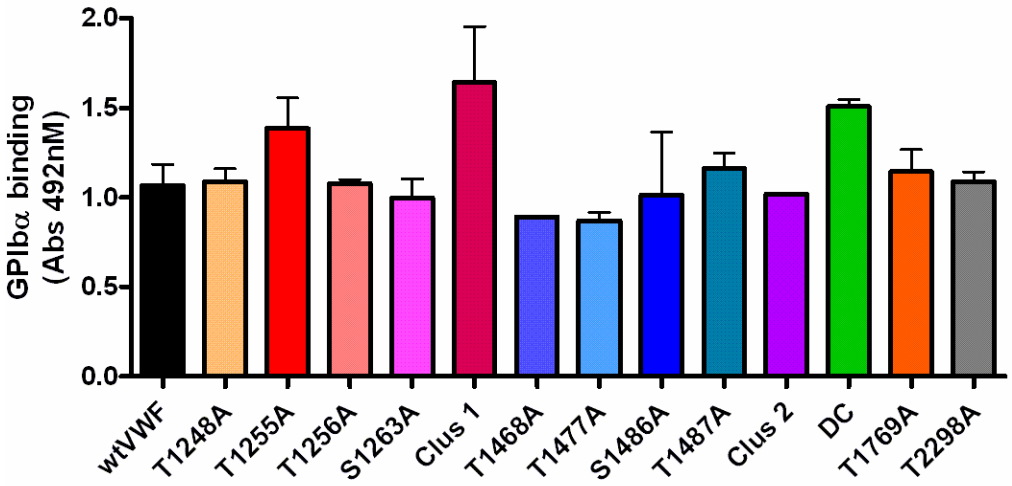


Figure 7.5 Interaction between GPIbα and VWF glycosylation variants in the presence 1mg/ml ristocetin

GPIbα coated plate was incubated with 4nM wtVWF and VWF variants and 1mg/ml of ristocetin, and bound VWF was detected. No binding was detected for wtVWF without the modulator. When compared to wtVWF the T1255A variant, the Clus 1 variant and the DC variant showed increased, whilst the T1468A and the T1468A demonstrated somewhat decreased GPIbα binding potential in the presence of ristocetin. All other *O*-linked glycans exhibited similar ristocetin dependent GPIbα binding to wtVWF.

The changes in the capability of VWF to bind to GPIbα following removal of certain glycan chains were observed in the presence of saturating concentrations of ristocetin. To further elucidate the effect of *O*-linked glycans on the VWF interaction with GPIbα,

binding was tested using a range of ristocetin concentrations between 0 and 1mg/ml. wtVWF binding to GPIbα was evident in the presence of 0.6 mg/ml ristocetin and thereafter the amount of bound VWF increased with increase in ristocetin concentration. (Figure 7.6)

All single N-terminal glycosylation variants apart from the T1255A showed similar sensitivity to ristocetin mediated GPIbα binding as wtVWF. The T1255A variant exhibited increased binding to GPIbα at any ristocetin concentration as shown in Figure 7.6. Moreover, distinctly enhanced GPIbα binding was observed for the T1255A variant in the presence of 0.5mg/ml ristocetin. This is a striking result as wtVWF and the adjacent mutant T1256A were unable to bind GPIbα when incubated with ristocetin concentrations below 0.6mg/ml.

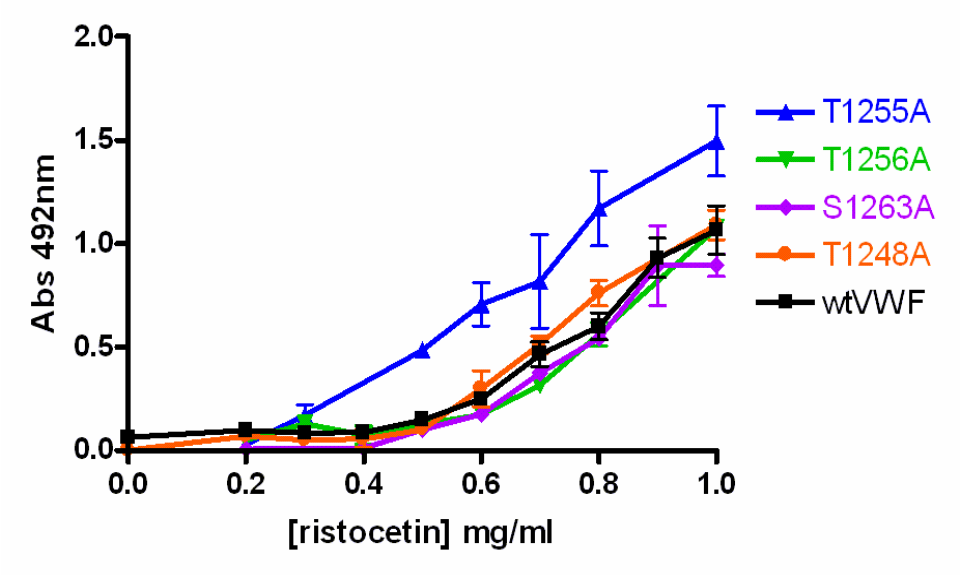
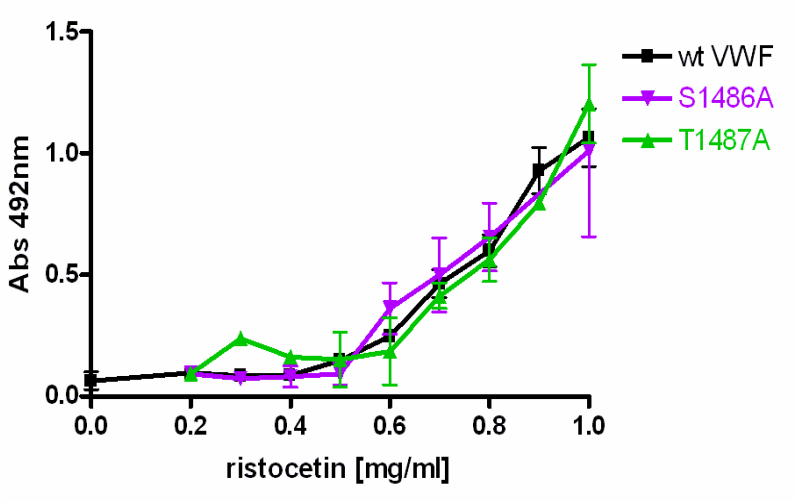


Figure 7.6 Binding between VWF *O*-glycosylation variants (N-terminal side) and recombinant GPIbα in the presence of various ristocetin concentrations

A GPIbα coated plate was incubated with 4nM wtVWF and VWF variants with a range of ristocetin concentrations (0-1mg/ml), and bound VWF was detected. Single glycosylation variants T1248A, T1256A and S1263A and wtVWF showed comparable GPIbα binding in the presence of ristocetin. The T1255A, showed increased GPIbα binding at any ristocetin concentration when compared to wtVWF and in contrast to wtVWF was able to bind to GPIbα at a ristocetin concentration of 0.5mg/ml. (Values shown here are mean ± SEM of 4 separate experiments performed in duplicate).

As illustrated on Figure 7.7a, two single glycosylation variants S1486A and T1487A that flank the C-terminal side of the A1 domain showed similar sensitivity to ristocetin mediated GPIbα binding as wtVWF at any ristocetin concentration. The other two variants T1468A and T1477A demonstrated reduced GPIbα binding at concentrations of ristocetin above 0.6mg/ml when compared to wtVWF, however the difference in binding was not so significant at 1mg/ml of ristocetin (Figure 7.7b).

A



B

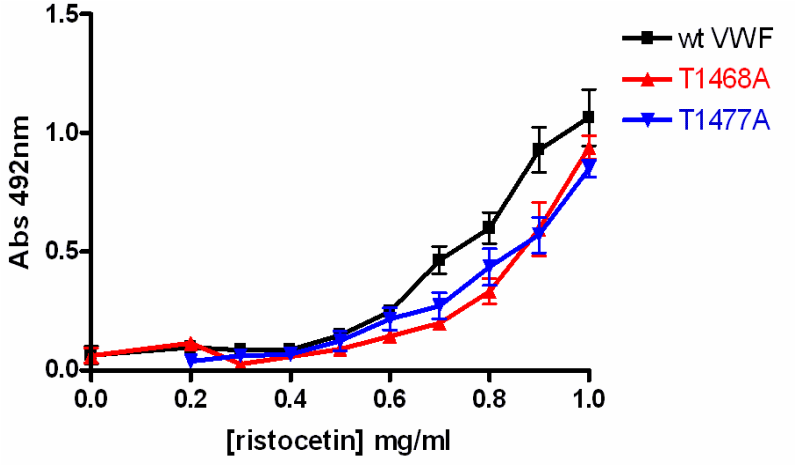
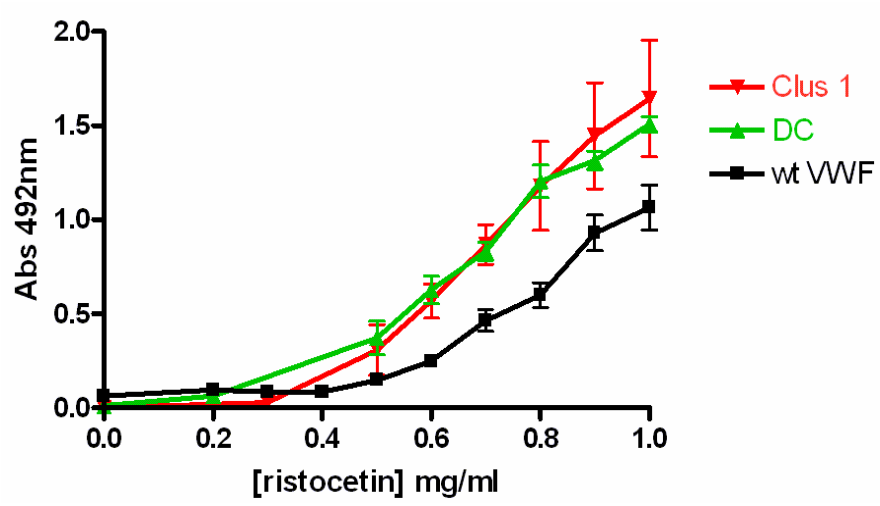


Figure 7.7 Binding between VWF *O*-glycosylation variants (C-terminal side) and recombinant GPIbα in the presence of various ristocetin concentrations

A GPIbα coated plate was incubated with 4nM wtVWF and VWF variants with a range of ristocetin concentrations (0-1mg/ml), and bound VWF was detected. The S1486A and T1487A variants showed similar GPIbα binding; while the T1468A and T1477A variants showed decreased GPIbα when compared to wtVWF (Values shown are mean ± SEM of 4 separate experiments performed in duplicate).

Intriguingly, the cluster 2 variant bound GPIbα in an identical manner as wtVWF (Figure 7.8b). This result is surprising given that the Cluster 2 variant includes the T1468A and T1477A mutations which resulted in decreased sensitivity to ristocetin mediated GPIbα binding. Furthermore, significantly enhanced sensitivity to ristocetin mediated GPIbα binding was observed for both the Clus 1 and DC variants when compared to wtVWF (Figure 7.8a). Importantly, notable binding for those mutants was observed at ristocetin concentrations of 0.5mg/ml, which was too low to induce GPIbα binding by wtVWF. On the basis of this data, it is apparent that the glycans clustered at the N-terminal side of the A1 domain have a major influence on ristocetin mediated GPIbα binding.

A



B

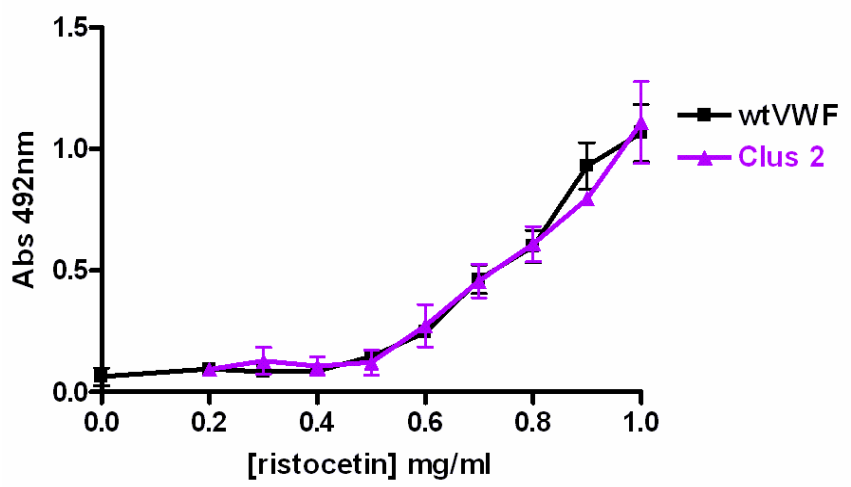


Figure 7.8 Binding between *O*-linked glycosylation cluster variants and recombinant GPIbα in the presence of various ristocetin concentrations

A GPIbα coated plate was incubated with 4nM wtVWF and VWF cluster variants with a range of ristocetin concentrations (0-1mg/ml), and bound VWF was detected.**(A)** The Clus 1 and DC variants showed significantly increased GPIbα binding compared to wtVWF at any ristocetin concentration. (**B**) The Clus 2 variant exhibited unaltered ristocetin dependent GPIbα binding. (Values shown here are mean ±SEM of 4 separate experiments performed in duplicate)

Finally the single glycan variants T1679A and T2298A localised in the A3 and D4 domains respectively were analysed and showed unaltered sensitivity to ristocetin mediated GPIbα binding (Figure 7.9). This suggests that glycan chains remote from the A1 domain have no influence on the VWF sensitivity to ristocetin mediated GPIbα binding.

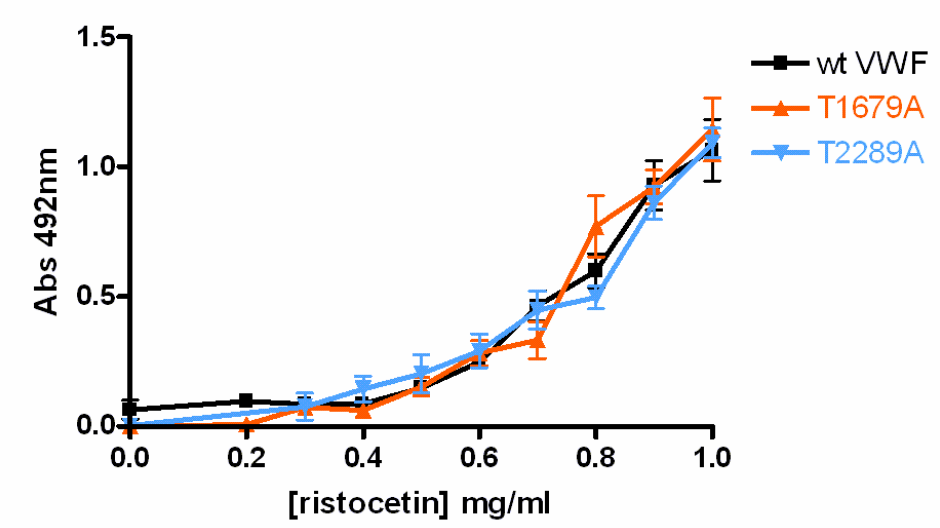


Figure 7.9 Binding between T1679A and T2289A variants and recombinant GPIbα in the presence of various ristocetin concentrations

A GPIbα coated plate was incubated with 4nM wtVWF and VWF variants with a range of ristocetin concentrations (0-1mg/ml), and bound VWF was detected. Both T1679A and T2298A variants showed similar GPIbα binding as the wtVWF. (Values shown here are mean ± SEM of 4 separate experiments performed in duplicate)

In summary, the T1255A, cluster 1 and double cluster variants were demonstrated to have enhanced sensitivity to ristocetin mediated GPIbα and required lower concentrations of ristocetin for the interaction to occur. This indicates that *O*-linked glycans flanking the N-terminal side of the A1 domain have an inhibitory effect on ristocetin mediated GPIbα binding. Strikingly, the absence of only one *O*-linked glycan chain from T1255 residue has a similar effect on ristocetin mediated GPIbα binding as the absence of the entire cluster of glycans flanking the A1 domain.

Interestingly, elimination of a single *O*-linked glycan from either threonine residue 1468 or 1477 resulted in diminished sensitivity of VWF to ristocetin mediated GPIbα binding. Paradoxically, the Clus 2 variant that included these two mutations showed unaltered capacity to interact with GPIbα in the presence of ristocetin.

Finally a type 2B VWD-mutant V1316M was analysed in the plate assay. It has been demonstrated that similarly to the T1255A, Clus1 and DC variants the V1316M variant exhibited an enhanced sensitivity to ristocetin mediated GPIbα binding (Figure 7.11).

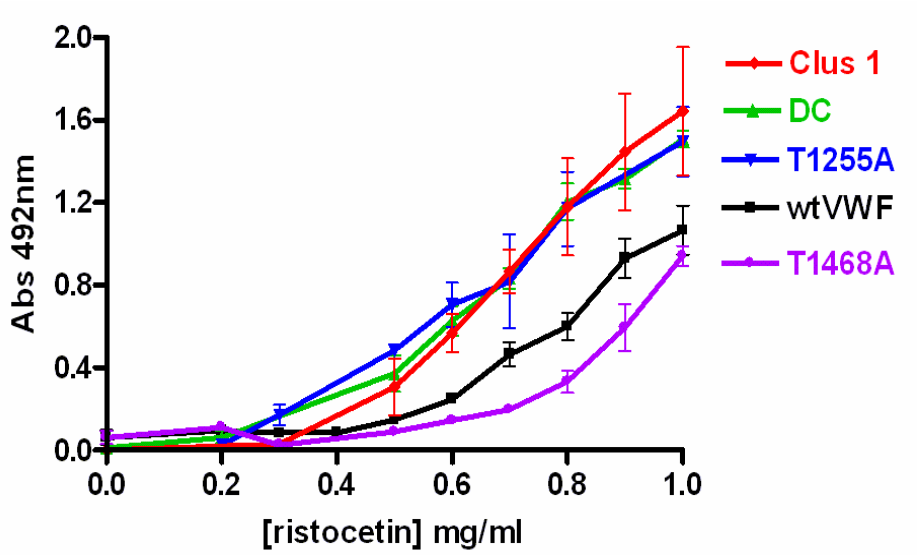


Figure 7.10 Binding between VWF *O*-glycosylation variants and recombinant GPIbα in the presence of various ristocetin concentrations

Summary of mutants with altered sensitivity to ristocetin mediated GPIbα binding. The T1255A, cluster 1 and double cluster variants showed increased sensitivity while the T1468A and T1477A variants showed reduced sensitivity to ristocetin mediated GPIbα binding when compared with wtVWF at any ristocetin concentration from 0.6mg/ml. All other mutants have similar sensitivity to ristocetin mediated GPIbα as wtVWF (results not shown).

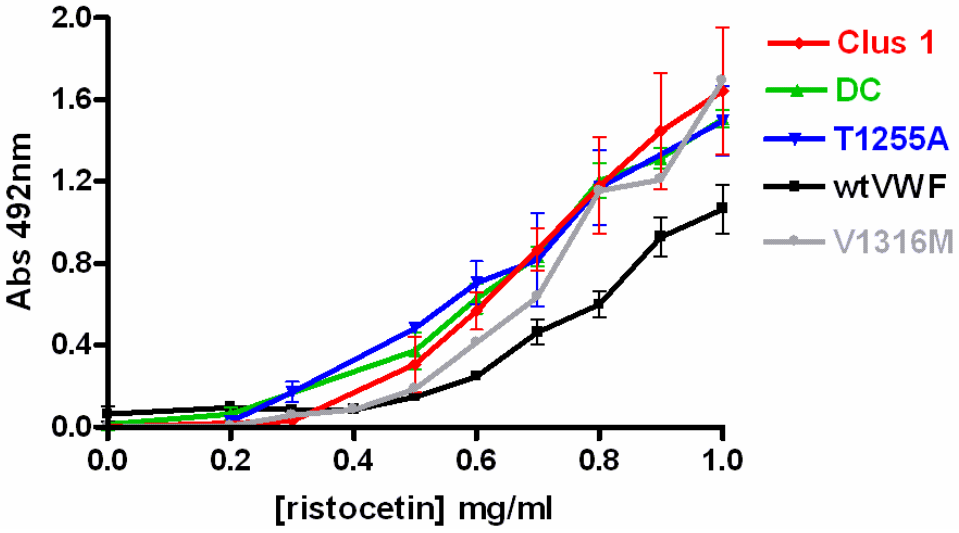


Figure 7.11 Comparison of ristocetin mediated GPIbα binding for wtVWF, VWF *O*-glycosylation variants and type 2B VWD variant

When compared to wtVWF, the type 2B-VWD variant V1316M shows increased sensitivity to ristocetin mediated GPIbα binding. The increase in binding is comparable to that observed for the T1255A, Clus1 and DC variant.

7.5 GPIbα binding and VWF sialylation

Although previous studies have been conflicting, some studies have suggested that VWF devoid of sialic acid is able to interact with GPIbα in vitro without the need for ristocetin. Since *O*-linked glycans predominantly terminate in sialic acid residues any effect of sialic acid on GPIbα binding is likely to be mediated by sialic acid residues present on the VWF *O*-linked glycans.

Firstly GPIbα binding to VWF was investigated after the enzymatic removal of sialic acid by treatment with neuraminidase in the absence and presence of ristocetin. In contrast to some previously published reports no spontaneous binding of desialylated wtVWF (+Neu-wtVWF) to GPIbα was observed in the absence of ristocetin (Figure 7.12). However, in the presence of 1mg/ml ristocetin, Neu-wtVWF demonstrated appreciably increased GPIbα binding compared to wtVWF, suggesting a role for sialic acid in the interaction of VWF with GPIb. However this procedure will have removed sialic acid from both *N* and *O*-linked glycans.

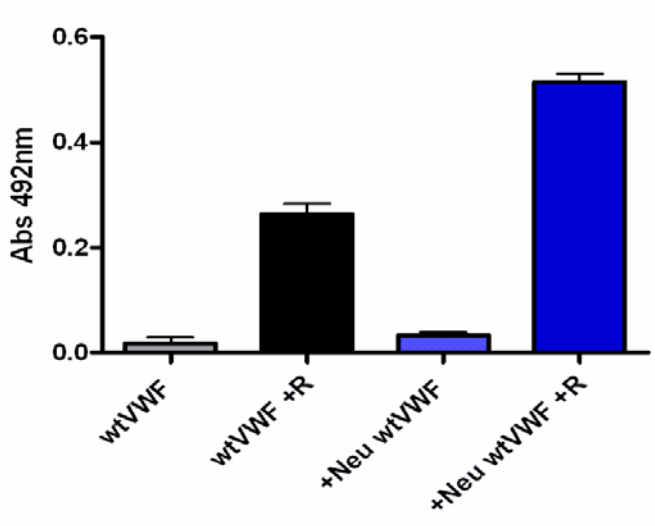


Figure 7.12 GPIbα binding for wtVWF and desialylated wtVWF in the absence and presence of ristocetin

Microtitre plates coated with GPIbα were incubated with wtVWF or desialylated VWF (+Neu-wtVWF) in the absence or presence of 1mg/ml ristocetin. No binding was detected for either sialyated or neuraminidase treated VWF without ristocetin. Desialylated VWF displayed markedly increased sensitivity to ristocetin mediated GPIbα binding in the presence of 1mg/ml when compared to sialylated VWF.

Following on from this, GPIbα binding by desialylated plasma derived (pd) and recombinant VWF was investigated at increasing ristocetin concentrations (0-1 mg/ml) (Figure 7.13). For both pdVWF and rVWF, GPIbα binding was detected first in the presence of 0.6mg/ml ristocetin and gradually increased with increasing concentration of ristocetin. Subsequently, GPIbα binding was compared before and after removal of sialic acid residues. It was observed that more pdVWF (Figure 7.13a) and rVWF (Figure 7.13b) bound to GPIbα following neuraminidase treatment. The increase in binding was observed at ristocetin concentrations above 0.6mg/m. These results clearly indicate that removal of sialic acid residues from VWF results in increased sensitivity to ristocetin mediated GPIbα binding.

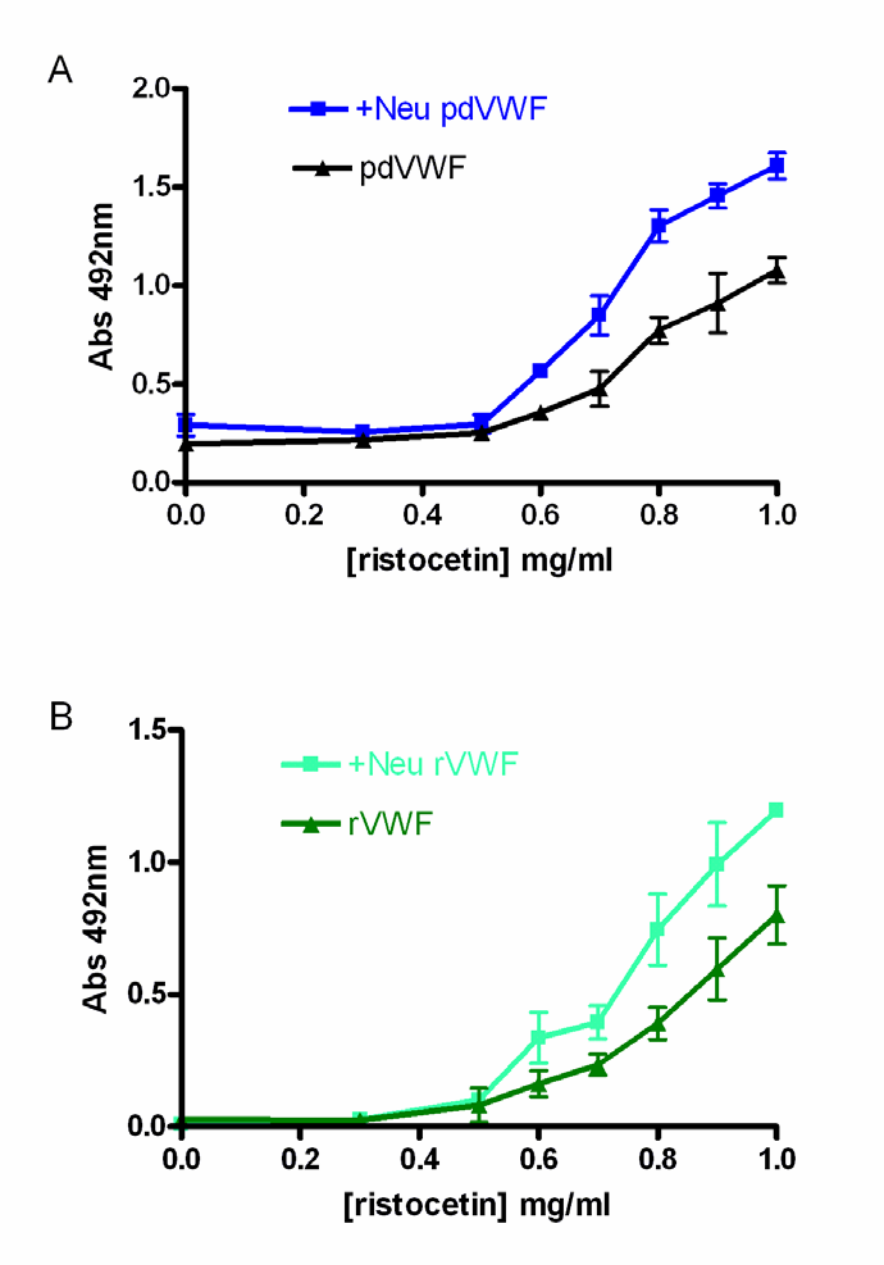


Figure 7.13 Interaction between GPIbα and sialyated and desialyated plasma derived and recombinant VWF

GPIbα binding affinity was investigated for pdVWF (**A**) and rVWF (**B**) in the presence of various ristocetin concentrations (0-1mg/ml). Both pdVWF and rVWF start to bind to GPIbα at 0.6mg/ml of ristocetin. In addition GPIbα binding was compared for sialyated and desialyated VWF (+Neu). More GPIbα binding was detected for desialyated (+Neu) pdVWF and rVWF at each ristocetin concentration (above 0.6mg/ml). +Neu-neuraminidase treated desialyated VWF.

7.5.1 Desialylation of *O*-linked glycosylation variants

Since an increase in sensitivity to ristocetin dependent binding to GPIbα was observed for the Clus 1 and DC variants and for Neu-VWF, I investigated the combined effect of removing sialic acid from these variants on ristocetin mediated GPIbα binding. Confirming my previous observations, Neu-VWF demonstrated increased GPIbα binding at and above ristocetin concentrations of 0.6mg/ml. The Clus2 variant bound GPIbα in similar fashion to wtVWF. Interestingly, removal of sialic acid from the Clus 2 variant did not enhance its binding to GPIbα, with binding at all ristocetin concentrations similar to wtVWF (Figure 7.14b). In contrast, the Clus1 variant, that has increased GPIbα binding, demonstrated a similar binding profile to Neu-VWF and binding of the Clus1 variant was further enhanced by the removal of sialic acid, with the Neu-Clus1 variant showing interaction with GPIbα at a ristocetin concentration of 0.4mg/ml. (Figure 7.14a). This is a remarkable result as neither wtVWF, single cluster mutants or desialylated VWF were able to interact with GPIbα at such a low concentrations of ristocetin.

Finally, the DC variant demonstrated markedly increased GPIbα binding compared to desialylated wtVWF (+Neu-wtVWF) at any ristocetin concentration (above 0.5 mg/ml). Significantly, the DC variant bound to GPIbα in the presence of as little as 0.4mg/ml of ristocetin in a manner comparable to the +Neu-Cluster 1 variant. Intriguingly, removal of sialic acid residues from the double cluster did not alter its GPIbα binding.(Figure 7.15a) Since the DC variant has only 2 more *O*-linked glycan chains left, neuraminidase treatment in this case will have resulted in removal of terminal sialic acid mainly from the *N*-linked glycans. Consequently it seems highly probable that the loss of sialic acid from the *O*-linked glycans is responsible for the increased sensitivity to ristocetin mediated GPIbα binding.

To further confirm this conclusion and to assess the role of sialic acid from the *O*-linked but not *N*-linked glycans in GPIbα binding, neuraminidase with highly specific activity towards α2-3 linked sialic acid was used in contrast to general neuraminidase that removes α2-3,6,8,9 sialic acid. This assay was performed based on the fact that the terminal sialic acid residues on the *N*-linked glycans are predominantly α2-6 linked to penultimate galactose residues,[20,383] whilst sialic acid on *O*-linked glycans may be either α2-3 or α2-6 linked[452] As shown in Figure 7.15b the wtVWF with majority of α2-3

linked sialic acid removed, exhibited identical ability to bind GPIbα in the presence of ristocetin as the wtVWF with α2-3,6,8,9 sialic acid residues removed and the fully sialylated wtVWF. This tends to confirm the conclusion that it is loss of sialic acid primarily from the *O*-linked glycans which lead to increased sensitivity to ristocetin dependent GPIbα binding.

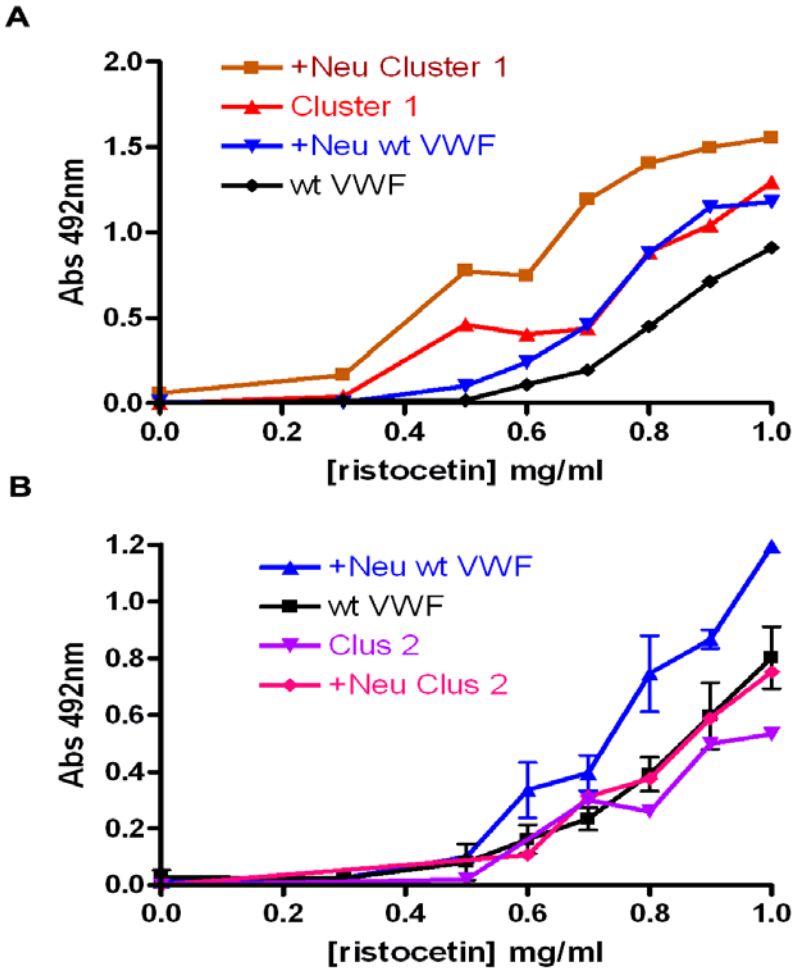


Figure 7.14 GPIbα binding by desialyted wtVWF, Clus 1 and Clus 2 variants in the presence of various ristocetin concentrations

A microtitre plate was coated with rGPIbα fragment via an antibody, and incubated with 4nM sialylated and desialylated wtVWF and VWF cluster variants in the presence of 0-1mg/ml ristocetin. (**A**) Cluster 1 bound to GPIbα similarly to desialylated wtVWF, and even greater increase in binding was observed for neuraminidase treated cluster 1. (**B**) No change in GPIbα binding was observed following removal of sialic acid form the Clus 2 variant.

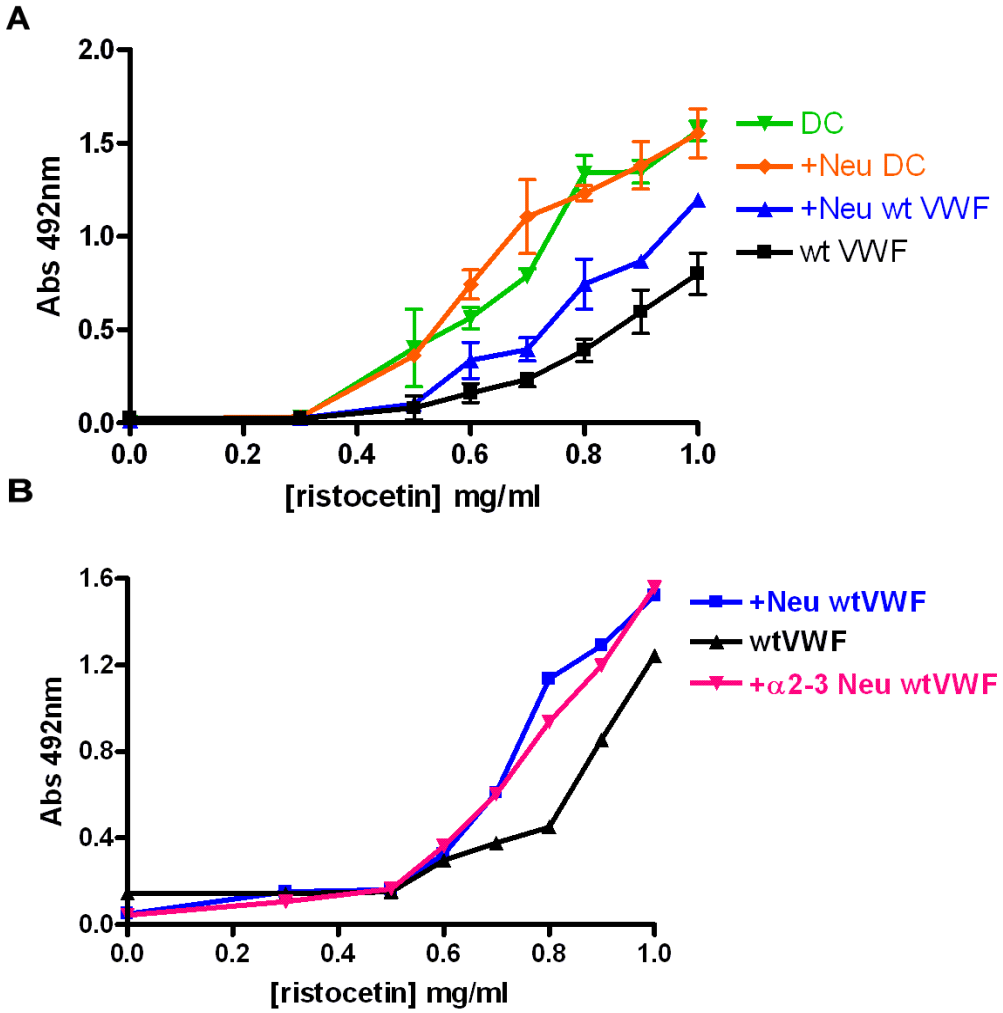


Figure 7.15 Binding between GPIbα and desialylated DC variant in the presence of a range of ristocetin concentrations

A microtitre plate was coated with rGPIbα fragment via an antibody and incubated with 4nM sialylated and neuraminidase treated wtVWF and DC variant in the presence of 0-1mg/ml ristocetin. (**A**) The DC variant bound to GPIbα significantly more readily than desialylated wtVWF, no additional increase in binding was observed for desialylated double cluster.(**B**) WtVWF was incubated with the α2-3 neuraminidase to specifically remove α2-3 linked sialic acid. The same amount of ristocetin dependent GPIbα binding was detected for wtVWF devoid of all sialic acid residues (+Neu wtVWF) and VWF lacking only α2-3 linked sialic acid (α2,3 Neu VWF).

7.6 Binding between GPIbα and wtVWF in the presence of botrocetin

To obtain more information regarding the role of *O*-linked glycans flanking the A1 domain of VWF in its interaction with GPIbα, plate binding assays were performed for wtVWF and double cluster in the presence of botrocetin since the mechanism by which botrocetin supports platelet binding and aggregation is different from that of ristocetin. However due to time constraints only preliminary data for the DC cluster variant was obtained.

rGPIbα was immobilised onto a plate via anti-GPIb antibody and incubated with increasing concentrations of VWF in the presence of 5µg/ml purified botrocetin. As shown on Figure 7.16 botrocetin dependent GPIbα binding was detected for wtVWF. Interestingly no difference in binding was detected for double cluster variant, suggesting that *O*-linked glycans have no influence on GPIbα binding in the presence of botrocetin.

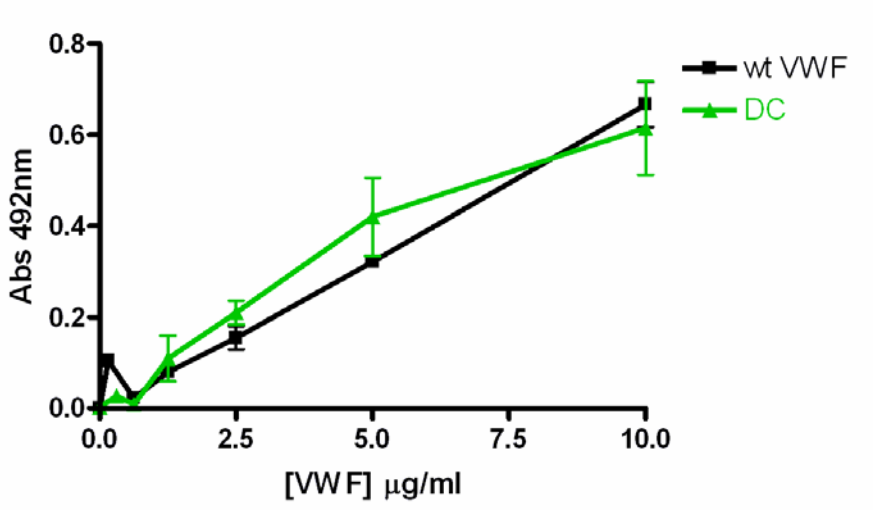


Figure 7.16 Binding of wtVWF and double cluster variant to GPIbα in the presence of botrocetin

A microtitre plate was coated with rGPIbα via anti-CD42b antibody and incubated with increasing concentrations of wtVWF or DC variant in the presence of 5µg/ml botrocetin. Interestingly, both wtVWF and double cluster exhibit similar botrocetin-dependent GPIbα binding.

7.7 Ristocetin co-factor activity assay- Influence of *O*-linked glycans on platelet aggregation

The ristocetin co-factor activity assay (VWF:RCo) is used in the diagnosis of patients with suspected VWD as it reproduces, *in vitro*, the ability of VWF to interact with platelets. The original method for this assay was described by MacFarlane and is based on the property of ristocetin to agglutinate formalin-fixed platelets in the presence of VWF.[515] Recombinant wild type and mutated VWF were sent to a diagnostic laboratory and their ristocetin co-factor activity analysed. (Assays performed by Ms Gillian Angus, Hammersmith hospital, London and Dr Anne Riddell, Royal Free hospital, London). The results from two separate assays performed on proteins expressed at different times are shown on Figure 7.17. It was demonstrated that all single glycosylation mutants localised on the N-terminal side of the A1 domain (T1248A, T1255A, T1256A) and their cluster (Clus 1) showed an increase in ristocetin dependent platelet aggregation when compared with wtVWF. The T1468A variant, on the C-terminal side of the A1 domain, had significantly diminished ristocetin co-factor activity. Interestingly the cluster 2 variant had the same capability to agglutinate platelets in the presence of ristocetin as wtVWF.

The results from the VWF:RCo assays generally correlate with the results obtained with the static GPIbα binding assays. The VWF variants that demonstrated increased ristocetin dependent binding to GPIbα also demonstrated enhanced platelet aggregation (e.g. T1255A, Cluster 1). Furthermore, the S1468A mutant showed both decreased R:Co activity and GPIbα binding, while the cluster 2 variant performed like wtVWF in both assays. However the T1248 and T1256A variants showed increased platelet aggregation, in contrast to results obtained in the plate assay where they showed similar GPIbα binding as wtVWF.

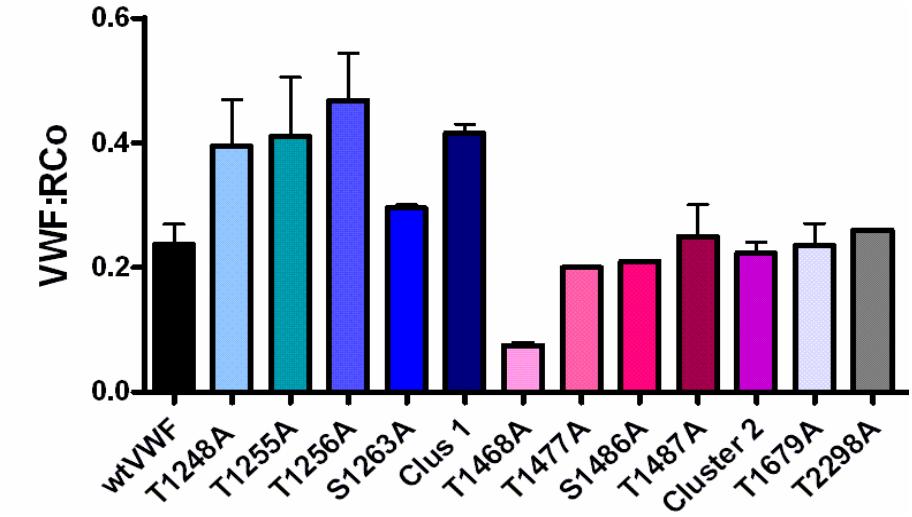


Figure 7.17 Ristocetin co-factor activity assay of recombinant VWF variants

Platelet agglutination in the presence of 1mg/ml ristocetin was analysed for wtVWF and VWF glycosylation variants. When compared with wtVWF the Cluster 2 shows the same VWF:RCo activity while decrease in activity is observed for the T1468A variant. The T1248A, T1255A, T1256A and Cluster 1 demonstrate increased platelet aggregation in the presence of ristocetin. All other single glycosylation variants showed unaltered platelet ristocetin dependent platelet aggregation.

7.8 Discussion

Existing published data regarding the function of VWF *O*-linked glycans in mediating the VWF-platelet interaction are conflicting and inconclusive; therefore in this project the role of *O*-linked glycans flanking the VWF-A1 domain on GPIbα binding has been investigated.

Traditionally, the ristocetin cofactor activity assay (VWF:RCo) has been used to investigate the platelet aggregatory potential of VWF; however this assay is known to have a high intra-assay coefficient of variation (CV) and is often not highly reproducible.[516] Recent attempts to improve the assay have made use of a plate based ELISA assay that utilises a recombinant fragment of GPIbα.[514] Therefore in this project I have constructed an expression vector for recombinant GPIbα, and used purified rGPIbα to establish a more reliable, reproducible and sensitive plate based assay to examine the interaction of VWF with GPIbα. In this assay GPIbα is captured to an anti-GPIbα antibody that doesn't affect the VWF-GPIbα interaction and then VWF is applied in the presence or absence of ristocetin.

Consistent with previous reports, I confirmed that larger VWF multimers bind more readily to GPIbα and since the *O*-linked glycosylation mutants analysed have similar multimeric patterns, any changes in GPIbα binding will not be due to variations in multimer distribution. In the absence of ristocetin, no GPIbα binding was detected for wild type or mutated VWF demonstrating that removal of even all the *O*-linked glycans flanking the A1 domain does not allow VWF to bind platelets spontaneously, or at least not in the assay used. Subsequently, I have analysed the ability of the VWF variants to bind GPIbα in the presence of 1mg/ml ristocetin. Interestingly, compared to wtVWF, markedly increased sensitivity to ristocetin mediated GPIbα binding was detected for the T1255A, Clus 1 and DC variants. Conversely, the T1468A and T1477A variants demonstrated slightly reduced binding to GPIbα; however, despite the Clus2 variant encompassing both of these mutations, its binding to GPIbα was unaltered. The changes in the ability of VWF to bind to GPIbα following removal of certain glycan chains were observed in the presence of saturating concentrations of ristocetin, therefore binding was investigated using a range of ristocetin concentrations. Ristocetin response curves generated for the *O*-linked glycan mutants on the N-terminal side of the A1 domain demonstrated that the T1255A, the cluster 1 and double cluster variants exhibited an increased response to ristocetin compared to wtVWF. These results indicate that *O*-linked glycans clustered at the N-terminal side of the A1 domain have an inhibitory effect on GPIbα binding at least in the presence of ristocetin, however the mechanisms of this effect are likely to be complex.

The crystal structure of the A1-GPIbα complex demonstrates that the N-terminal A1 flanking region interacts with the β-finger of GPIbα, and is displaced when GPIbα binds.[276] Moreover, recombinant A1 domain lacking the N-terminal extension has significantly enhanced GPIbα binding and the N-terminal flanking region is dislocated away from the interaction site in the type 2B VWD gain of function R1306Q mutant.[276,137] These data suggest that the N-terminal A1 flanking region has an inhibitory effect on GPIbα binding and that dislocation of the N-terminal extension, for example by shear stress may be a crucial mechanism physiologically allows GPIbα binding. Therefore, it may be hypothesised that dislocation of the N-terminal flanking region can also occur following removal of *O*-linked glycans, reducing its inhibitory properties and enhancing platelet binding. In addition, the N-terminal *O*-linked glycan cluster could modulate the interaction of the A1 domain with the D'-D3 domains. A

recent study suggested that when VWF is in a globular conformation the D'-D3 region shields the A1 domain, preventing GPIbα binding.[138] As discussed in the previous chapter, *O*-linked glycans provide rigidity to peptide backbones and for that reason it is suggested that the A1-N-terminal *O*-linked glycan cluster can stabilize the linker region between the D3 and A1 domains.[439] Consequently, loss of *O*-linked glycans can potentially increase the flexibility of the linker region and decrease any shielding effect of the D'D3 domains which would in turn result in increased exposure of the GPIbα binding site and augmented GPIbα binding. Change in the rigidity of the linker region and the interaction between the D'D3 and A1 domain might also result from the loss of negative charges associated with terminal sialic acid residues present on VWF *O*-linked glycans.

Alternatively, it could be hypothesised that the T1255A, cluster 1 and double cluster variants have an altered structure and as a result less ristocetin is required to promote an adequate conformational change required for interaction with GPIbα. In the nanobody binding assay, discussed in the previous chapter, a lower concentration of ristocetin was required to activate VWF and allow binding, as only partial activation of the VWF A1 domain is required for nanobody binding. The conformational change following removal of all the *O*-linked glycans flanking the A1 domain allows VWF to weakly bind to the nanobody in solution suggesting that the A1 domain is partially activated, however this activation is not large enough to result in spontaneous GPIbα binding. In addition removal of both clusters resulted in increased GPIbα binding at various ristocetin concentrations suggesting increased availability of the GPIbα binding site. The effect observed for the double cluster variant is possibly attributed to the removal of *O*-linked glycans from the N-terminal cluster, as removal of cluster 2 alone does not influence GPIbα binding.

In contrast, the S1468A variant (C-terminal side of A1) showed decreased GPIbα binding and platelet aggregation. These results are in keeping with previous data in which membrane-expressed A1 domain, devoid of *O*-glycan at position T1468, showed decreased platelet aggregatory potential.[455] It is hypothesised that the reduction in GPIbα binding is either due to destabilisation of the GPIbα or the ristocetin binding sites. Two regions have been implicated in VWF interaction with ristocetin the C1237-P1251 region at the N-terminal site of the A1 domain[288,289] and the proline-rich

sequence, E1463 to N1472, C-terminal to the disulphide bond in the VWF-A1 domain.[288-291] (Figure 7.18)

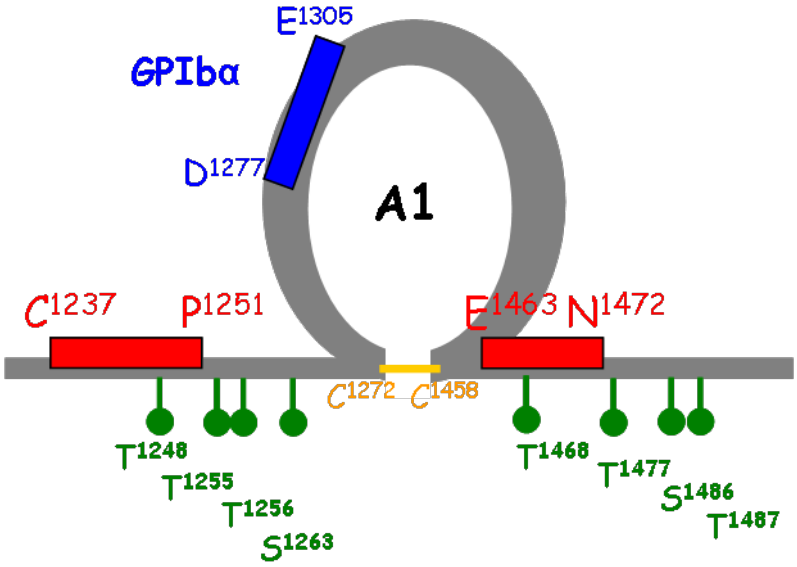
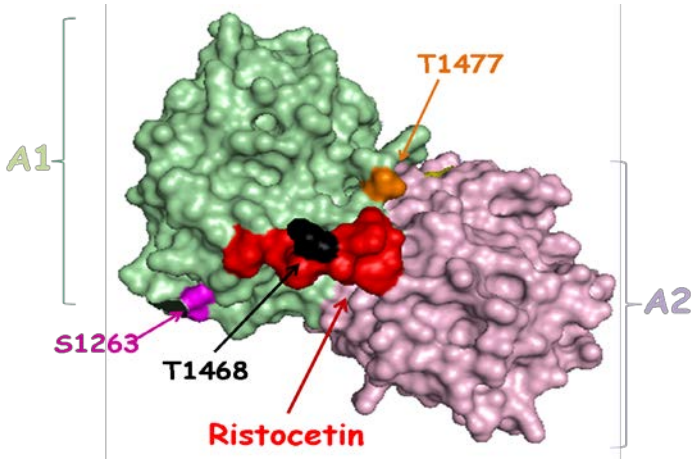


Figure 7.18 The A1 domain diagram

Schematic illustration of the A1 domain and its flanking regions with *O*-linked glycan sites indicated in green. Disulphide bond in yellow; sites implicated in ristocetin binding red boxes; GPIb binding site in blue box.

On the basis of that data, the N-terminal ristocetin binding site encompasses the glycosylated T1468 residue.[291,517,518] Cationic ristocetin would be expected to interact with a region of VWF having a net negative charge; therefore removal of T1468 glycan with its putative sialic acid terminus would reduce ristocetin binding. Moreover, as graphically illustrated on a predicted model of the folded A1-A2 domain complex, the ristocetin binding site and the T1468 glycosylation site are positioned on the surface of the A1 domain, while the putative GPIbα binding site is located on the opposite face of the A1 domain (Figure 7.19). On the basis of this observation I propose that the absence of an *O*-linked glycan at the T1468 residue alters ristocetin binding, rather than having any direct effect on the GPIbα binding site. However, as discussed in the previous chapter the proposed model needs to be interpreted with a degree of caution, as neither the crystal structures of the A1 or the predicted structure of the A2 domain[519] include the linker region between the two domains. The crystal structure of the A1 domain obtained by Emsley *et al.*,[125] included only the *O*-linked glycan sites S1263 and S1468 however the A1 protein was expressed in *E.coli* and therefore would not have been *O*-linked glycosylated in any case.

A



B

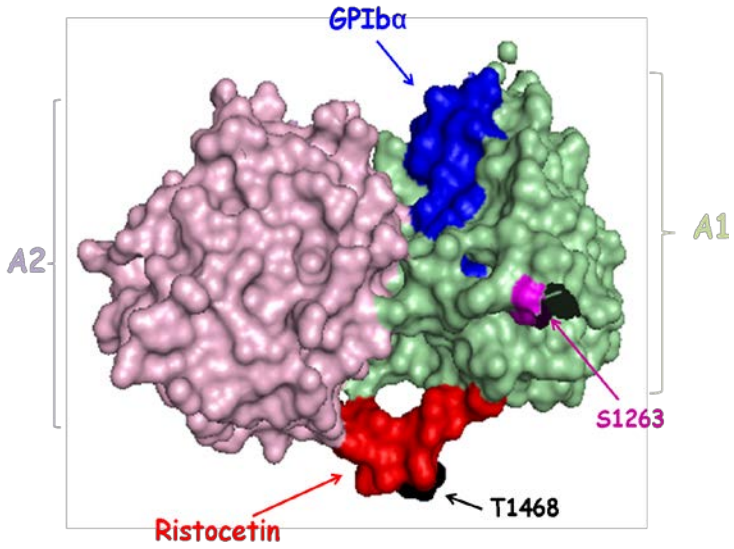


Figure 7.19 Predicted model of the A1-A2 domain complex based on the A1 domain crystal structure and predicted A2 domain structure with sites implicated in GPIb*α* and ristocetin binding

Surface model is based on the crystal structure of the A1 domain[125] and predicted crystal structure of the A2 domain[519] and was provided by Wei Chen (**A**) Two *O*-linked glycosylation sites in the A1-A2 linker region mapped to the surface of the A1 domain are indicated, the T1468 residue in black and the T1477 amino acid in orange. S1263 glycosylation site located in the N-terminal A1 domain flanking region marked in purple. The putative C-terminal ristocetin binding site is showed in red.(**B**) The major GPIbα binding site is indicated in blue and positioned on the opposite side of the A1 domain than the ristocetin binding site (in red).

Surprisingly, removal of all the C-terminal cluster *O*-linked glycans does not alter GPIbα binding even though it includes the T1468A mutation. This discordance is as yet unexplained. As discussed in the previous chapter *O*-linked glycans provide rigidity and stability to peptide backbones, therefore it is likely that removal of a whole glycan cluster from the A1-A2 linker increases flexibility of the peptide backbone enhancing the interaction between the A1 and A2 domains. Increasing the proximity (folding) between the A domains due to removal of *O*-linked glycans could limit the exposure of the C-terminal ristocetin binding site, but could at the same time enhance the exposure of the ristocetin biding site at the N-terminus of the A1 domain, and thus the cluster 2 variant would retain its GPIbα binding ability. Conversely, the removal of single glycan from this region may not alter the flexibility of the linker region enough to change the availability of ristocetin binding sites but could still limit the VWF interaction with ristocetin by removing the negative charge. It needs to be stated however that the sites implicated in ristocetin binding are not necessarily the only ones and are were not precisely mapped. In addition, it is not known how and if putative *O*-linked glycosylation sites are occupied in the recombinant *O*-glycosylation variants. Inhibition of glycosylation at the T1468 might modify utilisation of other sites within the cluster, and this could alter GPIbα binding.

Increased platelet aggregation in the presence and absence of ristocetin was previously observed for desialylated VWF (Neu-VWF).[512] In this study I have shown that desialylated recombinant and plasma derived VWF did not bind GPIbα in the absence of ristocetin but exhibited increased ristocetin dependent GPIbα binding. It has been previously shown that VWF sialic acid is decreased in patients with primary pulmonary hypertension (PPH).[520,521] PPH is characterised by presence of defective VWF, lacking large multimers and of chronic endogenous platelet activation. The authors of the study suggested that the presence of only lower molecular weight multimers in PPH patients is due to the increased consumption of VWF due to increased platelet binding and/or increased cleavage of VWF. This hypothesis is consistent with the observations made in this study that desialylated VWF has increased GPIbα binding and that larger VWF multimers exhibit greater GPIbα binding in the presence of ristocetin.

Furthermore, the Cluster 1 variant had similar binding to GPIbα Neu-wtVWF at various ristocetin concentrations and a further increase in binding was observed following removal of sialic acid residues. Interestingly Neu-Cluster 2 bound GPIbα in a similar

manner to wtVWF, suggesting that loss of entire *O*-linked oligosaccharide chains in the N-terminal cluster, not just terminal sialic acids is responsible for the increased binding observed for Cluster 1. However, it has to be also considered that removal of sialic acid from the N-terminal glycan cluster can have a different effect on VWF conformation and GPIbα binding than removal of both the C-terminal glycan cluster and sialic acid from the N-terminal glycan cluster. No additional increase in GPIbα binding was observed for the desialylated double cluster variant, which implies that removal of sialic acid from *O*-linked oligosaccharides not *N*-linked glycans is responsible for the increased GPIbα binding detected for Neu-wtVWF. Is has been shown that the terminal sialic acid on the *N*-linked glycans are predominantly α2-6 linked to penultimate galactose residues,[20,383] whilst sialic acid on *O*-linked glycans may be either α2-3 or α2-6 linked.[452] This property was used to further assess the role of sialic acid on the *O*-linked but not *N*-linked glycans. The wtVWF was treated with α2-3 neuraminidase which resulted in reduction of sialic acid mainly on *O*-linked glycans. Interestingly no difference in GPIbα binding was observed between wtVWF with no terminal sialic acid, and wtVWF with no α2-3 linked sialic acid, with all both having increased binding when compared to wild type VWF. Consequently it seems highly probable that the loss of sialic acid from the *O*-linked glycans is responsible for the increased GPIbα binding.

It needs to be considered, however, that the static GPIbα binding assay described in this thesis looks only at the first stage of the interaction with platelets. The VWF:RCo assay utilises ristocetin as an *in vitro* agonist to stimulate VWF-platelet interactions. Therefore the ability of the *O*-linked glycan variants to bind and agglutinate platelets was investigated using the traditional Ristocetin Cofactor Assay. Results obtained from the VWF:RCo assay were generally consistent with the results obtained using the GPIbα plate binding assay, with the T1255A, Clus1 and DC variants showing increased and the T1468A variant showing decreased ristocetin dependent platelet aggregation. However the T1248A and T1256A single glycosylation variants showed increased VWF:RCo, which contradictory to results from the plate assay were the variants had similar sensitivity to ristocetin mediated GPIbα binding. The exact reason why T1256A and T1248A have increased VWF:RCo but do not demonstrate increased ristocetin mediated GPIbα binding is not clear. However it is widely viewed that the VWF:RCo assay has a high intra-assay coefficient of variation (CV) and is often not highly reproducible.[516] Additionally, the high concentration of ristocetin (1mg/ml) used in the

assay, can precipitate plasma proteins, including VWF, and can bind platelets directly, thus further confounding the data.

In order to further elucidate if the changes in GPIbα binding where due to altered interaction with the *O*-linked glycan mutants I have attempted to investigated the binding with a different modulator; botrocetin. The snake venom protein botrocetin promotes the VWF-GPIbα interaction *in vitro,* however it interacts with distinct region of VWF and GPIbα (Figure 7.20), and induces GPIbα binding through different mechanisms compared to ristocetin.[270,292] In contrast to ristocetin, botrocetin does not induce any conformational change in the A1 domain but can provide an additional binding surface for GPIbα.[293,294] It has been demonstrated that botrocetin first binds to the A1 domain but not GPIbα and than subsequently slides around the A1 surface to form a new interface. Unlike ristocetin which is readily purchased as a ready to use reagent, botrocetin is only available as crude venom from *Bothrops jararaca* and requires purification prior to use. It has only recently been possible to optimise a purification protocol and only a small quantity of purified botrocetin was obtained. Thus the data I have obtained with botrocetin is very limited.

Nevertheless I have demonstrated that interestingly, in the presence of botrocetin, the DC variant bound to GPIb in a similar fashion to wtVWF. This could imply that the increase in binding observed for the DC variant in the presence of ristocetin reflects an enhanced response to ristocetin, not the accessibility of the GPIbα binding site. Furthermore, it is suggested that the double cluster variant could bind ristocetin more readily and less ristocetin would be required to induce conformational change in VWF. Alternatively VWF with *O*-linked glycans removed could be less stable and more susceptible to deformation.

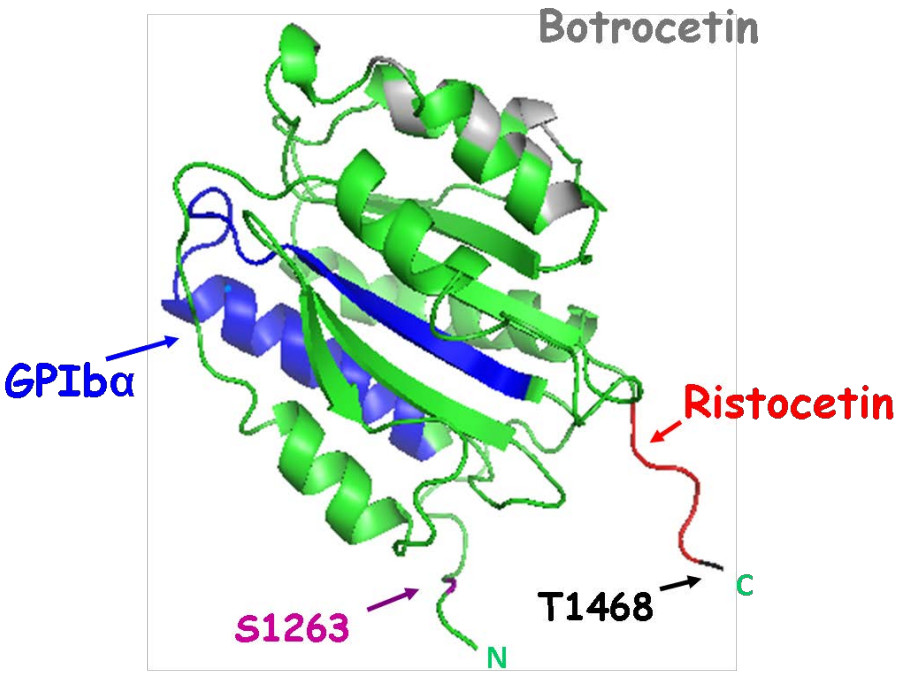


Figure 7.20 The A1 domain crystal structure

The A1 domain crystal structure[125] with the main GPIbα binding site in blue. Residues implicated in ristocetin binding are coloured in red. Residues implicated in polar interaction with botrocetin binding are also indicated (in grey).[294] The *O*- glycosylated residues S1263 (purple) and T1468 are also indicated in the A1 N-and C-terminal flanking region respectively.

In conclusion, the data presented in this chapter demonstrates that the *O*-linked glycans flanking the N-terminal side of the A1 domain have a negative effect on sensitivity to ristocetin mediated GPIbα binding in the plate assay and platelet aggregation in the VWF:RCo assay. In addition the absence of T1486A and T1477A glycans appears to impair VWF sensitivity to ristocetin mediated GPIbα binding and platelet aggregation. However these effects have all been observed under static conditions in the presence of artificial modulators. To assess the role of VWF *O*-linked glycans under more physiological conditions an *in vitro* flow assay was optimised and used to investigate the interaction of VWF with platelets under shear stress conditions.

8 VWF *O*-LINKED GLYCANS ROLE IN VWF-PLATELET INTERACTION UNDER CONDITIONS OF FLOW

8.1 Introduction

It is evident from the previous chapter that the *O*-linked glycans clustered around the VWF A1 domain alter the ability of VWF to interact with GPIbα in the presence of ristocetin. *In vivo*, platelets bind to VWF under conditions of physiological blood flow, thus the limitation of the assays performed in the previous chapter are the requirement for ristocetin and the absence of shear stress. To more effectively analyse the interaction of VWF with platelets, I have developed an *in vitro* flow based assay system to assess the VWF-platelet interaction under conditions of physiological flow. The developed flow assay allows direct visualization of the VWF-platelet interaction in real time, negating the need for ristocetin and providing a more physiological setting in which to investigate the role that VWF *O*-linked glycans play in mediating this interaction. In this chapter I will firstly discuss the optimisation of the flow assay and then its application to investigate the effect of VWF sialic acid and *O*-linked glycosylation on the ability of VWF to capture platelets under conditions of shear stress.

8.2 Expression and purification of D'A3

In majority of the flow assays performed a VWF fragment spanning the D' to A3 domains was used. The D'A3 construct, (designated VWF-D'A3) had been previously cloned in our laboratory and was chosen for several reasons; firstly the construct encompasses both clusters of *O*-linked glycans and domains vicinal to the A1 domain which could influence the A1 domain exposure and GPIbα binding (e.g. it contains the D'D3 domains that have been shown to shield the A1 domain[138]); secondly, it is readily expressed and purified at high levels and thirdly, for kinetic analysis of the VWF-GPIbα bond under flow conditions a monomeric fragment of VWF was required because spatial separation of VWF A1 domains is critical for these assays.

The *O*-linked glycosylation mutations were inserted into VWF-D'A3 by sub-cloning from the pcDNA3.1-FL-VWF construct using *KpnI* and *BamHI* restriction sites. D'A3 proteins which contained a C-terminal *c-myc*/His tag, were transiently expressed in HEK293T cells and purified by Nickel affinity chromatography. Eluted fractions were analysed by SDS-PAGE followed by Coomassie staining to determine the presence and purity of D'A3-VWF. In the fraction eluted with 25mM imidazole a band of ~115kDa

corresponding to D'A3 protein was present, with very little other contaminating proteins (Figure 8.1).

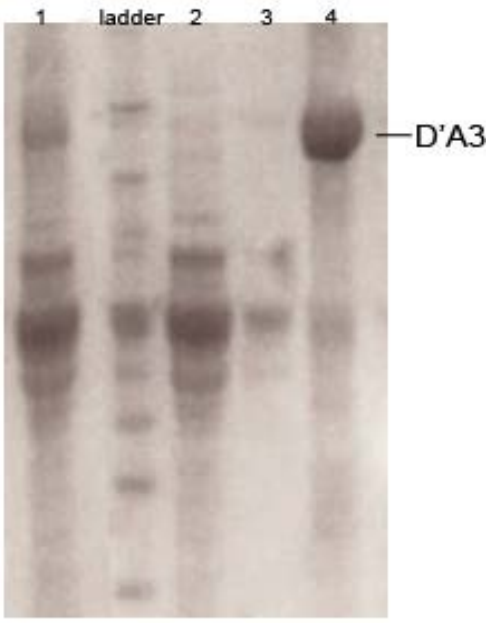


Figure 8.1 SDS-PAGE gel showing the expression and purification of wtD'A3-VWF

VWF-D'A3-*myc/his* protein was expressed in HEK293T cells and purified using a Ni^{2+}-chelating HiTrap column. Fractions from the purification were analysed by SDS-PAGE followed by Coomasie blue staining. Lane 1 - total mixture of proteins in the culture medium. Lane 2 - flow through material that did not bind to the column, Lane 3 - column wash fraction. Lane 4 - material eluted with 25mM imidazole.

8.3 Flow assay optimisation

8.3.1 Experimental setup

A schematic overview of the components used in the flow assay system is presented in Figure 8.2. The system comprises a syringe connected to a syringe driver that is set to predefined flow rates and is used to pump fluids through the flow slides. The flow slides are mounted under an Olympus U-TV1X-2 inverted stage fluorescent microscope that is coupled to a high speed RoleraXR digital camera and the camera is connected to a PC system to allow real-time visualisation and recording of fluorescently labelled platelets. StreamPix 6 software was used to capture images at a rate of 20-30 frames per second, these were then processed using VirtualDub software (freely available from http://www.virtualdub.org) and analysed using ImageJ software (freely available from http://www.ibidi.de).

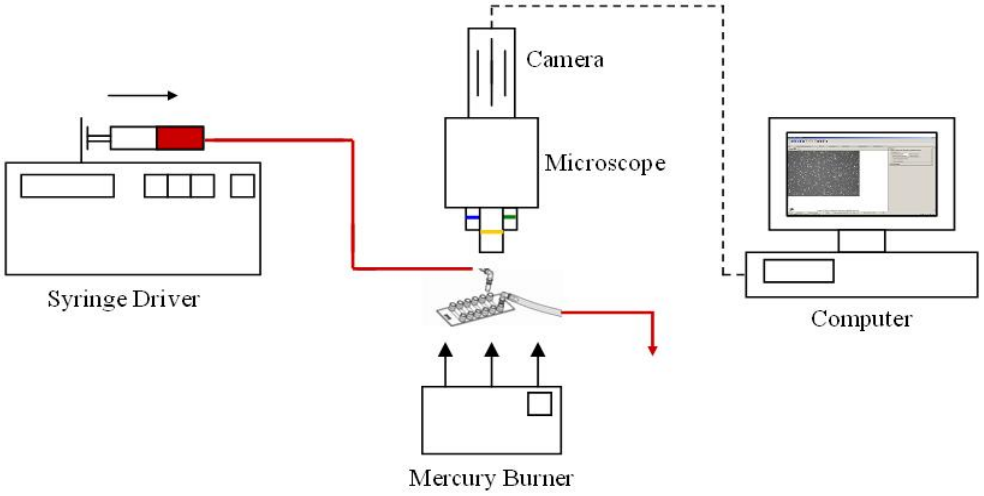


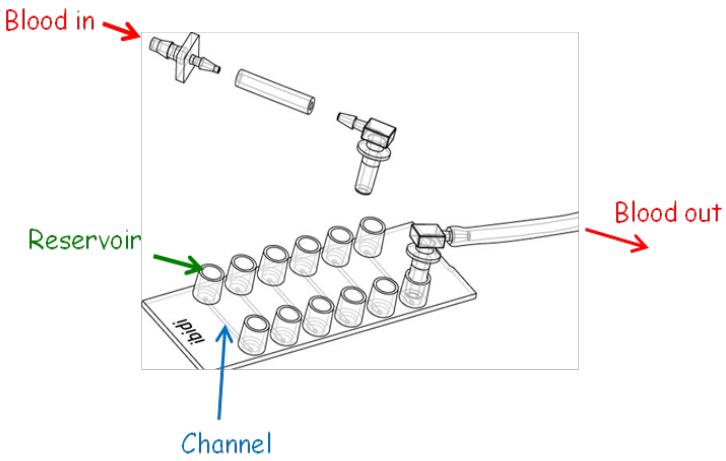
Figure 8.2 Experimental setup for flow assays

8.3.2 Flow slides

Previous work using physiological flow assays have generally utilised parallel plate flow chamber systems. This normally involved coating glass coverslips with proteins (or cells) and mounting the coverslip on a glass or plastic slide; this would then be covered with a rubber gasket and then a second slide on top. This was subsequently clamped and sealed tight with a vacuum source to prevent leakages. While these systems were effective, they could be cumbersome to assemble and the glass coverslips were often prone to breakage or the whole system prone to leakage. Recently, a number of products have become commercially available that have simplified the normal parallel plate system. These flow chamber slides are normally made of disposable plastic and are constructed to comprise a narrow channel with a low chamber height through which fluid can be perfused. The slides used in this project are manufactured by ibidi® and are made of hydrophobic plastic that has been optimised for efficient protein coating and fluorescent microscopy. Two types of ibidi slide were used, µ-slides $VI^{0.1}$and $VI^{0.4}$. As shown in Figure 8.3a these slides contain 6 separate flow channels with an inlet and outlet reservoir at either end, the inlet port is connected via plastic tubing to the syringe, while the outlet port is put to waste. The 0.1 and 0.4 refer to the channel heights of 100 and 400µm respectively, with the smaller channel height and volume of the µ-slide $VI^{0.1}$ resulting in a low pump speed to high shear ratio, thus minimising the amount of blood required for each experiment. The desired shear rate was obtained by setting the syringe driver to pump at a flow rate defined by the slide

manufacturer and as shown in Figure 8.3b, the recommended observation area is the central portion of the each channel which gives the greatest area of homogenous shear stress.

A



B

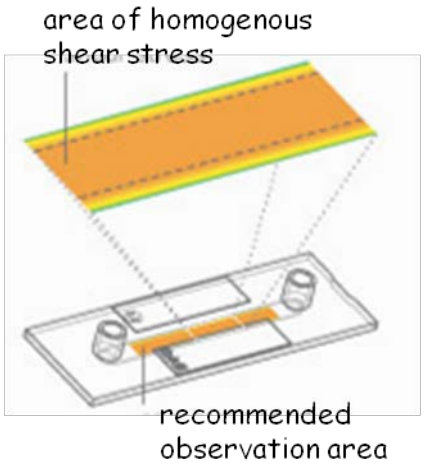


Figure 8.3 Flow slide-design and setup

Images acquired from Ibidi® web-site http://www.ibidi.de/

8.3.3 Platelet preparation

In this project flow assays were performed using purified and fluorescently labelled platelets and washed erythrocytes. Platelets were isolated by centrifugation from whole blood collected form healthy donors into ACD anticoagulant. Since in this project only the interaction between the platelet receptor GPIbα and the VWF-A1 domain was investigated, platelet activation was inhibited by the addition of prostaglandin E1,

apyrase and EDTA. Apyrase was used as it rapidly metabolizes ADP and ATP released from platelets thereby reducing platelet activation and recruitment whilst EDTA inhibits integrin receptor function. Isolated platelets were labelled with Calcein acetoxymethylester (AM) fluorescent dye. Calcein AM is cell permeable compound that is hydrolyzed by intracellular esterases enabling calcein to readily bind intracellular calcium, resulting in a green fluorescence (excitation and emission maxima ~494 and 517nm respectively). In parallel, erythrocytes were washed to remove any plasma VWF. As illustrated on Figure 8.4 erythrocytes require four saline washes to eliminate all plasma VWF. Washed erythrocytes were re-suspended with HEPES/Tyrodes buffer supplemented with 3.5mg/ml BSA to the original starting volume of blood, to maintain a normal hematocrit and the required amount of labelled platelets were added. In the assays where slides were coated with collagen the full platelet count was perfused (~200000 platelets per μl), while in the assays with immobilised VWF 14000 platelets per μl were used.

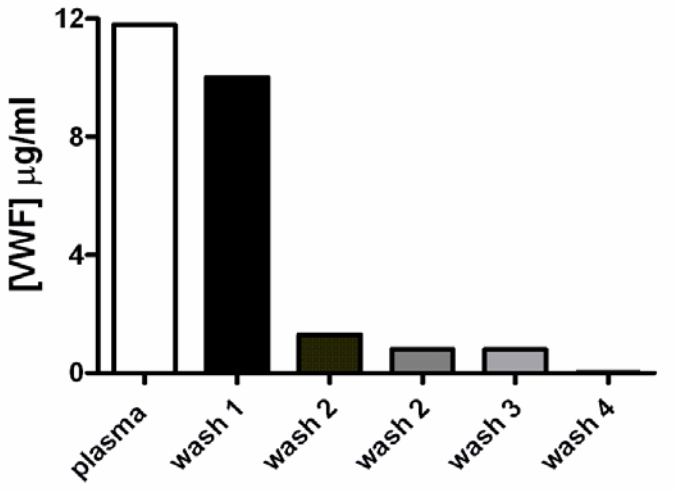


Figure 8.4 Preparation of plasma free blood – washing erythrocytes

Erythrocytes were separated from plasma and platelets, and washed with NaCl (by repeating re-suspension and centrifugation) to remove any residual VWF. Levels of VWF after the washes were measured by VWF ELISA. After the first wash majority of VWF was removed, but VWF free RBCs suspension was obtained only after the fourth wash.

8.3.4 Coating VWF concentration

Since the majority of experiments were to be performed with immobilised VWF and platelets in solution, preliminary experiments were performed to determine the optimal concentration of VWF to coat onto the flow slide surface.

Initially, the coating concentrations of full length VWF and VWF-D'A3 that would support platelet attachment and rolling were determined. No platelet attachment was seen when plasma free blood was perfused over a BSA blocked channel, indicating that platelets do not interact directly with the flow surface or the BSA used to block the surface (Figure 8.5). When channels were coated with 10µg/ml FL-VWF, minimal platelet interaction was observed and the platelets that did interact were observed to translocate rapidly across the surface in the direction of the flow (Figure 8.5). When coated at 25µg/ml or above, FL-VWF was able to capture large numbers of platelets (~500 per field of view, 0.4x0.3mm), with higher coating concentrations of VWF capturing similar numbers of platelets, indicating that at 25µg/ml the surface of the slide is saturated with VWF (Figure 8.5). Based on these results, in all subsequent assays full length VWF was immobilised at a concentration of 25µg/ml. No dose response was observed as the aim was to determine the saturating concentration. One would see a dose response if concentrations between 10 and 25µg/ml were used.

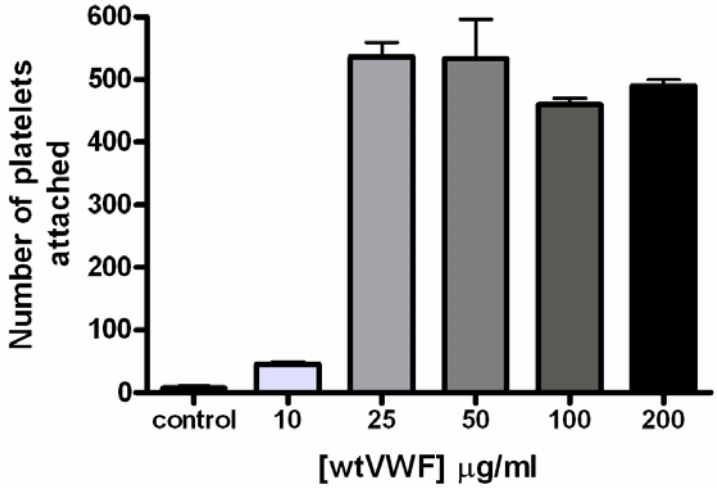


Figure 8.5 Optimal FL-VWF coating concentrations for the flow assay

Full length VWF was diluted in carbonate buffer, coated directly onto the flow slides at specified concentrations and blocked with BSA. Platelets reconstituted with erythrocytes were passed over at a shear rate of 1500 s^{-1} for 4 minutes. The number of residual platelets was determined for each VWF coating concentration and control lane coated with BSA per field of view-0.4x0.3mm. No non-specific binding was observed and VWF concentrations above 25µg/ml bound similar platelets numbers.

Similarly, the concentration of wtD'A3 required to saturate the slide surface was determined. Appreciably less platelet capture was detected for the slides coated with 15 and 20μg/ml of protein when compared with slides coated with 30 and 40 μg/ml of VWF-D'A3 (Figure 8.6). Since comparable platelet capture was observed when VWF-D'A3 was immobilised at 30μg/ml and 40μg/ml, the lower concentration of protein was used in all subsequent assays in which the platelet attachment and rolling were assessed. In addition, the coating concentration of VWF-D'A3 that would support only transient tethering events was established and will be discussed later.

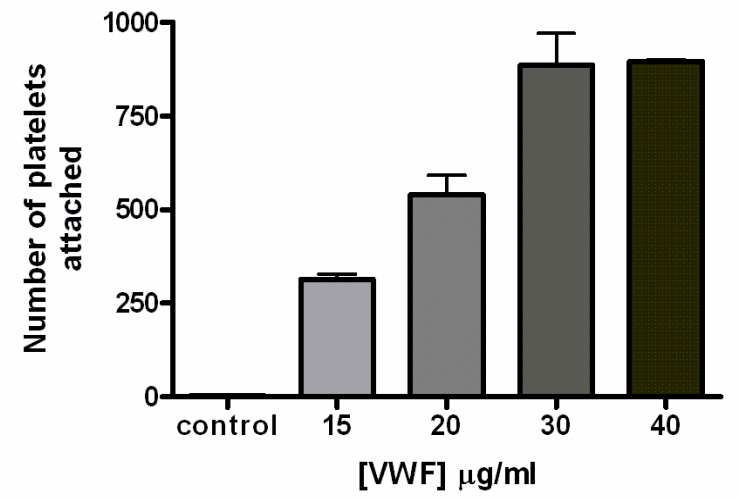


Figure 8.6 Optimal D'A3 coating concentration saturating the flow sides

WtD'A3 -VWF was diluted in carbonate buffer, coated directly onto the flow slides at specified concentrations and blocked with BSA. Platelets reconstituted with erythrocytes were passed over at a shear rate of 1500 s^{-1} for 4 minutes. The number of residual platelets was determined for each D'A3 coating concentration and control lane coated with BSA. No non-specific binding was observed. Slides were saturated with wtD'A3 at a concentrations above 30μg/ml.

8.3.5 Optimal collagen source

Following vessel injury VWF binds to exposed collagen, unravels and binds flowing platelets. This can be replicated in flow assays by coating the flow chamber surface with collagen and perfusing over whole blood or plasma free blood supplemented with VWF. To determine the optimal collagen source to use with the Ibidi slides, five collagen sources that are routinely used in our laboratory were selected (Table 8.1). Ibidi slides were coated with these collagens at 100μg/ml and a control channel coated with BSA. Plasma free blood supplemented with 10μg/ml pdVWF was then perfused over for

5mins at 1500s^{-1} and the extent of VWF mediated platelet capture measured as the percentage surface covered by labelled platelets. Firstly, validating the specificity of the assay, no platelet binding was detected in a control channel coated with BSA only (Figure 8.7a). In addition, no platelet attachment was observed in the absence of VWF. Of the five collagens tested, only two were able to capture platelets via VWF (Figure 8.7a,b). These were Sigma type III collagen and Southern Biosceinces type III collagen, both derived from human placenta. While the Sigma collagen, demonstrated platelet capture, the coating appeared to be non-uniform, as opposed to the SB collagen which coated the surface evenly and gave good VWF mediated platelet captured.

Finally the coating concentration of collagen type III was tested. The manufacturer's protocol for the Ibidi VI slides recommended using collagen at a concentration of 300µg/ml. Nonetheless, I have detected similar number of captured platelets on slides coated with 300 and 100µg/ml of SB type collagen III (Figure 8.7c) implying the 100 µg/ml of collagen is sufficient to saturate the surface. On the basis of presented data, in subsequent experiments, flow slides were coated with Southern Biosciences collagen type III at a concentration of 100µg/ml.

Source	Preparation	Collagen type	Supplier
Human	Trypsin digestion from human placenta	III	Sigma
Human	Trypsin digestion from human placenta	I	Sigma
Human	Pepsin digestion from human placenta	III	Southern Biosciences
Rat	Rat tail	I	Invitrogen
Bovine	Unspecified	I	Invitrogen

Table 8.1 Collagen sources tested

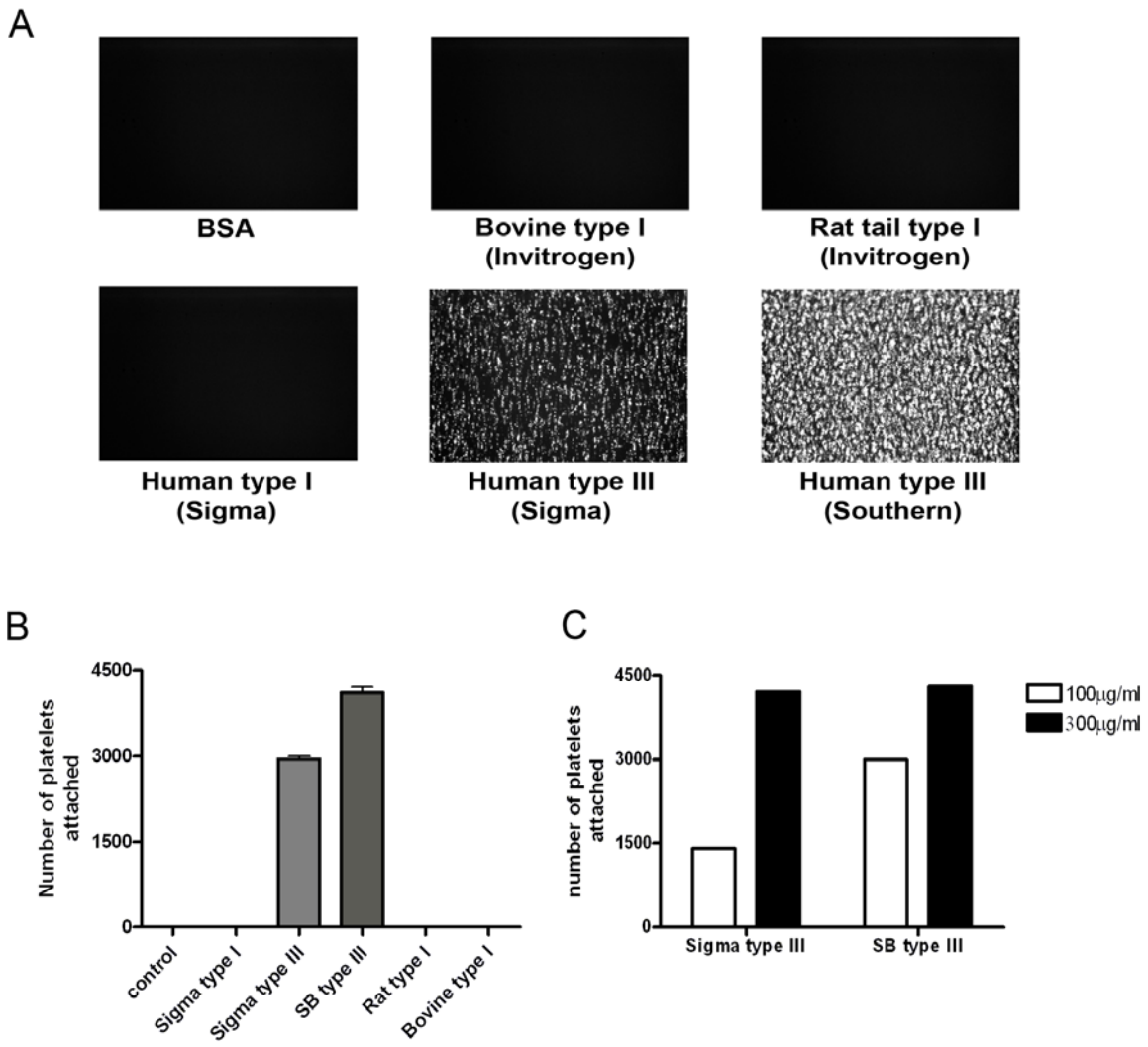


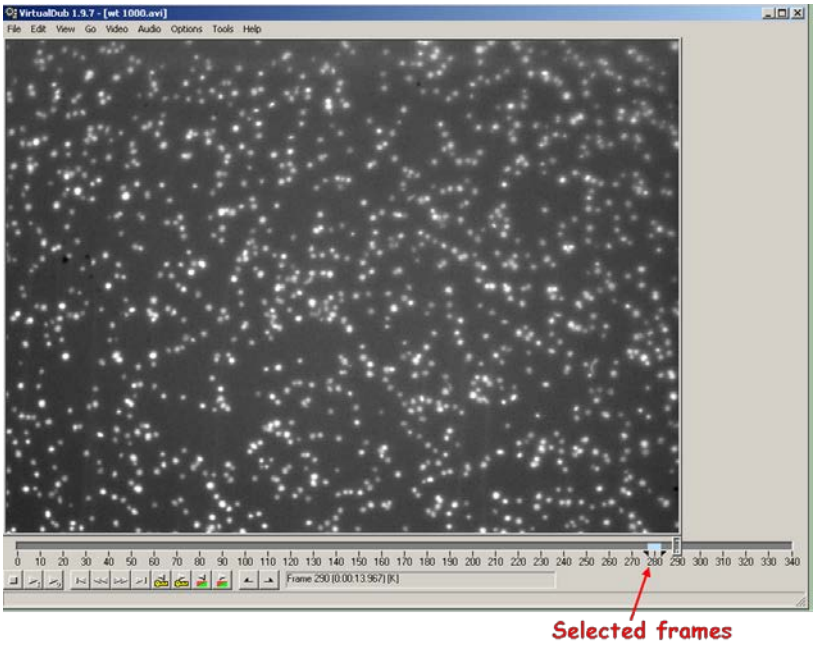
Figure 8.7 Determination of optimal collagen source for the flow assay

(A) Individual frames from videos recorded after 3 minutes of flow assay in which labelled platelets with VWF were passed over collagen coated slides at a shear rate of $1500s^{-1}$.Platelet attachment was only detected for type III collagen from Sigma and Southern Biosciences (SB). **(B)** 5 types of collagen (Table 8.1) were immobilised onto flow slides at a concentration of 300µg/ml). Labelled platelets reconstituted with erythrocytes and 10µg/ml of VWF were passed over at a shear rate of $1500s^{-1}$ for 4 minutes, and the number of adherent platelets was measured. The greatest platelet adhesion was detected for SB Type III collagen, followed by type III sigma collagen. Other types of collagen failed to support VWF mediated platelet adhesion. No binding was detected for surface coated with BSA (control). **(C)** Platelet adhesion to collagen type III was than compared at coating concentration of 100 and 300µg/ml. The SB type III collagen showed similar VWF mediated platelet binding at both coating concentrations unlike Sigma type III which exhibited reduced platelet binding at 100µg/ml

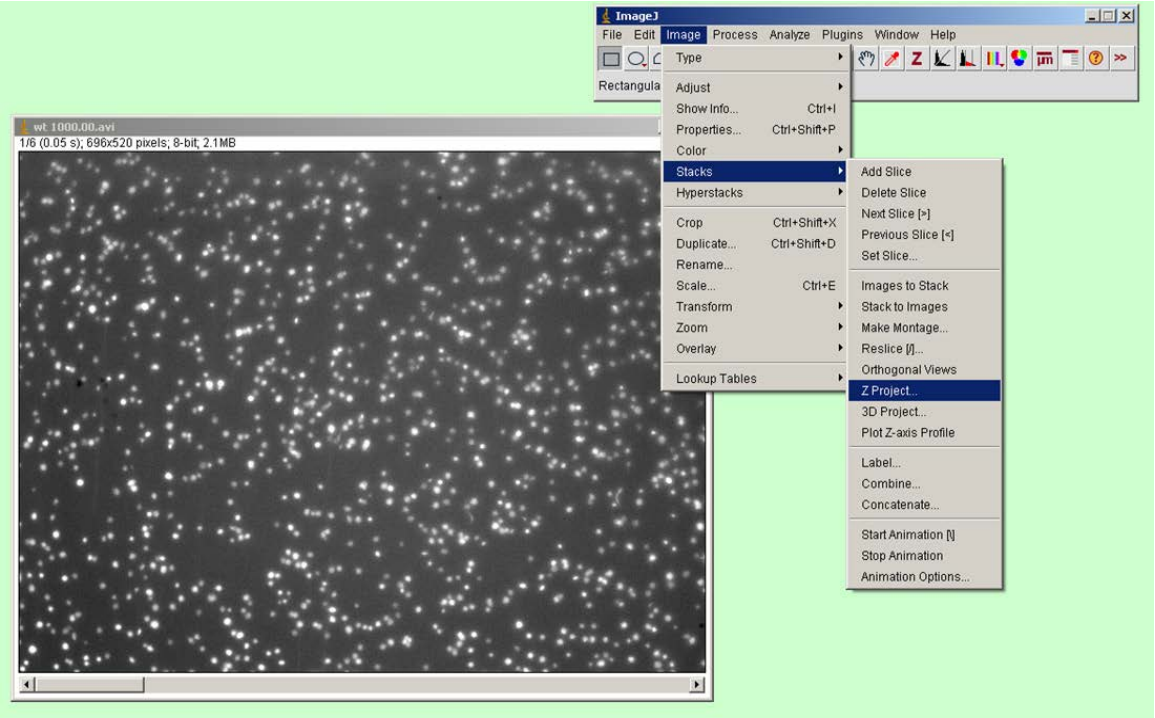
8.4 Kinetics and mechanics of platelet interaction with immobilised VWF-D'A3: method optimisation and data analysis

8.4.1 Platelet capture

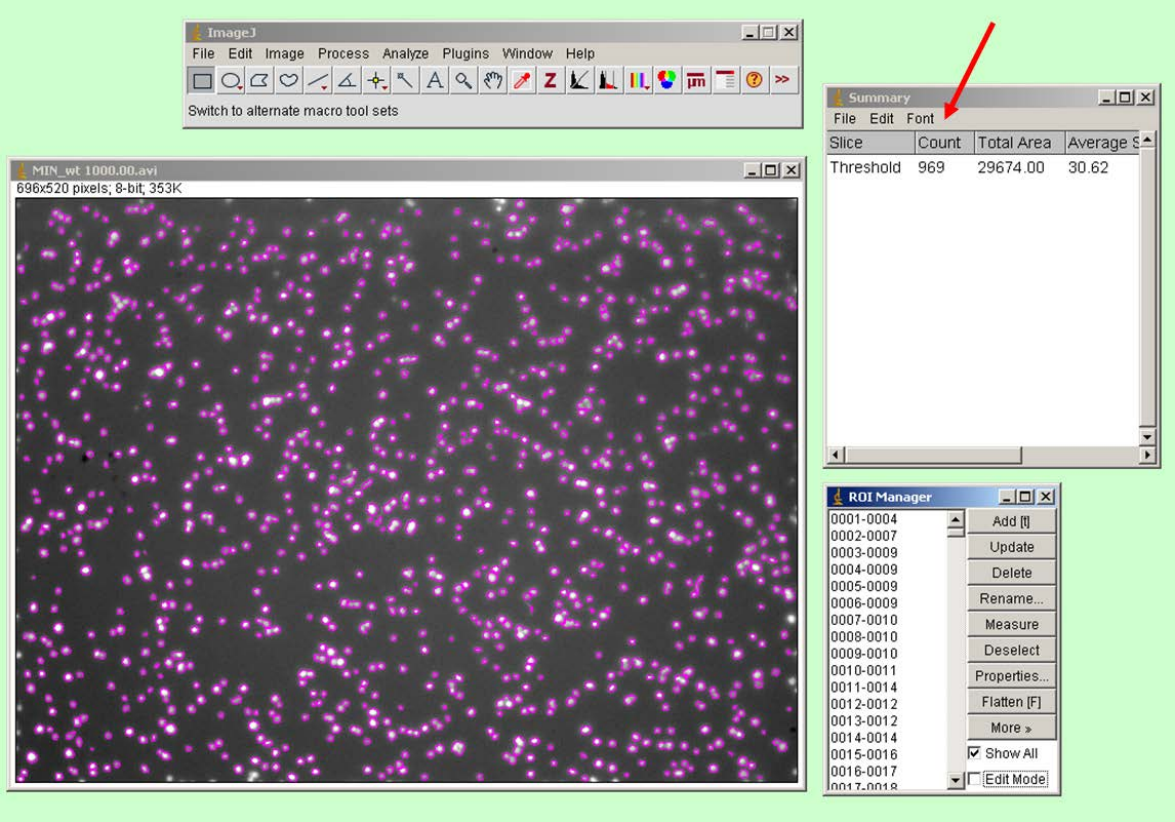
Once the coating conditions were optimised, I investigated the ability of immobilised VWF-D'A3 to capture platelets at a range of shear rates (200 to 2000s^{-1} corresponding to low and high shear stresses respectively). Briefly, slides were coated with VWF-D'A3 at a saturating concentration of 30µg/ml for 1 hour, blocked with BSA and washed with PBS prior to use. Fluorescently labelled platelets were re-suspended with erythrocytes and Hepes-Tyrodes buffer and perfused for 4 minutes at a given shear rate to allow adequate time for initial platelet interaction. Real-time movies of ~20sec for three separate fields of view were captured at a frame rate of ~20fps. Image J was used to determine the number of platelets captured via a series of steps outlined in Figure 8.8. Required video clips were saved as 'avi' files, and subsequently processed with VirtualDub to separate the movies into individual frames. In the case of platelet attachment measurements, three subsequent frames were saved and then processed using ImageJ software. Firstly, a minimal intensity Z-projection was performed to stack the three frames. This stacks objects that have remained stationary over the duration of the three frames and removes background noise and non-stationary objects, thus only platelets that had remained attached over three frames (0.15sec) would remain and any non-attached platelets or moving objects close to the surface would be removed from the composite image. Platelets were then counted using the "nucleus counter" function supplied with the ImageJ "particle analysis" plug-in. This works by selecting objects with intensity higher than the average background threshold intensity. The process was repeated for 3 different fields of view and the average number of attached platelets calculated for each shear rate.



1. Video files were first processed by the VirtualDub which allows viewing movies frame by frame. Required frames were selected and saved. These were then opened in Image J program.



2. Firstly Z-stack function was used to select an image with only platelets that remained residual for the duration of 3 frames (0.15s)



3. The number of platelets in the created image was calculated using a Particle analysis Plugin. The Nucleus counter function was selected where the minimal and maximal size of particles to be counted was determined and the 'Otsu' threshold method was applied. Each platelet counted by the program was outlined in purple and assigned a number. Among other parameters, platelet count was presented in a table (red arrow). In addition, it was possible to manually deselect particles that did not correspond to platelets and add platelets that the program had overlooked.

Figure 8.8 A step by step diagram showing and explaining the individual stages used to count the number of platelets bound to D'A3-VWF

Platelet attachment to wtD'A3 at a range of shear rates is illustrated in Figure 8.9. In keeping with previous studies, the number of interacting platelets increased as function of shear rate. It is clear that when the shear rate increases from 400 to 1000s^{-1} a greater number of bound plates is detected, while only a slight increase in platelet binding is observed when the shear rate is further increased to 2000s^{-1}. The specificity of interaction was demonstrated by the inability of platelets to adhere to BSA coated slides (Figure 8.9). Unexpectedly, in contrast to previously reports, more bound platelets were detected at 200s^{-1} compared to 400s^{-1}, however at the lower shear rate it was noted that the flow appeared uneven and almost pulsatile. This reflected the inability of the

available syringe pump to accurately pump at this shear rate: therefore 400s^{-1} was the minimal shear rate that could be accurately used in subsequent experiments.

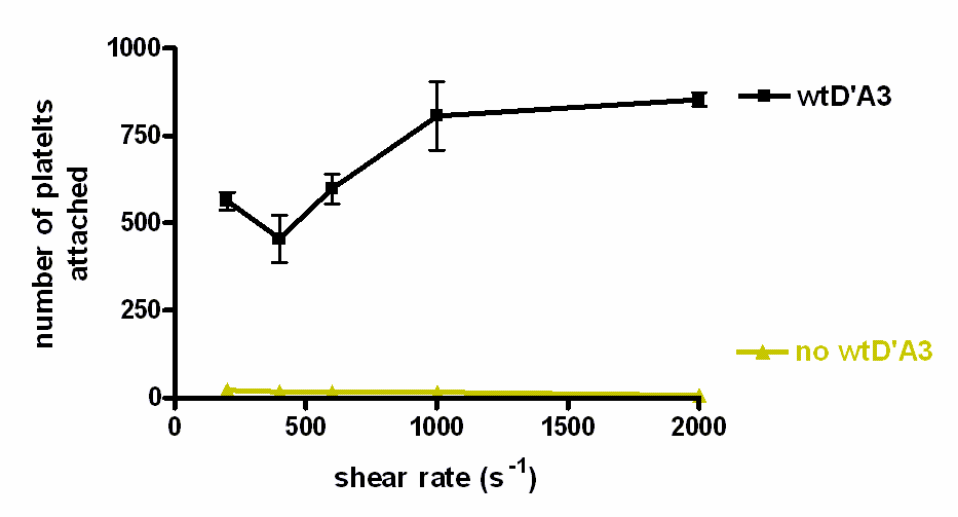


Figure 8.9 Shear rate dependence of platelet adhesion to wtD'A3-VWF

Purified fluorescently labelled platelets were perfused over slide surface coated with 30µg/ml of wtD'A3 at shear rates ranging from 200 to 2000s^{-1} for 4 minutes. The images were taken after that time and 3 different fields of view on the slides were recorded. The number of platelets that remained stationary for the duration of 3 frames (0.15s) as a function of shear rates was determined. Values are SEM of three separate experiments. As expected, increased platelet binding to immobilised D'A3 was observed with increasing shear rates. No platelet attachment was detected on surface coated with BSA only.

8.4.2 Platelet rolling velocities

The GPIbα-A1 interaction cannot support irreversible platelet adhesion but allows tethering and translocation which slows the platelet velocity, allowing establishment of additional bonds through other receptors on activated platelets. Importantly, when analysing platelet attachment to wtD'A3 I observed that platelet interaction with immobilised protein appears as a continuous translocation. Interacting platelets moved in the direction of flow, albeit at a markedly reduced velocity relative to freely flowing platelets. Since this translocation occurred in a "stop-start" manner it can therefore be described as rolling. Consequently I proceeded to analyse platelet rolling velocities at a variety of shear stresses. As described previously, video clips saved as 'avi' files, were subsequently processed with VirtualDub. For platelet rolling assays, longer movies comprising approximately 50 successive frames were created. Next the rolling

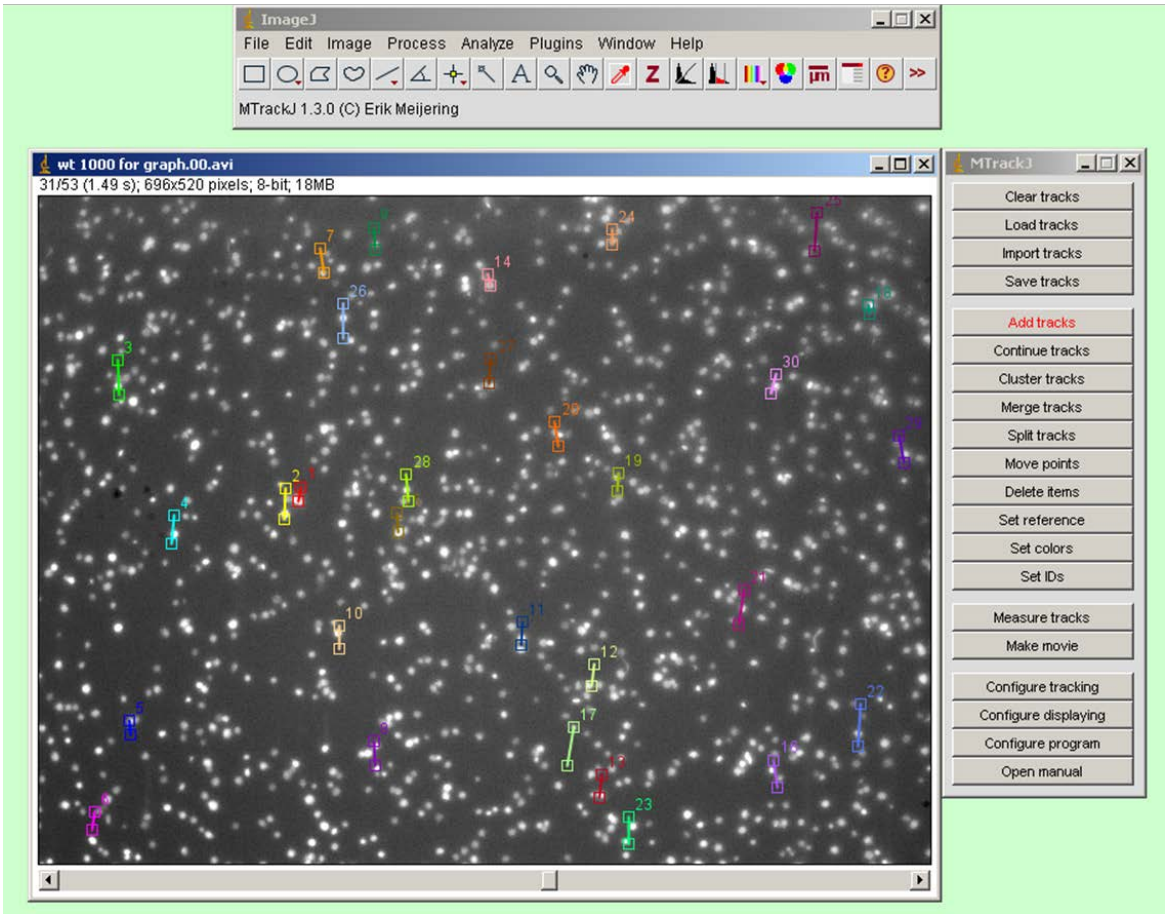
velocities were measured by tracking individual platelets frame-by-frame at intervals of 0.05s, and the velocity was calculated using the ImageJ plug-in MtrackJ. This measures the distance in pixels an object travels over time. The microscope was calibrated so that 1 pixel corresponded to a distance of 0.64μm. The time that one platelet spent continuously moving while maintaining contact with the VWF coated surface is defined as the rolling duration, and rolling velocity was calculated from the distance that the platelet translocated during this period (Figure 8.10). Approximately 25-40 platelets were tracked in 3 random fields of view, and 3 separate experimental runs were completed for each flow rate.

Next page-

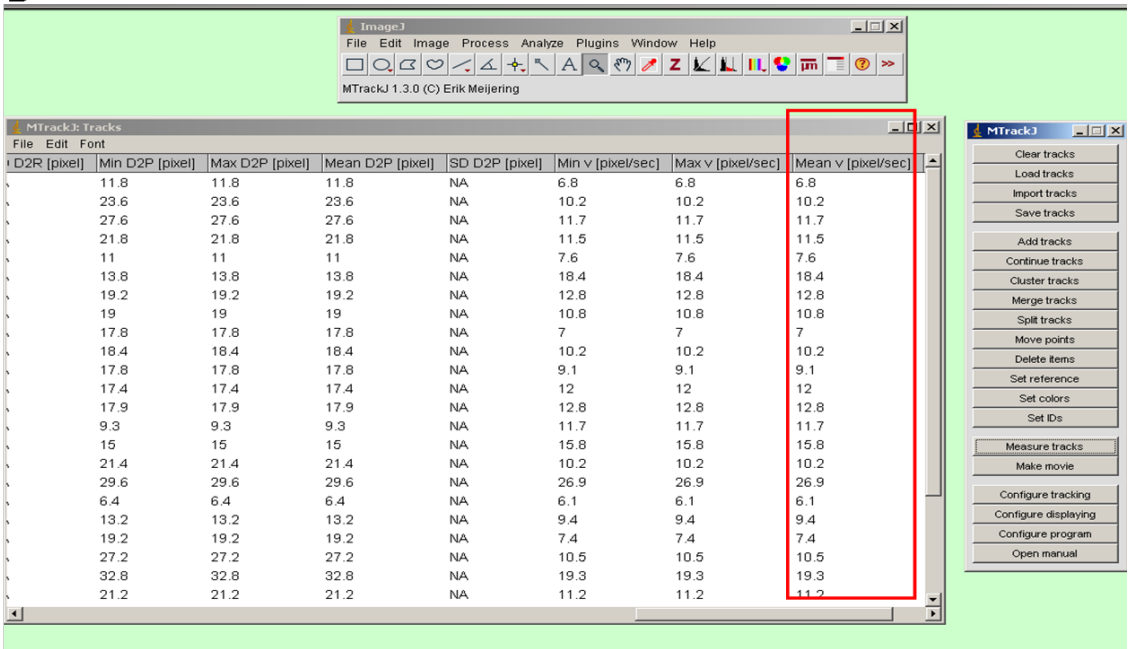
Figure 8.10 Platelet rolling velocities measurement using Image J

A fragmented movie consisting of 53 frames was used to determined platelet rolling velocities on immobilised wtD'A3. **(A)** Selected platelet translocation was tracked frame by frame. Start and end point were manually marked on respective frames (coloured lines on the picture) using a MtrackJ plug-in. Information regarding the frame duration was inserted and function 'measure tracks' was selected **(B)** Among other information Image J determined mean rolling velocities (red box) of selected platelets from the distance that they translocated depending on the time that the translocation has taken. Distance was measured in pixels per second, which was then converted manually to μm per second. Using a calibration slide it was determined that 1 pixel in the movie corresponded to 0.64 μm.

A


ImageJ
File Edit Image Process Analyze Plugins Window Help
MTrackJ 1.3.0 (C) Erik Meijering
wt 1000 for graph.00.avi
31/53 (1.49 s); 696x520 pixels; 8-bit; 18MB
MTrackJ
Clear tracks
Load tracks
Import tracks
Save tracks
Add tracks
Continue tracks
Cluster tracks
Merge tracks
Split tracks
Move points
Delete items
Set reference
Set colors
Set IDs
Measure tracks
Make movie
Configure tracking
Configure displaying
Configure program
Open manual

B


ImageJ
File Edit Image Process Analyze Plugins Window Help
MTrackJ 1.3.0 (C) Erik Meijering
MTrackJ: Tracks
File Edit Font
D2R [pixel] | Min D2P [pixel] | Max D2P [pixel] | Mean D2P [pixel] | SD D2P [pixel] | Min v [pixel/sec] | Max v [pixel/sec] | Mean v [pixel/sec]
11.8 | 11.8 | 11.8 | NA | 6.8 | 6.8 | 6.8
23.6 | 23.6 | 23.6 | NA | 10.2 | 10.2 | 10.2
27.6 | 27.6 | 27.6 | NA | 11.7 | 11.7 | 11.7
21.8 | 21.8 | 21.8 | NA | 11.5 | 11.5 | 11.5
11 | 11 | 11 | NA | 7.6 | 7.6 | 7.6
13.8 | 13.8 | 13.8 | NA | 18.4 | 18.4 | 18.4
19.2 | 19.2 | 19.2 | NA | 12.8 | 12.8 | 12.8
19 | 19 | 19 | NA | 10.8 | 10.8 | 10.8
17.8 | 17.8 | 17.8 | NA | 7 | 7 | 7
18.4 | 18.4 | 18.4 | NA | 10.2 | 10.2 | 10.2
17.8 | 17.8 | 17.8 | NA | 9.1 | 9.1 | 9.1
17.4 | 17.4 | 17.4 | NA | 12 | 12 | 12
17.9 | 17.9 | 17.9 | NA | 12.8 | 12.8 | 12.8
9.3 | 9.3 | 9.3 | NA | 11.7 | 11.7 | 11.7
15 | 15 | 15 | NA | 15.8 | 15.8 | 15.8
21.4 | 21.4 | 21.4 | NA | 10.2 | 10.2 | 10.2
29.6 | 29.6 | 29.6 | NA | 26.9 | 26.9 | 26.9
6.4 | 6.4 | 6.4 | NA | 6.1 | 6.1 | 6.1
13.2 | 13.2 | 13.2 | NA | 9.4 | 9.4 | 9.4
19.2 | 19.2 | 19.2 | NA | 7.4 | 7.4 | 7.4
27.2 | 27.2 | 27.2 | NA | 10.5 | 10.5 | 10.5
32.8 | 32.8 | 32.8 | NA | 19.3 | 19.3 | 19.3
21.2 | 21.2 | 21.2 | NA | 11.2 | 11.2
MTrackJ
Clear tracks
Load tracks
Import tracks
Save tracks
Add tracks
Continue tracks
Cluster tracks
Merge tracks
Split tracks
Move points
Delete items
Set reference
Set colors
Set IDs
Measure tracks
Make movie
Configure tracking
Configure displaying
Configure program
Open manual

The mean rolling velocities for platelets perfused over wtD'A3 (in µm per second) were plotted against shear rate and illustrated in Figure 8.11. In agreement with previously published data, a biphasic velocity curve was observed.[335] This is characteristic for the flow dependent interaction of GPIbα with the A1 domain involving the formation of 'catch and slip' bonds. As the shear rate increased from 400 to 1000s^{-1} platelet translocation velocity decreased from ~12µm/s to ~7µm/s (catch regime). Once the shear rate was raised to 2000s^{-1} rolling speed increased back to 12µm/s (slip regime).

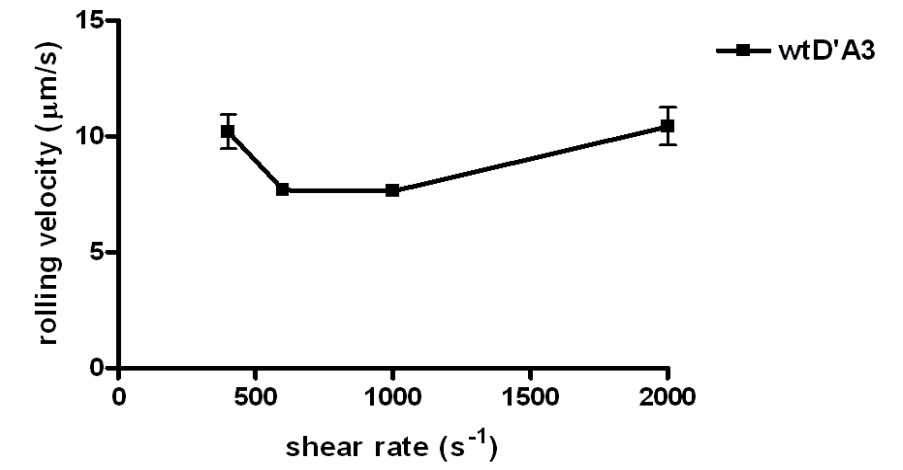
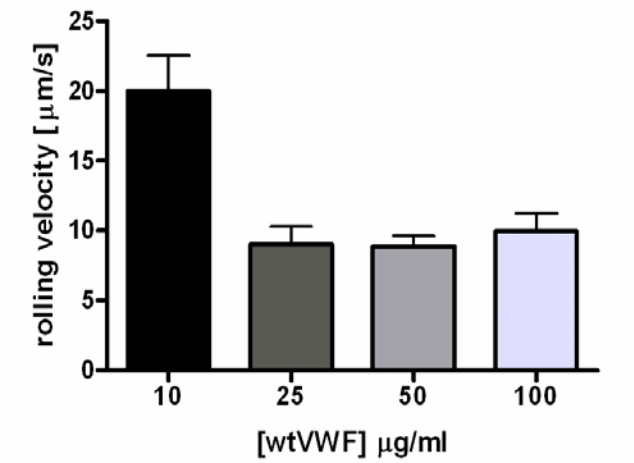


Figure 8.11 Shear rate depended platelets rolling velocity on wtD'A3-VWF
VWF-D'A3 was coated onto a flow slide at a saturating concentrations of 30µg/ml and labelled platelets with erythrocytes were perfused over at shear rates ranging from 400 to 2000s^{-1} for 4 minutes. Movies were recorded after this time and rolling velocities were measured by tracking an individual platelet frame by frame at an interval of 0.05s, in the direction of flow and mean velocity was determined by Image J. The data are mean ±SEM of 3 independent experiments. Platelets rolling velocities first decreased with increasing shear rate until 1000s^{-1} and then increased when shear rate increased to a value of 2000s^{-1}.

To determine the influence of A1 domain density on platelet rolling velocities, slides were coated with varying concentrations of either FL-VWF or wtD'A3 at a shear rate of 1000s^{-1}. The velocity of platelets decreased by ~50% when the concentration of immobilised FL-VWF was increased from 10 to 25µg/ml (Figure 8.12a). No significant difference in translocation speed was observed on slides coated with 25, 50, 100µg/ml , presumably because at 25µg/ml the surface was saturated with FL-VWF. Similarly, in the case of wtD'A3 the fastest platelet rolling was detected on slides coated with the lowest concentration of protein (20µg/ml), and the velocity decreased appreciably with

increasing concentrations of protein (Figure 8.12b). When the surface was saturated with wtD'A3 (>30µg/ml) cells exhibited similar lowest translocation velocities. The presented results show that the surface density of VWF and its A1 domain influence platelet rolling velocities.

A



B

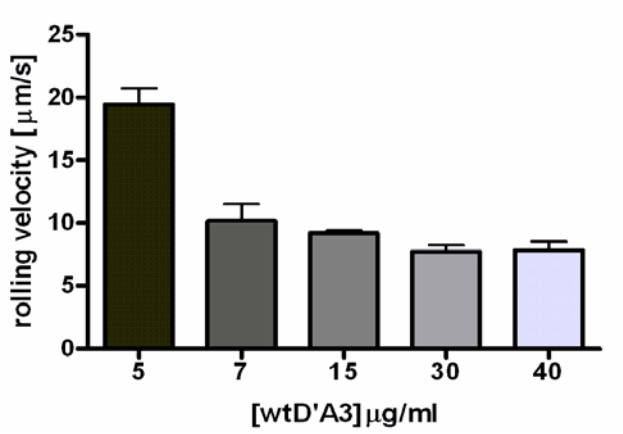


Figure 8.12 Comparison of platelets rolling velocities on various concentrations of immobilised FL-VWF and D'A3 at a shear stress of 1000s^{-1}

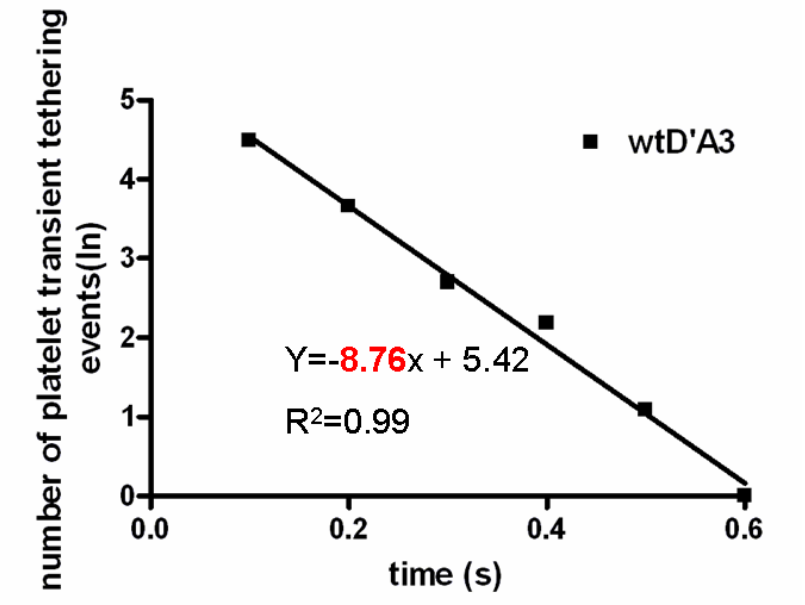
Platelets were perfused over slide surface coated with various concentrations of FL-VWF **(A)** or wtD'A3 **(B)** at shear rate of 1000s^{-1} for 4 minutes. Movies were recorded after this time and rolling velocities were measured by tracking an individual platelet frame by frame at an interval of 0.05s, in the direction of **(A)** platelets exhibited highest rolling velocities on the surfaces coated with 10µg/ml of FL-wtVWF, when the slides were saturated with VWF (>25µg/ml) platelet translocated notably slower.**(B)** The fastest platelet rolling was observed when wtD'A3 was immobilised at 5µg/ml, and velocity decreased with increasing concentration of immobilised protein, with the slowest value reached at the saturating concentrations of wtD'A3 (>30µg/ml)

8.4.3 Dissociation rate constant

The interaction between platelet receptor GPIbα and the A1 domain of VWF has a fast association and fast dissociation rate. To estimate the GPIbα-A1 disassociation rate (k_{off}) in the presence of shear stress, flow slides were coated with 2µg/ml VWF-D'A3 and purified labelled platelets and RBC perfused over the surface as increasing shear rates.

The coating concentration of 2µg/ml was selected because it allowed spatial separation of D'A3 domains and I have observed that it was the highest concentration at which no platelet rolling or other forms of translocation occurred. This condition limited the possibility of multiple bond formation and allowed the determination of single GPIbα-A1 bond lifetimes at various shear rates. A transient tether was defined as a flowing platelet that suddenly arrested, without evidence of translocation and then resumed a velocity equivalent to that of a non-interacting platelet. Only one tethering event per platelet (in the field of view) was counted during the observation period. The duration of tethers was determined by recording images at a rate of 22 frames per second and measuring the length of time each platelet remained bound to the surface. Recorded movies were opened in VirtualDub to separate the movie sequences into individual frames and the number and length of individual transient tethering events was determined manually. On average, 150 tethering events were measured to determine the k_{off} in each independent experimental run. The dissociation rate constants were then determined by plotting the natural logarithm of the number of platelets that interacted as a function of duration of tethering (Figure 8.13a). For first-order dissociation kinetics, the resultant plot is a straight line, and the slope of the line = $-k_{off.}$ As an example, bond lifetimes between VWF-D'A3 and platelets at a shear rate of $1000s^{-1}$ are illustrated on Figure 8.13a. The negative slope of the straight line was calculated as $8.7s^{-1}$ and the R^2 value of 0.99 indicated a good linear relationship between the natural log of the number of tethering events and the duration of the events. Analogous measurements were performed at the shear rates of 400, 600 and $2000s^{-1}$. Average wtD'A3-GPIbα dissociation rates values are listed in the Figure 8.13b. The lowest k_{off} value was determined at a shear rate of $400s^{-1}$, it was slightly higher at shear rates of 600 and $1000s^{-1}$ and then increased at $2000s^{-1}$. However the changes in k_{off} were minimal, indicating that the wtD'A3-GPIbα bond lifetime was similar across the shear range tested.

A



B

Shear rate (s^{-1})	Dissociation rate constant - K_{off} (s^{-1})
400	6.7 ± 1.3
600	7.1 ± 1.1
1000	7.1 ±1.4
2000	9.2 ± 1.6

Figure 8.13 Kinetics of dissociation of transiently tethered platelets from wtD'A3

Labelled platelets were perfused over flow slides coated with 2µg/ml coating concentration of wtD'A3, the lowest concentration capable of supporting adhesion to assure occurrence of only transient tethering events. Disassociation rate constants were estimated at various wall shear stresses and based on the duration of transient tether events for approximately 150 platelets. **(A)** Representative experiment for wtD'A3 variant at a shear rate of $1000s^{-1}$ The natural logarithm of the number of platelets that interacted as a function of time that platelet remained attached was plotted in Excel. The plot was a straight line whose slope corresponded to $-k_{off}$. **(B)** Disassociation rates values for the tether bond between GPIbα- and wtD'A3 at range of shear rates ($400-1000s^{-1}$).

8.4.4 Transient tethering

Finally, the number of transient tethering events occurring over a set time frame at increasing shear rates was calculated. The number of transient tethering events is indicative of VWF-GPIbα association rate. Platelets were perfused over slides coated with low concentration of wtD'A3 at a range of shear rates (400-1000s^{-1}) and the number of interacting platelets over 5 seconds counted. As shown in Figure 8.14 the number of tether events was the highest at the shear rate of 600s^{-1} and subsequently decreased with increasing shear rate, with very few events taking place at 2000s^{-1}. Moreover, a high number of platelet tethering events was observed at a lower shear rate of 400s^{-1}. These experiments demonstrate that increase in the shear rate promotes transient tethering but over a certain threshold value it then has a negative effect.

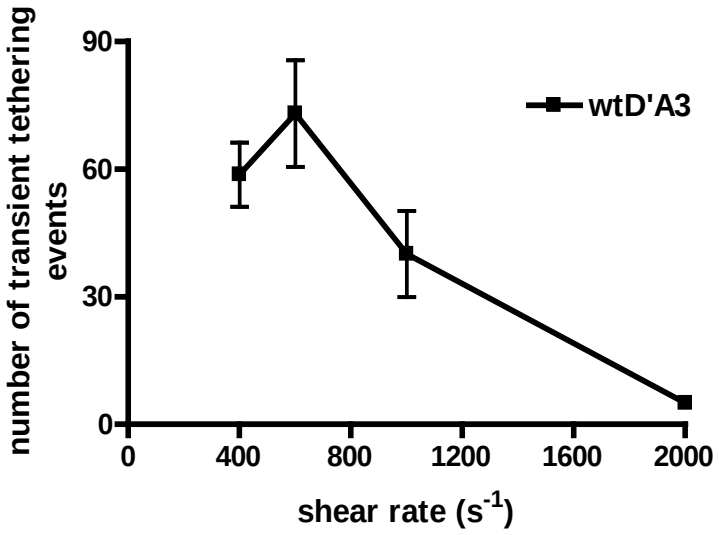


Figure 8.14 Shear rate dependence of transient platelet tethering on flow slides coated with wtD'A3

Labelled platelets were perfused over slides coated with 2µg/ml of wtD'A3- VWF fragment at shear rates ranging from 400 to 2000s^{-1}. The number of platelets that transiently tethered during 5 s observation period was quantified for 3 different fields of view for 3 independent experiments.

8.5 Desialylated wtVWF interaction with platelets under shear stress

8.5.1 Platelet adhesion and rolling

As presented in the previous chapter, the removal of sialic acid from VWF *O*-linked glycans enhanced the ability of VWF to bind to GPIbα in the presence of ristocetin. Therefore the flow assay was used to determine if VWF sialic acid also affected the interaction under shear stress conditions. As shown above, platelet capture on immobilised wtD'A3 increased with increasing shear stress. Interestingly, for desialylated wtD'A3 (+Neu-wtD'A3) the number of captured platelets at 400 and 600s^{-1} was considerably increased compared to wtD'A3. However, at 1000 and 2000s^{-1} platelet capture was similar for both wild type and neuraminidase treated protein (Figure 8.15).

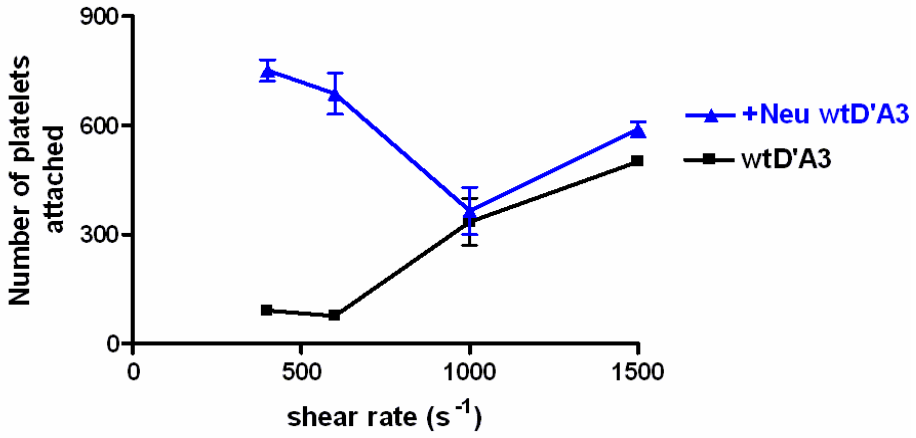


Figure 8.15 Platelets attachment to wtD'A3 and desialylated wtD'A3 under shear stress

Purified platelets were perfused over slide surface coated with 30µg/ml wtD'A3 and desialylated wtD'A3 (+Neu wtD'A3) at shear rates ranging from 200 to 2000 s^{-1} for 4 minutes. The number of platelets that remained stationery for the duration of 3 frames (0.15s) on the indicated substrates as a function of shear rates was determined. 0.4x0.3mm

From observation of the real time interaction of platelets with Neu-wtD'A3 it was apparent that at the lower shear rates platelets appeared to move slower across the VWF surface when compared to platelets interacting with wtD'A3, therefore rolling velocities were calculated. As with wtVWF-D'A3, a biphasic shear dependent velocity curve was observed, albeit with smaller changes in rolling velocity (Figure 8.16). Significantly, at 400 and 600s^{-1}, platelets rolled slower over Neu-wtD'A3, (~16 µm/s) compared to

wtVWF-D'A3, (~9μm/s), where as similar rolling velocities were determined at 1000 and 2000s^{-1} (Figure 8.16).

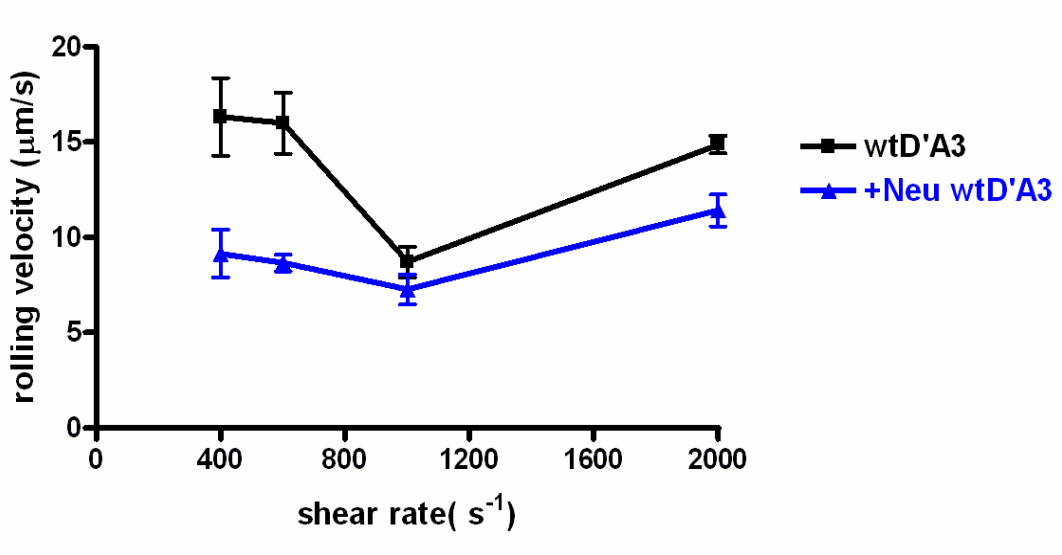


Figure 8.16 Platelet rolling on wtD'A3 and desialylated wtD'A3

wtD'A3 and desialylated wtD'A3 (+Neu wtD'A3) were coated at a saturating concentrations of 30μg/ml and platelets with erythrocytes were passed over at shear rates ranging from 400 to 2000s^{-1} for 4 minutes. Rolling velocities were measured by tracking individual platelets frame by frame at an interval of 0.05s, in the direction of flow and mean velocity was calculated by Image J. Approximately 25-40 platelets were tracked in 3 random fields of views, and 3 separate experimental runs were completed for each flow rate. Mean ±SEM shown.

8.5.2 Transient tethering

Since at the lower shear rates Neu-wtD'A3 bound greater numbers of platelets and slowed the decreased the platelet rolling velocity the kinetics of the interaction were investigated. To limit the possibility of multiple bond formation and to ensure that only transient tethering events take place, the concentration of immobilised proteins was low (2μg/ml). Initially, the number of transient tethering events occurring in specified time at a given shear rate was quantified as described in section 1.4.2. As shown on Figure 8.17 at all shear values tested, the number of platelets transiently tethering was similar for wtD'A3 and Neu-wtD'A3. Moreover as previously described, the number of tether events decreased with increasing shear rate.

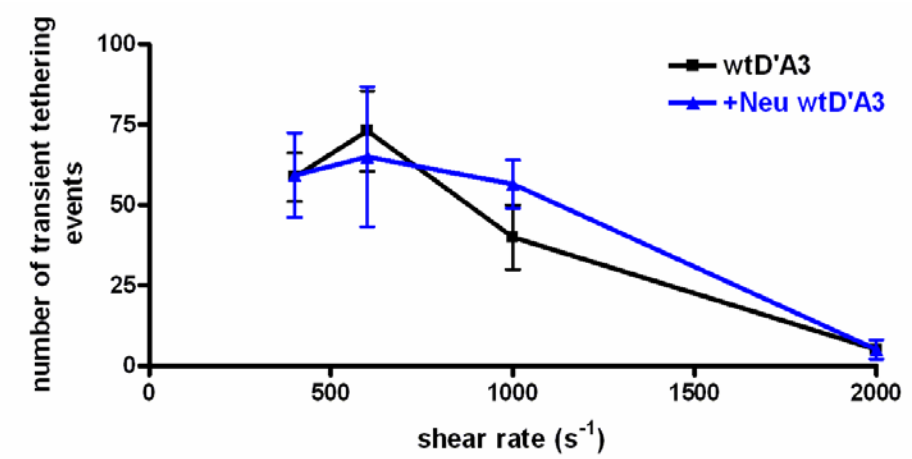


Figure 8.17 Shear dependence of transient tethering between platelets and wtD'A3 and desialylated wtD'A3

Platelets were perfused over slides coated with 2µg/ml of wtD'A3 and desialylated D'A3 (+Neu-D'A3) at shear rates ranging from 400 to 2000s^{-1}. The number of platelets that transiently tethered to the substrate was quantified for 3 different fields of view (0.4x0.3mm) for 3 independent experiments during 5s of flow. Both wtD'A3 and Neu-D'A3 participated in equivalent number of tethering events across the shear rates range tested.

Finally, I determined the GPIbα-A1 bond lifetime and quantified the dissociation rate constant under shear stress (as described in detail in section 3.4.3).. The values of the dissociation rate constant, K_{off} were calculated for both wtD'A3 and Neu-wtD'A3 at shear rates ranging from 400 to 2000s^{-1}. As demonstrated in Table 8.2 I established that under all shear rates tested, k_{off} values for GPIbα binding to wtD'A3 and Neu-wtD'A3 were comparable. This data suggests that removal of sialic acid from VWF does not alter GPIbα-A1 bond dissociation under the shear stress rates tested.

Shear rate (s^{-1})	k_{off} 400s-1	600 s-1	1000 s-1	2000 s-1
wtD'A3	6.7 ±1.3	7.1 ±1.1	7.1 ±1.4	9.2 ±1.6
+Neu wtD'A3	6.7 ±1	7.4 ±1.2	6.6 ±1.1	8.6 ±1.1

Table 8.2 Disassociation rate constants for the tether bond between GPIbα- and wtD'A3 and desialyated wtD'A3

Estimation of the K_{off} values for the GPIbα VWF tether bond was based on the duration of transient tether events. Experiments were conducted for wtD'A3 and desialylated wtD'A3 (+Neu-wtD'A3) at coating concentrations supporting only transient tethering events (2μg/ml) under a range of shear rates. Similar dissociation rates were estimated for platelet interaction with both immobilised wtD'A3 and Neu-wtD'A3 under shear stress.($p>0.05$)

8.6 Platelet accumulation and rolling on wtD'A3 and *O*-linked glycosylation variants

In the plate based ELISA assay the T1255A, Clus1 and DC variants all exhibited increased sensitivity to ristocetin mediated GPIbα binding, while the T1468A variant demonstrated decreased binding. I have therefore investigated if these mutations have a similar effect on the interaction with GPIbα under flow conditions. Firstly, the ability of platelets to accumulate and translocate on VWF *O*-glycosylation variants was compared to that of wild type VWF. The assays were performed under a range of shear rates from 400 to 2000s^{-1} using slides saturated with wild type and mutated D'A3 proteins.

Initially, platelet attachment to the immobilised and T1255A and the Clus1 variants double cluster variant (DC-D'A3) was examined. Interestingly when compared to wild type protein, the T1255A-D'A3 single glycosylation variant and Clus1-D'A3 and DC-D'A3 showed similar capability to binding platelets at shear rates up to 1000s^{-1}, and decreased platelet capture at the shear rate of 2000s^{-1}(Figure 8.18). Importantly, similarly to wild type protein, wtD'A3 variants exhibited a shear dependent increase in platelet binding, except at 2000s^{-1} where the number of platelets bound to the D'A3 glycosylation variants decreased.

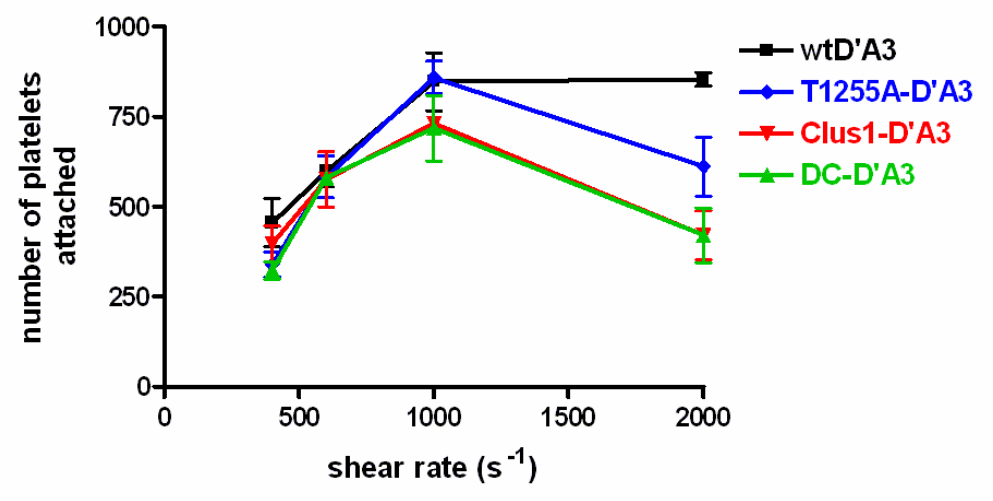


Figure 8.18 Comparison of platelets attachment to immobilised Clus1-, 1255- , DC-D'A3 variants and wtD'A3 under flow

Purified platelets were perfused over immobilised wtD'A3, T1255A-D'A3, Clus1-D'A3 and DC-D'A3 at shear rates ranging from 400 to 2000 s^{-1} for 4 minutes. The number of platelets that remained stationery for the duration of 3 frames (0.15s) on the indicated substrates as a function of shear rates was determined. At the shear rates up to 1000s^{-1} platelet accumulation on the T1255A-, Clus1- and DC-D'A3, variants was similar to wtD'A3. At 2000s^{-1} less platelet binding was observed on immobilised variants.

Subsequently, platelet rolling velocities were determined for platelets translocating over T1255A-, Clus1- and DC-D'A3 variants, and compared to wtD'A3. As shown in Figure 8.19 platelets rolling over D'A3 glycosylation variants generally followed a biphasic shear dependent pattern similar to wtD'A3. However at all shear rates tested the rolling velocity was significantly higher for the T1255A-, Clus1 and DC variants. This indicates that platelets translocate faster over VWF molecules lacking *O*-linked glycan chains. Interestingly at 600s^{-1} platelets had higher rolling velocities on the cluster 1 variant compared to the T1255A and DC variants.

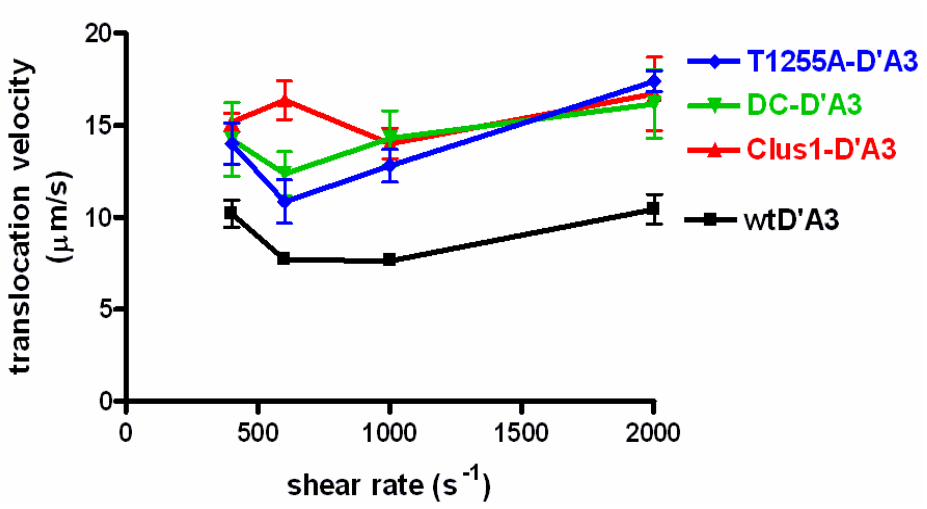


Figure 8.19 Platelets translocation velocities on the immobilised T1255A-D'A3 and Clus1-D'A3 *O*-linked glycosylation variant under flow

Translocation velocities were measured by tracking an individual platelet frame by frame at an interval of 0.05s, in the direction of flow. Mean translocation velocities ($\mu m/s^{-1}$) were calculated by ImageJ at indicated wall shear stresses. Platelets translocation velocities were notably higher on both immobilised T1255A-, Clus1- and DC-D'A3 variant when compared to wtD'A3 at all shear rates tested.

In the plate binding assay the T1468A variant showed reduced sensitivity to ristocetin mediated GPIbα binding and platelet aggregation. To investigate if this was due to an altered interaction with ristocetin or a true effect on GPIbα binding, the interaction of platelets with VWF-D'A3-T1468A was investigated under flow. As demonstrated in Figure 8.20a under all flow rates tested the number of bound platelets was similar on immobilised T1468A-D'A3 compared to wtD'A3. Furthermore, mean platelet rolling velocities were calculated and plotted against the shear rate. The velocity curves for both wtD'A3 and T1468A-D'A3 have the same biphasic shape. Platelets rolled with the same speed on immobilised T148A-D'A3 as on wtD'A3 under shear rates from 400 to $2000s^{-1}$ (Figure 8.20b). These results indicate that removal of *O*-glycan chain from position T1468 has no influence on the ability of bound VWF to mediate platelet capture and subsequent translocation.

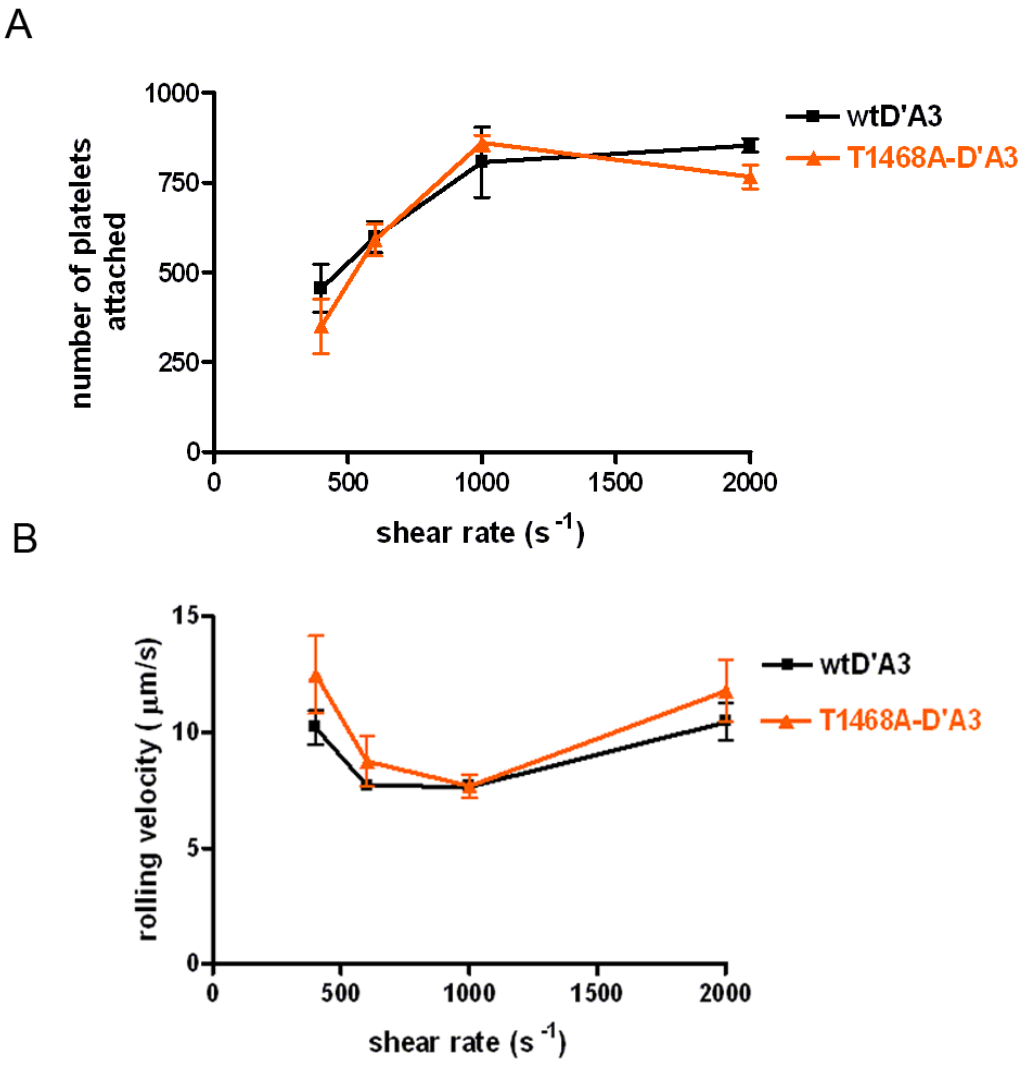


Figure 8.20 The impact of the T1468A mutation on platelet attachment and translocation in flow

Labelled platelets were perfused over immobilised wtD'A3 and the T1468A –D'A3 variant for 4 minutes under flow rates from 400 to 2000s^{-1}. **(A)** After that time the number of attached platelets in the field of view (0.5x0.4) was counted at indicated shear rates for both substrates. The platelet accumulation was the same on wtD'A3 and T1468A-D'A3. **(B)** Mean platelet rolling velocities were measured and plotted against shear rates. Platelets translocated with the same speed on immobilised wtD'A3 and the T148A-D'A3 glycosylation variant. Values shown here are mean ± SEM of 3 separate experiments, with ~30-40 platelets analysed for each shear rate in each experiments.

In addition, it was necessary to compare the platelet interaction with the VWF variants present in D'A3 and full length VWF. For that purpose, I have determined platelet attachment to immobilised full length wtVWF as well as T1255A, Cluster 1 and the double cluster variants under shear rates from 400 to 2000s^{-1}. Firstly the number of

platelets attached increased with increasing shear rates for wtVWF and all mutated proteins (Figure 8.21). Correspondingly to the results obtained with immobilised D'A3 variants, platelets bound similarly to wtVWF as to T1255A-Clus1 and DC-VWF variants when exposed to shear rates up to $1000s^{-1}$. Also similar platelet attachment was observed for full length wtVWF and glycosylation variants at the shear rate $2000s^{-1}$. This is in contrast to when D'A3 fragment were used, as at the shear rate of $2000s^{-1}$ the T1255A-Clus1 and DC-variants exhibited decreased binding when compared to wild type protein.

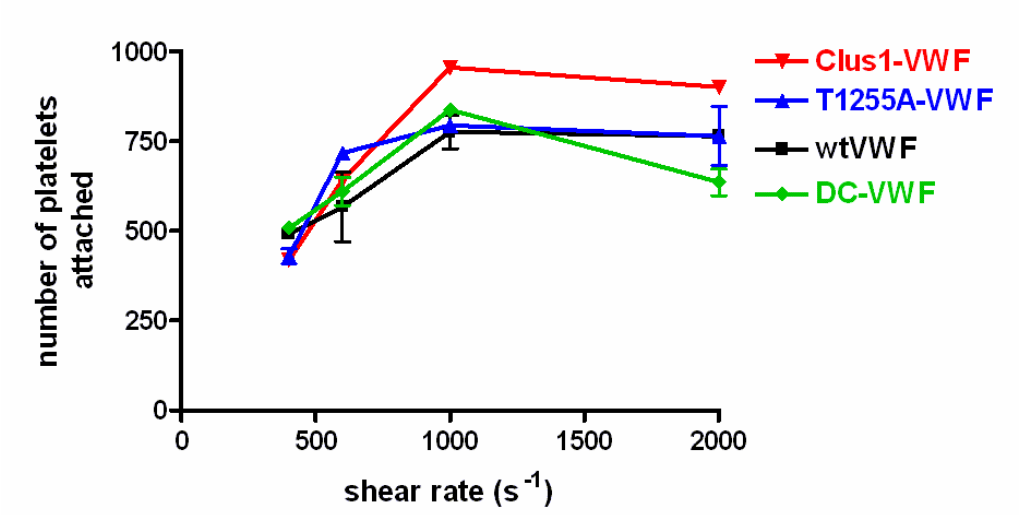


Figure 8.21 Comparison of platelet attachment to immobilised full length Clus1-, 1255- DC-VWF variants and wtVWF

Purified platelets were perfused over immobilised wtVWF, T1255A, Cluster 1 and double cluster at shear rates ranging from 400 to 2000 s^{-1} for 4 minutes. The number of platelets that remained stationery for the duration of 3 frames (0.15s) on the indicated substrates as a function of shear rates was determined. At all the shear rates tested platelet accumulation on VWF variants was similar to that of wtVWF.

8.7 The influence of VWF *O*-linked glycosylation on the kinetics of GPIbα-A1 tether bond

The interaction between platelet receptor GPIbα and the A1 domain of VWF has a fast association and fast dissociation rate. The increased platelet rolling velocity on immobilised T1255A-, Clus1- and DC-D'A3 variants is suggestive of altered kinetics of the receptor-ligand bond. For that reason the influence of the *O*-linked glycan mutants on the rate of bond formation and bond dissociation rates under various shear stress rates was investigated. To directly measure the kinetic parameters, I have analysed the formation and dissociation of transient adhesive events between platelets and D'A3 proteins coated at low site density to limit multiple bond formation.

8.7.1 Dissociation rate

The duration of transient tethers on each immobilised D'A3 variant was measured under shear rates ranging from 400 to 1000s^{-1}. When the initiation of tethering was synchronised to t=0, transient tethers were seen to dissociate with first order kinetics. The log transformed data fitted into a single straight line with a high correlation coefficient and the slope of the regression line corresponded to the dissociation constant. A representative graph depicting the distribution of interaction times for approximately 150 transient tethering events that occurred between platelets and DC-D'A3 at various shear rates is shown in Figure 8.22. The same analysis was applied to wtD'A3 and T1255A-, Clus1-D'A3 variants in three separate experiments and the K_{off} values at respective shear rates are gathered in Table 8.3. No major difference between the k_{off} values at shear rates between 200 and 2000s^{-1} was detected for any of the proteins. Importantly, the dissociation rates appeared quite similar for wtD'A3 and all the variants tested. Based on this results it appears that the increased rolling velocity seen with the VWF *O*-linked glycan variants is not due to increased dissociation of the GPIbα-A1 bond.

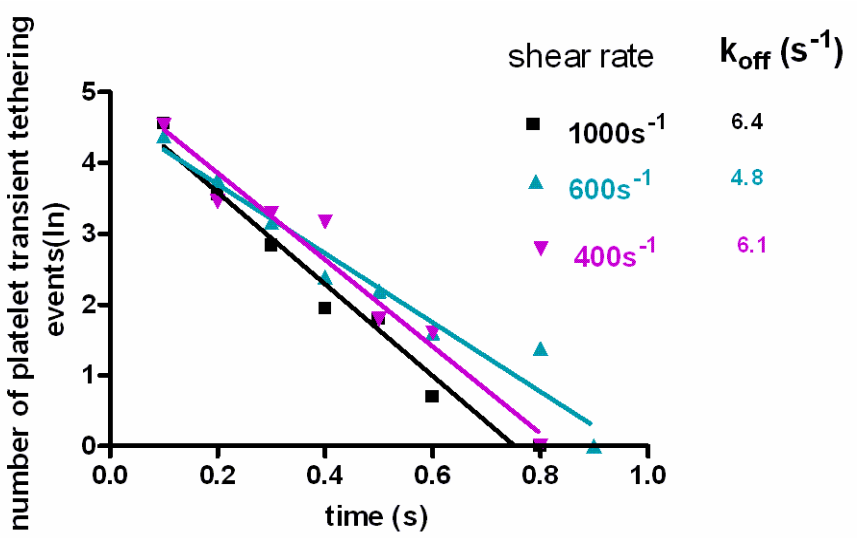


Figure 8.22 Kinetics of dissociation of transiently tethered platelets on DC-D'A3

Disassociation rate constants were estimated at various wall shear stresses using a 2µg/ml coating concentration of recombinant protein. Kinetics of transient tethering between platelets and DC-D'A3 variant at a shear rates of 400, 600 and 1000s^{-1} is demonstrated as an example. The natural logarithm of the number of tethering events was plotted against the duration of tethering and the negative slope of the lines is the $k_{off.}$. Disassociation rate values at each shear rate are indicated. (R^2 values were ~0.9)

Shear rate (s^{-1})	k_{off} 400s^{-1}	600 s^{-1}	1000 s^{-1}	2000 s^{-1}
wtD'A3	6.7±1.3	7.1 ±1.1	7.1 ±1.4	9.2 ±1.6
DC-D'A3	5.4±0.9	4.7±0.6	5.7±0.9	3.7 ±0.4
T1255-D'A3	6.6±0.1	6.6±0.8	6±0.2	7.4 ±1.7
Clus1-D'A3	5.5±1.0	6.4 ±1.2	5.1 ±0.5	7.5 ±1.6
T1468A	5.9±0.9	6.9±0.8	6.9±0.9	7.9±1.5

Table 8.3 Disassociation rates values for the tether bond between GPIbα- and wild type and mutated D'A3

Estimation of the K_{off} values for the GPIbα -VWF tether bond was based on the duration of transient tether events. Experiments were conducted for wtD'A3 and D'A3 *O*-linked glycosylation variants at coating concentrations supporting only transient tethering events (2µg/ml) under a range of shear rates. Similar dissociation rates were estimated for platelet interaction with both immobilised wtD'A3 and mutated-D'A3. Values shown here are SEM of 3 separate experiments. Calculated p values between koff between mutants and shear rates were above 0.05.

8.7.2 Transient tethering rate

Firstly the effect of the T1255A, Clus1- and DC- mutations on the flow dependent transient tethering of platelets to immobilised D'A3 was investigated. Briefly, platelets were perfused over VWF at a range of shear rates for 3 minutes and the number and behaviour of interacting platelets was determined as a function of the bulk concentration of D'A3 absorbed on the slides. As before, the formation of platelet tethers with wtD'A3 was inversely correlated with shear rate, with decreasing numbers of tethers formed as the shear rate increased.(Figure 8.23) Interestingly, the number of transient tethers formed on the T1255A, Clus 1 and DC variants was greatly decreased at all shear rates, with the T1255A and Clus 1 variants only able to tether minimal numbers of platelets and the DC variant able to support marginally more tethering events at all shear rates compared to the T1255A and Clus1 variants. (Figure 8.23) The specificity of this adhesive event was demonstrated by the inability of platelets to interact with BSA coated surface under all flow conditions tested.

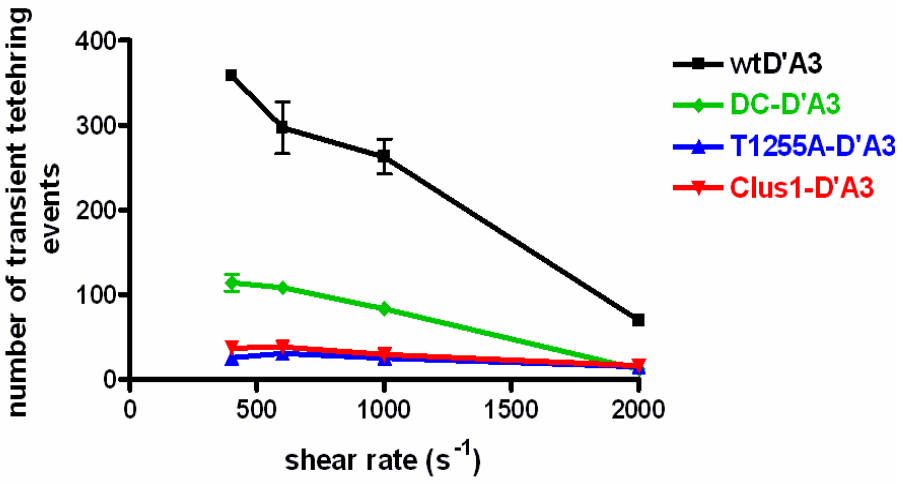


Figure 8.23 Platelet tethering to immobilised wtD'A3 and D'A3 glycosylation variants as a function of shear rate

Platelets were perfused over slides coated with 2µg/ml of wtD'A3 and T1255A-, Clus1,and DC D'A3 glycosylation variants at shear rates ranging from 200 to 5000s^{-1} for 3 minutes. The graph shows the number of platelets that transiently tethered to each substrate at a given shear rate, during 5 seconds at 3 different fields of view (0.4x0.3mm). Values are shown as SEM of three experiments at each protein concentration tested. The number of transient tethering events was markedly lower on immobilised T1255A, Clus1 and DC variants than on wild type protein at all shear rates except 2000s^{-1}.

8.7.3 Effect of coating concentration on platelet adhesion to VWF-D'A3

Since the analysed VWF *O*-linked glycan variants had faster rolling velocity it was hypothesised that this could be the result of a decrease in the bond lifetime and therefore, would result in alteration of the K_{off} for the interaction. However, as shown, the calculated K_{off} values for the T1255A, Clus1 and DC variants were all similar to wtD'A3 indicating that the K_{off} was unaltered, and therefore the difference in rolling velocity could not be attributed to a decrease in bond lifetime. Intriguingly, as also shown, at low coating concentrations, the T1255A, Clus1 and DC variants were significantly less efficient than wild type protein at supporting transient tethering events, however when flow slides were saturated with these proteins they were able to effectively capture platelets. It was therefore hypothesised that when coated below saturating concentrations, the mutant VWF molecules were less efficient at capturing platelets. To test this hypothesis, separate flow channels were coated with increasing concentrations of either wild type D'A3 or T1255A-D'A3 and platelets perfused over at $1500s^{-1}$.The number of platelets interacting and the type of interaction (i.e. transient tethering, rolling) were compared at each protein concentration. (Figure 8.24) At a coating concentration of 2µg/ml, transient tether formation was the only type of interaction observed on either T1255A-D'A3 or wtD'A3, with significantly more tethers seen on wtD'A3 compared to T1255A-D'A3. At 3ug/ml, more platelets tethered to wtD'A3 with a small proportion being rolling events. However, only a few tethering events were observed on T1255A-D'A3. At 7 and 15µg/ml, more platelets interacted with wtD'A3 and the proportion of rolling events increased. In contrast at 7 and 15µg/ml, although more platelets were observed to tether to T1255A-D'A3, the number of events was still less than for wtD'A3, and furthermore very few rolling events were observed. It was only at 30µg/ml that T1255A-D'A3 was able to support platelet rolling and capture platelets to the same extent as wtD'A3

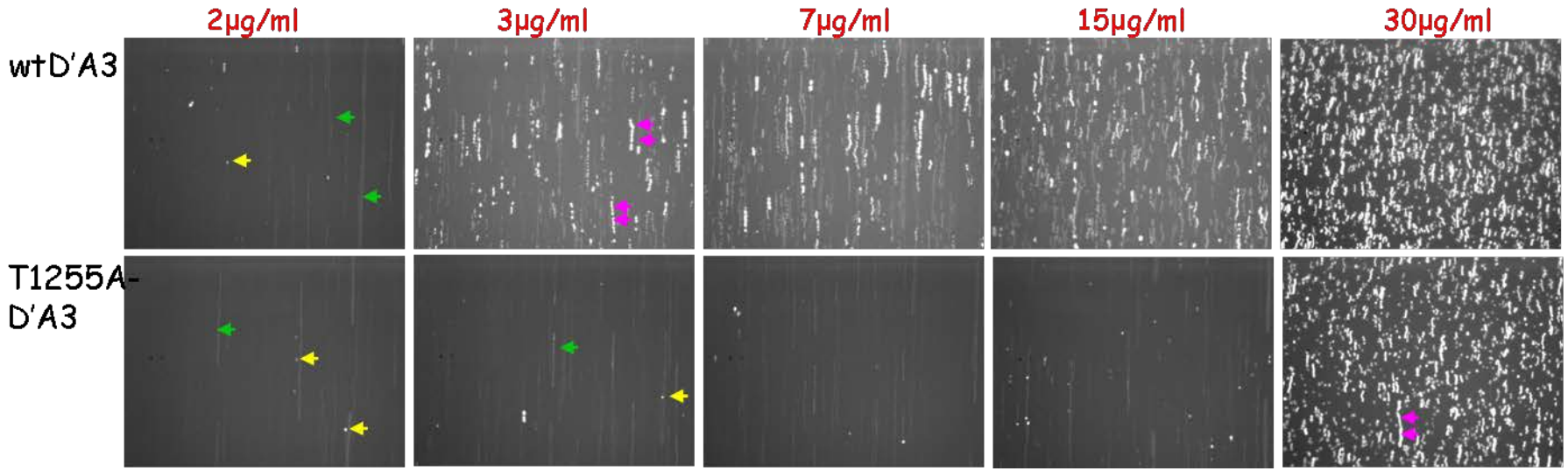


Figure 8.24Interaction of platelets with various concentrations of wtD'A3 and T1255A-D'A3

Flow slides were coated with wtD'A3 (top panels) and T1255-D'A3 (bottom panels) at concentrations from 2 to 30µg/ml (as indicated), and labelled platelets were perfused at 1500s^{-1} for 4 minutes. At the lowest coating concentration of 2µg/ml transient tethering (yellow arrows) was the only type of interaction between platelets and immobilised wtD'A3 and T1255A-D'A3. When the concentration increased to 3µg/ml the wtD'A3 supported significantly more interaction than the T1255A, majority of which could be described as platelet rolling (pink arrows). With increasing wtD'A3 concentration, an increasing number of tethers resulted in rolling. The T1255A-D'A3 was unable to mediate platelet translocation until it was immobilised at a concentration of 30µg/ml. Platelets flowing near the surface, but not binding were visible as a white smear (green arrows).

Since the number of tethering events was notably lower on immobilised T1255A, Clus1 and DC-D'A3 variants than on the wtD'A3, it was necessary to verify whether *O*-glycosylation variant were coated on the slide to the same extent, and remained attached after subject to hydrodynamic flow. To this end, after incubation with protein, slides were washed; blocked and HEPES/Tyrodes buffer was perfused for 4 minutes at the shear rate of $1500s^{-1}$. Then proteins were stripped from the slide surface and subject to SDS-PAGE under reducing conditions followed by WB and immunostaining with anti-c-myc antibodies. As demonstrated in Figure 8.25 same amount of protein was detected in each well, suggesting that both wtD'A3 and D'A3 variants were present on the flow slides in equal amounts and were not removed by shear stress.

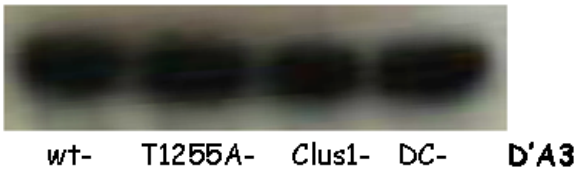


Figure 8.25 Western Blot analysis of the wtD'A3 and mutated D'A3 fragments coated on a flow slide surface

wtD'A3 and T1255A, Clus-1, and DC-D'A3 glycosylation variants were removed from the slide surface, reduced and subject to SDS-PAGE under reducing conditions and blotted. Detection of D'A3 was carried out the using anti-c-myc antibodies. The same signal was detected in each lane, implying the same amount of D'A3 was present.

8.8 Comparison of platelet translocation pattern over immobilised wtD'A3 and *O*-glycosylation variants

On closer inspection of the recorded movies of platelet rolling, it was observed that platelets did not appear to translocate across the T1255A, Clus1 and DC variants in the same way when compared to wtD'A3. While platelets moved in a smooth and consistent manner across wtD'A3, the translocation across the mutant D'A3 surfaces appeared less uniform and more erratic. To investigate this further, 35 individual frames from selected movies were stacked using the maximal intensity Z-projection function in ImageJ to assess the movement of individual platelets over the duration of the 35 frames.

As illustrated in Figure 8.26, on surfaces coated with the *O*-glycosylation variants, platelets appeared to "jump", as gaps are visible between points of binding when subsequent movie frames are analysed. In the case of interaction wtD'A3 platelets stopped more often, indicating that the distance between bonds and therefore presumably between available A1 domains, was shorter.

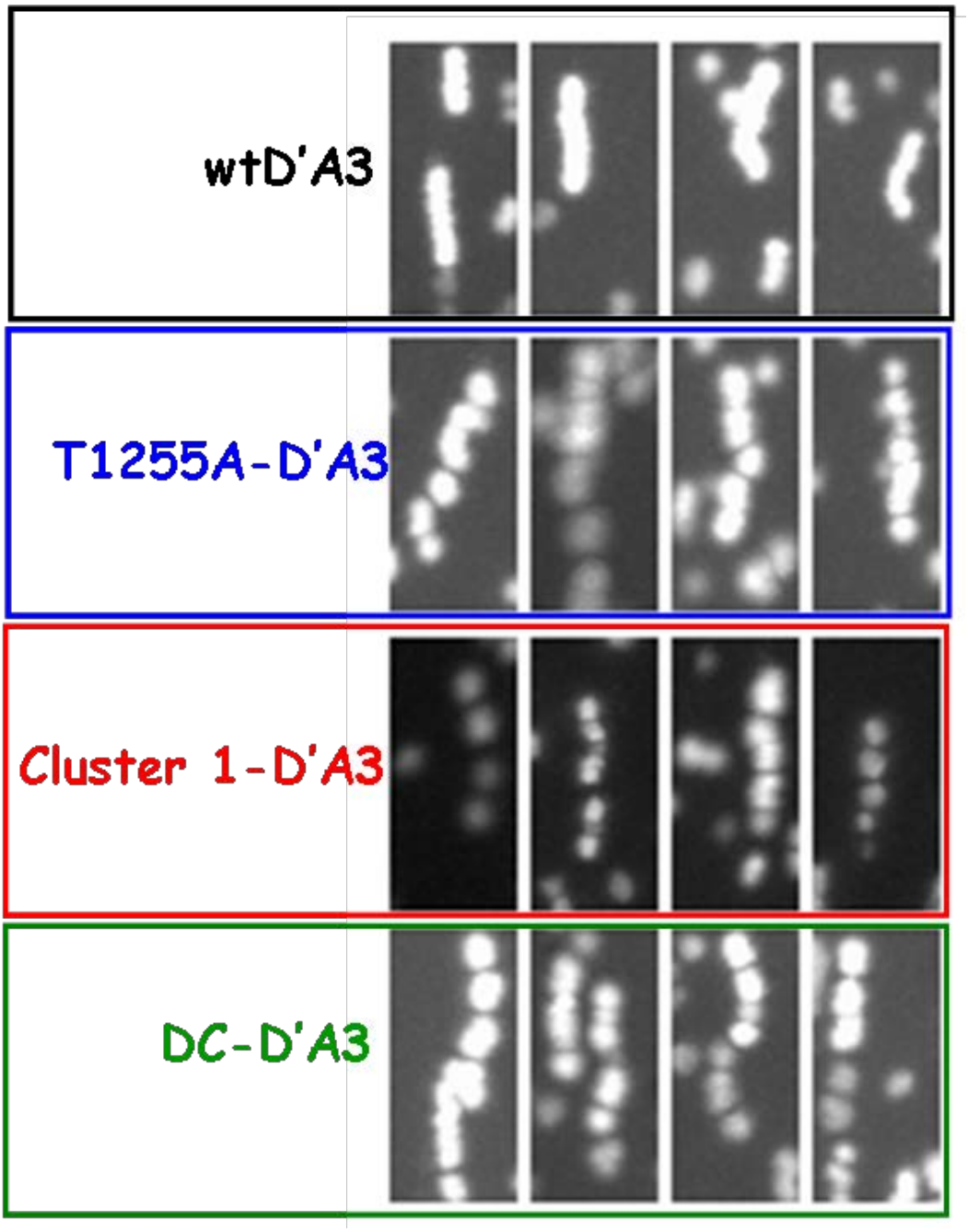


Figure 8.26 Platelet translocation pattern on immobilised wtD'A3 and T1255-, Cluster1- and DC-D'A3 glycosylation variants

Purified platelets were perfused over wtD'A3, T1255A-D'A3, Clus1-D'A3 and DC-D'A3 immobilised (at a concentration of 30µg/ml) at shear rates of 1000 s^{-1} for 4 minutes after that time movies were recorded. 35 subsequent frames were superimposed (~1.75s) to track the translocation of individual platelets. Examples of platelets translocation paths on wild type and mutated proteins are shown. It is clear that platelets roll uniformly on the surface coated with wtD'A3. In contrast platelets translocate less consistently and smoothly on immobilised glycosylation variants and appear to jump rather than roll as indicated by the larger gaps between points of platelets attachment. (Images were acquired at x20 magnification and analysed following x3 zoom in ImageJ)

8.9 Influence of *O*-linked glycosylation variants on VWF mediated platelet adhesion to collagen

Removal of the *O*-linked glycan from position T1255 or the entire N-terminal glycan cluster or all *O*-linked glycans clustered around the A1 domain resulted in altered interaction with platelets. However these experiments were performed using D'A3 fragments immobilised on to flow slides. While this is more physiological than static assays used to examine VWF function, *in vivo* platelets bind to VWF that is immobilised on collagen surfaces under high shear stress. Therefore to analyse further the effect of the *O*-linked glycan variants on VWF platelet capture function, flow assays were performed in which flow slides were coated with collagen and these were perfused with plasma free blood supplemented with wild type FL-VWF or its variants.

The number of bound platelets was determined every 0.5min of perfusion and the results were expressed as a percentage of the collagen surface covered. Firstly, no significant collagen binding was detected when platelets without VWF or with the type 2M-VWD variant (G1324S-VWF) were used, confirming the specificity of the interaction (Figure 8.27). The amount of binding increased with perfusion time for wtVWF and the *O*-glycosylation variants. As demonstrated in Figure 8.27, after 0.5min of flow notable platelet binding was observed in the presence of T1255A- and Clus1-VWF, whilst only a minimal binding occurred in the presence of wtVWF. Increased T1255A and Clus1-VWF mediated platelet capture to collagen was observed at time points between 2-5 minutes when compared to wtVWF, with approximately 10% more surface covered in the presence of glycosylation variants. Surprisingly, these data indicate that the removal of *O*-linked glycans from the position T1255 or the entire N-terminal glycan cluster results in enhanced platelet capture to collagen type III under high shear rate of $1500s^{-1}$.

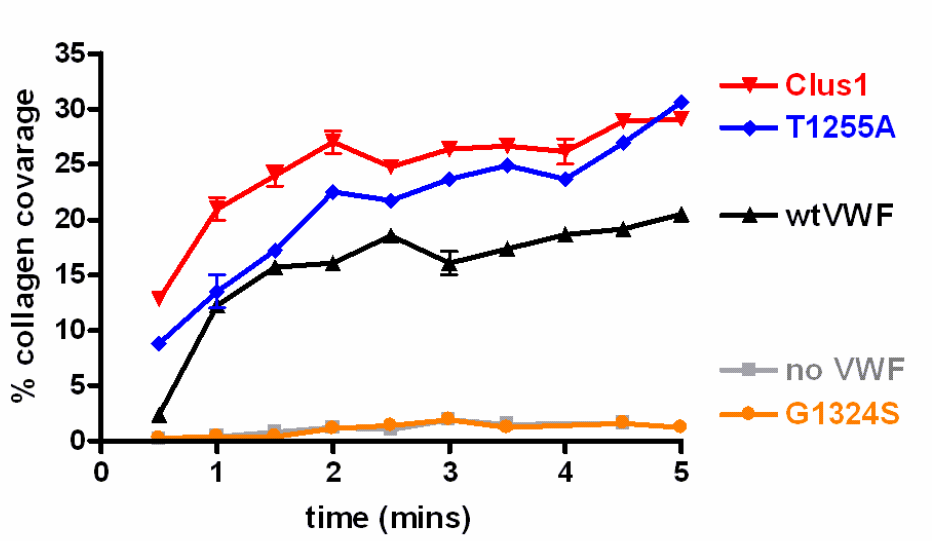


Figure 8.27 Platelet adhesion to collagen type III in the presence of wtVWF and VWF glycosylation variants

Labelled platelets with wtVWF and VWF variants were perfused over collagen type III coated surface at shear rate of $1500s^{-1}$. The number of bound platelets was expressed as the percentage of surface coverage and plotted against time after the start of perfusion. No significant collagen binding was detected when platelets without VWF (noVWF) or with type 2M-VWD variant (1324-VWF) were used. The amount of captured platelets was higher in the presence of T1255- and Clus1-VWF than in the presence of wtVWF. Mean ± SEM

8.10 Discussion

It is apparent from the previous chapter that the *O*-linked glycans clustered around the VWF A1 domain alter VWF sensitivity to ristocetin mediated GPIbα binding. However, these assays do not accurately reflect how the interaction occurs in vivo, due to the requirement of an artificial modulator and the absence of flow. To study the VWF-GPIbα interaction in a more physiological setting I have optimised an *in vitro* flow based assay system to assess the VWF-platelet interaction in real time under shear stress which closely mimics blood flow.

In this project flow assays were performed using purified and fluorescently labelled platelets and washed erythrocytes. Since only the interaction between the platelet receptor GPIbα and the VWF-A1 domain was investigated, platelet activation was inhibited by the addition of prostaglandin E1, apyrase and EDTA. Platelet isolation and labelling involved a series of centrifugations and it was important to keep buffers and platelets at room temperature and be very slow and careful when re-suspending the

platelets to minimise activation. In addition, I have observed that the presence of erythrocytes is essential to observe platelet adhesion to immobilised VWF under flow. This finding is in agreement with previous data showing that in the presence of erythrocytes, shear enhances radial transport of platelets to the surface due to shear induced tumbling of erythrocytes.[348,522] Under flow, especially high shear, erythrocytes tend to move towards the centre of the vessel pushing platelets towards the vascular wall creating a near-wall platelet excess.[523] Interestingly, it has been previously shown that platelet adhesion to VWF coated slides under high shear rate (1500 s^{-1}) is still efficient even when the platelet count was reduced by up to 90% further confirming the importance of erythrocytes.[523] Importantly I have determined that erythrocytes had to be washed four times in order to remove any residual VWF. Subsequently I have optimised coating conditions for VWF and collagen. The type III collagen from Southern Biosciences immobilised overnight at a concentration of 100µg/ml was identified as the most suitable for the flow assays. Furthermore, the concentrations of VWF-D'A3 and FL-VWF required to saturate the slide surface and which would support platelet attachment and rolling were determined. In addition a coating concentration of VWF-D'A3 that would support only transient tethering events was established.

In the majority of the assays described in this project a fragment of VWF comprising of D' to A3 domains was used as it allowed me to study the kinetics of the bond formation between platelet GPIbα and the VWF-A1 domain, which would not be feasible if multimeric VWF was used. In the majority of previously published studies, the isolated A1 domain expressed in *E.coli* was used to study the kinetics of the VWF-GPIbα bond formation. It was assumed that the isolated A1 domain would perform in the flow assay identically as full length VWF. This assumption is based on the studies which have shown that under shear flow platelet attachment to a surface saturated with immobilised bacterial A1 or a glycosylated VWF fragment containing the A1 domain and part of the D3 domain (residues 1208-1496) was comparable to multimeric VWF.[524,285] However, in these studies only platelet attachment was evaluated, which provides little insight into the biomechanical properties of the GPIb-VWF-A1 bond. Therefore a more detailed analysis such as platelet rolling and kinetic analysis of bond formation is necessary before a direct comparison can be made. Using static assays I have demonstrated that *O*-linked glycans flanking the A1 domain modulate VWF-GPIbα binding. In previous studies, domains neighbouring the A1 domain have been implicated in modulating its

accessibility. The D'D3 domains and N-terminal A1 domain flanking region have an inhibitory effect on GPIbα binding[137,138] and it has also been suggested that the A2 domain interacts with the A1 domain.[286] Based on these data, the D'A3 fragment was chosen for the flow experiments, as in contrast to the isolated A1 domain, it encompasses structural elements that may influence GPIbα binding in multimeric VWF.

It has been well documented that GPIbα mediates platelet attachment and translocation of platelets on immobilised VWF *in vitro*. I have confirmed this observation by examining the interaction of platelets with immobilised full length VWF and D'A3-VWF. Initially, the effect of increasing shear rate (400 to 2000s^{-1}) on platelet attachment and rolling on immobilised wtD'A3 was investigated. The specificity of this interaction was demonstrated by inability of platelets to adhere to surface coated with BSA. Platelets were able to bind to immobilised wtD'A3 in a shear dependent manner, however since the A1-GPIbα interaction cannot support irreversible adhesion, they translocated in the direction of flow, albeit at a markedly reduced velocity relative to freely flowing platelets. In accordance with previously published studies[1] platelet rolling velocities were dependent on the shear rate, with a biphasic velocity curve at shear rates between 400 and 2000s^{-1}. I have observed that with increasing shear rates platelets rolled more slowly due to increasing bond-lifetimes (catch bond) until a threshold shear rate value was reached. A further increase in the shear rate caused faster platelet rolling (slip bond). The shear stress dependent bond formation between platelet GPIbα and the VWF-A1 domain has been previously documented and is similar to that of selectins with their glycoconjugate ligands which mediate leukocyte rolling on inflamed vascular surfaces.[525] The force applied on the bond initially increases and the bond lifetime increases (catch bond) until a maximal value is reached and then as the force increases further, bond lifetimes decreases (slip bond).[526] Platelet attachment and rolling experiments were performed under conditions that support multiple bond formation at a time between platelet and VWF-A1 domains, and as such, provide limited insight into the biomechanical properties of the GPIbα-A1 bond. To gain insight into the kinetics of transient tether events between platelets and wtD'A3 under flow conditions, protein was immobilised at a concentration that limited multiple bond formation. Initially, shear rate dependence of transient tethering was examined. It is well established that tether formation is related to shear rate and therefore is limited by the time that the receptor and ligand are in proximity to one another, rather than by the

force exerted on forming bonds.[332] It has been shown for selectin-ligand bond formation that the initial increase in shear rate increases the collision probability and allows it to overcome a repulsive barrier.[353,355] However, above a certain threshold shear rate, the tether formation becomes limited by the time that the receptor and ligand are in proximity to one another. Similarly, the GPIbα-A1 tether bond formation requires a critical level of hydrodynamic flow to initiate adhesion and an increase in shear rate promotes bond formation up to a point where shear rate becomes the limiting factor. In accordance with these studies I have observed that as the flow rates increased, the number of platelet-wtD'A3 transient tethering events increased until a shear rate of $600s^{-1}$ was reached. Above that point the number of platelet-wtD'A3 tethering events started to decrease and at shear rates above $5000s^{-1}$ no transient tethering was observed.

Transient tethers are the smallest unit of adhesive interaction observed in shear flow, and have a distribution of bond lifetimes that obey first order dissociation kinetics.[333,354,527,528] The wtD'A3 platelet tether time distribution followed first-order dissociation kinetics implying we have indeed looked at single bond formation. Based on the bond lifetimes, the dissociation rate constants of transient tethers were calculated at a range of shear rates ($400\text{-}2000s^{-1}$). The k_{off} values for wtD'A3 appear to fall in to the same order of magnitude as reported in the literature, although previously obtained dissociation rates were determined for tethers between the isolated A1 domain-platelet interaction and at lower shear rates (up to approximately $200s^{-1}$).[262] To our knowledge this is the first time the dissociation rate values for the GPIbα-VWF-A1 interaction under condition of medium and high shear stress have been derived. Interestingly no apparent differences were detected in the k_{off} values across the shear range tested ($400\text{-}2000s^{-1}$). The viscosity of plasma is approximately 5 fold higher that blood preparations used in this study. In the future a HEPES-TYRODES buffer supplemented with Ficoll to increase viscosity is going to be used. This may help to resolve changes in bond lifetime across the ranges of shear rates that were previously reported, and observe the influence of shear stress values on bond lifetimes. So far I have only modified the shear stress by increasing the shear rate values; however by increasing those I am also decreasing the probability of bond formation, which could mean that the effect of increasing force on the bond will not be observed, as the bond will not be formed in the first place. By increasing the viscosity we increase the shear stress therefore increase the

force acting on a bond and in result the bond lifetime and dissociation rate but not the velocity of blood and probability of bond formation.

In addition, I have observed that the shear rates that supported the maximal number of platelet-wtD'A3 tethering events, were lower than the shear rates at which platelet attachment was maximal and rolling velocity was the slowest. I propose that the force acting on an entire platelet is the same in both experiments, however in platelet adhesion and rolling experiments the force acting on the platelet is distributed among several bonds, thus the force acting on an individual bond is decreased. In the platelet transient tethering experiments, the entire force acting on a platelet is loaded onto a single GPIbα-VWFA1 bond. When the surface is saturated with VWF, multiple bonds mediate platelet adhesion and rolling, which could reduce the force on individual bonds below the levels that produce the catch and slip bond transition. At low shear stresses, bond lifetimes are too short to support rolling and platelet attachment that would be long enough to be measured in the experiments performed in this project. However low shear rates are large enough to mediate platelets transient tethering.

8.10.1 The influence of *O*-linked glycans on platelet interaction with immobilised D'A3-VWF under various shear rates

With the flow assays optimised, I investigated the influence of *O*-linked glycosylation on VWF-platelet interactions under hydrodynamic shear stress. To begin with, I investigated the properties of the T1468A variant which exhibited decreased sensitivity to ristocetin mediated GPIbα binding in the plate assay and diminished ability to support platelets aggregation in the VWF:RCo assay. I have shown that platelet adhesion and platelet rolling velocities on the slide surface densely coated with T1468A-D'A3 are comparable to that on immobilised wtD'A3 at all shear rates tested. Furthermore, the transient tethering rate and dissociation rate constant of bonds formed between GPIbα and T1468A-D'A3 were similar to that of GPIbα-wtD'A3. These results indicate that the decreased GPIbα binding observed for T1468A variant under static conditions was likely due to distorted interaction with ristocetin not GPIbα. As discussed in the previous chapter the T1468 glycosylation site resides in one of the regions implicated in ristocetin binding, therefore removal of the glycan chain might directly affect ristocetin binding or ristocetin effect on VWF-A1 domain conformation.[288,290]

It has been previously suggested that ristocetin dependent assays may not entirely reliable in assessing VWF function.[516] Significantly decreased ristocetin dependent platelet binding was observed for VWF from patients with the type 2M-P1467S mutation or individuals with the D1472H polymorphism even though they had no bleeding phenotype. Conversely VWF containing those mutations exhibited normal GPIbα binding when the assay was performed under shear conditions or static conditions in an assay that did not require presence of ristocetin (using GPIbα with gain of function mutations).[516,529] The discrepancy in the binding studies performed dependent and independently of ristocetin was attributed by the authors to altered ristocetin binding.

Subsequently the flow assay was employed to examine platelet interaction with the *O*-linked glycosylation variants that exhibited increased sensitivity to ristocetin mediated GPIbα. The T1255A- Clus1- and DC-D'A3 variants exhibited a generally similar ability to mediate platelet capture as wtD'A3 at the shear rates up to $1000s^{-1}$, however decreased platelet capture was observed at $2000s^{-1}$. Interestingly the calculated platelet rolling velocities showed that platelets translocated faster on all three immobilised *O*-linked glycosylation variants than on wild type protein at all shear rates tested. Interestingly, the Cluster 1 showed higher rolling velocity then the other two variants at a shear rate of $600s^{-1}$. This has been observed several times however an adequate explanation cannot be determined for this observation. Importantly, platelet rolling velocity curves followed a biphasic pattern, implying that removal of *O*-linked glycans does not affect the ability of VWF to form catch and slip bonds with GPIbα. The rolling velocity is thought to depend on the bond lifetime and dissociation rate constant. However, platelet rolling also relies on the efficiency at which primary transient tethers transform into stable tethers by forming new bonds at the front edge of the platelets as previous bonds in the rear edge dissociate.

To further elucidate the differences in rolling I have attempted to characterise the kinetics of tether bonds for mutated proteins. Unexpectedly, I have shown that there is no significant difference in the dissociation rate values for bonds formed between platelets and T1255A, Clus1 and DC-D'A3 when compared to wtD'A3 under all flow conditions tested. This finding implies that the difference in platelet rolling observed for these *O*-glycosylation variants is caused by reasons other than the change in bond dissociation under shear stress. Subsequently, I have shown that immobilised T1255A-,

Clus1- and DC-D'A3 variants support notably lower numbers of transient tethering events when compared to wtD'A3 at the shear rates between 400 and 1000s^{-1}. This finding shows that a proportion of immobilised D'A3 variants are unable to bind GPIbα under shear stress therefore the probability of bond formation is lower, which suggests that the accessibility of GPIbα binding sites is limited in the absence of *O*-glycans. This finding is intriguing since the immobilised glycosylation variants were able to effectively capture platelets when flow slides were saturated with protein. It can be proposed that this dissimilarity is due to the concurrent GPIbα-A1 bonds being formed between individual platelet and densely immobilised D'A3, whereas transient tethering engages an individual A1 domain and GPIbα receptor. It can be hypothesised that when the surface is saturated with D'A3, the distance between A1 domains is significantly smaller; therefore individual platelets can interact with more than one A1 domain, thus allowing adhesion even if a proportion of GPIbα binding sites are not available. Corroborating this hypothesis I have shown that the number of bound platelets was similar for wtD'A3 and T1255A-D'A3 only when both were coated at saturating conditions allowing multivalent contacts to form due to clustering of A1 domains. Furthermore it was observed that T1255A-D'A3 had to be immobilised at concentrations ten times higher than wtD'A3 in order to support platelet rolling.

In view of the fact that the bond dissociation rates were comparable for wtD'A3 and the T1255A, Cluster 1 and DC D'A3 variants, the faster platelet rolling on the *O*-glycosylation variants has to be attributed to decreased accessibility of their GPIbα binding sites. I propose that since a proportion of GPIbα binding sites are unavailable as indicated by the reduced number of transient tethering events taking place (figure C,D) the distance between the A1 domains that a translocating platelet can bind to is increased. Thus transloacting platelets pause less often on the VWF variants (B) than on wild type protein (A) and appear to cover a larger distance during the same time, which is reflected in a higher platelet translocation velocity. When analysing movies of platelet translocation frame by frame it is becomes apparent that platelet translocation on immobilised wtD'A3 appears as consistent and smooth rolling. In contrast platelet translocation over immobilised T1255A-, Cluster1 and DC-D'A3 variants appears less continuous, more erratic and platelet appear to 'jump' as well as roll.

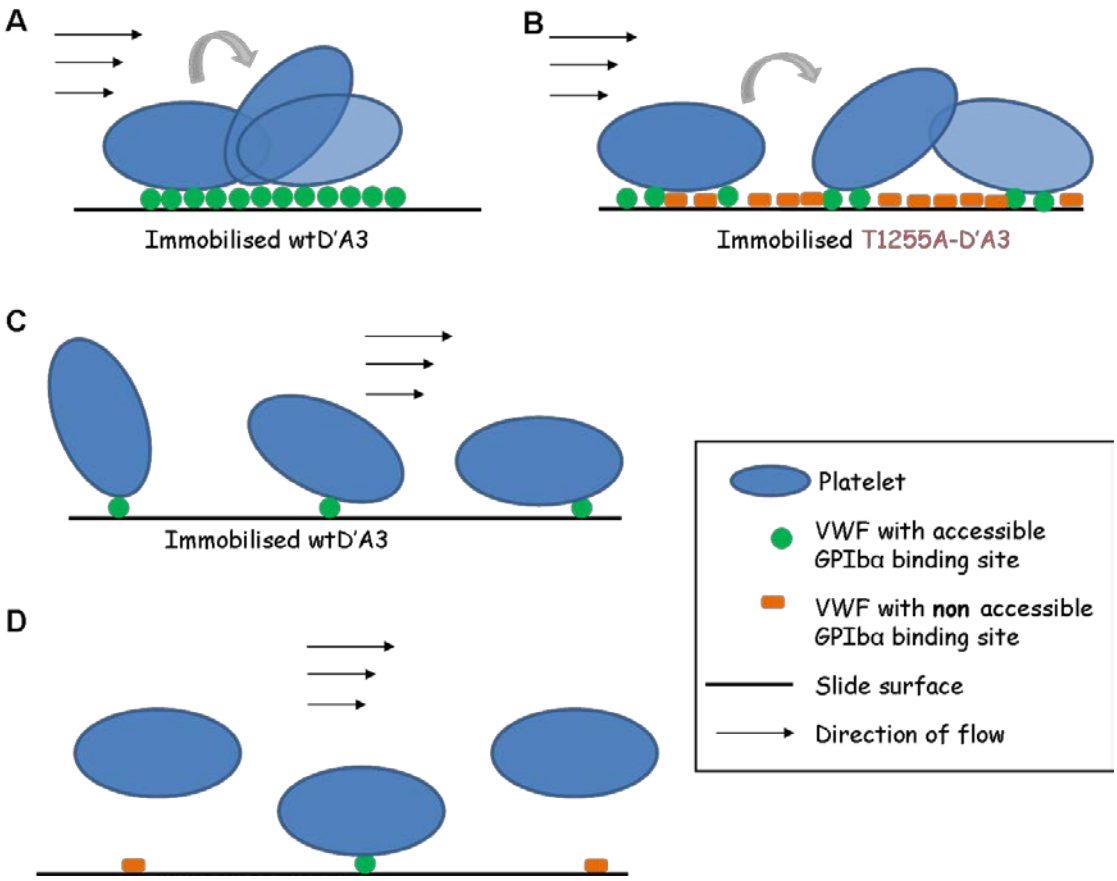


Figure 8.28 Illustration of proposed pattern of platelet translocation and transient tethering on immobilised wtD'A3 and the T1255A, Clus1 and DC glycosylation variants under shear stress

Graphic representation of platelet rolling on a slide surface saturated with wtD'A3 **(A)** and T1255A-, Clus1 or DC-D'A3 variants **(B)** under shear stress. (A) All the GPIbα binding sites of the wtD'A3 are available, therefore platelets bind and pause more often, rolling consistently. **(B)** A proportion of GPIbα binding sites of the *O*-glycosylation variants is non-accessible, therefore platelets bind and pause less often which allows them to cover a larger distance in a shorter space of time, which is reflected by faster translocation velocity. Similarly if more of GPIbα binding sites are available in the wtD'A3 **(C)** than glycosylation variants **(D)** platelet transiently tether more often on immobilised wtD'A3 than the T1255A-, Clus1 or DC-D'A3 variants under conditions of shear stress.

To further elucidate this hypothesis I have investigated platelet rolling velocities on FL-VWF and wtD'A3 coated at different concentrations. Platelets rolled faster on the lowest concentration of protein immobilised and slower when the surface was saturated with the protein. Moreover, I have shown that platelets roll faster on a surface saturated with immobilised FL-VWF (15.2±0.5μm/s) than wtD'A3 (9.7±0.2μm/s). These results further support the concept that the shorter the distance between A1 domains the more frequently platelets can bind and pause, which results in slower translocation velocity. The dependence of rolling velocity on the density of potential interaction sites has been previously demonstrated by Fredrickson *et al*., in a study using mammalian cells expressing GPIbα and immobilised VWF.[530] Cells with a lower GPIbα receptor density rolled significantly faster than cells with medium or high density of GPIbα. Importantly, the number of interacting cells was independent of receptor density. In addition it was observed that GPIbα expressing cells rolled on immobilised VWF notably faster when VWF was coated at low concentrations.[530]

Finally, the other *O*-glycosylation variants were able to interact with platelets under shear stress in a similar manner as wtD'A3. Importantly, the Cluster 2 variant exhibited unaltered interaction with platelets suggesting that the differences in GPIbα binding observed for the double cluster variant is only due to the absence of glycans on the N-terminal side of the A1 domain.

On the basis of the presented data, I propose that removal of *O*-linked glycans from the N-terminal side of the A1 domain can induce a change in the conformation of VWF D'A3. As a result the accessibility of the GPIbα binding site in the A1 domain becomes limited, at least when the D'A3 protein is immobilised on the slide surface and exposed to shear stress. As discussed in chapter 3, *O*-linked glycans are positioned in close proximity to the peptide backbone, which facilitates close interaction between the sugar and protein, and clustering of glycans can further amplify this effect.[400,502] *O*-linked glycans are known to provide rigidity to peptide backbones and stabilize otherwise flexible regions, thus stabilising protein conformation.[439] Glycans introduce steric hindrance, and the polypeptide they are attached to can adopt a rigid, extended conformation.[438-445] The removal of *O*-linked glycan(s) from the N-terminal A1 flanking region may change its flexibility, and allow VWF to adopt a more tightly folded conformation, limiting the exposure of the A1 domain. Furthermore, the absence of *O*-linked glycans may allow formation of nonspecific interactions between A1 and

neighbouring domains, possibly increasing shielding by D'D3 domain, and as a result, altering the accessibility of the GPIbα binding site.

8.10.2 Sialic acid effect on VWF-platelet interaction under conditions of shear flow

In the static assay removal of sialic acid residues from VWF resulted in increased sensitivity to ristocetin mediated GPIbα binding. In the present study I have therefore investigated the ability of desialylated VWF to interact with platelet receptor GPIbα under various shear rates. Firstly I demonstrated that both sialylated and desialylated proteins were able to support the same number of transient tethering events. Moreover the GPIbα-A1 dissociation rate constants were similar for both proteins at all shear rates tested. Seemingly contradictory, the number of bound platelets was higher for the desialylated D'A3 when proteins were immobilised at saturated concentrations under shear rates up to $1000s^{-1}$ but no difference was observed at higher shear rates. Furthermore platelets rolled with markedly slower velocities on immobilised desialylated D'A3 when compared to sialylated D'A3 at shear rates up to $1000s^{-1}$.

Even though a similar number of primary transient tethering events were supported by desialylated D'A3 and sialylated D'A3, I propose that the number of primary tethering events that transform into rolling events was higher on surface saturated with desialylated D'A3. This hypothesis could explain why the calculated number of attached platelets was greater on the desialylated wtD'A3 compared to sialylated wtD'A3 when proteins were immobilised at saturating concentrations, but not when they were coated at low concentrations and only transient tethering events were measured.

I hypothesise that the slower platelet rolling velocity on desialylated wtD'A3 could be a result of increased affinity of platelets that are already tethered to VWF when terminal sialic acid residues are absent from the protein. The ability of platelets to interact with the next available GPIbα binding site could increase when VWF is devoid of sialic acid. Consequently rolling platelets bound to more A1 domains and paused more frequently. Therefore over a given time period platelets translocated over a shorter distance than if they were rolling on sialylated D'A3, even though the actual bond lifetime was unaltered. The molecular mechanism of this effect of sialic acid residues is not clear. GPIbα contains a negatively charged aspartate and glutamate residues and sulphated

tyrosines[295,297] (which are also present in the recombinant GPIbα fragment used in the static assays) as well as a highly glycosylated mucin stalk. It has been previously demonstrated that inhibiting the sulfaation of GPIbα reduced ristocetin dependent VWF binding.[297] It could be hypothesised that removal of terminal sialic acid residues which confer a negative charge to glycans[505] from VWF promote electrostatic interaction of VWF with GPIbα under lower shear stress and static conditions. Interestingly, the difference in platelet adhesion and rolling occurs until a certain shear rate value ($1000s^{-1}$). It can be assumed that after this point shear stress becomes the crucial factor that limiting GPIbα-A1 bond formation and platelet translocation, and conformational changes that occur in GPIb and VWF structure are more important that an electrostatic interaction between the proteins. An increase in GPIbα binding was also observed following removal of sialic acid in the static assay in the presence of ristocetin, further confirming increased affinity of desialylated VWF towards GPIbα.

8.10.3 Platelets interaction with collagen in the presence of VWF under high shear stress the role of *O*-linked glycans

In the experiments discussed above VWF was immobilised directly onto the flow slides, while this is more physiological than static assays used to examine VWF function, it is perhaps not a true reflection of platelet-VWF interactions *in vivo* where platelets bind to VWF that is immobilised on collagen surfaces under high shear stress. For that reason I have also investigated platelet capture to slides coated with collagen in the presence of wild type FL-VWF or T1255A and Cluster 1 variants. Experiments were performed under high shear stress ($1500s^{-1}$) to prevent platelet binding directly to collagen. Moreover, since both platelet and collagen binding depend on VWF multimeric content, I ensured that purified VWF samples of the same multimeric composition were used. Surprisingly the number of platelets captured to collagen via T1255A or Cluster1 was greater than platelet capture mediated by the wtVWF. These results imply that the removal of *O*-linked glycans from the N-terminal side of the A1 domain has a different effect on the ability of VWF to interact with platelets when VWF is immobilised directly on the slide to when it is bound to collagen. The observed difference might be either to an increased ability of collagen bound VWF variants to capture platelets or e a consequence of increased ability of these mutants to bind to collagenunder shear stress. However it appears from the static assays and preliminary flow experiments performed

towards the end of the study that is not the case, as both variant showed normal collagen binding however is more studies are needed to confirm this.

Based on the presented data, it can be hypothesised that the effect of VWF *O*-linked glycans on platelet binding under shear stress is dependent on the way VWF is attached to the slide surface. VWF adheres to collagen mainly via its A3 domain and putatively via A1 domain; direct binding to the slide surface is possibly less uniform and might involve several domains. Currently, it is not apparent how diverse methods of VWF immobilisation affect its conformation. Moreover, shear stress could potentially exert different effects on immobilised VWF depending on the way it has been captured. It has been previously demonstrated that the hydrophobicity of the surface can influence the structure of immobilised VWF. On a hydrophilic mica surface VWF appears in more extended structure, while on a hydrophobic surface VWF adopts a more compact coiled structure, thought to resemble VWF in solution.[93] In this study a hydrophobic plastic surface was used; therefore the immobilisation should not influence the conformation of D'A3 domains. It has been previously shown that surface immobilised VWF may undergo a conformational change under the influence of high shear stress and acquire an elongated structure rather than a loosely coiled structure observed under static conditions.[89,90] However a change in the overall (molecular) shape does need not induce a conformational transition in the A1 domain. Following absorption on the slide the tight globular conformation of the D'-A3 domains might still be retained whilst the C-terminal domains might undergo elongation. Indeed tapping force atomic force microscopy (TM-AFM) studies demonstrated that VWF multimers and dimers immobilised on hydrophobic mica surfaces consist of intramolecular repeat units of globular and stretched domains.[94] Moreover, the overall structural change in VWF exposed to shear before immobilisation did not cause a significant change in the diameter of its globular repeat units.[94]

It has also been previously demonstrated that the structural conformation of the isolated VWF-A1 domain changes when it binds to collagen.[132] The presence of *O*-linked glycans might influence this change in conformation; for example their absence could provide more flexibility to VWF A domains structure so that they are more prone to unfolding. The isolated A1 domain is able to interact with collagen and bind platelets but in the presence of other domains, the interaction of VWF-A3 domain with collagen is essential to mediate platelet attachment.[134] It has been shown that the binding of VWF

to collagen via the A3 domain induces a conformational change in VWF, exposing its cryptic A1 collagen binding site.[134] I hypothesise that when VWF is bound to collagen, *O*-linked glycans influence the ability of the A1 domain to interact with the A2 and A3 domains and to participate in the shielding effect of D'D3 domains on the A1 domain. Moreover the absence of *O*-linked glycans could result in destabilisation of the A1A2A3 tridomain complex. This destabilisation can augment the effect that collagen binding via the A3 domains has on the exposure of A1 domain and its GPIbα binding site under shear stress

Importantly, platelet adhesion to collagen under high shear stress depends on the presence of both soluble and collagen bound VWF, whereas in the experiments where VWF is immobilised directly onto the slides surface no soluble VWF is present. It has been previously demonstrated that under shear stress the additional inter-molecular interaction between VWF domains of both soluble and collagen bound VWF facilitate formation of a VWF network, which anchors circulating platelets.[95,164,362] It can be hypothesised that the removal of *O*-linked glycans could enhance this VWF self-association under shear stress, resulting in increased platelet capture.

It has been shown that under static conditions ristocetin mediated VWF self-aggregation can also take place.[531] It has been suggested that ristocetin induces large conformational changes that disrupt the multiple domain interactions that occur within globular VWF. Ristocetin binding to VWF possibly alters domain interactions within a VWF monomer, thereby allowing inter-domain interactions between different VWF molecules that contribute to the formation of aggregates. Since I have observed increased ristocetin dependent platelet capture for the T1255A- Cluster 1 and DC cluster in my static GPIbα binding assay it could be tentatively suggested that the absence of *O*-linked glycans might increase the efficiency of ristocetin mediated VWF self-aggregation which could result in increased GPIbα binding. This hypothesis is however unlikely as the concentration of ristocetin used in the previously published study was three times higher than the highest concentration I have used in the static assay

In summary, I have demonstrated that the T1255A, Cluster 1 and double cluster variants have a distorted ability to interact with platelets in the presence of hydrodynamic shear stress. Importantly however, the effect of the glycans on GPIbα binding depends on the manner in which VWF is immobilised. Previous studies investigating the interaction of platelets with VWF under flow conditions have demonstrated that the initial, and crucial, tethering and translocation of platelets is mediated by the GPIbα receptor interaction with the A1 domain, whereas firm adhesion requires binding by integrin αIIbβ3 of activated platelets.[245] In view of the presented data it is clear that GPIbα binding to VWF is a complex event and distinct structural characteristic can control the ability to establish stable bonds or to initiate platelets tethering. The results presented in this chapter emphasise the importance of immobilisation method on receptor-ligand interaction under shear flow. Moreover, it is the first time the role and kinetic effects of *O*-linked glycans on platelet binding under shear stress has been studied and my results could be important in understanding the fundamental mechanism of platelets tethering and rolling.

9 CONCLUSION AND FUTURE DIRECTIONS

Glycosylation is a co- and post-translational modification that involves the covalent attachment of carbohydrate structures to the protein backbone and has been shown to be crucial for the expression and functioning of many eukaryotic proteins. The two major types of glycans produced by eukaryotic cells are *N*- and *O*-linked glycans. While the former has been extensively studied, fewer data exist regarding the function of *O*-linked glycosylation. Mucin type *O*-linked glycosylation is well known to support the structure and function of mucin proteins on endothelial cell surfaces, by assisting in tissue hydration, protecting cells against stress and pathogen infection and altering accessibility of the peptide backbone to proteases therefore protecting it from degradation.[1-3] *O*-linked glycans have been shown to mediate specific functions such as regulating the serum half-life of chemokines and hormones and also to mediate intracellular trafficking of proteins as well as signalling and interaction with receptors.[4-10] However *O*-linked oligosaccharides can also have a general nonspecific effect on the properties of proteins. *O*-glycans are suggested to influence the secondary, tertiary, and quaternary structure of the folded protein by introducing steric hindrance, and causing the polypeptide to which they are attached to adopt a rigid, extended conformation.[11-18] For example, it has been shown that ovine submaxillary mucine (OSM) has an elongated filamentous conformation, however following removal of *O*-glycans it assumes a globular conformation.[19] There are not many examples of studies on proteins with isolated mucin type glycans. It has been shown that a single *O*-linked glycan on human granulocyte colony stimulating factor contributes to stability of the glycoprotein by suppressing polymerisation and conformational change of the protein, allowing it to keep its biological activity.[20] Clusters of *O*-linked glycans are located in the hinge regions of immunoglobulins IgD and IgA, where up to 6 *O*-linked glycans chains can be present.[21-23] *O*-linked glycans in these hinge regions have been shown to mediate binding of IgA and IgD to a lectin binding site on T-lymphocytes *in vitro*.[22,24]Abnormalities in IgA *O*-glycosylation have been implicated in diseases such as Sjogren's syndrome and IgA nephropathy (IgAN).[25-27] In IgAN, patients have abnormalities in glycan biosynthesis which can results in the exposure of GalNAc residues[22,28-30] Aberrantly glycosylated IgA molecules have a tendency to self aggregate as the exposed GalNAc residues are recognised by anti-IgG or IgA antibodies, leading to the formation of large circulating immune complexes that deposit in the kidney and

activate Complement.[31-33] In addition, IgA molecules lacking terminal Gal residues have increased affinity for the extracellular matrix components fibronectin and collagen type IV, as shown by studies *in vitro*.[34,35]

VWF is a large multimeric plasma glycoprotein that plays a crucial role in haemostasis by mediating platelet capture to thrombogenic surfaces under conditions of high shear stress.[36] A considerable proportion (18.7%) of the molecular mass of VWF is comprised of *N*- and *O*- linked oligosaccharides.[37] Based on previous studies, VWF contains 16 *N*-linked and 10 *O*-linked glycosylation sites.[37] VWF *N*-glycans have been studied extensively and their roles in VWF dimerisation, intracellular processing and storage as well as susceptibility to ADAMTS13 proteolysis have been well established[38-42] In contrast, prior to this study, only limited data were available on the function of VWF *O*-linked glycans.

Currently there are very few approaches available to study the role of *O*-linked glycans. Firstly, one might compare the properties of the native glycoprotein to the enzymatically deglycosylated counterpart. In the case of *N*-linked glycans this is possible by the use of PNGase-F which removes whole *N*-linked glycan chains from the peptide or protein. Unfortunately there is not an equivalent enzyme that allows the removal of entire *O*-linked glycan chains. Instead, monosaccharides have to be removed by a series of exoglycosidases until only the Galβ(1-3)GalNAc core remains attached to the serine or threonine residues. In the case of VWF, the glycans initially would have to be desialyated which would also mean removal of terminal sialic acid residues from the *N*-linked glycans, and therefore could confound any functional results. Subsequently the enzyme *O*-glycanase (endo-α-N-acetylgalactosaminidase) could be used to remove the core 1 structures with no modification of the serine or threonine residues. However, *O*-glycanase cannot recognise core 2 structures and since VWF contains core 2 structures this approach could not be used.

Alternatively, VWF could be expressed in the ldlD-CHO cell line, which cannot incorporate either Gal or GalNAc into carbohydrate chains when provided with medium lacking this sugars.[43] This cell line was however not available for this study and furthermore the entire proteome of these cells would lack *O*-linked glycans with unpredictable secondary effects.

As mentioned above VWF contains 10 *O*-glycosylation sites, eight of which are clustered around the A1 domain, therefore it has been suggested they might be part of mechanisms regulating the exposure of the GPIbα binding site.[44] To date, the published data regarding the role of *O*-glycans in platelet binding is partial and often contradictory. VWF devoid of *O*-linked glycans demonstrated decreased ristocetin mediated platelet binding and normal binding potential in the presence of botrocetin.[45] On the other hand, the A1 domain lacking glycans at the N-terminal side exhibited increased platelet aggregatory potential in the presence of ristocetin.[46] Previous studies have demonstrated that VWF expressed in ldlD-CHO cells lacking *O*-linked glycans was secreted normally and had unaltered multimeric structure and heparin and collagen binding.

In an attempt to further characterise the function of VWF *O*-glycans, individual and multiple mutations (threonine/serine into alanine) were made to *O*-linked glycan sites to prevent addition of oligosaccharides. The variants consisted of ten single point mutations (T1248A, T1248A, T1255A, S1263A, T1468A, T1477A, S1486A, T1679A and T1679A and T2298A) and three types of cluster variants created by mutating all of the 4 sites either side of the A1 domain (cluster 1 and cluster 2) or all 8 sites around the A1 domain (double cluster). Mutated proteins were then expressed in HEK293T cells and characterised. Firstly, in keeping with a preceding study, I have demonstrated that absence of *O*-linked glycans does not influence VWF expression or secretion.[45] Furthermore all the variants had normal multimeric composition and an ability to bind collagens type I and III similar to that of recombinant wild type protein. The absence of *O*-linked glycans did not influence the binding between VWF and heparin or isolated bacterial A2 domain.

9.1 Susceptibility to ADAMTS13 proteolysis

Next, I have analysed the susceptibility of VWF variants to ADAMTS13 proteolysis and binding. Firstly, I have shown than the S1486A, Cluster 2 and double cluster variants were proteolysed slower than wtVWF both in the presence of urea and under the pseudo-shear stress generated using a bench top vortex mixer.[47] Based on the fact that *O*-linked glycans are known to provide rigidity to peptide backbones[11-15] I hypothesised that removal of *O*-glycans from the linker region between the A1 and the A2 domain may increase its flexibility. Change in the flexibility of the linker region

could alter any potential interactions between the A1 and the A2 domains, consequently altering the accessibility of the ADAMTS13 cleavage site. Furthermore, I also hypothesised that the *O*-glycans may participate in stabilising the extended conformation of VWF, allowing efficient exposure of the ADAMTS13 cleavage site. Interestingly, the VWF S1486A, Clus2 and DC variants immobilised on a microtitre plate (therefore in at least a partially elongated confirmation) bound ADAMTS13 with similar affinity to wtVWF. Intriguingly, the mutations that resulted in decreased susceptibility to ADAMTS13 proteolysis, enhanced binding of VWF to ADAMTS13 in solution. I suggested that a change in the local conformation of the VWF A1A2A3 domains, due to removal of glycans, may have a downstream effect and alter the exposure of other domains and the binding sites they encompass. To further confirm this effect, and determine kinetic parameters of the interaction, binding will be investigated in further detail using surface plasmon resonance analysis. Ultimately, to confirm the effect of *O*-linked glycans on VWF proteolysis by ADAMTS13 it will be necessary to adapt the flow assays to analyse ADAMTS13 cleavage under conditions of physiological shear stress. Blood outgrowth endothelial cells (BOECs) isolated from a dog with VWD type 3 will be used to create an EC model of VWF expression. BOECs will be seeded onto flow slides and transfected with VWF variants; provided they can form WPBs the cell will be stimulated with histamine. ADAMTS13 cleavage of UL-VWF released from WPBs will be analysed under high shear stress.

9.2 VWF interaction with platelet GPIbα – the role of *O*-linked glycans

Platelet adhesion at sites of vascular injury contributes to the arrest of bleeding, and at high shear stress this interaction is dependent on the interaction between VWF and the platelet receptor GPIbα. A major aim of this project was to establish the influence of *O*-linked glycans on the VWF-GPIbα interaction. To facilitate this I developed a plate based ELISA method to analyse the interaction of VWF with a recombinant fragment of GPIbα in the presence of ristocetin and optimised an *in vitro* flow assay to study platelet-VWF interactions under conditions of flow.

The data presented in this thesis extends previous observations which demonstrated that the *O*-linked glycans attached to residues T1248 and T1256 negatively modulated the ristocetin dependent platelet binding to COS-7 cell anchored A1 domains in the

presence of ristocetin.[46] Firstly I have shown that the T1255A, Cluster 1 and DC variants have significantly increased sensitivity to ristocetin mediated GPIbα binding and platelet agglutination. The effect was evidenced both as a higher overall binding to GPIbα, and binding to GPIbα at a lower concentration than required by wtVWF.

In vivo, platelets bind to VWF under conditions of physiological blood flow, thus the plate binding assay is limited by the requirement for ristocetin and the absence of shear stress. To explore and define the mechanics and kinetics of the VWF-GPIbα interaction and investigate the influence of *O*-linked glycans on this interaction under shear stress, which closely mimics conditions in the blood flow, I have optimised and employed an *in vitro* flow based assay system. Images of fluorescently labelled platelet motion over surfaces coated with a D'A3-VWF fragment or collagen coated with FL-VWF were visualised under a microscope equipped with a camera and recorded during flow experiments at a range of fluid shear rates (400-2000s^{-1}). Firstly I measured the number of platelets interacting with saturated surfaces and platelet rolling velocities on wtD'A3 and D'A3 glycosylation variants. I have demonstrated that platelets bound transiently to both wtD'A3 and glycosylation variants in a generally similar, shear dependent manner. Moreover platelet rolling velocities on all proteins tested followed a biphasic curve, as the platelets rolling velocity firstly decreased with increasing shear and then after a certain point started to increase with increasing shear rate, indicating catch and slip transition. Interestingly, when compared to wtVWF the T1255A-, Cluster 1- and DC-D'A3 supported faster platelet rolling at the shear rates between 400 and 2000s^{-1}. Subsequently I have analysed the kinetics of GPIbα-VWF bond formation. It has been observed that the rate of transient platelet tethering is notably decreased on immobilised T1255A-, Clus 1- and DC-D'A3 variants. Interestingly the dissociation rate is the same for bonds formed between GPIbα and wild type as well as mutated D'A3.

These results imply that faster platelet translocation on glycosylation variants is not due to shortening in the lifetime of the GPIbα-A1 bond, but is related to the reduced ability of the VWF variants to support platelet tethering. The exact nature of this change has not yet been elucidated, however based on the obtained results I hypothesise that removal of *O*-linked glycans from the N-terminal *O*-linked glycan cluster results in reduced accessibility of the GPIbα binding site when VWF is immobilised directly onto the flow slide and exposed to shear stress. Furthermore since a proportion of GPIbα binding sites is inaccessible the distance between potential binding sites is increased. As

a result platelets translocate on the slide surface irregularly and jump rather than roll, therefore they move further in a given time.

In all these experiments VWF was captured directly onto the flow slides: even though it is a standard approach used in flow studies and allows us to study kinetic parameters of the GPIbα-A1 interaction, it may not be a true reflection of the platelet-VWF interaction *in vivo* where platelets bind to VWF that is captured to collagen surfaces under flow. For that reason I have also investigated platelet capture to slides coated with collagen in the presence of FL-VWF under high shear stress. Surprisingly I have shown that platelet capture to collagen was higher in the presence of T1255A- and Cluster 1 VWF than wtVWF. The increase platelet capture would not be correlated directly to the multimeric size as all glycosylation variants have identical multimer distribution to the wild type protein. Moreover they exhibit similar affinity for collagen under static conditions. The difference in binding could be related to the altered ability of VWF variants to bind to collagen under flow. It has been proposed that the VWF-A1 domain contains a cryptic collagen binding site which aids the capture of VWF to collagen under high shear stress.[48] The *O*-linked glycan variants could potentially cause greater exposure of this site or may enhance its function under flow conditions. Further work will be needed to develop an assay to directly determine VWF-collagen binding function under shear stress that can then be used to determine if VWF *O*-linked glycans alter collagen binding under flow conditions. Alternatively, I hypothesise that increased platelet capture in the presence of T1255A and Cluster 1 variants could be attributable to the influence of *O*-linked glycans on VWF self-assembly under high shear stress on collagen surface. It has been previously demonstrated that that upon application of high shear forces VWF multimers and self-assemble to form "spider web" like structures which facilitates capture of flowing platelets.[49-51] Moreover, as recently shown, the formation of macro-aggregates (VWF self-assembly) may also be induced by VWF binding of ristocetin. In order to further examine this hypothesis additional studies are going to be devised. The amount of VWF bound to collagen as well as its multimeric structure will have to be compared. Studies under static conditions correlate well with studies where platelet capture by VWF variants immobilised on collagen was investigated under high shear stress. Conversely these studies provide different results than the studies under shear flow where platelet interactions with D'A3-VWF immobilised directly on the slide surface were studied. This observation must be

examined with respect to the various differences between the flow assays such as the size and multimerisation of the VWF constructs used and the method of VWF immobilisation, as well as the presence of soluble VWF. In the assays where VWF was immobilised directly onto a slide surface a fragment of VWF encompassing the D'-A3 domains was used while the experiment using collagen coated slides involved the full length multimeric VWF. Domains after the A3 domain might influence the accessibility of the GPIbα binding site, for instance it has been previously shown that a peptide directed against the region between A3 and D4 domains inhibited VWF binding to collagen type I.[52] In addition, the length of VWF molecule might affect its conformational stability and unfolding under shear stress. Moreover, the extent of conformational changes caused by VWF immobilisation directly on the slide surface or caused by VWF binding to collagen has not been fully clarified. Importantly, in the assays involving collagen coated slides, the soluble VWF has the potential to bind to collagen and to also self-associate. In the future platelet capture to collagen will be analysed at other shear rates and also platelet capture under flow with VWF immobilised on the slide and present in solution will be investigated to determine if VWF *O*-linked glycans affect self-association in the absence of collagen.

Considering the number of possible differences between the two flow assays, i.e. collagen coated slides or VWF coated slides, it is not surprising that the effects of *O*-linked glycans on VWF-platelet interactions differ. Importantly both assays provide unique information and parameters regarding the mechanism of the VWF-GPIbα interaction. Both assays complement each other, and the results highlight the need for varied approaches when studying the effects and mechanism of VWD mutations. Significantly the results presented in this thesis emphasise the importance of using VWF expressed in mammalian cells. Most of the previous studies on VWF-platelet interactions have been limited to experiments using isolated bacterial A1 domain. This study clearly indicates that the *O*-glycosylation status of VWF strongly influences properties of VWF and its interaction with various ligands. In future studies, especially when designing pro- or anti-thrombotic therapies it will be important to consider the influence of VWF glycans on its function. For example, several companies are producing recombinant VWF and it will be crucial to determine that the glycan chains present on these molecules do not drastically alter VWF function. The GPIbα plate binding assay correlates well with the current laboratory assay used in the diagnosis of

VWD; the VWF:RCo, nevertheless, both assays are dependent on the presence of ristocetin and not laminar flow, which is not a physiological situation, even though it has been previously suggested that interaction with ristocetin closely mimics changes induced by flow.[53] Aggregation in the VWF:RCo is evaluated with platelets in suspension and the absence of interactions with immobilised substrates, as such the assay does not provide an accurate assessment on *in vivo* function. Alternatively, a cone and plate viscometer can be used to generate shear stress to measure VWF mediated platelet aggregation, however the fluid dynamic parameters are poorly defined and again may not truly reflect *in vivo* shear stress.

In contrast, in flow assays, platelet adhesion and aggregation involve the transition from free flow to arrest on a surface. The other disadvantage is the fact that the VWF:RCo assay has a high coefficient of variation and may display abnormal results due to polymorphism or mutations in the VWF ristocetin binding regions.[54,55] In this study the removal of the glycan from the threonine localised in the ristocetin binding site (T1468A) resulted in the diminished GPIbα binding in the static assay and platelet aggregation, however the mutated protein was able to support platelet binding under shear stress, in the absence of ristoecetin. Based on the results from the flow assay I attributed decreased GPIbα binding by the T1468A mutants in the static assay to an abnormal interaction with ristocetin rather than GPIbα. Interestingly, a plate based GPIbα binding assay has been recently described where a novel gain of function GPIbα mutant was used to eliminate the need for ristocetin. As part of my future work I plan to generate this mutant and use it to analyse binding of the VWF *O*-linked glycans variants.

9.3 VWF *O*-linked glycans as stabilisers of linker regions

Overall, based on the results presented in this thesis it can be hypothesised that the interaction between VWF domains is stabilised and modulated by the presence of the *O*-linked glycans. Removal of all or specific *O*-glycan chains from the linker regions can destabilise the A1A2A3 tri-domain structure and result in a reduced interaction between the three domains. In addition the absence of *O*-linked glycans could alter the shielding of the A1 domain by the D'D3 domains[56] or even more distal domains. The altered interface between the A1A2A3 domains induces changes in their interaction with ligands such as GPIbα and ADAMTS13. It appears that the glycans clustered at the C-

terminal side of the A1 domain influence VWF interaction with ADAMTS13, whilst *O*-glycans clustered at the N-terminal side of the A1 domain strongly control its interaction with platelet receptor GPIbα. The *O*-linked glycans might mediate this effect by number of mechanisms. It is known that due to steric hindrance introduced by the *O*-glycans, glycosylated protein backbones adopt a stiff extended conformation.[11-15] I propose that VWF *O*-glycans provide rigidity to the proline rich and flexible linker regions and thereby influence the position of the VWF domains towards each other and as a result the accessibility of various binding sites. As discussed, I hypothesise that *O*-glycans in the A1-A2 linker region stabilise the interaction of those domains as well as allowing VWF to more readily adopt an extended conformation when unfolding, therefore reducing residual interactions which could hinder its interaction with ADAMTS13. It has been previously demonstrated that isolated bacterial A2 domain interacts with the A1 domain and it may block the VWF-GPIbα interaction in the native protein.[57] Moreover, it has been demonstrated that binding of FVIII and platelets to VWF accelerates proteolytic cleavage of VWF by ADAMTS13 under mechanically induced fluid shear stress.[58-60] The interplay between platelet binding and ADAMTS13 cleavage may play a role in regulating plasma multimer distribution under flow conditions and glycans might be a part of this mechanism. Recent data using small angle neutron scattering (SANS) spectroscopy to study VWF dynamics in response to shear flow, suggests that fluid shear forces may be able to maintain structural alterations at the domain level of VWF in solution which may then augment the A1 domain binding function and the A2 domain proteolysis rate.[61] Based on results presented in this thesis I propose that *O*-linked glycans are an important part of that mechanism.

It has been previously shown that the D'D3 domains shield the GPIb binding site in the A1 domain.[56] It has been also demonstrated that the GPIbα binding site remains cryptic in a fragment of VWF starting at 1238; thus including only part of the D3 domain.[62,63] Moreover the N-terminal flanking regions of the A1 domain (1260-1271) and the C-terminal region of the D3 domain (1204-1259) shield the GPIbα binding site, while the peptides derived from these regions inhibited ristocetin-induced binding of purified VWF to platelets.[44] In addition it was demonstrated that the shorter the D3-A1 linker region the greater the ability of VWF to bind platelet in the presence of ristocetin.[64] From those studies it appears that the A1 domain N-terminal flanking region is an important determinant of the availability of the A1 domain for GPIbα. Based on the

obtained results, I postulate that the *O*-linked glycans clustered in the D3-A1 linker region are crucial modifiers of the linker region function as they can determine its rigidity and as result accessibility of the A1 domain.

Interestingly the local changes may have an allosteric effect; rearrangement of the VWF-A domains complex can propagate to the other end of the protein influencing, for instance, ADAMTS13 binding or more complex aspect of VWF function such as self association. To my knowledge the data presented in this thesis is one of very few studies that demonstrate that linker regions between domains of glycoproteins can be stabilised by only a small number of *O*-linked oligosaccharide chains, and the flexibility of linker regions has a significant influence on the function of the entire protein.

9.4 Structure of VWF *O*-linked glycans

Prior to the start of this project the only structural study suggested that *O*-glycome is heterogeneous but only a single major structure desialylated core 1 was identified.[65] A detailed analysis of the plasma derived VWF *O*-glycom has been published to facilitate characterisation of VWF *O*-linked glycans function.[66] Since in this project recombinant VWF was used it was necessary to compare its *O*-glycome to that of plasma VWF. In collaboration with Dr. K.Canis, by performing mass spectrometry analysis on purified recombinant VWF I have demonstrated that plasma derived and recombinant VWF present similar *O*-glycan structures, with both core 1 and core 2 structures present. The desialylated core 1 was shown to be the major moiety and also tri-sialylated core 1 glycans were detected. In contrast to pdVWF no tetrasialylated core 1 or ABH antigen-containing core 2 glycans were detected. Identification of the disialosyl motif (two sialic acid residues linked together) is particularly interesting as it requires a particular sialyl-transferase activity usually known to synthesise polysialic acid structures. The fact that HEK293T cells produce this unusual moiety on VWF *O*-glycans implies a direct importance for VWF structure and function. The disialosyl motif is recognised by SIGLEC 7 (sialic acid binding Immunoglobulin-like lectin 7) which is expressed in abundance on natural killer (NK) cells.[67] I therefore propose that that VWF *O*-glycans might be able to interact with SIGLECs which are a family of sialic acid-binding receptors, expressed on the cells of hematopoietic origin.[68] Indeed recently an abstract was published on a study which identified one murine and six human SIGLEC-family members (including SIGLEC7) as novel partners for pdVWF.[69] Moreover the VWF-

SIGLEC interaction was shown to be mediated by sialic acid residues present on VWF glycans. In addition, the majority of identified structures terminated in sialic acid residues which confer a negative charge and therefore might be an important element of *O*-glycans' influence on the rigidity of the A1 domain flanking regions as discussed above. Current data clearly demonstrates that *N*-glycans modulate the interaction between VWF and ADAMTS13. The ABO antigens influence VWF susceptibility to ADAMTS13 proteolysis.[70] It was recently shown that a very small proportion of *O*-linked glycans also present ABH antigens they also might participate in mediating this a effect.

It is fascinating that individual glycan chains at specific sites have an impact on VWF function comparable to the removal of entire clusters. The differences in binding observed for the single glycosylation variants T1255A and S1486A are similar to that obtained with the respective cluster variants, which could suggest that the observed effects result from loss of single *O*-linked carbohydrate attachment sites rather that a cumulative response to the loss of several *O*-glycans. It has been previously suggested that the glycosylation of different sites takes place in a specific order and can be influenced by steric hindrance of neighbouring glycosylation sites.[71,72] However, to date we have not been able to ascertain whether mutation of a given *O*-linked glycosylation site of VWF affects glycosylation of nearby residues. It would have been useful to characterise the composition of *O*-linked oligosaccharides at specific sites. Regrettably, due to proximity of the *O*-glycosylation sites within the clusters it will not be possible to determine occupancy of individual sites, however we will attempt to characterise separately the two clusters. In order to perform the structural analysis of glycans clusters peptides carrying *O*-linked glycans have to be isolated, which is technically difficult. To aid this process I am currently performing studies with the Click-iT™ O-GalNAc enzymatic labelling system (Invitrogen). Briefly *O*-linked glycan containing proteins expressed in HEK293T cells are metabolically labelled by incorporating an azide modified sugar in to the glycan structure on the newly synthesised proteins. This is performed by incubating cultured VWF cDNA transfected cells with modified GalNac sugar–GalNAz. Recombinant VWF is then purified using both ion-exchange and heparin-Sepharose chromatography. VWF containing the modified sugar is then detected using the Click-iT detection kit where the GalNAz sugar is tagged with biotinylated alkyne. Next VWF is digested with trypsin and *O*-linked glycans

containing peptides purified using Streptavidin affinity chromatography. Isolated glycopeptides will be then analysed by mass spectrometry.

9.5 Sialic acid and VWF function

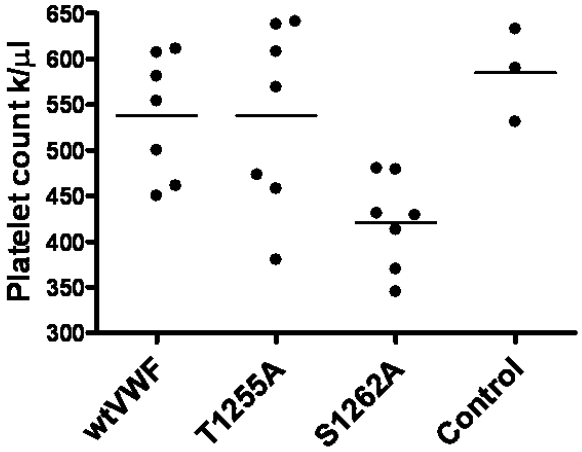
Another aspect of VWF *O*- and *N*-glycans is the presence of terminal sialic acid residues. Sialylation was shown to protect VWF from ADAMTS13 proteolysis but it was demonstrated that this effect is mediated primarily by sialic acid presented on the *N*-linked glycans.[73] Desialylated VWF was previously shown to support enhanced platelet adhesion in flow assays which was confirmed in this study.[74,75] I have also demonstrated that desialylation (treatment with neuraminidase) of VWF increased its sensitivity to ristocetin mediated GPIbα binding and I have attributed this effect to absence of terminal sialic acid residues from the *O*-linked glycans. Moreover it is reasonable to suggest that negatively charged sialic acid residues participate in the effect of *O*-linked glycans clustered in the A1-A2 linker region on VWF's interaction with ADAMTS13. In addition, I have demonstrated that the neuraminidase treated (Neu)-D'A3-VWF supports increased platelet attachment and slower platelet rolling up to a shear rate of $1000s^{-1}$. Conversely it does not alter the GPIbα-A1 bond dissociation rate or probability of transient tethering events taking place. The mechanism of increased binding exhibited by Neu-D'A3 has not been fully elucidated, however as discussed in the previous chapter I propose that removal of sialic acid residues increases the electrostatic interaction between VWF and GPIbα for the platelets that are already tethered to the D'A3 coated surface, as a result more primary transient tethering events are transformed into rolling events.

9.6 Role of VWF *O*-linked glycans *in vivo*

Additional studies are ongoing to further specify the physiological implications of VWF *O*-linked glycans. The relationship between VWF proteolysis and clearance has not yet been fully established. Animal models used to investigate the clearance of VWF have returned conflicting results.[76-80] It has been previously suggested that VWF levels are associated with variations in the presence of the sialylated T-antigen.[81] Moreover we have detected that a small proportion of plasma VWF *O*-linked glycans carry ABO blood group antigens[66] which is interesting because the ABO-carbohydrate structures are implicated in regulating VWF plasma levels and clearance.[82-84] In the view of this data is seems feasible that *O*-linked glycans might influence VWF clearance. In

collaboration with Dr James O'Donnell (Trinity College, Dublin) I am performing studies to determine the effect of the *O*-linked variants on VWF clearance using the $VWF^{-/-}$ murine model. In addition the $VWF^{-/-}$ mouse will also be used to investigate the role of *O*-linked glycans on VWF function *in vivo*. The murine and human VWF sequences differ to some extent (86% identity); moreover one putative glycosylation site is different in murine VWF as it contains a serine residue in position 1262 instead of position 1263 which is glycosylated in humans. Importantly human VWF has impaired capacity to support murine platelet adhesion and murine VWF-A1 supports limited binding of human platelets.[85] Thus in order to study VWF function in the murine model I have created murine VWF *O*-linked glycosylation variants. In collaboration with Prof K Vanhoorelbeke, (KU Leuven, Belgium) the vector pcDNA6-VWF was injected hydrodynamically into the murine tail vein for in vivo expression of murine VWF. In these preliminary experiments a reduced platelet count was observed following expression of the T1262A variant and a slight increase in bleeding time was observed with the T1255A variant(Figure 9.1). However, expression levels of all the injected variants were quite low To increase VWF levels the experiments are going to be repeated using the vector pBS-HCRHPi-MCS with liver-specific expression cassette, which allows for high level hepatic gene expression.[86] As before, platelets and VWF levels as well as bleeding time will be measured for mice with wtVWF and VWF glycosylation variants and thrombus formation will be investigated.

A



B

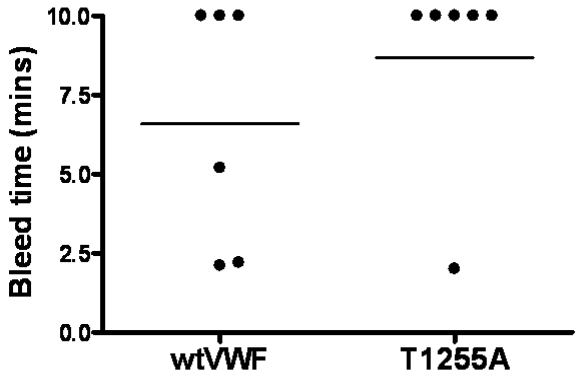


Figure 9.1 Platelet numbers and bleeding time after VWF gene transfer in VWF deficient mice

Hydrodynamic gene transfer was performed as described previously in VWF deficient mice strain.[86,87] **(A)** Mice were bled 48 hours after gen transfers in order to evaluate VWF expression, and platelet count. Reduced platelet count was observed for mice with T1262A-VWF variant present. **(B)** Function of mutated VWF was assessed by measuring a tail clipping bleeding time. Increased bleeding tine was detected for the T1262A-VWF variant when compared with wtVWF, however since the VWF levels were very low the bleeding time is not very informative. (All experiments were performed in accordance with protocols by the Institutional Animal Care and Use Committee of the K.U. Leuven, Belgium).

I have made several observations that highlight the role of *O*-linked glycans in mediating VWF function and have also raised a number of questions that require further investigation. Several experiments are already in progress that will enable me to obtain even further insight into the mechanism by which VWF function is modulated by its *O*-linked glycans.

In conclusion the work presented in this thesis clearly demonstrates important roles for VWF *O*-linked glycans in mediating different aspects of VWF function. While the *O*-linked glycans chains presented on VWF do not affect the expression, secretion, multimerisation or collagen and heparin binding functions of VWF, they have profound effects on the susceptibility of VWF to ADAMTS13 cleavage and the interaction of VWF with platelets. These effects appear to, certainly in part, be attributed to the *O*-linked glycans stabilising the conformation of the VWF molecule, particularly the linker regions either side of the A1 domain. These data not only demonstrate a critical role for *O*-linked glycans in mediating VWF function but also confirm the importance of *O*-linked glycosylation as a major determinant of protein structure and function.

10 REFERENCES

1. Sadler JE. Biochemistry and genetics of von Willebrand factor. Annu Rev Biochem. 1998;67:395-424.
2. Federici AB. The factor VIII/von Willebrand factor complex: basic and clinical issues. Haematologica. 2003;88:EREP02.
3. Mancuso DJ, Tuley EA, Westfield LA, et al. Structure of the gene for human von Willebrand factor. J Biol Chem. 1989;264:19514-19527.
4. Bonthron D, Orkin SH. The human von Willebrand factor gene. Structure of the 5' region. Eur J Biochem. 1988;171:51-57.
5. Mancuso DJ, Tuley EA, Westfield LA, et al. Human von Willebrand factor gene and pseudogene: structural analysis and differentiation by polymerase chain reaction. Biochemistry. 1991;30:253-269.
6. Patracchini P, Calzolari E, Aiello V, et al. Sublocalization of von Willebrand factor pseudogene to 22q11.22-q11.23 by in situ hybridization in a 46,X,t(X;22)(pter;q11.21) translocation. Hum Genet. 1989;83:264-266.
7. Jahroudi N, Lynch DC. Endothelial-cell-specific regulation of von Willebrand factor gene expression. Mol Cell Biol. 1994;14:999-1008.
8. Schwachtgen JL, Janel N, Barek L, et al. Ets transcription factors bind and transactivate the core promoter of the von Willebrand factor gene. Oncogene. 1997;15:3091-3102.
9. Jahroudi N, Ardekani AM, Greenberger JS. An NF1-like protein functions as a repressor of the von Willebrand factor promoter. J Biol Chem. 1996;271:21413-21421.
10. Mayadas TN, Wagner DD. von Willebrand factor biosynthesis and processing. Ann N Y Acad Sci. 1991;614:153-166.
11. Nichols TC, Samama CM, Bellinger DA, et al. Function of von Willebrand factor after crossed bone marrow transplantation between normal and von Willebrand disease pigs: effect on arterial thrombosis in chimeras. Proc Natl Acad Sci U S A. 1995;92:2455-2459.
12. Titani K, Kumar S, Takio K, et al. Amino acid sequence of human von Willebrand factor. Biochemistry. 1986;25:3171-3184.
13. Katsumi A, Tuley EA, Bodo I, Sadler JE. Localization of disulfide bonds in the cystine knot domain of human von Willebrand factor. J Biol Chem. 2000;275:25585-25594.
14. Marti T, Rosselet SJ, Titani K, Walsh KA. Identification of disulfide-bridged substructures within human von Willebrand factor. Biochemistry. 1987;26:8099-8109.
15. Niemann H, Klenk HD. Coronavirus glycoprotein E1, a new type of viral glycoprotein. J Mol Biol. 1981;153:993-1010.
16. Wagner DD, Mayadas T, Marder VJ. Initial glycosylation and acidic pH in the Golgi apparatus are required for multimerization of von Willebrand factor. J Cell Biol. 1986;102:1320-1324.
17. McKinnon TA, Goode EC, Birdsey GM, et al. Specific N-linked glycosylation sites modulate synthesis and secretion of von Willebrand factor. Blood. 2010;116:640-648.
18. Wise RJ, Pittman DD, Handin RI, Kaufman RJ, Orkin SH. The propeptide of von Willebrand factor independently mediates the assembly of von Willebrand multimers. Cell. 1988;52:229-236.

19. Kornfeld R, Kornfeld S. Assembly of asparagine-linked oligosaccharides. Annu Rev Biochem. 1985;54:631-664.
20. Matsui T, Titani K, Mizuochi T. Structures of the asparagine-linked oligosaccharide chains of human von Willebrand factor. Occurrence of blood group A, B, and H(O) structures. J Biol Chem. 1992;267:8723-8731.
21. Carew JA, Browning PJ, Lynch DC. Sulfation of von Willebrand factor. Blood. 1990;76:2530-2539.
22. Voorberg J, Fontijn R, van Mourik JA, Pannekoek H. Domains involved in multimer assembly of von willebrand factor (vWF): multimerization is independent of dimerization. Embo J. 1990;9:797-803.
23. Mayadas TN, Wagner DD. In vitro multimerization of von Willebrand factor is triggered by low pH. Importance of the propolypeptide and free sulfhydryls. J Biol Chem. 1989;264:13497-13503.
24. Mayadas TN, Wagner DD. Vicinal cysteines in the prosequence play a role in von Willebrand factor multimer assembly. Proc Natl Acad Sci U S A. 1992;89:3531-3535.
25. Shapiro J, Sciaky N, Lee J, Bosshart H, Angeletti RH, Bonifacino JS. Localization of endogenous furin in cultured cell lines. J Histochem Cytochem. 1997;45:3-12.
26. Wise RJ, Barr PJ, Wong PA, Kiefer MC, Brake AJ, Kaufman RJ. Expression of a human proprotein processing enzyme: correct cleavage of the von Willebrand factor precursor at a paired basic amino acid site. Proc Natl Acad Sci U S A. 1990;87:9378-9382.
27. van de Ven WJ, Voorberg J, Fontijn R, et al. Furin is a subtilisin-like proprotein processing enzyme in higher eukaryotes. Mol Biol Rep. 1990;14:265-275.
28. Hilbert L, Nurden P, Caron C, et al. Type 2N von Willebrand disease due to compound heterozygosity for R854Q and a novel R763G mutation at the cleavage site of von Willebrand factor propeptide. Thromb Haemost. 2006;96:290-294.
29. Vischer UM, Wagner DD. von Willebrand factor proteolytic processing and multimerization precede the formation of Weibel-Palade bodies. Blood. 1994;83:3536-3544.
30. Journet AM, Saffaripour S, Wagner DD. Requirement for both D domains of the propolypeptide in von Willebrand factor multimerization and storage. Thromb Haemost. 1993;70:1053-1057.
31. Wagner DD, Saffaripour S, Bonfanti R, et al. Induction of specific storage organelles by von Willebrand factor propolypeptide. Cell. 1991;64:403-413.
32. Haberichter SL, Fahs SA, Montgomery RR. von Willebrand factor storage and multimerization: 2 independent intracellular processes. Blood. 2000;96:1808-1815.
33. Yamamoto K, de Waard V, Fearns C, Loskutoff DJ. Tissue distribution and regulation of murine von Willebrand factor gene expression in vivo. Blood. 1998;92:2791-2801.
34. Hollestelle MJ, Thinnes T, Crain K, et al. Tissue distribution of factor VIII gene expression in vivo--a closer look. Thromb Haemost. 2001;86:855-861.
35. Rand JH, Badimon L, Gordon RE, Uson RR, Fuster V. Distribution of von Willebrand factor in porcine intima varies with blood vessel type and location. Arteriosclerosis. 1987;7:287-291.
36. Rosenberg RD, Aird WC. Vascular-bed--specific hemostasis and hypercoagulable states. N Engl J Med. 1999;340:1555-1564.
37. van Mourik JA, Romani de Wit T, Voorberg J. Biogenesis and exocytosis of Weibel-Palade bodies. Histochem Cell Biol. 2002;117:113-122.

38. Borchiellini A, Fijnvandraat K, ten Cate JW, et al. Quantitative analysis of von Willebrand factor propeptide release in vivo: effect of experimental endotoxemia and administration of 1-deamino-8-D-arginine vasopressin in humans. Blood. 1996;88:2951-2958.
39. Wagner DD. The Weibel-Palade body: the storage granule for von Willebrand factor and P-selectin. Thromb Haemost. 1993;70:105-110.
40. Harrison P, Cramer EM. Platelet alpha-granules. Blood Rev. 1993;7:52-62.
41. Cramer EM, Vainchenker W, Vinci G, Guichard J, Breton-Gorius J. Gray platelet syndrome: immunoelectron microscopic localization of fibrinogen and von Willebrand factor in platelets and megakaryocytes. Blood. 1985;66:1309-1316.
42. Voorberg J, Fontijn R, Calafat J, Janssen H, van Mourik JA, Pannekoek H. Biogenesis of von Willebrand factor-containing organelles in heterologous transfected CV-1 cells. EMBO J. 1993;12:749-758.
43. Sengel A, Stoebner P. Golgi origin of tubular inclusions in endothelial cells. J Cell Biol. 1970;44:223-226.
44. Zenner HL, Collinson LM, Michaux G, Cutler DF. High-pressure freezing provides insights into Weibel-Palade body biogenesis. J Cell Sci. 2007;120:2117-2125.
45. Weibel ER, Palade GE. New Cytoplasmic Components in Arterial Endothelia. J Cell Biol. 1964;23:101-112.
46. Gebrane-Younes J, Drouet L, Caen JP, Orcel L. Heterogeneous distribution of Weibel-Palade bodies and von Willebrand factor along the porcine vascular tree. Am J Pathol. 1991;139:1471-1484.
47. Huang RH, Wang Y, Roth R, et al. Assembly of Weibel-Palade body-like tubules from N-terminal domains of von Willebrand factor. Proc Natl Acad Sci U S A. 2008;105:482-487.
48. Berriman JA, Li S, Hewlett LJ, et al. Structural organization of Weibel-Palade bodies revealed by cryo-EM of vitrified endothelial cells. Proc Natl Acad Sci U S A. 2009;106:17407-17412.
49. Michaux G, Abbitt KB, Collinson LM, Haberichter SL, Norman KE, Cutler DF. The physiological function of von Willebrand's factor depends on its tubular storage in endothelial Weibel-Palade bodies. Dev Cell. 2006;10:223-232.
50. Bonfanti R, Furie BC, Furie B, Wagner DD. PADGEM (GMP140) is a component of Weibel-Palade bodies of human endothelial cells. Blood. 1989;73:1109-1112.
51. Fiedler U, Scharpfenecker M, Koidl S, et al. The Tie-2 ligand angiopoietin-2 is stored in and rapidly released upon stimulation from endothelial cell Weibel-Palade bodies. Blood. 2004;103:4150-4156.
52. Wolff B, Burns AR, Middleton J, Rot A. Endothelial cell "memory" of inflammatory stimulation: human venular endothelial cells store interleukin 8 in Weibel-Palade bodies. J Exp Med. 1998;188:1757-1762.
53. Ozaka T, Doi Y, Kayashima K, Fujimoto S. Weibel-Palade bodies as a storage site of calcitonin gene-related peptide and endothelin-1 in blood vessels of the rat carotid body. Anat Rec. 1997;247:388-394.
54. Metcalf DJ, Nightingale TD, Zenner HL, Lui-Roberts WW, Cutler DF. Formation and function of Weibel-Palade bodies. J Cell Sci. 2008;121:19-27.
55. Michaux G, Pullen TJ, Haberichter SL, Cutler DF. P-selectin binds to the D'-D3 domains of von Willebrand factor in Weibel-Palade bodies. Blood. 2006;107:3922-3924.

56. Zannettino AC, Holding CA, Diamond P, et al. Osteoprotegerin (OPG) is localized to the Weibel-Palade bodies of human vascular endothelial cells and is physically associated with von Willebrand factor. J Cell Physiol. 2005;204:714-723.
57. Denis CV, Andre P, Saffaripour S, Wagner DD. Defect in regulated secretion of P-selectin affects leukocyte recruitment in von Willebrand factor-deficient mice. Proc Natl Acad Sci U S A. 2001;98:4072-4077.
58. Haberichter SL, Merricks EP, Fahs SA, Christopherson PA, Nichols TC, Montgomery RR. Re-establishment of VWF-dependent Weibel-Palade bodies in VWD endothelial cells. Blood. 2005;105:145-152.
59. Haberichter SL, Jozwiak MA, Rosenberg JB, Christopherson PA, Montgomery RR. The von Willebrand factor propeptide (VWFpp) traffics an unrelated protein to storage. Arterioscler Thromb Vasc Biol. 2002;22:921-926.
60. Lui-Roberts WW, Collinson LM, Hewlett LJ, Michaux G, Cutler DF. An AP-1/clathrin coat plays a novel and essential role in forming the Weibel-Palade bodies of endothelial cells. J Cell Biol. 2005;170:627-636.
61. Hamilton KK, Sims PJ. Changes in cytosolic Ca2+ associated with von Willebrand factor release in human endothelial cells exposed to histamine. Study of microcarrier cell monolayers using the fluorescent probe indo-1. J Clin Invest. 1987;79:600-608.
62. Rondaij MG, Bierings R, Kragt A, van Mourik JA, Voorberg J. Dynamics and plasticity of Weibel-Palade bodies in endothelial cells. Arterioscler Thromb Vasc Biol. 2006;26:1002-1007.
63. Levine JD, Harlan JM, Harker LA, Joseph ML, Counts RB. Thrombin-mediated release of factor VIII antigen from human umbilical vein endothelial cells in culture. Blood. 1982;60:531-534.
64. Matsushita K, Yamakuchi M, Morrell CN, et al. Vascular endothelial growth factor regulation of Weibel-Palade-body exocytosis. Blood. 2005;105:207-214.
65. Vischer UM, Wollheim CB. Epinephrine induces von Willebrand factor release from cultured endothelial cells: involvement of cyclic AMP-dependent signalling in exocytosis. Thromb Haemost. 1997;77:1182-1188.
66. Kaufmann JE, Oksche A, Wollheim CB, Gunther G, Rosenthal W, Vischer UM. Vasopressin-induced von Willebrand factor secretion from endothelial cells involves V2 receptors and cAMP. J Clin Invest. 2000;106:107-116.
67. Vischer UM, Barth H, Wollheim CB. Regulated von Willebrand factor secretion is associated with agonist-specific patterns of cytoskeletal remodeling in cultured endothelial cells. Arterioscler Thromb Vasc Biol. 2000;20:883-891.
68. Cohen RJ, Epstein SE, Cohen LS, Dennis LH. Alterations of fibrinolysis and blood coagulation induced by exercise, and the role of beta-adrenergic-receptor stimulation. Lancet. 1968;2:1264-1266.
69. Rickles FR, Hoyer LW, Rick ME, Ahr DJ. The effects of epinephrine infusion in patients with von Willebrand's disease. J Clin Invest. 1976;57:1618-1625.
70. Galbusera M, Zoja C, Donadelli R, et al. Fluid shear stress modulates von Willebrand factor release from human vascular endothelium. Blood. 1997;90:1558-1564.
71. Pinsky DJ, Naka Y, Liao H, et al. Hypoxia-induced exocytosis of endothelial cell Weibel-Palade bodies. A mechanism for rapid neutrophil recruitment after cardiac preservation. J Clin Invest. 1996;97:493-500.
72. Mannucci PM. Desmopressin (DDAVP) in the treatment of bleeding disorders: the first 20 years. Blood. 1997;90:2515-2521.

73. Matsushita K, Morrell CN, Cambien B, et al. Nitric oxide regulates exocytosis by S-nitrosylation of N-ethylmaleimide-sensitive factor. Cell. 2003;115:139-150.
74. Lowenstein CJ, Morrell CN, Yamakuchi M. Regulation of Weibel-Palade body exocytosis. Trends Cardiovasc Med. 2005;15:302-308.
75. Matsushita K, Morrell CN, Mason RJ, et al. Hydrogen peroxide regulation of endothelial exocytosis by inhibition of N-ethylmaleimide sensitive factor. J Cell Biol. 2005;170:73-79.
76. Cai H, Griendling KK, Harrison DG. The vascular NAD(P)H oxidases as therapeutic targets in cardiovascular diseases. Trends Pharmacol Sci. 2003;24:471-478.
77. Qian Z, Gelzer-Bell R, Yang Sx SX, et al. Inducible nitric oxide synthase inhibition of weibel-palade body release in cardiac transplant rejection. Circulation. 2001;104:2369-2375.
78. Kuhlencordt PJ, Chen J, Han F, Astern J, Huang PL. Genetic deficiency of inducible nitric oxide synthase reduces atherosclerosis and lowers plasma lipid peroxides in apolipoprotein E-knockout mice. Circulation. 2001;103:3099-3104.
79. Kuhlencordt PJ, Gyurko R, Han F, et al. Accelerated atherosclerosis, aortic aneurysm formation, and ischemic heart disease in apolipoprotein E/endothelial nitric oxide synthase double-knockout mice. Circulation. 2001;104:448-454.
80. Davignon J, Ganz P. Role of endothelial dysfunction in atherosclerosis. Circulation. 2004;109:III27-32.
81. Hansson GK. Inflammation, atherosclerosis, and coronary artery disease. N Engl J Med. 2005;352:1685-1695.
82. Nakayama T, Sato W, Yoshimura A, et al. Endothelial von Willebrand factor release due to eNOS deficiency predisposes to thrombotic microangiopathy in mouse aging kidney. Am J Pathol. 2010;176:2198-2208.
83. Babich V, Meli A, Knipe L, et al. Selective release of molecules from Weibel-Palade bodies during a lingering kiss. Blood. 2008;111:5282-5290.
84. Valentijn KM, van Driel LF, Mourik MJ, et al. Multigranular exocytosis of Weibel Palade bodies in vascular endothelial cells. Blood. 2010.
85. Mayadas T, Wagner DD, Simpson PJ. von Willebrand factor biosynthesis and partitioning between constitutive and regulated pathways of secretion after thrombin stimulation. Blood. 1989;73:706-711.
86. Tsai HM, Nagel RL, Hatcher VB, Seaton AC, Sussman, II. The high molecular weight form of endothelial cell von Willebrand factor is released by the regulated pathway. Br J Haematol. 1991;79:239-245.
87. Sporn LA, Marder VJ, Wagner DD. Inducible secretion of large, biologically potent von Willebrand factor multimers. Cell. 1986;46:185-190.
88. Giblin JP, Hewlett LJ, Hannah MJ. Basal secretion of von Willebrand factor from human endothelial cells. Blood. 2008.
89. Siedlecki CA, Lestini BJ, Kottke-Marchant KK, Eppell SJ, Wilson DL, Marchant RE. Shear-dependent changes in the three-dimensional structure of human von Willebrand factor. Blood. 1996;88:2939-2950.
90. Fowler WE, Fretto LJ, Hamilton KK, Erickson HP, McKee PA. Substructure of human von Willebrand factor. J Clin Invest. 1985;76:1491-1500.
91. Ohmori K, Fretto LJ, Harrison RL, Switzer ME, Erickson HP, McKee PA. Electron microscopy of human factor VIII/Von Willebrand glycoprotein: effect of reducing reagents on structure and function. J Cell Biol. 1982;95:632-640.
92. Fretto LJ, Fowler WE, McCaslin DR, Erickson HP, McKee PA. Substructure of human von Willebrand factor. Proteolysis by V8 and characterization of two functional domains. J Biol Chem. 1986;261:15679-15689.

93. Raghavachari M, Tsai H, Kottke-Marchant K, Marchant RE. Surface dependent structures of von Willebrand factor observed by AFM under aqueous conditions. Colloids Surf B Biointerfaces. 2000;19:315-324.
94. Seyfried BK, Friedbacher G, Rottensteiner H, et al. Comparison of plasma-derived and recombinant von Willebrand factor by atomic force microscopy. Thromb Haemost. 2010;104.
95. Schneider SW, Nuschele S, Wixforth A, et al. Shear-induced unfolding triggers adhesion of von Willebrand factor fibers. Proc Natl Acad Sci U S A. 2007;104:7899-7903.
96. Verweij CL, Diergaarde PJ, Hart M, Pannekoek H. Full-length von Willebrand factor (vWF) cDNA encodes a highly repetitive protein considerably larger than the mature vWF subunit. Embo J. 1986;5:1839-1847.
97. Wagner DD. Cell biology of von Willebrand factor. Annu Rev Cell Biol. 1990;6:217-246.
98. Rosenberg JB, Haberichter SL, Jozwiak MA, et al. The role of the D1 domain of the von Willebrand factor propeptide in multimerization of VWF. Blood. 2002;100:1699-1706.
99. Allen S, Abuzenadah AM, Hinks J, et al. A novel von Willebrand disease-causing mutation (Arg273Trp) in the von Willebrand factor propeptide that results in defective multimerization and secretion. Blood. 2000;96:560-568.
100. Gaucher C, Uno H, Yamazaki T, Mashiba H, Mazurier C. A new candidate mutation (N528S) within the von Willebrand factor propeptide identified in a Japanese patient with phenotype IIC of von Willebrand disease. Eur J Haematol. 1998;61:145-148.
101. Schneppenheim R, Thomas KB, Krey S, et al. Identification of a candidate missense mutation in a family with von Willebrand disease type IIC. Hum Genet. 1995;95:681-686.
102. Gaucher C, Dieval J, Mazurier C. Characterization of von Willebrand factor gene defects in two unrelated patients with type IIC von Willebrand disease. Blood. 1994;84:1024-1030.
103. Foster PA, Fulcher CA, Marti T, Titani K, Zimmerman TS. A major factor VIII binding domain resides within the amino-terminal 272 amino acid residues of von Willebrand factor. J Biol Chem. 1987;262:8443-8446.
104. Fujimura Y, Titani K, Holland LZ, et al. von Willebrand factor. A reduced and alkylated 52/48-kDa fragment beginning at amino acid residue 449 contains the domain interacting with platelet glycoprotein Ib. J Biol Chem. 1986;261:381-385.
105. Dong Z, Thoma RS, Crimmins DL, McCourt DW, Tuley EA, Sadler JE. Disulfide bonds required to assemble functional von Willebrand factor multimers. J Biol Chem. 1994;269:6753-6758.
106. Schooten CJ, Tjernberg P, Westein E, et al. Cysteine-mutations in von Willebrand factor associated with increased clearance. J Thromb Haemost. 2005;3:2228-2237.
107. Hommais A, Stepanian A, Fressinaud E, et al. Mutations C1157F and C1234W of von Willebrand factor cause intracellular retention with defective multimerization and secretion. J Thromb Haemost. 2006;4:148-157.
108. Purvis AR, Gross J, Dang LT, et al. Two Cys residues essential for von Willebrand factor multimer assembly in the Golgi. Proc Natl Acad Sci U S A. 2007;104:15647-15652.

109. Allen S, Abuzenadah AM, Blagg JL, et al. Two novel type 2N von Willebrand disease-causing mutations that result in defective factor VIII binding, multimerization, and secretion of von Willebrand factor. Blood. 2000;95:2000-2007.
110. Hilbert L, Jorieux S, Fontenay-Roupie M, et al. Expression of two type 2N von Willebrand disease mutations identified in exon 18 of von Willebrand factor gene. Br J Haematol. 2004;127:184-189.
111. Lenting PJ, van Mourik JA, Mertens K. The life cycle of coagulation factor VIII in view of its structure and function. Blood. 1998;92:3983-3996.
112. Vlot AJ, Koppelman SJ, van den Berg MH, Bouma BN, Sixma JJ. The affinity and stoichiometry of binding of human factor VIII to von Willebrand factor. Blood. 1995;85:3150-3157.
113. Vlot AJ, Koppelman SJ, Meijers JC, et al. Kinetics of factor VIII-von Willebrand factor association. Blood. 1996;87:1809-1816.
114. Bendetowicz AV, Wise RJ, Gilbert GE. Collagen-bound von Willebrand factor has reduced affinity for factor VIII. J Biol Chem. 1999;274:12300-12307.
115. Morfini M, Mannucci PM, Tenconi PM, et al. Pharmacokinetics of monoclonally-purified and recombinant factor VIII in patients with severe von Willebrand disease. Thromb Haemost. 1993;70:270-272.
116. Weiss HJ, Sussman, II, Hoyer LW. Stabilization of factor VIII in plasma by the von Willebrand factor. Studies on posttransfusion and dissociated factor VIII and in patients with von Willebrand's disease. J Clin Invest. 1977;60:390-404.
117. Koedam JA, Meijers JC, Sixma JJ, Bouma BN. Inactivation of human factor VIII by activated protein C. Cofactor activity of protein S and protective effect of von Willebrand factor. J Clin Invest. 1988;82:1236-1243.
118. Lenting PJ, Donath MJ, van Mourik JA, Mertens K. Identification of a binding site for blood coagulation factor IXa on the light chain of human factor VIII. J Biol Chem. 1994;269:7150-7155.
119. Lenting PJ, Neels JG, van den Berg BM, et al. The light chain of factor VIII comprises a binding site for low density lipoprotein receptor-related protein. J Biol Chem. 1999;274:23734-23739.
120. Cao W, Krishnaswamy S, Camire RM, Lenting PJ, Zheng XL. Factor VIII accelerates proteolytic cleavage of von Willebrand factor by ADAMTS13. Proc Natl Acad Sci U S A. 2008.
121. McEver RP, Beckstead JH, Moore KL, Marshall-Carlson L, Bainton DF. GMP-140, a platelet alpha-granule membrane protein, is also synthesized by vascular endothelial cells and is localized in Weibel-Palade bodies. J Clin Invest. 1989;84:92-99.
122. Padilla A, Moake JL, Bernardo A, et al. P-selectin anchors newly released ultralarge von Willebrand factor multimers to the endothelial cell surface. Blood. 2004;103:2150-2156.
123. Bernardo A, Ball C, Nolasco L, Choi H, Moake JL, Dong JF. Platelets adhered to endothelial cell-bound ultra-large von Willebrand factor strings support leukocyte tethering and rolling under high shear stress. J Thromb Haemost. 2005;3:562-570.
124. Sadler JE, Shelton-Inloes BB, Sorace JM, Harlan JM, Titani K, Davie EW. Cloning and characterization of two cDNAs coding for human von Willebrand factor. Proc Natl Acad Sci U S A. 1985;82:6394-6398.
125. Emsley J, Cruz M, Handin R, Liddington R. Crystal structure of the von Willebrand Factor A1 domain and implications for the binding of platelet glycoprotein Ib. J Biol Chem. 1998;273:10396-10401.

126. Huizinga EG, Martijn van der Plas R, Kroon J, Sixma JJ, Gros P. Crystal structure of the A3 domain of human von Willebrand factor: implications for collagen binding. Structure. 1997;5:1147-1156.
127. Zhang Q, Zhou YF, Zhang CZ, Zhang X, Lu C, Springer TA. Structural specializations of A2, a force-sensing domain in the ultralarge vascular protein von Willebrand factor. Proc Natl Acad Sci U S A. 2009;106:9226-9231.
128. Auton M, Cruz MA, Moake J. Conformational stability and domain unfolding of the Von Willebrand factor A domains. J Mol Biol. 2007;366:986-1000.
129. Mohri H, Yoshioka A, Zimmerman TS, Ruggeri ZM. Isolation of the von Willebrand factor domain interacting with platelet glycoprotein Ib, heparin, and collagen and characterization of its three distinct functional sites. J Biol Chem. 1989;264:17361-17367.
130. Hoylaerts MF, Yamamoto H, Nuyts K, Vreys I, Deckmyn H, Vermylen J. von Willebrand factor binds to native collagen VI primarily via its A1 domain. Biochem J. 1997;324 (Pt 1):185-191.
131. Mazzucato M, Spessotto P, Masotti A, et al. Identification of domains responsible for von Willebrand factor type VI collagen interaction mediating platelet adhesion under high flow. J Biol Chem. 1999;274:3033-3041.
132. Morales LD, Martin C, Cruz MA. The interaction of von Willebrand factor-A1 domain with collagen: mutation G1324S (type 2M von Willebrand disease) impairs the conformational change in A1 domain induced by collagen. J Thromb Haemost. 2006;4:417-425.
133. Bonnefoy A, Romijn RA, Vandervoort PA, I VANR, Vermylen J, Hoylaerts MF. von Willebrand factor A1 domain can adequately substitute for A3 domain in recruitment of flowing platelets to collagen. J Thromb Haemost. 2006;4:2151-2161.
134. Lankhof H, van Hoeij M, Schiphorst ME, et al. A3 domain is essential for interaction of von Willebrand factor with collagen type III. Thromb Haemost. 1996;75:950-958.
135. Koivunen E, Ranta TM, Annila A, et al. Inhibition of beta(2) integrin-mediated leukocyte cell adhesion by leucine-leucine-glycine motif-containing peptides. J Cell Biol. 2001;153:905-916.
136. Berndt MC, Ward CM, Booth WJ, Castaldi PA, Mazurov AV, Andrews RK. Identification of aspartic acid 514 through glutamic acid 542 as a glycoprotein Ib-IX complex receptor recognition sequence in von Willebrand factor. Mechanism of modulation of von Willebrand factor by ristocetin and botrocetin. Biochemistry. 1992;31:11144-11151.
137. Sugimoto M, Dent J, McClintock R, Ware J, Ruggeri ZM. Analysis of structure-function relationships in the platelet membrane glycoprotein Ib-binding domain of von Willebrand's factor by expression of deletion mutants. J Biol Chem. 1993;268:12185-12192.
138. Ulrichts H, Udvardy M, Lenting PJ, et al. Shielding of the A1 domain by the D'D3 domains of von Willebrand factor modulates its interaction with platelet glycoprotein Ib-IX-V. J Biol Chem. 2006;281:4699-4707.
139. Fujimura Y, Titani K, Holland LZ, et al. A heparin-binding domain of human von Willebrand factor. Characterization and localization to a tryptic fragment extending from amino acid residue Val-449 to Lys-728. J Biol Chem. 1987;262:1734-1739.
140. Sobel M, Soler DF, Kermode JC, Harris RB. Localization and characterization of a heparin binding domain peptide of human von Willebrand factor. J Biol Chem. 1992;267:8857-8862.

141. Sixma JJ, Schiphorst ME, Verweij CL, Pannekoek H. Effect of deletion of the A1 domain of von Willebrand factor on its binding to heparin, collagen and platelets in the presence of ristocetin. Eur J Biochem. 1991;196:369-375.
142. Adachi T, Matsushita T, Dong Z, et al. Identification of amino acid residues essential for heparin binding by the A1 domain of human von Willebrand factor. Biochem Biophys Res Commun. 2006;339:1178-1183.
143. Rastegar-Lari G, Legendre P, Ajzenberg N, Warszawski J, Meyer D, Baruch D. von Willebrand factor binding to heparin in various types of von Willebrand disease. Hematol J. 2000;1:190-198.
144. Guidetti GF, Bartolini B, Bernardi B, et al. Binding of von Willebrand factor to the small proteoglycan decorin. FEBS Lett. 2004;574:95-100.
145. Roberts DD, Williams SB, Gralnick HR, Ginsburg V. von Willebrand factor binds specifically to sulfated glycolipids. J Biol Chem. 1986;261:3306-3309.
146. Data RE, Williams SB, Roberts DD, Gralnick HR. Platelets adhere to sulfatides by von Willebrand factor dependent and independent mechanisms. Thromb Haemost. 1991;65:581-587.
147. Christophe O, Obert B, Meyer D, Girma JP. The binding domain of von Willebrand factor to sulfatides is distinct from those interacting with glycoprotein Ib, heparin, and collagen and resides between amino acid residues Leu 512 and Lys 673. Blood. 1991;78:2310-2317.
148. Devaiah AK, Raife TJ, Barton JA, Olson JD. Inhibition of human platelet function by sulfatides. Blood Coagul Fibrinolysis. 2000;11:543-550.
149. Borthakur G, Cruz MA, Dong JF, et al. Sulfatides inhibit platelet adhesion to von Willebrand factor in flowing blood. J Thromb Haemost. 2003;1:1288-1295.
150. van der Plas RM, Gomes L, Marquart JA, et al. Binding of von Willebrand factor to collagen type III: role of specific amino acids in the collagen binding domain of vWF and effects of neighboring domains. Thromb Haemost. 2000;84:1005-1011.
151. Zanardelli S, Chion AC, Groot E, et al. A novel binding site for ADAMTS13 constitutively exposed on the surface of globular VWF. Blood. 2009;114:2819-2828.
152. Feys HB, Anderson PJ, Vanhoorelbeke K, Majerus EM, Sadler JE. Multi-step binding of ADAMTS-13 to von Willebrand factor. J Thromb Haemost. 2009;7:2088-2095.
153. Hunt LT, Barker WC. von Willebrand factor shares a distinctive cysteine-rich domain with thrombospondin and procollagen. Biochem Biophys Res Commun. 1987;144:876-882.
154. Beacham DA, Wise RJ, Turci SM, Handin RI. Selective inactivation of the Arg-Gly-Asp-Ser (RGDS) binding site in von Willebrand factor by site-directed mutagenesis. J Biol Chem. 1992;267:3409-3415.
155. Szanto T, Vanhoorelbeke K, Toth G, et al. Identification of a VWF peptide antagonist that blocks platelet adhesion under high shear conditions by selectively inhibiting the VWF-collagen interaction. J Thromb Haemost. 2009;7:1680-1687.
156. Voorberg J, Fontijn R, Calafat J, Janssen H, van Mourik JA, Pannekoek H. Assembly and routing of von Willebrand factor variants: the requirements for disulfide-linked dimerization reside within the carboxy-terminal 151 amino acids. J Cell Biol. 1991;113:195-205.
157. Schneppenheim R, Brassard J, Krey S, et al. Defective dimerization of von Willebrand factor subunits due to a Cys-> Arg mutation in type IID von Willebrand disease. Proc Natl Acad Sci U S A. 1996;93:3581-3586.
158. Farndale RW, Sixma JJ, Barnes MJ, de Groot PG. The role of collagen in thrombosis and hemostasis. J Thromb Haemost. 2004;2:561-573.

159. Sixma JJ, van Zanten GH, Huizinga EG, et al. Platelet adhesion to collagen: an update. Thromb Haemost. 1997;78:434-438.
160. Sixma JJ, van Zanten GH, Saelman EU, et al. Platelet adhesion to collagen. Thromb Haemost. 1995;74:454-459.
161. Moroi M, Jung SM. A mechanism to safeguard platelet adhesion under high shear flow: von Willebrand factor-glycoprotein Ib and integrin alphabeta-collagen interactions make complementary, collagen-type-specific contributions to adhesion. J Thromb Haemost. 2007;5:797-803.
162. Pareti FI, Niiya K, McPherson JM, Ruggeri ZM. Isolation and characterization of two domains of human von Willebrand factor that interact with fibrillar collagen types I and III. J Biol Chem. 1987;262:13835-13841.
163. Wu D, Vanhoorelbeke K, Cauwenberghs N, et al. Inhibition of the von Willebrand (VWF)-collagen interaction by an antihuman VWF monoclonal antibody results in abolition of in vivo arterial platelet thrombus formation in baboons. Blood. 2002;99:3623-3628.
164. Savage B, Almus-Jacobs F, Ruggeri ZM. Specific synergy of multiple substrate-receptor interactions in platelet thrombus formation under flow. Cell. 1998;94:657-666.
165. Romijn RA, Bouma B, Wuyster W, et al. Identification of the collagen-binding site of the von Willebrand factor A3-domain. J Biol Chem. 2001;276:9985-9991.
166. Romijn RA, Westein E, Bouma B, et al. Mapping the collagen-binding site in the von Willebrand factor-A3 domain. J Biol Chem. 2003;278:15035-15039.
167. Nishida N, Sumikawa H, Sakakura M, et al. Collagen-binding mode of vWF-A3 domain determined by a transferred cross-saturation experiment. Nat Struct Biol. 2003;10:53-58.
168. Cruz MA, Yuan H, Lee JR, Wise RJ, Handin RI. Interaction of the von Willebrand factor (vWF) with collagen. Localization of the primary collagen-binding site by analysis of recombinant vWF A domain polypeptides. J Biol Chem. 1995;270:19668.
169. Wu YP, van Breugel HH, Lankhof H, et al. Platelet adhesion to multimeric and dimeric von Willebrand factor and to collagen type III preincubated with von Willebrand factor. Arterioscler Thromb Vasc Biol. 1996;16:611-620.
170. Denis C, Baruch D, Kielty CM, Ajzenberg N, Christophe O, Meyer D. Localization of von Willebrand factor binding domains to endothelial extracellular matrix and to type VI collagen. Arterioscler Thromb. 1993;13:398-406.
171. Furlan M, Robles R, Lamie B. Partial purification and characterization of a protease from human plasma cleaving von Willebrand factor to fragments produced by in vivo proteolysis. Blood. 1996;87:4223-4234.
172. Zheng X, Chung D, Takayama TK, Majerus EM, Sadler JE, Fujikawa K. Structure of von Willebrand factor-cleaving protease (ADAMTS13), a metalloprotease involved in thrombotic thrombocytopenic purpura. J Biol Chem. 2001;276:41059-41063.
173. Anderson PJ, Kokame K, Sadler JE. Zinc and calcium ions cooperatively modulate ADAMTS13 activity. J Biol Chem. 2006;281:850-857.
174. Zhang P, Pan W, Rux AH, Sachais BS, Zheng XL. The cooperative activity between the carboxyl-terminal TSP1 repeats and the CUB domains of ADAMTS13 is crucial for recognition of von Willebrand factor under flow. Blood. 2007;110:1887-1894.
175. Zhou W, Inada M, Lee TP, et al. ADAMTS13 is expressed in hepatic stellate cells. Lab Invest. 2005;85:780-788.

176. Liu L, Choi H, Bernardo A, et al. Platelet-derived VWF-cleaving metalloprotease ADAMTS-13. J Thromb Haemost. 2005;3:2536-2544.
177. Turner N, Nolasco L, Tao Z, Dong JF, Moake J. Human endothelial cells synthesize and release ADAMTS-13. J Thromb Haemost. 2006;4:1396-1404.
178. Chion CK, Doggen CJ, Crawley JT, Lane DA, Rosendaal FR. ADAMTS13 and von Willebrand factor and the risk of myocardial infarction in men. Blood. 2007;109:1998-2000.
179. Soejima K, Nakamura H, Hirashima M, Morikawa W, Nozaki C, Nakagaki T. Analysis on the molecular species and concentration of circulating ADAMTS13 in Blood. J Biochem. 2006;139:147-154.
180. Feys HB, Liu F, Dong N, et al. ADAMTS-13 plasma level determination uncovers antigen absence in acquired thrombotic thrombocytopenic purpura and ethnic differences. J Thromb Haemost. 2006;4:955-962.
181. Furlan M, Robles R, Morselli B, Sandoz P, Lammle B. Recovery and half-life of von Willebrand factor-cleaving protease after plasma therapy in patients with thrombotic thrombocytopenic purpura. Thromb Haemost. 1999;81:8-13.
182. Tsai HM. Physiologic cleavage of von Willebrand factor by a plasma protease is dependent on its conformation and requires calcium ion. Blood. 1996;87:4235-4244.
183. Majerus EM, Anderson PJ, Sadler JE. Binding of ADAMTS13 to von Willebrand factor. J Biol Chem. 2005;280:21773-21778.
184. Dong JF, Moake JL, Nolasco L, et al. ADAMTS-13 rapidly cleaves newly secreted ultralarge von Willebrand factor multimers on the endothelial surface under flowing conditions. Blood. 2002;100:4033-4039.
185. Dong JF, Moake JL, Bernardo A, et al. ADAMTS-13 metalloprotease interacts with the endothelial cell-derived ultra-large von Willebrand factor. J Biol Chem. 2003;278:29633-29639.
186. Dong JF. Cleavage of ultra-large von Willebrand factor by ADAMTS-13 under flow conditions. J Thromb Haemost. 2005;3:1710-1716.
187. Jin SY, Skipwith CG, Shang D, Zheng XL. von Willebrand factor cleaved from endothelial cells by ADAMTS13 remains ultralarge in size. J Thromb Haemost. 2009;7:1749-1752.
188. Turner N, Nolasco L, Dong JF, Moake J. ADAMTS-13 cleaves long von Willebrand factor multimeric strings anchored to endothelial cells in the absence of flow, platelets or conformation-altering chemicals. J Thromb Haemost. 2009;7:229-232.
189. Chauhan AK, Motto DG, Lamb CB, et al. Systemic antithrombotic effects of ADAMTS13. J Exp Med. 2006;203:767-776.
190. Shim K, Anderson PJ, Tuley EA, Wiswall E, Sadler JE. Platelet-VWF complexes are preferred substrates of ADAMTS13 under fluid shear stress. Blood. 2008;111:651-657.
191. Vomund AN, Majerus EM. ADAMTS13 bound to endothelial cells exhibits enhanced cleavage of von Willebrand factor. J Biol Chem. 2009;284:30925-30932.
192. Sporn LA, Marder VJ, Wagner DD. von Willebrand factor released from Weibel-Palade bodies binds more avidly to extracellular matrix than that secreted constitutively. Blood. 1987;69:1531-1534.
193. Arya M, Anvari B, Romo GM, et al. Ultralarge multimers of von Willebrand factor form spontaneous high-strength bonds with the platelet glycoprotein Ib-IX complex: studies using optical tweezers. Blood. 2002;99:3971-3977.
194. Tsai HM. Deficiency of ADAMTS13 in thrombotic thrombocytopenic purpura. Int J Hematol. 2002;76 Suppl 2:132-138.

195. Tsai HM. Current concepts in thrombotic thrombocytopenic purpura. Annu Rev Med. 2006;57:419-436.
196. Levy GG, Nichols WC, Lian EC, et al. Mutations in a member of the ADAMTS gene family cause thrombotic thrombocytopenic purpura. Nature. 2001;413:488-494.
197. Moake JL. Thrombotic microangiopathies. N Engl J Med. 2002;347:589-600.
198. Lyons SE, Bruck ME, Bowie EJ, Ginsburg D. Impaired intracellular transport produced by a subset of type IIA von Willebrand disease mutations. J Biol Chem. 1992;267:4424-4430.
199. Tsai HM, Sussman, II, Ginsburg D, Lankhof H, Sixma JJ, Nagel RL. Proteolytic cleavage of recombinant type 2A von Willebrand factor mutants R834W and R834Q: inhibition by doxycycline and by monoclonal antibody VP-1. Blood. 1997;89:1954-1962.
200. Tsai HM. Shear stress and von Willebrand factor in health and disease. Semin Thromb Hemost. 2003;29:479-488.
201. Vincentelli A, Susen S, Le Tourneau T, et al. Acquired von Willebrand syndrome in aortic stenosis. N Engl J Med. 2003;349:343-349.
202. Fujioka M, Hayakawa K, Mishima K, et al. ADAMTS13 gene deletion aggravates ischemic brain damage: a possible neuroprotective role of ADAMTS13 by ameliorating post-ischemic hypoperfusion. Blood. 2009.
203. Huang J, Roth R, Heuser JE, Sadler JE. Integrin alpha(v)beta(3) on human endothelial cells binds von Willebrand factor strings under fluid shear stress. Blood. 2009;113:1589-1597.
204. Shida Y, Nishio K, Sugimoto M, et al. Functional imaging of shear-dependent activity of ADAMTS13 in regulating mural thrombus growth under whole blood flow conditions. Blood. 2008;111:1295-1298.
205. Kleinschnitz C, De Meyer SF, Schwarz T, et al. Deficiency of von Willebrand factor protects mice from ischemic stroke. Blood. 2009;113:3600-3603.
206. Zhao BQ, Chauhan AK, Canault M, et al. von Willebrand factor-cleaving protease ADAMTS13 reduces ischemic brain injury in experimental stroke. Blood. 2009;114:3329-3334.
207. Fujioka M, Hayakawa K, Mishima K, et al. ADAMTS13 gene deletion aggravates ischemic brain damage: a possible neuroprotective role of ADAMTS13 by ameliorating postischemic hypoperfusion. Blood. 2010;115:1650-1653.
208. Nieswandt B, Stoll G. The smaller, the better: VWF in stroke. Blood. 2010;115:1477-1478.
209. De Meyer SF, Schwarz T, Deckmyn H, et al. Binding of von Willebrand Factor to Collagen and Glycoprotein Ib{alpha}, But Not to Glycoprotein IIb/IIIa, Contributes to Ischemic Stroke in Mice. Arterioscler Thromb Vasc Biol.
210. Ono T, Mimuro J, Madoiwa S, et al. Severe secondary deficiency of von Willebrand factor-cleaving protease (ADAMTS13) in patients with sepsis-induced disseminated intravascular coagulation: its correlation with development of renal failure. Blood. 2006;107:528-534.
211. Chauhan AK, Kisucka J, Brill A, Walsh MT, Scheiflinger F, Wagner DD. ADAMTS13: a new link between thrombosis and inflammation. J Exp Med. 2008;205:2065-2074.
212. Nguyen TC, Liu A, Liu L, et al. Acquired ADAMTS-13 deficiency in pediatric patients with severe sepsis. Haematologica. 2007;92:121-124.
213. Reiter RA, Varadi K, Turecek PL, Jilma B, Knobl P. Changes in ADAMTS13 (von-Willebrand-factor-cleaving protease) activity after induced release of von

Willebrand factor during acute systemic inflammation. Thromb Haemost. 2005;93:554-558.
214. Gawaz M. Role of platelets in coronary thrombosis and reperfusion of ischemic myocardium. Cardiovasc Res. 2004;61:498-511.
215. Kroll MH, Hellums JD, McIntire LV, Schafer AI, Moake JL. Platelets and shear stress. Blood. 1996;88:1525-1541.
216. Methia N, Andre P, Denis CV, Economopoulos M, Wagner DD. Localized reduction of atherosclerosis in von Willebrand factor-deficient mice. Blood. 2001;98:1424-1428.
217. Sramek A, Bucciarelli P, Federici AB, et al. Patients with type 3 severe von Willebrand disease are not protected against atherosclerosis: results from a multicenter study in 47 patients. Circulation. 2004;109:740-744.
218. Whincup PH, Danesh J, Walker M, et al. von Willebrand factor and coronary heart disease: prospective study and meta-analysis. Eur Heart J. 2002;23:1764-1770.
219. Gao W, Anderson PJ, Sadler JE. Extensive contacts between ADAMTS13 exosites and von Willebrand factor domain A2 contribute to substrate specificity. Blood. 2008.
220. Akiyama M, Takeda S, Kokame K, Takagi J, Miyata T. Crystal structures of the noncatalytic domains of ADAMTS13 reveal multiple discontinuous exosites for von Willebrand factor. Proc Natl Acad Sci U S A. 2009;106:19274-19279.
221. Soejima K, Matsumoto M, Kokame K, et al. ADAMTS-13 cysteine-rich/spacer domains are functionally essential for von Willebrand factor cleavage. Blood. 2003;102:3232-3237.
222. Zheng X, Nishio K, Majerus EM, Sadler JE. Cleavage of von Willebrand factor requires the spacer domain of the metalloprotease ADAMTS13. J Biol Chem. 2003;278:30136-30141.
223. Gao W, Anderson PJ, Majerus EM, Tuley EA, Sadler JE. Exosite interactions contribute to tension-induced cleavage of von Willebrand factor by the antithrombotic ADAMTS13 metalloprotease. Proc Natl Acad Sci U S A. 2006;103:19099-19104.
224. Wu JJ, Fujikawa K, McMullen BA, Chung DW. Characterization of a core binding site for ADAMTS-13 in the A2 domain of von Willebrand factor. Proc Natl Acad Sci U S A. 2006;103:18470-18474.
225. Pos W, Crawley JT, Fijnheer R, Voorberg J, Lane DA, Luken BM. An autoantibody epitope comprising residues R660, Y661, and Y665 in the ADAMTS13 spacer domain identifies a binding site for the A2 domain of VWF. Blood;115:1640-1649.
226. Tao Z, Wang Y, Choi H, et al. Cleavage of ultralarge multimers of von Willebrand factor by C-terminal-truncated mutants of ADAMTS-13 under flow. Blood. 2005;106:141-143.
227. de Groot R, Bardhan A, Ramroop N, Lane DA, Crawley JT. Essential role of the disintegrin-like domain in ADAMTS13 function. Blood. 2009;113:5609-5616.
228. Bode W, Gomis-Ruth FX, Stockler W. Astacins, serralysins, snake venom and matrix metalloproteinases exhibit identical zinc-binding environments (HEXXHXXGXXH and Met-turn) and topologies and should be grouped into a common family, the 'metzincins'. FEBS Lett. 1993;331:134-140.
229. Gardner MD, Chion CK, de Groot R, Shah A, Crawley JT, Lane DA. A functional calcium-binding site in the metalloprotease domain of ADAMTS13. Blood. 2009;113:1149-1157.
230. Tsai HM, Sussman, II, Nagel RL. Shear stress enhances the proteolysis of von Willebrand factor in normal plasma. Blood. 1994;83:2171-2179.

231. Tsai HM, Lian EC. Antibodies to von Willebrand factor-cleaving protease in acute thrombotic thrombocytopenic purpura. N Engl J Med. 1998;339:1585-1594.
232. Zanardelli S, Crawley JT, Chion CK, Lam JK, Preston RJ, Lane DA. ADAMTS13 substrate recognition of von Willebrand factor A2 domain. J Biol Chem. 2006;281:1555-1563.
233. Banno F, Chauhan AK, Kokame K, et al. The distal carboxyl-terminal domains of ADAMTS13 are required for regulation of in vivo thrombus formation. Blood. 2009;113:5323-5329.
234. Shankaran H, Neelamegham S. Hydrodynamic forces applied on intercellular bonds, soluble molecules, and cell-surface receptors. Biophys J. 2004;86:576-588.
235. Nishio K, Anderson PJ, Zheng XL, Sadler JE. Binding of platelet glycoprotein Ibalpha to von Willebrand factor domain A1 stimulates the cleavage of the adjacent domain A2 by ADAMTS13. Proc Natl Acad Sci U S A. 2004;101:10578-10583.
236. Skipwith C, Cao W, Zheng XL. Factor VIII and platelets synergistically accelerate cleavage of von Willebrand factor by ADAMTS13 under fluid shear stress. J Biol Chem. 2010.
237. Ricketts LM, Dlugosz M, Luther KB, Haltiwanger RS, Majerus EM. O-fucosylation is required for ADAMTS13 secretion. J Biol Chem. 2007;282:17014-17023.
238. Zhou W, Tsai HM. N-Glycans of ADAMTS13 modulate its secretion and von Willebrand factor cleaving activity. Blood. 2009;113:929-935.
239. McKinnon TA, Chion AC, Millington AJ, Lane DA, Laffan MA. N-linked glycosylation of VWF modulates its interaction with ADAMTS13. Blood. 2007.
240. Fujikawa K, Suzuki H, McMullen B, Chung D. Purification of human von Willebrand factor-cleaving protease and its identification as a new member of the metalloproteinase family. Blood. 2001;98:1662-1666.
241. Xie L, Chesterman CN, Hogg PJ. Control of von Willebrand factor multimer size by thrombospondin-1. J Exp Med. 2001;193:1341-1349.
242. Pimanda JE, Ganderton T, Maekawa A, et al. Role of thrombospondin-1 in control of von Willebrand factor multimer size in mice. J Biol Chem. 2004;279:21439-21448.
243. Staatz WD, Rajpara SM, Wayner EA, Carter WG, Santoro SA. The membrane glycoprotein Ia-IIa (VLA-2) complex mediates the Mg++-dependent adhesion of platelets to collagen. J Cell Biol. 1989;108:1917-1924.
244. Saelman EU, Nieuwenhuis HK, Hese KM, et al. Platelet adhesion to collagen types I through VIII under conditions of stasis and flow is mediated by GPIa/IIa (alpha 2 beta 1-integrin). Blood. 1994;83:1244-1250.
245. Savage B, Saldivar E, Ruggeri ZM. Initiation of platelet adhesion by arrest onto fibrinogen or translocation on von Willebrand factor. Cell. 1996;84:289-297.
246. Ruggeri ZM. Von Willebrand factor: looking back and looking forward. Thromb Haemost. 2007;98:55-62.
247. Chauhan AK, Kisucka J, Lamb CB, Bergmeier W, Wagner DD. von Willebrand factor and factor VIII are independently required to form stable occlusive thrombi in injured veins. Blood. 2007;109:2424-2429.
248. Du X, Beutler L, Ruan C, Castaldi PA, Berndt MC. Glycoprotein Ib and glycoprotein IX are fully complexed in the intact platelet membrane. Blood. 1987;69:1524-1527.
249. Modderman PW, Admiraal LG, Sonnenberg A, von dem Borne AE. Glycoproteins V and Ib-IX form a noncovalent complex in the platelet membrane. J Biol Chem. 1992;267:364-369.

250. Vicente V, Houghten RA, Ruggeri ZM. Identification of a site in the alpha chain of platelet glycoprotein Ib that participates in von Willebrand factor binding. J Biol Chem. 1990;265:274-280.
251. Cruz MA, Diacovo TG, Emsley J, Liddington R, Handin RI. Mapping the glycoprotein Ib-binding site in the von willebrand factor A1 domain. J Biol Chem. 2000;275:19098-19105.
252. Matsushita T, Sadler JE. Identification of amino acid residues essential for von Willebrand factor binding to platelet glycoprotein Ib. Charged-to-alanine scanning mutagenesis of the A1 domain of human von Willebrand factor. J Biol Chem. 1995;270:13406-13414.
253. Simon DI, Chen Z, Xu H, et al. Platelet glycoprotein ibalpha is a counterreceptor for the leukocyte integrin Mac-1 (CD11b/CD18). J Exp Med. 2000;192:193-204.
254. Romo GM, Dong JF, Schade AJ, et al. The glycoprotein Ib-IX-V complex is a platelet counterreceptor for P-selectin. J Exp Med. 1999;190:803-814.
255. Baglia FA, Shrimpton CN, Emsley J, et al. Factor XI interacts with the leucine-rich repeats of glycoprotein Ibalpha on the activated platelet. J Biol Chem. 2004;279:49323-49329.
256. Bradford HN, Pixley RA, Colman RW. Human factor XII binding to the glycoprotein Ib-IX-V complex inhibits thrombin-induced platelet aggregation. J Biol Chem. 2000;275:22756-22763.
257. Fuster V, Badimon L, Badimon JJ, Chesebro JH. The pathogenesis of coronary artery disease and the acute coronary syndromes (2). N Engl J Med. 1992;326:310-318.
258. Fuster V, Badimon L, Badimon JJ, Chesebro JH. The pathogenesis of coronary artery disease and the acute coronary syndromes (1). N Engl J Med. 1992;326:242-250.
259. Tangelder GJ, Slaaf DW, Arts T, Reneman RS. Wall shear rate in arterioles in vivo: least estimates from platelet velocity profiles. Am J Physiol. 1988;254:H1059-1064.
260. Goldsmith HL, Turitto VT. Rheological aspects of thrombosis and haemostasis: basic principles and applications. ICTH-Report--Subcommittee on Rheology of the International Committee on Thrombosis and Haemostasis. Thromb Haemost. 1986;55:415-435.
261. Cruz MA, Handin RI, Wise RJ. The interaction of the von Willebrand factor-A1 domain with platelet glycoprotein Ib/IX. The role of glycosylation and disulfide bonding in a monomeric recombinant A1 domain protein. J Biol Chem. 1993;268:21238-21245.
262. Doggett TA, Girdhar G, Lawshe A, et al. Alterations in the intrinsic properties of the GPIbalpha-VWF tether bond define the kinetics of the platelet-type von Willebrand disease mutation, Gly233Val. Blood. 2003;102:152-160.
263. Chen S, Alon R, Fuhlbrigge RC, Springer TA. Rolling and transient tethering of leukocytes on antibodies reveal specializations of selectins. Proc Natl Acad Sci U S A. 1997;94:3172-3177.
264. Kumar RA, Dong JF, Thaggard JA, Cruz MA, Lopez JA, McIntire LV. Kinetics of GPIbalpha-vWF-A1 tether bond under flow: effect of GPIbalpha mutations on the association and dissociation rates. Biophys J. 2003;85:4099-4109.
265. Doggett TA, Girdhar G, Lawshe A, et al. Selectin-like kinetics and biomechanics promote rapid platelet adhesion in flow: the GPIb(alpha)-vWF tether bond. Biophys J. 2002;83:194-205.
266. Ozaki Y, Asazuma N, Suzuki-Inoue K, Berndt MC. Platelet GPIb-IX-V-dependent signaling. J Thromb Haemost. 2005;3:1745-1751.

267. Du X. Signaling and regulation of the platelet glycoprotein Ib-IX-V complex. Curr Opin Hematol. 2007;14:262-269.
268. Ruggeri ZM, Zimmerman TS. von Willebrand factor and von Willebrand disease. Blood. 1987;70:895-904.
269. Ruggeri ZM. Structure and function of von Willebrand factor. Thromb Haemost. 1999;82:576-584.
270. Matsushita T, Meyer D, Sadler JE. Localization of von willebrand factor-binding sites for platelet glycoprotein Ib and botrocetin by charged-to-alanine scanning mutagenesis. J Biol Chem. 2000;275:11044-11049.
271. Miller JL, Cunningham D, Lyle VA, Finch CN. Mutation in the gene encoding the alpha chain of platelet glycoprotein Ib in platelet-type von Willebrand disease. Proc Natl Acad Sci U S A. 1991;88:4761-4765.
272. Russell SD, Roth GJ. Pseudo-von Willebrand disease: a mutation in the platelet glycoprotein Ib alpha gene associated with a hyperactive surface receptor. Blood. 1993;81:1787-1791.
273. Berndt MC, Fournier DJ, Castaldi PA. Bernard-Soulier syndrome. Baillieres Clin Haematol. 1989;2:585-607.
274. Roth GJ. Molecular defects in the Bernard-Soulier syndrome: assessment of receptor genes, transcripts and proteins. C R Acad Sci III. 1996;319:819-826.
275. Uff S, Clemetson JM, Harrison T, Clemetson KJ, Emsley J. Crystal structure of the platelet glycoprotein Ib(alpha) N-terminal domain reveals an unmasking mechanism for receptor activation. J Biol Chem. 2002;277:35657-35663.
276. Huizinga EG, Tsuji S, Romijn RA, et al. Structures of glycoprotein Ibalpha and its complex with von Willebrand factor A1 domain. Science. 2002;297:1176-1179.
277. Dumas JJ, Kumar R, McDonagh T, et al. Crystal structure of the wild-type von Willebrand factor A1-glycoprotein Ibalpha complex reveals conformation differences with a complex bearing von Willebrand disease mutations. J Biol Chem. 2004;279:23327-23334.
278. Berndt MC, Shen Y, Dopheide SM, Gardiner EE, Andrews RK. The vascular biology of the glycoprotein Ib-IX-V complex. Thromb Haemost. 2001;86:178-188.
279. Lou J, Zhu C. Flow induces loop-to-{beta}-hairpin transition on the {beta}-switch of platelet glycoprotein Ib{alpha}. Proc Natl Acad Sci U S A. 2008.
280. Zou X, Liu Y, Chen Z, Cardenas-Jiron GI, Schulten K. Flow-induced beta-hairpin folding of the glycoprotein Ibalpha beta-switch. Biophys J;99:1182-1191.
281. Sadler JE. Biomedicine. Contact--how platelets touch von Willebrand factor. Science. 2002;297:1128-1129.
282. Sheinerman FB, Norel R, Honig B. Electrostatic aspects of protein-protein interactions. Curr Opin Struct Biol. 2000;10:153-159.
283. Auton M, Sedlak E, Marek J, Wu T, Zhu C, Cruz MA. Changes in thermodynamic stability of von Willebrand factor differentially affect the force-dependent binding to platelet GPIbalpha. Biophys J. 2009;97:618-627.
284. Sugimoto M, Mohri H, McClintock RA, Ruggeri ZM. Identification of discontinuous von Willebrand factor sequences involved in complex formation with botrocetin. A model for the regulation of von Willebrand factor binding to platelet glycoprotein Ib. J Biol Chem. 1991;266:18172-18178.
285. Miyata S, Ruggeri ZM. Distinct structural attributes regulating von Willebrand factor A1 domain interaction with platelet glycoprotein Ibalpha under flow. J Biol Chem. 1999;274:6586-6593.

286. Martin C, Morales LD, Cruz MA. Purified A2 domain of von Willebrand factor binds to the active conformation of von Willebrand factor and blocks the interaction with platelet glycoprotein Ibalpha. J Thromb Haemost. 2007;5:1363-1370.
287. Scott JP, Montgomery RR, Retzinger GS. Dimeric ristocetin flocculates proteins, binds to platelets, and mediates von Willebrand factor-dependent agglutination of platelets. J Biol Chem. 1991;266:8149-8155.
288. Girma JP, Takahashi Y, Yoshioka A, Diaz J, Meyer D. Ristocetin and botrocetin involve two distinct domains of von Willebrand factor for binding to platelet membrane glycoprotein Ib. Thromb Haemost. 1990;64:326-332.
289. Mohri H, Fujimura Y, Shima M, et al. Structure of the von Willebrand factor domain interacting with glycoprotein Ib. J Biol Chem. 1988;263:17901-17904.
290. Azuma H, Sugimoto M, Ruggeri ZM, Ware J. A role for von Willebrand factor proline residues 702-704 in ristocetin-mediated binding to platelet glycoprotein Ib. Thromb Haemost. 1993;69:192-196.
291. De Luca M, Facey DA, Favaloro EJ, et al. Structure and function of the von Willebrand factor A1 domain: analysis with monoclonal antibodies reveals distinct binding sites involved in recognition of the platelet membrane glycoprotein Ib-IX-V complex and ristocetin-dependent activation. Blood. 2000;95:164-172.
292. Fujimura Y, Miyata S, Nishida S, et al. The interaction of botrocetin with normal or variant von Willebrand factor (types IIA and IIB) and its inhibition by monoclonal antibodies that block receptor binding. Thromb Haemost. 1992;68:464-469.
293. Fukuda K, Doggett T, Laurenzi IJ, Liddington RC, Diacovo TG. The snake venom protein botrocetin acts as a biological brace to promote dysfunctional platelet aggregation. Nat Struct Mol Biol. 2005;12:152-159.
294. Fukuda K, Doggett TA, Bankston LA, Cruz MA, Diacovo TG, Liddington RC. Structural basis of von Willebrand factor activation by the snake toxin botrocetin. Structure. 2002;10:943-950.
295. Ward CM, Andrews RK, Smith AI, Berndt MC. Mocarhagin, a novel cobra venom metalloproteinase, cleaves the platelet von Willebrand factor receptor glycoprotein Ibalpha. Identification of the sulfated tyrosine/anionic sequence Tyr-276-Glu-282 of glycoprotein Ibalpha as a binding site for von Willebrand factor and alpha-thrombin. Biochemistry. 1996;35:4929-4938.
296. Marchese P, Murata M, Mazzucato M, et al. Identification of three tyrosine residues of glycoprotein Ib alpha with distinct roles in von Willebrand factor and alpha-thrombin binding. J Biol Chem. 1995;270:9571-9578.
297. Dong JF, Li CQ, Lopez JA. Tyrosine sulfation of the glycoprotein Ib-IX complex: identification of sulfated residues and effect on ligand binding. Biochemistry. 1994;33:13946-13953.
298. Shen Y, Romo GM, Dong JF, et al. Requirement of leucine-rich repeats of glycoprotein (GP) Ibalpha for shear-dependent and static binding of von Willebrand factor to the platelet membrane GP Ib-IX-V complex. Blood. 2000;95:903-910.
299. Dong JF, Berndt MC, Schade A, McIntire LV, Andrews RK, Lopez JA. Ristocetin-dependent, but not botrocetin-dependent, binding of von Willebrand factor to the platelet glycoprotein Ib-IX-V complex correlates with shear-dependent interactions. Blood. 2001;97:162-168.
300. Ajzenberg N, Ribba AS, Rastegar-Lari G, Meyer D, Baruch D. Effect of recombinant von Willebrand factor reproducing type 2B or type 2M mutations on shear-induced platelet aggregation. Blood. 2000;95:3796-3803.

301. Ikeda Y, Handa M, Kawano K, et al. The role of von Willebrand factor and fibrinogen in platelet aggregation under varying shear stress. J Clin Invest. 1991;87:1234-1240.
302. Goto S, Ikeda Y, Saldivar E, Ruggeri ZM. Distinct mechanisms of platelet aggregation as a consequence of different shearing flow conditions. J Clin Invest. 1998;101:479-486.
303. Peterson DM, Stathopoulos NA, Giorgio TD, Hellums JD, Moake JL. Shear-induced platelet aggregation requires von Willebrand factor and platelet membrane glycoproteins Ib and IIb-IIIa. Blood. 1987;69:625-628.
304. Lefkovits J, Plow EF, Topol EJ. Platelet glycoprotein IIb/IIIa receptors in cardiovascular medicine. N Engl J Med. 1995;332:1553-1559.
305. Gralnick HR, Williams SB, Coller BS. Fibrinogen competes with von Willebrand factor for binding to the glycoprotein IIb/IIIa complex when platelets are stimulated with thrombin. Blood. 1984;64:797-800.
306. Hantgan RR, Nichols WL, Ruggeri ZM. von Willebrand factor competes with fibrin for occupancy of GPIIb:IIIa on thrombin-stimulated platelets. Blood. 1990;75:889-894.
307. Moake JL, Turner NA, Stathopoulos NA, Nolasco LH, Hellums JD. Involvement of large plasma von Willebrand factor (vWF) multimers and unusually large vWF forms derived from endothelial cells in shear stress-induced platelet aggregation. J Clin Invest. 1986;78:1456-1461.
308. Moake JL, Turner NA, Stathopoulos NA, Nolasco L, Hellums JD. Shear-induced platelet aggregation can be mediated by vWF released from platelets, as well as by exogenous large or unusually large vWF multimers, requires adenosine diphosphate, and is resistant to aspirin. Blood. 1988;71:1366-1374.
309. Ruggeri ZM, Dent JA, Saldivar E. Contribution of distinct adhesive interactions to platelet aggregation in flowing blood. Blood. 1999;94:172-178.
310. Ni H, Denis CV, Subbarao S, et al. Persistence of platelet thrombus formation in arterioles of mice lacking both von Willebrand factor and fibrinogen. J Clin Invest. 2000;106:385-392.
311. Sadler JE, Budde U, Eikenboom JC, et al. Update on the pathophysiology and classification of von Willebrand disease: a report of the Subcommittee on von Willebrand Factor. J Thromb Haemost. 2006;4:2103-2114.
312. Weiss HJ, Rogers J. Fibrinogen and platelets in the primary arrest of bleeding. Studies in two patients with congenital afibrinogenemia. N Engl J Med. 1971;285:369-374.
313. Ruggeri ZM, Orje JN, Habermann R, Federici AB, Reininger AJ. Activation-independent platelet adhesion and aggregation under elevated shear stress. Blood. 2006;108:1903-1910.
314. Santoro SA. Identification of a 160,000 dalton platelet membrane protein that mediates the initial divalent cation-dependent adhesion of platelets to collagen. Cell. 1986;46:913-920.
315. Nieuwenhuis HK, Akkerman JW, Houdijk WP, Sixma JJ. Human blood platelets showing no response to collagen fail to express surface glycoprotein Ia. Nature. 1985;318:470-472.
316. Sarratt KL, Chen H, Zutter MM, Santoro SA, Hammer DA, Kahn ML. GPVI and alpha2beta1 play independent critical roles during platelet adhesion and aggregate formation to collagen under flow. Blood. 2005;106:1268-1277.

317. Moroi M, Jung SM, Okuma M, Shinmyozu K. A patient with platelets deficient in glycoprotein VI that lack both collagen-induced aggregation and adhesion. J Clin Invest. 1989;84:1440-1445.
318. Moroi M, Jung SM, Shinmyozu K, Tomiyama Y, Ordinas A, Diaz-Ricart M. Analysis of platelet adhesion to a collagen-coated surface under flow conditions: the involvement of glycoprotein VI in the platelet adhesion. Blood. 1996;88:2081-2092.
319. Jung SM, Sonoda M, Tsuji K, et al. Are integrin alpha(2)beta(1), glycoprotein Ib and vWf levels correlated with their contributions to platelet adhesion on collagen under high-shear flow? Platelets;21:101-111.
320. Nieswandt B, Watson SP. Platelet-collagen interaction: is GPVI the central receptor? Blood. 2003;102:449-461.
321. Van de Walle GR, Schoolmeester A, Iserbyt BF, et al. Activation of alphaIIbbeta3 is a sufficient but also an imperative prerequisite for activation of alpha2beta1 on platelets. Blood. 2007;109:595-602.
322. Goto S, Tamura N, Handa S, Arai M, Kodama K, Takayama H. Involvement of glycoprotein VI in platelet thrombus formation on both collagen and von Willebrand factor surfaces under flow conditions. Circulation. 2002;106:266-272.
323. Nieswandt B, Brakebusch C, Bergmeier W, et al. Glycoprotein VI but not alpha2beta1 integrin is essential for platelet interaction with collagen. EMBO J. 2001;20:2120-2130.
324. Kato K, Kanaji T, Russell S, et al. The contribution of glycoprotein VI to stable platelet adhesion and thrombus formation illustrated by targeted gene deletion. Blood. 2003;102:1701-1707.
325. Corral J, Gonzalez-Conejero R, Rivera J, Ortuno F, Aparicio P, Vicente V. Role of the 807 C/T polymorphism of the alpha2 gene in platelet GP Ia collagen receptor expression and function--effect in thromboembolic diseases. Thromb Haemost. 1999;81:951-956.
326. Arthur JF, Dunkley S, Andrews RK. Platelet glycoprotein VI-related clinical defects. Br J Haematol. 2007;139:363-372.
327. Barrett NE, Holbrook L, Jones S, et al. Future innovations in anti-platelet therapies. Br J Pharmacol. 2008;154:918-939.
328. Bell GI. Models for the specific adhesion of cells to cells. Science. 1978;200:618-627.
329. Thomas WE, Trintchina E, Forero M, Vogel V, Sokurenko EV. Bacterial adhesion to target cells enhanced by shear force. Cell. 2002;109:913-923.
330. Marshall BT, Long M, Piper JW, Yago T, McEver RP, Zhu C. Direct observation of catch bonds involving cell-adhesion molecules. Nature. 2003;423:190-193.
331. Guo B, Guilford WH. Mechanics of actomyosin bonds in different nucleotide states are tuned to muscle contraction. Proc Natl Acad Sci U S A. 2006;103:9844-9849.
332. Chen S, Springer TA. Selectin receptor-ligand bonds: Formation limited by shear rate and dissociation governed by the Bell model. Proc Natl Acad Sci U S A. 2001;98:950-955.
333. Alon R, Chen S, Puri KD, Finger EB, Springer TA. The kinetics of L-selectin tethers and the mechanics of selectin-mediated rolling. J Cell Biol. 1997;138:1169-1180.
334. Hanley WD, Wirtz D, Konstantopoulos K. Distinct kinetic and mechanical properties govern selectin-leukocyte interactions. J Cell Sci. 2004;117:2503-2511.

335. Yago T, Lou J, Wu T, et al. Platelet glycoprotein Ibalpha forms catch bonds with human WT vWF but not with type 2B von Willebrand disease vWF. J Clin Invest. 2008;118:3195-3207.
336. Rinko LJ, Lawrence MB, Guilford WH. The molecular mechanics of P- and L-selectin lectin domains binding to PSGL-1. Biophys J. 2004;86:544-554.
337. Evans E, Leung A, Heinrich V, Zhu C. Mechanical switching and coupling between two dissociation pathways in a P-selectin adhesion bond. Proc Natl Acad Sci U S A. 2004;101:11281-11286.
338. Heinrich V, Leung A, Evans E. Nano- to microscale dynamics of P-selectin detachment from leukocyte interfaces. II. Tether flow terminated by P-selectin dissociation from PSGL-1. Biophys J. 2005;88:2299-2308.
339. Tees DF, Waugh RE, Hammer DA. A microcantilever device to assess the effect of force on the lifetime of selectin-carbohydrate bonds. Biophys J. 2001;80:668-682.
340. Evans EA, Calderwood DA. Forces and bond dynamics in cell adhesion. Science. 2007;316:1148-1153.
341. Yakovenko O, Sharma S, Forero M, et al. FimH forms catch bonds that are enhanced by mechanical force due to allosteric regulation. J Biol Chem. 2008;283:11596-11605.
342. Thomas WE. Mechanochemistry of receptor-ligand bonds. Curr Opin Struct Biol. 2009;19:50-55.
343. Ruggeri ZM. Type IIB von Willebrand disease: a paradox explains how von Willebrand factor works. J Thromb Haemost. 2004;2:2-6.
344. Turitto VT, Baumgartner HR. Effect of temperature on platelet interaction with subendothelium exposed to flowing blood. Haemostasis. 1974;3:224-236.
345. van Breugel HF, de Groot PG, Heethaar RM, Sixma JJ. Role of plasma viscosity in platelet adhesion. Blood. 1992;80:953-959.
346. Basmadjian D. The effect of flow and mass transport in thrombogenesis. Ann Biomed Eng. 1990;18:685-709.
347. Wang SK, Hwang NH. On transport of suspended particulates in tube flow. Biorheology. 1992;29:353-377.
348. Aarts PA, van den Broek SA, Prins GW, Kuiken GD, Sixma JJ, Heethaar RM. Blood platelets are concentrated near the wall and red blood cells, in the center in flowing blood. Arteriosclerosis. 1988;8:819-824.
349. Eckstein EC, Belgacem F. Model of platelet transport in flowing blood with drift and diffusion terms. Biophys J. 1991;60:53-69.
350. Turitto VT. Blood viscosity, mass transport, and thrombogenesis. Prog Hemost Thromb. 1982;6:139-177.
351. Dembo M, Torney DC, Saxman K, Hammer D. The reaction-limited kinetics of membrane-to-surface adhesion and detachment. Proc R Soc Lond B Biol Sci. 1988;234:55-83.
352. Evans E, Ritchie K. Dynamic strength of molecular adhesion bonds. Biophys J. 1997;72:1541-1555.
353. Chang KC, Hammer DA. The forward rate of binding of surface-tethered reactants: effect of relative motion between two surfaces. Biophys J. 1999;76:1280-1292.
354. Alon R, Hammer DA, Springer TA. Lifetime of the P-selectin-carbohydrate bond and its response to tensile force in hydrodynamic flow. Nature. 1995;374:539-542.
355. Chen S, Springer TA. An automatic braking system that stabilizes leukocyte rolling by an increase in selectin bond number with shear. J Cell Biol. 1999;144:185-200.

356. Mehta P, Cummings RD, McEver RP. Affinity and kinetic analysis of P-selectin binding to P-selectin glycoprotein ligand-1. J Biol Chem. 1998;273:32506-32513.
357. Nicholson MW, Barclay AN, Singer MS, Rosen SD, van der Merwe PA. Affinity and kinetic analysis of L-selectin (CD62L) binding to glycosylation-dependent cell-adhesion molecule-1. J Biol Chem. 1998;273:763-770.
358. Mody NA, Lomakin O, Doggett TA, Diacovo TG, King MR. Mechanics of transient platelet adhesion to von Willebrand factor under flow. Biophys J. 2005;88:1432-1443.
359. Bell GI, Dembo M, Bongrand P. Cell adhesion. Competition between nonspecific repulsion and specific bonding. Biophys J. 1984;45:1051-1064.
360. Savage B, Sixma JJ, Ruggeri ZM. Functional self-association of von Willebrand factor during platelet adhesion under flow. Proc Natl Acad Sci U S A. 2002;99:425-430.
361. Shankaran H, Alexandridis P, Neelamegham S. Aspects of hydrodynamic shear regulating shear-induced platelet activation and self-association of von Willebrand factor in suspension. Blood. 2003;101:2637-2645.
362. Choi H, Aboulfatova K, Pownall HJ, Cook R, Dong JF. Shear-induced disulfide bond formation regulates adhesion activity of von Willebrand factor. J Biol Chem. 2007;282:35604-35611.
363. Li Y, Choi H, Zhou Z, et al. Covalent regulation of ULVWF string formation and elongation on endothelial cells under flow conditions. J Thromb Haemost. 2008;6:1135-1143.
364. Ulrichts H, Vanhoorelbeke K, Girma JP, Lenting PJ, Vauterin S, Deckmyn H. The von Willebrand factor self-association is modulated by a multiple domain interaction. J Thromb Haemost. 2005;3:552-561.
365. Di Stasio E, Romitelli F, Lancellotti S, Arcovito A, Giardina B, De Cristofaro R. Kinetic study of von Willebrand factor self-aggregation induced by ristocetin. Biophys Chem. 2009;144:101-107.
366. Gezsi A, Budde U, Deak I, et al. Accelerated clearance alone explains ultra-large multimers in von Willebrand disease Vicenza. J Thromb Haemost;8:1273-1280.
367. Casonato A, Pontara E, Sartorello F, et al. Reduced von Willebrand factor survival in type Vicenza von Willebrand disease. Blood. 2002;99:180-184.
368. Lenting PJ, Westein E, Terraube V, et al. An experimental model to study the in vivo survival of von Willebrand factor. Basic aspects and application to the R1205H mutation. J Biol Chem. 2004;279:12102-12109.
369. Julenius K, Molgaard A, Gupta R, Brunak S. Prediction, conservation analysis, and structural characterization of mammalian mucin-type O-glycosylation sites. Glycobiology. 2005;15:153-164.
370. Varki A. Biological roles of oligosaccharides: all of the theories are correct. Glycobiology. 1993;3:97-130.
371. Hart GW. Dynamic O-linked glycosylation of nuclear and cytoskeletal proteins. Annu Rev Biochem. 1997;66:315-335.
372. Parekh RB, Dwek RA, Thomas JR, et al. Cell-type-specific and site-specific N-glycosylation of type I and type II human tissue plasminogen activator. Biochemistry. 1989;28:7644-7662.
373. Raman R, Sasisekharan V, Sasisekharan R. Structural insights into biological roles of protein-glycosaminoglycan interactions. Chem Biol. 2005;12:267-277.
374. Venkataraman G, Shriver Z, Raman R, Sasisekharan R. Sequencing complex polysaccharides. Science. 1999;286:537-542.

375. Samor B, Mazurier C, Goudemand M, Debeire P, Fournet B, Montreuil J. Preliminary results on the carbohydrate moiety of factor VIII/von Willebrand factor (FVIII/vWf). Thromb Res. 1982;25:81-89.
376. Sodetz JM, Paulson JC, McKee PA. Carbohydrate composition and identification of blood group A, B, and H oligosaccharide structures on human Factor VIII/von Willebrand factor. J Biol Chem. 1979;254:10754-10760.
377. Moremen KW, Trimble RB, Herscovics A. Glycosidases of the asparagine-linked oligosaccharide processing pathway. Glycobiology. 1994;4:113-125.
378. Spiro RG, Zhu Q, Bhoyroo V, Soling HD. Definition of the lectin-like properties of the molecular chaperone, calreticulin, and demonstration of its copurification with endomannosidase from rat liver Golgi. J Biol Chem. 1996;271:11588-11594.
379. Oliver JD, van der Wal FJ, Bulleid NJ, High S. Interaction of the thiol-dependent reductase ERp57 with nascent glycoproteins. Science. 1997;275:86-88.
380. Helenius A, Aebi M. Intracellular functions of N-linked glycans. Science. 2001;291:2364-2369.
381. Lowe JB. The blood group-specific human glycosyltransferases. Baillieres Clin Haematol. 1993;6:465-492.
382. Samor B, Michalski JC, Debray H, et al. Primary structure of a new tetraantennary glycan of the N-acetyllactosaminic type isolated from human factor VIII/von Willebrand factor. Eur J Biochem. 1986;158:295-298.
383. Debeire P, Montreuil J, Samor B, et al. Structure determination of the major asparagine-linked sugar chain of human factor VIII--von Willebrand factor. FEBS Lett. 1983;151:22-26.
384. Mitra N, Sinha S, Ramya TN, Surolia A. N-linked oligosaccharides as outfitters for glycoprotein folding, form and function. Trends Biochem Sci. 2006;31:156-163.
385. Shental-Bechor D, Levy Y. Effect of glycosylation on protein folding: a close look at thermodynamic stabilization. Proc Natl Acad Sci U S A. 2008;105:8256-8261.
386. Goudemand J, Mazurier C, Samor B, Bouquelet S, Montreuil J, Goudemand M. Effect of carbohydrate modifications of factor VIII/von Willebrand factor on binding to platelets. Thromb Haemost. 1985;53:390-395.
387. Gralnick HR, Williams SB, Rick ME. Role of carbohydrate in multimeric structure of factor VIII/von Willebrand factor protein. Proc Natl Acad Sci U S A. 1983;80:2771-2774.
388. Kessler CM, Floyd CM, Frantz SC, Orthner C. Critical role of the carbohydrate moiety in human von Willebrand factor protein for interactions with type I collagen. Thromb Res. 1990;57:59-76.
389. Federici AB, Elder JH, De Marco L, Ruggeri ZM, Zimmerman TS. Carbohydrate moiety of von Willebrand factor is not necessary for maintaining multimeric structure and ristocetin cofactor activity but protects from proteolytic degradation. J Clin Invest. 1984;74:2049-2055.
390. O'Donnell J, Boulton FE, Manning RA, Laffan MA. Amount of H antigen expressed on circulating von Willebrand factor is modified by ABO blood group genotype and is a major determinant of plasma von Willebrand factor antigen levels. Arterioscler Thromb Vasc Biol. 2002;22:335-341.
391. Souto JC, Almasy L, Muniz-Diaz E, et al. Functional effects of the ABO locus polymorphism on plasma levels of von Willebrand factor, factor VIII, and activated partial thromboplastin time. Arterioscler Thromb Vasc Biol. 2000;20:2024-2028.
392. Gill JC, Endres-Brooks J, Bauer PJ, Marks WJ, Jr., Montgomery RR. The effect of ABO blood group on the diagnosis of von Willebrand disease. Blood. 1987;69:1691-1695.

393. Bowen DJ. An influence of ABO blood group on the rate of proteolysis of von Willebrand factor by ADAMTS13. J Thromb Haemost. 2003;1:33-40.
394. Shimizu Y, Shaw S. Cell adhesion. Mucins in the mainstream. Nature. 1993;366:630-631.
395. Carraway KL, Hull SR. Cell surface mucin-type glycoproteins and mucin-like domains. Glycobiology. 1991;1:131-138.
396. Hanisch FG. O-glycosylation of the mucin type. Biol Chem. 2001;382:143-149.
397. Harris RJ, Spellman MW. O-linked fucose and other post-translational modifications unique to EGF modules. Glycobiology. 1993;3:219-224.
398. Anttinen H, Hulkko A. Regulation of the glycosylations of collagen hydroxylysine in chick embryo tendon and cartilage cells. Biochim Biophys Acta. 1980;632:417-427.
399. Kieliszewski MJ, O'Neill M, Leykam J, Orlando R. Tandem mass spectrometry and structural elucidation of glycopeptides from a hydroxyproline-rich plant cell wall glycoprotein indicate that contiguous hydroxyproline residues are the major sites of hydroxyproline O-arabinosylation. J Biol Chem. 1995;270:2541-2549.
400. Comer FI, Hart GW. O-Glycosylation of nuclear and cytosolic proteins. Dynamic interplay between O-GlcNAc and O-phosphate. J Biol Chem. 2000;275:29179-29182.
401. Hollingsworth MA, Swanson BJ. Mucins in cancer: protection and control of the cell surface. Nat Rev Cancer. 2004;4:45-60.
402. Brockhausen I, Schutzbach J, Kuhns W. Glycoproteins and their relationship to human disease. Acta Anat (Basel). 1998;161:36-78.
403. Wang H, Tachibana K, Zhang Y, et al. Cloning and characterization of a novel UDP-GalNAc:polypeptide N-acetylgalactosaminyltransferase, pp-GalNAc-T14. Biochem Biophys Res Commun. 2003;300:738-744.
404. Ten Hagen KG, Fritz TA, Tabak LA. All in the family: the UDP-GalNAc:polypeptide N-acetylgalactosaminyltransferases. Glycobiology. 2003;13:1R-16R.
405. Van den Steen P, Rudd PM, Dwek RA, Opdenakker G. Concepts and principles of O-linked glycosylation. Crit Rev Biochem Mol Biol. 1998;33:151-208.
406. Cheng L, Tachibana K, Iwasaki H, et al. Characterization of a novel human UDP-GalNAc transferase, pp-GalNAc-T15. FEBS Lett. 2004;566:17-24.
407. Kinarsky L, Suryanarayanan G, Prakash O, et al. Conformational studies on the MUC1 tandem repeat glycopeptides: implication for the enzymatic O-glycosylation of the mucin protein core. Glycobiology. 2003;13:929-939.
408. Bennett EP, Hassan H, Hollingsworth MA, Clausen H. A novel human UDP-N-acetyl-D-galactosamine:polypeptide N-acetylgalactosaminyltransferase, GalNAc-T7, with specificity for partial GalNAc-glycosylated acceptor substrates. FEBS Lett. 1999;460:226-230.
409. Ten Hagen KG, Bedi GS, Tetaert D, et al. Cloning and characterization of a ninth member of the UDP-GalNAc:polypeptide N-acetylgalactosaminyltransferase family, ppGaNTase-T9. J Biol Chem. 2001;276:17395-17404.
410. Hanisch FG, Muller S, Hassan H, et al. Dynamic epigenetic regulation of initial O-glycosylation by UDP-N-Acetylgalactosamine:Peptide N-acetylgalactosaminyltransferases. site-specific glycosylation of MUC1 repeat peptide influences the substrate qualities at adjacent or distant Ser/Thr positions. J Biol Chem. 1999;274:9946-9954.

411. Hanisch FG, Chai W, Rosankiewicz JR, Lawson AM, Stoll MS, Feizi T. Core-typing of O-linked glycans from human gastric mucins. Lack of evidence for the occurrence of the core sequence Gal1-6GalNAc. Eur J Biochem. 1993;217:645-655.
412. Brockhausen I. Pathways of O-glycan biosynthesis in cancer cells. Biochim Biophys Acta. 1999;1473:67-95.
413. El-Battari A, Prorok M, Angata K, et al. Different glycosyltransferases are differentially processed for secretion, dimerization, and autoglycosylation. Glycobiology. 2003;13:941-953.
414. Sansom C, Markman O. Glycobiology. Bloxham: Scion; 2007.
415. Brockhausen I. Mucin-type O-glycans in human colon and breast cancer: glycodynamics and functions. EMBO Rep. 2006;7:599-604.
416. Tsuboi S, Fukuda M. Roles of O-linked oligosaccharides in immune responses. Bioessays. 2001;23:46-53.
417. Berger EG. Tn-syndrome. Biochim Biophys Acta. 1999;1455:255-268.
418. Gendler SJ, Spicer AP. Epithelial mucin genes. Annu Rev Physiol. 1995;57:607-634.
419. Tabak LA. In defense of the oral cavity: structure, biosynthesis, and function of salivary mucins. Annu Rev Physiol. 1995;57:547-564.
420. Garner B, Merry AH, Royle L, Harvey DJ, Rudd PM, Thillet J. Structural elucidation of the N- and O-glycans of human apolipoprotein(a): role of o-glycans in conferring protease resistance. J Biol Chem. 2001;276:22200-22208.
421. Smith KA. Interleukin-2: inception, impact, and implications. Science. 1988;240:1169-1176.
422. Altschuler Y, Kinlough CL, Poland PA, et al. Clathrin-mediated endocytosis of MUC1 is modulated by its glycosylation state. Mol Biol Cell. 2000;11:819-831.
423. Hang HC, Bertozzi CR. The chemistry and biology of mucin-type O-linked glycosylation. Bioorg Med Chem. 2005;13:5021-5034.
424. Jablonka-Shariff A, Garcia-Campayo V, Boime I. Evolution of lutropin to chorionic gonadotropin generates a specific routing signal for apical release in vivo. J Biol Chem. 2002;277:879-882.
425. Hermiston ML, Xu Z, Weiss A. CD45: a critical regulator of signaling thresholds in immune cells. Annu Rev Immunol. 2003;21:107-137.
426. Rosen SD. Ligands for L-selectin: homing, inflammation, and beyond. Annu Rev Immunol. 2004;22:129-156.
427. Lasky LA, Singer MS, Dowbenko D, et al. An endothelial ligand for L-selectin is a novel mucin-like molecule. Cell. 1992;69:927-938.
428. Ley K, Kansas GS. Selectins in T-cell recruitment to non-lymphoid tissues and sites of inflammation. Nat Rev Immunol. 2004;4:325-335.
429. Primakoff P, Myles DG. Penetration, adhesion, and fusion in mammalian sperm-egg interaction. Science. 2002;296:2183-2185.
430. Hooper LV, Gordon JI. Commensal host-bacterial relationships in the gut. Science. 2001;292:1115-1118.
431. Sullivan NJ, Peterson M, Yang ZY, et al. Ebola virus glycoprotein toxicity is mediated by a dynamin-dependent protein-trafficking pathway. J Virol. 2005;79:547-553.
432. Ono M, Hakomori S. Glycosylation defining cancer cell motility and invasiveness. Glycoconj J. 2004;20:71-78.
433. Kim YJ, Varki A. Perspectives on the significance of altered glycosylation of glycoproteins in cancer. Glycoconj J. 1997;14:569-576.

434. Kelly WG, Dahmus ME, Hart GW. RNA polymerase II is a glycoprotein. Modification of the COOH-terminal domain by O-GlcNAc. J Biol Chem. 1993;268:10416-10424.
435. Chou TY, Hart GW, Dang CV. c-Myc is glycosylated at threonine 58, a known phosphorylation site and a mutational hot spot in lymphomas. J Biol Chem. 1995;270:18961-18965.
436. Hart GW, Greis KD, Dong LY, et al. O-linked N-acetylglucosamine: the "yin-yang" of Ser/Thr phosphorylation? Nuclear and cytoplasmic glycosylation. Adv Exp Med Biol. 1995;376:115-123.
437. Hurtado-Guerrero R, Dorfmueller HC, van Aalten DM. Molecular mechanisms of O-GlcNAcylation. Curr Opin Struct Biol. 2008;18:551-557.
438. Coltart DM, Royyuru AK, Williams LJ, et al. Principles of mucin architecture: structural studies on synthetic glycopeptides bearing clustered mono-, di-, tri-, and hexasaccharide glycodomains. J Am Chem Soc. 2002;124:9833-9844.
439. Jentoft N. Why are proteins O-glycosylated? Trends Biochem Sci. 1990;15:291-294.
440. McMaster TJ, Berry M, Corfield AP, Miles MJ. Atomic force microscopy of the submolecular architecture of hydrated ocular mucins. Biophys J. 1999;77:533-541.
441. Shogren R, Gerken TA, Jentoft N. Role of glycosylation on the conformation and chain dimensions of O-linked glycoproteins: light-scattering studies of ovine submaxillary mucin. Biochemistry. 1989;28:5525-5536.
442. Gerken TA, Butenhof KJ, Shogren R. Effects of glycosylation on the conformation and dynamics of O-linked glycoproteins: carbon-13 NMR studies of ovine submaxillary mucin. Biochemistry. 1989;28:5536-5543.
443. Fong AM, Erickson HP, Zachariah JP, et al. Ultrastructure and function of the fractalkine mucin domain in CX(3)C chemokine domain presentation. J Biol Chem. 2000;275:3781-3786.
444. Cyster JG, Shotton DM, Williams AF. The dimensions of the T lymphocyte glycoprotein leukosialin and identification of linear protein epitopes that can be modified by glycosylation. EMBO J. 1991;10:893-902.
445. Li F, Wilkins PP, Crawley S, Weinstein J, Cummings RD, McEver RP. Post-translational modifications of recombinant P-selectin glycoprotein ligand-1 required for binding to P- and E-selectin. J Biol Chem. 1996;271:3255-3264.
446. Rose MC, Voter WA, Sage H, Brown CF, Kaufman B. Effects of deglycosylation on the architecture of ovine submaxillary mucin glycoprotein. J Biol Chem. 1984;259:3167-3172.
447. Rudd PM, Fortune F, Patel T, Parekh RB, Dwek RA, Lehner T. A human T-cell receptor recognizes 'O'-linked sugars from the hinge region of human IgA1 and IgD. Immunology. 1994;83:99-106.
448. Mestecky J, Kilian M. Immunoglobulin A (IgA). Methods Enzymol. 1985;116:37-75.
449. Mattu TS, Pleass RJ, Willis AC, et al. The glycosylation and structure of human serum IgA1, Fab, and Fc regions and the role of N-glycosylation on Fc alpha receptor interactions. J Biol Chem. 1998;273:2260-2272.
450. Barratt J, Smith AC, Feehally J. The pathogenic role of IgA1 O-linked glycosylation in the pathogenesis of IgA nephropathy. Nephrology (Carlton). 2007;12:275-284.
451. Allen AC, Harper SJ, Feehally J. Galactosylation of N- and O-linked carbohydrate moieties of IgA1 and IgG in IgA nephropathy. Clin Exp Immunol. 1995;100:470-474.

452. Samor B, Michalski JC, Mazurier C, et al. Primary structure of the major O-glycosidically linked carbohydrate unit of human von Willebrand factor. Glycoconj J. 1989;6:263-270.
453. Schachter H, Brockhausen I. The biosynthesis of branched O-glycans. Symp Soc Exp Biol. 1989;43:1-26.
454. Carew JA, Quinn SM, Stoddart JH, Lynch DC. O-linked carbohydrate of recombinant von Willebrand factor influences ristocetin-induced binding to platelet glycoprotein 1b. J Clin Invest. 1992;90:2258-2267.
455. Schulte am Esch J, 2nd, Robson SC, Knoefel WT, Eisenberger CF, Peiper M, Rogiers X. Impact of O-linked glycosylation of the VWF-A1-domain flanking regions on platelet interaction. Br J Haematol. 2005;128:82-90.
456. Stoddart JH, Jr., Andersen J, Lynch DC. Clearance of normal and type 2A von Willebrand factor in the rat. Blood. 1996;88:1692-1699.
457. van Schooten CJ, Denis CV, Lisman T, et al. Variations in glycosylation of von Willebrand factor with O-linked sialylated T antigen are associated with its plasma levels. Blood. 2007;109:2430-2437.
458. Schwarzkopf M, Knobeloch KP, Rohde E, et al. Sialylation is essential for early development in mice. Proc Natl Acad Sci U S A. 2002;99:5267-5270.
459. Harduin-Lepers A, Mollicone R, Delannoy P, Oriol R. The animal sialyltransferases and sialyltransferase-related genes: a phylogenetic approach. Glycobiology. 2005;15:805-817.
460. Ikehara Y, Kojima N, Kurosawa N, et al. Cloning and expression of a human gene encoding an N-acetylgalactosamine-alpha2,6-sialyltransferase (ST6GalNAc I): a candidate for synthesis of cancer-associated sialyl-Tn antigens. Glycobiology. 1999;9:1213-1224.
461. Samyn-Petit B, Krzewinski-Recchi MA, Steelant WF, Delannoy P, Harduin-Lepers A. Molecular cloning and functional expression of human ST6GalNAc II. Molecular expression in various human cultured cells. Biochim Biophys Acta. 2000;1474:201-211.
462. Kelm S, Schauer R. Sialic acids in molecular and cellular interactions. Int Rev Cytol. 1997;175:137-240.
463. Ashwell G, Morell A. The dual role of sialic acid in the hepatic recognition and catabolism of serum glycoproteins. Biochem Soc Symp. 1974:117-124.
464. Morell AG, Gregoriadis G, Scheinberg IH, Hickman J, Ashwell G. The role of sialic acid in determining the survival of glycoproteins in the circulation. J Biol Chem. 1971;246:1461-1467.
465. Durocher JR, Payne RC, Conrad ME. Role of sialic acid in erythrocyte survival. Blood. 1975;45:11-20.
466. Nelsestuen GL, Suttie JW. Properties of asialo and aglycoprothrombin. Biochem Biophys Res Commun. 1971;45:198-203.
467. Berkowitz SD, Federici AB. Sialic acid prevents loss of large von Willebrand factor multimers by protecting against amino-terminal proteolytic cleavage. Blood. 1988;72:1790-1796.
468. Sodetz JM, Pizzo SV, McKee PA. Relationship of sialic acid to function and in vivo survival of human factor VIII/von Willebrand factor protein. J Biol Chem. 1977;252:5538-5546.
469. McGrath RT, McKinnon TA, Byrne B, et al. Expression of terminal {alpha}2-6 linked sialic acid on von Willebrand factor specifically enhances proteolysis by ADAMTS13. Blood. 2009.

470. Shima M, Fujimura Y, Nishiyama T, et al. ABO blood group genotype and plasma von Willebrand factor in normal individuals. Vox Sang. 1995;68:236-240.
471. Gallinaro L, Cattini MG, Sztukowska M, et al. A shorter von Willebrand factor survival in O blood group subjects explains how ABO determinants influence plasma von Willebrand factor. Blood. 2008;111:3540-3545.
472. Turecek PL, Gritsch H, Pichler L, et al. In vivo characterization of recombinant von Willebrand factor in dogs with von Willebrand disease. Blood. 1997;90:3555-3567.
473. Millar CM, Riddell AF, Brown SA, et al. Survival of von Willebrand factor released following DDAVP in a type 1 von Willebrand disease cohort: influence of glycosylation, proteolysis and gene mutations. Thromb Haemost. 2008;99:916-924.
474. Badirou I, Kurdi M, Rayes J, et al. von Willebrand factor clearance does not involve proteolysis by ADAMTS13. J Thromb Haemost. 2010.
475. Ashwell G, Harford J. Carbohydrate-specific receptors of the liver. Annu Rev Biochem. 1982;51:531-554.
476. Sodetz JM, Paulson JC, Pizzo SV, McKee PA. Carbohydrate on human factor VIII/von Willebrand factor. Impairment of function by removal of specific galactose residues. J Biol Chem. 1978;253:7202-7206.
477. Park EI, Mi Y, Unverzagt C, Gabius HJ, Baenziger JU. The asialoglycoprotein receptor clears glycoconjugates terminating with sialic acid alpha 2,6GalNAc. Proc Natl Acad Sci U S A. 2005;102:17125-17129.
478. Ellies LG, Ditto D, Levy GG, et al. Sialyltransferase ST3Gal-IV operates as a dominant modifier of hemostasis by concealing asialoglycoprotein receptor ligands. Proc Natl Acad Sci U S A. 2002;99:10042-10047.
479. Sweeney JD, Novak EK, Reddington M, Takeuchi KH, Swank RT. The RIIIS/J inbred mouse strain as a model for von Willebrand disease. Blood. 1990;76:2258-2265.
480. Mohlke KL, Purkayastha AA, Westrick RJ, Ginsburg D. Comparative mapping of distal murine chromosome 11 and human 17q21.3 in a region containing a modifying locus for murine plasma von Willebrand factor level. Genomics. 1998;54:19-30.
481. Nichols WC, Cooney KA, Mohlke KL, et al. von Willebrand disease in the RIIIS/J mouse is caused by a defect outside of the von Willebrand factor gene. Blood. 1995;86:2461.
482. Mohlke KL, Purkayastha AA, Westrick RJ, et al. Mvwf, a dominant modifier of murine von Willebrand factor, results from altered lineage-specific expression of a glycosyltransferase. Cell. 1999;96:111-120.
483. van Schooten CJ, Shahbazi S, Groot E, et al. Macrophages contribute to the cellular uptake of von Willebrand factor and factor VIII in vivo. Blood. 2008.
484. Grewal PK, Uchiyama S, Ditto D, et al. The Ashwell receptor mitigates the lethal coagulopathy of sepsis. Nat Med. 2008;14:648-655.
485. Ceroni A, Maass K, Geyer H, Geyer R, Dell A, Haslam SM. GlycoWorkbench: a tool for the computer-assisted annotation of mass spectra of glycans. J Proteome Res. 2008;7:1650-1659.
486. Canis K, McKinnon TA, Nowak A, et al. The plasma von Willebrand factor O-glycome comprises a surprising variety of structures including ABH antigens and disialosyl motifs. J Thromb Haemost. 2010;8:137-145.
487. Budde U, Metzner HJ, Muller HG. Comparative analysis and classification of von Willebrand factor/factor VIII concentrates: impact on treatment of patients with von Willebrand disease. Semin Thromb Hemost. 2006;32:626-635.
488. Lethagen S, Carlson M, Hillarp A. A comparative in vitro evaluation of six von Willebrand factor concentrates. Haemophilia. 2004;10:243-249.

489. Tsuji S. Molecular cloning and functional analysis of sialyltransferases. J Biochem. 1996;120:1-13.
490. Kudo M, Takayama E, Tashiro K, et al. Cloning and expression of an alpha-2,8-polysialyltransferase (STX) from Xenopus laevis. Glycobiology. 1998;8:771-777.
491. Kleene R, Schachner M. Glycans and neural cell interactions. Nat Rev Neurosci. 2004;5:195-208.
492. Yasukawa Z, Sato C, Sano K, Ogawa H, Kitajima K. Identification of disialic acid-containing glycoproteins in mouse serum: a novel modification of immunoglobulin light chains, vitronectin, and plasminogen. Glycobiology. 2006;16:651-665.
493. Storr SJ, Royle L, Chapman CJ, et al. The O-linked glycosylation of secretory/shed MUC1 from an advanced breast cancer patient's serum. Glycobiology. 2008;18:456-462.
494. Lenting PJ, Pegon JN, Christophe OD, Denis CV. Factor VIII and von Willebrand factor--too sweet for their own good. Haemophilia. 2010;16 Suppl 5:194-199.
495. Yamaji T, Teranishi T, Alphey MS, Crocker PR, Hashimoto Y. A small region of the natural killer cell receptor, Siglec-7, is responsible for its preferred binding to alpha 2,8-disialyl and branched alpha 2,6-sialyl residues. A comparison with Siglec-9. J Biol Chem. 2002;277:6324-6332.
496. Hulstein JJ, de Groot PG, Silence K, Veyradier A, Fijnheer R, Lenting PJ. A novel nanobody that detects the gain-of-function phenotype of von Willebrand factor in ADAMTS13 deficiency and von Willebrand disease type 2B. Blood. 2005;106:3035-3042.
497. Auton M, Sowa KE, Smith SM, Sedlak E, Vijayan KV, Cruz MA. Destabilization of the A1 domain in von Willebrand factor dissociates the A1A2A3 tri-domain and provokes spontaneous binding to glycoprotein Ibalpha and platelet activation under shear stress. J Biol Chem;285:22831-22839.
498. Kirnarsky L, Nomoto M, Ikematsu Y, et al. Structural analysis of peptide substrates for mucin-type O-glycosylation. Biochemistry. 1998;37:12811-12817.
499. Wojczyk BS, Stwora-Wojczyk MM, Hagen FK, et al. cDNA cloning and expression of UDP-N-acetyl-D-galactosamine:polypeptide N-acetylgalactosaminyltransferase T1 from Toxoplasma gondii. Mol Biochem Parasitol. 2003;131:93-107.
500. Ten Hagen KG, Hagen FK, Balys MM, Beres TM, Van Wuyckhuyse B, Tabak LA. Cloning and expression of a novel, tissue specifically expressed member of the UDP-GalNAc:polypeptide N-acetylgalactosaminyltransferase family. J Biol Chem. 1998;273:27749-27754.
501. Tetaert D, Ten Hagen KG, Richet C, Boersma A, Gagnon J, Degand P. Glycopeptide N-acetylgalactosaminyltransferase specificities for O-glycosylated sites on MUC5AC mucin motif peptides. Biochem J. 2001;357:313-320.
502. Naganagowda GA, Gururaja TL, Satyanarayana J, Levine MJ. NMR analysis of human salivary mucin (MUC7) derived O-linked model glycopeptides: comparison of structural features and carbohydrate-peptide interactions. J Pept Res. 1999;54:290-310.
503. Baker EN, Hubbard RE. Hydrogen bonding in globular proteins. Prog Biophys Mol Biol. 1984;44:97-179.
504. Schuster O, Klich G, Sinnwell V, Kranz H, Paulsen H, Meyer B. 'Wave-type' structure of a synthetic hexaglycosylated decapeptide: a part of the extracellular domain of human glycophorin A. J Biomol NMR. 1999;14:33-45.
505. Reglero A, Rodriguez-Aparicio LB, Luengo JM. Polysialic acids. Int J Biochem. 1993;25:1517-1527.

506. Ying J, Ling Y, Westfield LA, Sadler JE, Shao JY. Unfolding the A2 domain of von Willebrand factor with the optical trap. Biophys J. 2010;98:1685-1693.
507. Wyss DF, Wagner G. The structural role of sugars in glycoproteins. Curr Opin Biotechnol. 1996;7:409-416.
508. Wang C, Eufemi M, Turano C, Giartosio A. Influence of the carbohydrate moiety on the stability of glycoproteins. Biochemistry. 1996;35:7299-7307.
509. DeKoster GT, Robertson AD. Thermodynamics of unfolding for Kazal-type serine protease inhibitors: entropic stabilization of ovomucoid first domain by glycosylation. Biochemistry. 1997;36:2323-2331.
510. Sola RJ, Rodriguez-Martinez JA, Griebenow K. Modulation of protein biophysical properties by chemical glycosylation: biochemical insights and biomedical implications. Cell Mol Life Sci. 2007;64:2133-2152.
511. Vermylen J. More on: 'new light on an old story: von Willebrand factor binding to collagen'. J Thromb Haemost. 2007;5:440-441.
512. De Marco L, Shapiro SS. Properties of human asialo-factor VIII. A ristocetin-independent platelet-aggregating agent. J Clin Invest. 1981;68:321-328.
513. Morisato DK, Gralnick HR. Selective binding of the factor VIII/von Willebrand factor protein to human platelets. Blood. 1980;55:9-15.
514. Caron C, Hilbert L, Vanhoorelbeke K, Deckmyn H, Goudemand J, Mazurier C. Measurement of von Willebrand factor binding to a recombinant fragment of glycoprotein Ibalpha in an enzyme-linked immunosorbent assay-based method: performances in patients with type 2B von Willebrand disease. Br J Haematol. 2006;133:655-663.
515. Macfarlane DE, Stibbe J, Kirby EP, Zucker MB, Grant RA, McPherson J. Letter: A method for assaying von Willebrand factor (ristocetin cofactor). Thromb Diath Haemorrh. 1975;34:306-308.
516. Flood VH, Friedman KD, Gill JC, et al. Limitations of the ristocetin cofactor assay in measurement of von Willebrand factor function. J Thromb Haemost. 2009;7:1832-1839.
517. Coller BS, Gralnick HR. Studies on the mechanism of ristocetin-induced platelet agglutination. Effects of structural modification of ristocetin and vancomycin. J Clin Invest. 1977;60:302-312.
518. Coller BS. The effects of ristocetin and von Willebrand factor on platelet electrophoretic mobility. J Clin Invest. 1978;61:1168-1175.
519. Sutherland JJ, O'Brien LA, Lillicrap D, Weaver DF. Molecular modeling of the von Willebrand factor A2 Domain and the effects of associated type 2A von Willebrand disease mutations. J Mol Model. 2004;10:259-270.
520. Collados MT, Sandoval J, Lopez S, et al. Characterization of von Willebrand factor in primary pulmonary hypertension. Heart Vessels. 1999;14:246-252.
521. Lopes AA, Ferraz de Souza B, Maeda NY. Decreased sialic acid content of plasma von Willebrand factor in precapillary pulmonary hypertension. Thromb Haemost. 2000;83:683-687.
522. Goldsmith HL. The flow of model particles and blood cells and its relation to thrombogenesis. Prog Hemost Thromb. 1972;1:97-127.
523. Ruggeri ZM. Platelet adhesion under flow. Microcirculation. 2009;16:58-83.
524. Miura S, Li CQ, Cao Z, Wang H, Wardell MR, Sadler JE. Interaction of von Willebrand factor domain A1 with platelet glycoprotein Ibalpha-(1-289). Slow intrinsic binding kinetics mediate rapid platelet adhesion. J Biol Chem. 2000;275:7539-7546.
525. McEver RP. Adhesive interactions of leukocytes, platelets, and the vessel wall during hemostasis and inflammation. Thromb Haemost. 2001;86:746-756.

526. Yago T, Wu J, Wey CD, Klopocki AG, Zhu C, McEver RP. Catch bonds govern adhesion through L-selectin at threshold shear. J Cell Biol. 2004;166:913-923.
527. Ramachandran V, Yago T, Epperson TK, et al. Dimerization of a selectin and its ligand stabilizes cell rolling and enhances tether strength in shear flow. Proc Natl Acad Sci U S A. 2001;98:10166-10171.
528. Smith MJ, Berg EL, Lawrence MB. A direct comparison of selectin-mediated transient, adhesive events using high temporal resolution. Biophys J. 1999;77:3371-3383.
529. Flood VH, Gill JC, Morateck PA, et al. Common VWF exon 28 polymorphisms in African Americans affecting the VWF activity assay by ristocetin cofactor. Blood;116:280-286.
530. Fredrickson BJ, Dong JF, McIntire LV, Lopez JA. Shear-dependent rolling on von Willebrand factor of mammalian cells expressing the platelet glycoprotein Ib-IX-V complex. Blood. 1998;92:3684-3693.
531. Papi M, Maulucci G, De Spirito M, et al. Ristocetin-induced self-aggregation of von Willebrand factor. Eur Biophys J.

APPENDICES

APPENDIX A - Buffers and solutions

10 X DNA loading buffer

0.125% (w/v) xilene cyanol, 0.125% (w/v) bromophenol blue, 0.625% SDS (w/v), 20% (v/v) glycerol

10 X TBE buffer

0.89 M Tris-borate (pH 8.3), 20 mM EDTA. Prior to use, this was diluted to 1 x TBE buffer with purified water

TE buffer

10 mM Tris (pH 8.0), 1 mM EDTA

SDS-PAGE Electrophoresis buffer

25 mM Tris-HCl (pH 8.3) 192 mM glycine and 0.1% (w/v) SDS

2 x Protein Loading buffer

150 mM Tris-HCl (pH 6.8), 20% (v/v) glycerol, 4% (w/v) SDS, 0.125% (w/v) bromophenol blue

Transfer buffer

25 mM Tris-HCl (pH 8.3), 192 mM glycine, 20% (v/v) methanol

PBS buffer

Dissolve 5 PBS tablets (Sigma) to 1 litre of distilled H_2O

LB (Luria-Bertani) broth

1% (w/v) bacto-tryptone, 0.5% (w/v) bacto-yeast extract, 1% (w/v) NaCl

LB agar

1% (w/v) bacto-tryptone, 0.5% (w/v) bacto-yeast extract, 1% (w/v) NaCl, 1.5% bacto-agar

(The components of each medium are dissolved in ultra-pure water and autoclaved)

APPENDIX B – Oligonucleotide primers

Primer	Sequnce (5'-3')
T1248A fwd	GGTGGTGCCTCCC**G**CAGATGCCCCGGTG
T1248A rev	CACCGGGGCATCTGCGGGAGGCACCACC
T1255A fwd	CCGGGTGAGCCCC**G**CCACTCTGTATGTGGAGGACATC
T1255A rev	GATGTCCTCCACATCAAGAGTGG**C**GGGGCTCACCCGG
T1256A fwd	GTGAGCCCCGCC**G**CTCTGTATGTGG
T1256A rev	CCACATACAGAG**C**GGCGGGGCTCAC
S12623A fwd	GTATGTGGAGGACATC**G**CGGAACCGCCGTTGC
S1263A rev	GCAACGGCGGTTCCG**C**GATGTCCTCCACATAC
T1468A fwd	GCCCCTCCTCCT**G**CTCTGCCCCCC
T1468A rev	GGGGGGGCAGAG**C**AGGAGGAGGGG
T1477A fwd	CATGGCACAAGTC**G**CTGTGGGCCCGG
T1477A rev	CCGGGCCCTCAG**C**GACTAGTGCCATG
S1486A fwd	CTCTTGGGGGTT**G**CGACCCTGGGG
S1486A rev	GCCCCAGGCTCG**C**AACCCCCAAGA
T1487A fwd	CTTGGGGGTTTCG**G**CCCTGGGGCCCAAG
T1487A rev	CTTGGGCCCCAGGG**C**CGAAACCCCCAAG
C3 fwd	CCCGGTGAGCCCC**G**CCACTCTGTATGTG
C3 rev	CACATACAGAGTGG**C**GGGGCTCACCGGG
C4 fed	GGTGAGCCCCGCCGCTCTGTATGTGGAG
C4 rev	CTCCACATACAGAGCGGCGGGGCTCACC
C6 fwd	CATGGCACAAGTC**G**CTGTGGGCCCG
C6 rev	CCGGGCCCACAG**C**GACTTGTGCCATG
C7 fwd	CTCTTGGGGGTT**G**CGGCCCTGGGGC
C7 rev	GCCCCAGGGCCG**C**AACCCCCAAGAG

T1679A fed	CTGCAGATCCCC**G**CCTCTCCCCAT
T1679A rev	ATGGGAGAGGG**C**GGGGATCTGCAG
T2298A fed	CAGCCCTGCCCC**G**CGGCCAAAGCTC
T2298A rev	GAGCTTTGGCCG**C**GGGGCAGGGCTG
G1324S fwd	GGAGTACCACGAC**A**GCTCCCACGCCTAC
G1324S rev	GTAGGCGTGGGAGC**T**GTCGTGGTACTC
GPIbá clone fwd	ATAAGCTTGATATCGAATTCATGCCTCTCCTCCTCTTGCT
GPIbá clone rev	GTGGATCCCCCGGGCTGCAGACGCACCTTATCGCCCTCA
GPIbá insert fwd	CTGAGGGCGATAAGGTGCGTGAACAAAAACTCATCTCAG
GPIbá insert rev	GTGGATCCCCCGGGCTGCAGTCAATGGTGATGGTGATGAT

PUBLICATIONS ARISING FROM THIS WORK

Papers arising from this thesis

The plasma von Willebrand factor *O*-glycom comprises a surprising verity of structures including ABH antigens and disialosyl motifs.
Canis K, McKinnon TAJ, **Nowak A,** Panico M, Morris HR, Laffan M, Dell A.
J Thromb Haemost. 2010 Jan;8(1):137-45

The role of VWF *O*-linked glycans in mediating the interaction with GPIb under shear stress.
Nowak AA, McKinnon TAJ, Canis K, Angus G, Riddell A, Laffan MA. Manuscript in preparation for submission to Blood.

Opposing effects of VWF *O*-linked glycans on the interaction with ADAMTS13.
Nowak AA, McKinnon TAJ, Hughes J, Chan ACK, Laffan MA. Manuscript in preparation for submission to J Thromb Haemost.

Characterisation of Von Willebrand factor A1 domain mutants I1416N and I1416T using an *in vitro* flow assay system.
McKinnon TAJ, **Nowak AA**, Laffan MA and Millar CM. (Manuscript in preparation for submission to Blood)

Abstracts leading to oral presentation

O-linked glycosylation of VWF is an important modulator of ADAMTS13 proteolysis and binding to GPIbα
AA Nowak, G Angus, MA Laffan, TAJ McKinnon.
British Society of Haemostasis and Thrombosis annual meeting, Newcastle upon Thyme, UK October 2009

Abstracts leading to poster presentation

O-linked glycosylation of VWF is an important modulator of ADAMTS13 proteolysis and binding to GPIbα
AANowak, G Angus, M. Laffan and TAJ McKinnon.
International Society on Thrombosis and Haemostasis Boston, USA, July 2009

Publications associated with this thesis

Specific N-linked glycosylation sites modulate synthesis and secretion of von Willebrand factor.
McKinnon TA, Goode EC, Birdsey GM, **Nowak AA,** Chan AC, Lane DA, Laffan MA. Blood 2010 Jul 29;116(4):640-8.

Poster presentations

The role of *N*-linked glycosylation in expression and function of ADAMTS13.
AANowak, Chan Kwo Chion, M. Laffan and TAJ McKinnon.
American Society of Haematology Meeting, San Francisco, USA,December 200